Physics and chemistry of stratospheric ozone and interactions with climate change

Jayanarayanan Kuttippurath

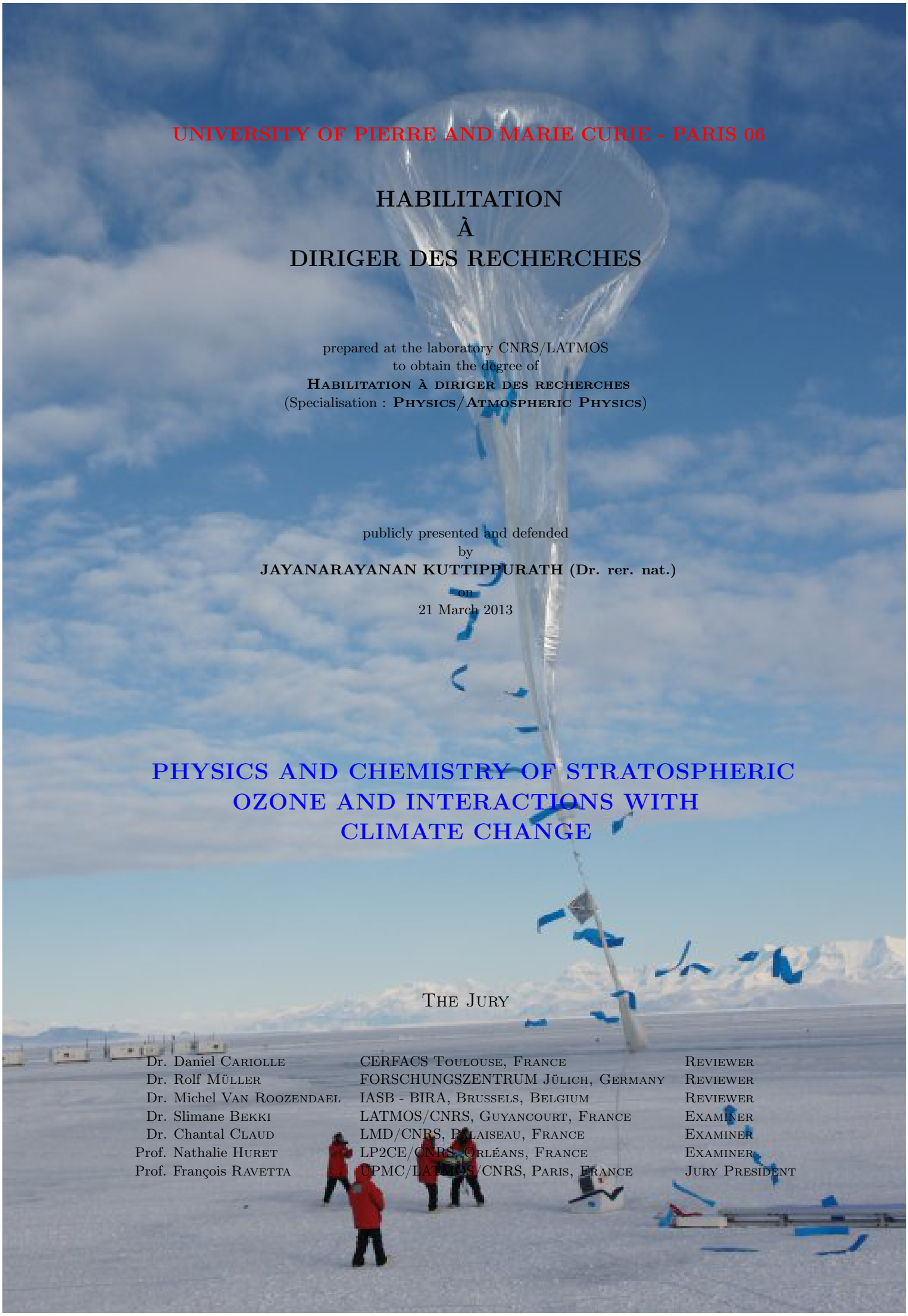

UNIVERSITY OF PIERRE AND MARIE CURIE - PARIS 06

HABILITATION À DIRIGER DES RECHERCHES

prepared at the laboratory CNRS/LATMOS
to obtain the degree of
Habilitation à diriger des recherches
(Specialisation : **Physics/Atmospheric Physics**)

publicly presented and defended
by
JAYANARAYANAN KUTTIPPURATH (Dr. rer. nat.)
on
21 March 2013

PHYSICS AND CHEMISTRY OF STRATOSPHERIC OZONE AND INTERACTIONS WITH CLIMATE CHANGE

The Jury

Dr. Daniel Cariolle	CERFACS Toulouse, France	Reviewer
Dr. Rolf Müller	FORSCHUNGSZENTRUM Jülich, Germany	Reviewer
Dr. Michel Van Roozendael	IASB - BIRA, Brussels, Belgium	Reviewer
Dr. Slimane Bekki	LATMOS/CNRS, Guyancourt, France	Examiner
Dr. Chantal Claud	LMD/CNRS, Palaiseau, France	Examiner
Prof. Nathalie Huret	LP2CE/CNRS, Orléans, France	Examiner
Prof. François Ravetta	UPMC/LATMOS/CNRS, Paris, France	Jury President

UNIVERSITY OF PIERRE AND MARIE CURIE - PARIS 06

HABILITATION
À
DIRIGER DES RECHERCHES

prepared at the laboratory CNRS/LATMOS
to obtain the degree of
Habilitation à diriger des recherches
(Specialisation : **Physics/Atmospheric Physics**)

publicly presented and defended
by
JAYANARAYANAN KUTTIPPURATH (Dr. rer. nat.)
on
21 March 2013

PHYSICS AND CHEMISTRY OF STRATOSPHERIC OZONE AND INTERACTIONS WITH CLIMATE CHANGE

The Jury

Dr. Daniel Cariolle	CERFACS Toulouse, France	Reviewer
Dr. Rolf Müller	FORSCHUNGSZENTRUM Jülich, Germany	Reviewer
Dr. Michel Van Roozendael	IASB - BIRA, Brussels, Belgium	Reviewer
Dr. Slimane Bekki	LATMOS/CNRS, Guyancourt, France	Examiner
Dr. Chantal Claud	LMD/CNRS, Palaiseau, France	Examiner
Prof. Nathalie Huret	LP2CE/CNRS, Orléans, France	Examiner
Prof. François Ravetta	UPMC/LATMOS/CNRS, Paris, France	Jury President

Contents

Key Findings

• 1. The dynamical activity in recent winters suggests that the occurrences of major warmings (MWs) in the Arctic is increasing at a rate of ∼1.1 events/winter against the historical value of 0.7 events/winter, which has implications for the ozone trends estimated during 1998/1999–2009/2010 in the northern hemisphere, and thus local and global climate.

• 2. A thorough diagnosis of the chemical ozone loss in the past 17 Arctic winters (1993/1994–2009/2010) suggests that the ozone loss is inversely proportional to the intensity and timing of MWs in each winter, where early (December–January) MWs lead to minimal loss.

• 3. The Arctic winter 2002/2003 was unique, as there were three minor warmings and a MW, but still experienced significant loss of ozone (∼1.3±0.2 ppmv at 450–500 K).

• 4. Large vortex-wide denitrification and the largest observed ozone loss until the year 2005 (∼1.5±0.2 ppmv at 450–550 K) were observed in the Arctic winter 2004/2005.

• 5. The Arctic winter 2010/2011 showed a record ozone loss (∼2.5±0.2 ppmv at 450–600 K or ∼160 DU over 350–850 K) and sign of an Arctic ozone hole. The nature of ozone loss with altitude (400–675 K) was comparable to that of relatively warmer Antarctic winters (e.g. 2004).

• 6. A method is introduced and applied to the Antarctic ground-based total column ozone measurements to construct a long-term ozone loss time series for the 1989–2012 period. The ozone loss analysis shows that the Antarctic ozone loss was around 35% (or 100 to 150 DU) during 1989–1991 and 48% (∼150 DU) during 1992–2012.

• 7. The comparatively reduced ozone loss and smaller ozone holes during the Antarctic winters 2004–2010 were due to relatively higher temperatures resulted from minor warmings in the period.

• 8. The peak ozone loss altitude in the Antarctic is around 500 K. However, the very cold winters (e.g. 2006) show a higher and the relatively warmer winters (e.g. 2010) show a lower shift in the peak loss altitudes of about 25 K, showing a clear distinction between various Antarctic winters in terms of the altitude of maximum ozone loss.

• 9. The contribution of various chemical cycles to the ozone loss for several Arctic and Antarctic winters is presented and compared. The study shows that about 85% of ozone loss in the lower stratosphere is dominated by the ClO–ClO and ClO–BrO cycles together and about 75% of the loss in the middle stratosphere is controlled by the NO–NO_2 cycle. The study also suggests that the contribution of the NO_x cycle to the total column ozone loss above 550 K in the Arctic is about 19±7 DU, whereas it is about three times larger in the Antarctic (50±5 DU).

• 10. An ozone trend of about +1 DU yr^{-1} is estimated from ground-based and satellite measurements in the Antarctic vortex for the 2000–2010 period. These trends are significant at 99% confidence intervals. This positive trend implies that the Antarctic ozone is recovering and hence, indicates a successful implementation of the Montreal Protocol.

• 11. Apart from the polar chemistry and dynamics studies, a detailed climatology of the equatorial waves (Kelvin, Rossby, and Rossby–Gravity) was also co-developed during the course of this thesis and is the first detailed study of its kind using observations and climate model simulations.

Acknowledgements

A lot of motivation is needed to prepare for an HDR and I greatly thank Dr. S. Bekki (Director of the SHTI research group of CNRS/LATMOS) and Dr. D. Hauser (Director, CNRS/LATMOS) for their motivation for making this HDR happen. I sincerely thank the president of the HDR screening committee Prof. P. Bouruet-Aubertot (UPMC/LOCEAN), the head of the HDR jury selection committee Prof. V. Zeitlin (UPMC/LMD) and other members of the HDR screening committee, for their approval for the preparation and presentation of this HDR.

This thesis comprises the studies during my research scientist tenure at CNRS/LATMOS and CNRS/LMD. Therefore, I deeply express my gratitude to Dr. F. Lott of CNRS/LMD, and Dr. F. Goutail and Dr. S. Godin-Beekmann of CNRS/LATMOS, who paved my way to these excellent research laboratories. I also thank for their continuous support and the scientific discussions I had with them.

I thank Dr. F. Lefèvre for his assistance to my modelling initiatives with the chemistry climate model (CCM) LMDz-reprobus, and the chemical transport models REPROBUS and MIMOSA-CHIM. I also remember the stimulating scientific discussions I had with him on various aspects of chemistry and climate modelling.

I thank Dr. J. Gazeaux for his help with the MIMOSA-CHIM CTM. I appreciate the help and support given by Dr. H. K. Roscoe (BAS, UK), Dr. J.-P. Pommereau, Dr. A. Pazmiño and Dr. M. Marchand of LATMOS, and Dr. F. Vial and Dr. A. Hertzog of LMD. I always cherish the good support given by my Bremen (Univ. Bremen, Germany) colleagues: Prof. J. Notholt, Dr. A. Kleinböhl, Dr. H. Bremer, Dr. H. Küllmann, Dr. B.-M. Sinnhuber and Dr. M. Sinnhuber.

I would like to thank the referees of this HDR thesis: Dr. D. Cariolle, Dr. R. Müller and Dr. M. van Roozendael. It is not an easy task to make a thorough review report in a limited time period, for an HDR memoir in particular. Therefore, I greatly thank them for their comments on the manuscript, the critical review reports and the time they spent for this evaluation. I also thank the examiners of the thesis: Dr. S. Bekki, Dr. C. Claud, Dr. N. Huret and Dr. F. Ravetta (President of the HDR defense jury) for their comments on the manuscript, discussions during the defense and the time they granted for these evaluation processes.

Publications make an integral part of this thesis. I, therefore, express my sincere gratitude to all my coauthors: Dr. M. Chipperfield (Univ. Leeds, UK), Dr. U. Cortesi (Univ. Waterloo, Canada), Dr. E. Dupuy (Univ. Waterloo, Canada), Dr. W. Feng (Univ. Leeds, UK), Dr. L. Froidevaux (JPL/NASA, USA), Dr. J. Gazeaux (CNRS, Paris) Dr. K. Künzi (Univ. Bremen, Germany), Dr. P. J. Nair (CNRS, France), Dr. G. Nikulin (SMHI, Sweden), Dr. S. Payan (LPMAA, France), Dr. M. Santee (JPL/NASA, USA), Dr. J. Shanklin (BAS, UK), Dr. S. Solomon (Univ. Bremen, Germany), Dr. K. Strong (Univ. Troronto, Canda), Dr. J. Urban (Chamlers', Seweden), Dr. M. von Hobe (FZJ, Germany), Dr. D. Wang (KIT, Germany), Dr. M. Wolf (Univ. Troronto, Canda) and Dr. E. Wolfram (CELIAP, Argentina).

Furthermore, I take this opportunity to thank Mrs. C. Boonne (IPSL, ETHER data manager) for her timely support with various data sets for my studies. I also thankfully remember the administrative help provided by Mrs. M. Roux of LMD, and Mrs. M. Moreau, Mrs. M. Grenier, Mrs. E. Quinsac, Mrs. C. Takacs and Mrs. V. Fleury of LATMOS, and I. Ferrand of CNRS Meudon.

I deeply thank my wife Prijitha for everything she did for me for the past five years: her sacrifice, unlimited love, deep patience, thorough understanding, encouraging words, constant support and wise counsel. Her listening to my ideas, the scientific discussions I had with her, and her editing and careful revision of the chapters have greatly helped to draft this thesis in a better way. I also thank for her tolerance of the absorption of all our evenings, weekends and holidays in the recent years.

Last, but certainly not least, I would like to thank the continuous and strong support received from my parents, siblings, teachers, friends, and to all unseen hands contributed directly or indirectly towards the fulfillment of this HDR. Thank you!

The studies presented in thesis were funded by the following projects as well: The EU-EuPLEx, SCIA–VALUE, ACCENT–BIAFLUX, PAVE, SCOUT–O3, ANR/ORACLE–O3 France, CNES, ESA/MULTI-TASTE, RECONCILE, and the CNRS post-doctoral fellowship (2005–2007).

Acronym

1-D	:	One–dimensional
2-D	:	Two–dimensional
3-D	:	Three–dimensional
AAO	:	Antarctic Oscillation
ACE-FTS	:	Atmospheric Chemistry Experiment-Fourier Transform Spectrometer
AK	:	Averaging Kernel
AMF	:	Air Mass Factor
AOS	:	Acousto-Optical Spectrometer
A_{PSC}	:	Area of Polar Stratospheric Clouds
ASUR	:	Airborne Sub-millimetre Radiometer
BD	:	Brewer-Dobson
BrO	:	Bromine Monoxide
CCM	:	Chemistry Climate Model
CCMVal	:	Chemistry Climate Model Validation
CFC	:	Chlorofluorocarbon
ClO	:	Chlorine monoxide
CTM	:	Chemical Transport Model
DOAS	:	Differential Optical Absorption Spectroscopy
DU	:	Dobson Unit
ECMWF	:	European Centre for Medium-Range Weather Forecasts
EESC	:	Equivalent Effective Stratospheric Chlorine
EEASC	:	Equivalent Effective Antarctic Stratospheric Chlorine
ENSO	:	El Niño–Southern Oscillation
ENVISAT	:	Environmental Satellite
EP flux	:	Eliassen-Palm flux
EqL	:	Equivalent Latitude
ERA	:	ECMWF Reanalysis
ERS	:	European Remote Sensing
EuPLEX	:	European Polar Lee-wave Experiment
FTIR	:	Fourier Transform Infrared
GAW	:	Global Atmosphere Watch
GCM	:	General Circulation Model
GOME	:	Global Ozone Monitoring Experiment
HALOE	:	Halogen Occultation Experiment
HF	:	Heat flux
HNO_3	:	Nitric Acid
IASI	:	Infrared Atmospheric Sounding Interferometer
ILAS	:	Improved Limb Atmospheric Spectrometer
IR	:	Infra-Red
MetOp	:	Meteorological Operational
MIMOSA	:	Modélisation Isentrope du transport Méso-échelle
	:	de lÓzone Stratosphérique par Advection
MIMOSA-CHIM	:	MIMOSA CTM
MLS	:	Microwave Limb Sounder
MSR	:	Multi-sensor Reanalysis
MW	:	Major Warming
MWR	:	Microwave Radiometer
NASA	:	National Aeronautics and Space Administration
NAT	:	Nitric Acid Trihydrate
NCAR	:	National Center for Atmospheric Research
NDACC	:	Network for the Detection of Atmospheric Composition Change
NH	:	Northern Hemisphere
N_2O	:	Nitrogen dioxide

NO	:	Nitrogen Oxide
NO_2	:	Nitrous Oxide
NOAA	:	National Oceanic and Atmospheric Administration
NILU	:	Norsk institutt for luftforskning
O_3	:	Ozone
ODS	:	Ozone Depleting Substance
OMI	:	Ozone Monitoring Instrument
OSIRIS	:	Optical Spectrograph InfraRed Imager System
POAM	:	Polar Ozone and Aerosol Measurement
ppbv	:	Parts per billion by volume
ppmv	:	Parts per million by volume
pptv	:	Parts per trillion by volume
PSC	:	Polar Stratospheric Cloud
PV	:	Potential Vorticity
pvu	:	PV Unit
PWLT	:	Piece–wise linear trend
QBO	:	Quasi Biennial Oscillation
REPROBUS	:	Reactive Processes Ruling the Ozone Budget in the Stratosphere
SAGE	:	Stratospheric Aerosol and Gas Experiment
SAOZ	:	Système d'Analyse par Observation Zénithale
SBUV	:	Solar Backscatter UltraViolet
SCIAMACHY	:	SCanning Imaging Absorption spectroMeter for Atmospheric CartograpHY
SCIA	:	SCIAMACHY
SCIA-VALUE	:	SCIAMACHY Utilisation and Validation Experiment
SF	:	Solar flux
SMR	:	Sub-millimetre Radiometer
SH	:	Southern Hemisphere
sh	:	sunlit hour
SPARC	:	Stratospheric Processes And their Role in Climate
SSW	:	Sudden Stratospheric Warming
SZA	:	Solar Zenith Angle
TOMS	:	Total Ozone Mapping Spectrometer
TOSOMI	:	Total Ozone retrieval scheme for SCIAMACHY based on the OMI/DOAS algorithm
TOGOMI	:	Total Ozone retrieval scheme for GOME based on the OMI/DOAS algorithm
UARS	:	Upper Atmosphere Research Satellite
UTLS	:	Upper Troposphere and Lower Stratosphere
UV	:	Ultra–Violet
UV-VIS	:	UV Visible
VMR	:	Volume Mixing Ratio
V_{PSC}	:	Volume of PSC
WMO	:	World Meteorological Organisation

Publications

1. **Kuttippurath, J.**, F. Lefèvre, J.-P. Pommereau, H. K. Roscoe, F. Goutail, A. Pazmiño and J. D. Shanklin: The Antarctic ozone loss in 1979–2010: First sign of ozone recovery, Atmos. Chem. Phys., 13, doi:10.5194/acp-13-1625-2013, 1625–1635, 2013.

2. Gazeaux, J. C. Clerbaux, M. George, J. HadjiLazaro, **J. Kuttippurath**, P.F. Coheur, D. Hurtmans, T. Deshler, M. Kovilakam, P. Campbell, V. Guidard, F. Rabier and J. N. Thepaut: Intercomparison of polar ozone profiles by IASI/MetOp sounder with 2010 Concordiasi ozonesonde observations, Atmos. Meas. Tech., 6, doi:10.5194/amt-6-613-2013, 613–620, 2013.

3. Nair, P. J., S. Godin-Beekmann, **J. Kuttippurath**, G. Ancellet, F. Goutail, A. Pazmiño, L. Froidevaux, J. M. Zawodny, R. D. Evans, J. H. Wang, J. Anderson and M Pastel: Ozone trends derived from the total column and vertical profiles at a northern mid-latitude station, Atmos. Chem. Phys., 13, doi:10.5194/acp-13-10373-2013, 10373–10384, 2013.

4. **Kuttippurath, J.** and G. Nikulin: A comparative study of the major sudden stratospheric warmings in the Arctic winters 2003/2004–2009/2010, Atmos. Chem. Phys., 12, doi:10.5194/acp-12-8115-2012, 8115–8129, 2012.

5. **Kuttippurath, J.**, S. Godin-Beekmann, F. Lefèvre, G. Nikulin, M. L. Santee and L. Froidevaux: Record-breaking ozone loss in the Arctic winter 2010/2011: comparison with 1996/1997, Atmos. Chem. Phys., 12, doi:10.5194/acp-12-7073-2012, 7073–7085, 2012.

6. Wolfram, E. A., J. Salvador, F. Orte, R. D'Elia, S. Godin-Beekmann, S., **J. Kuttippurath**, A. Pazmio, F. Goutail, C. Casiccia, F. Zamorano, N. Paes Leme and E. J. Quel: The unusual persistence of an ozone hole over a southern mid-latitude station during the Antarctic spring 2009: a multi-instrument study, Ann. Geophys., 30, doi:10.5194/angeo-30-1435-2012, 1435–1449, 2012.

7. **Kuttippurath, J.**, A. Kleinböhl, M. Sinnhuber, H. Bremer, H. Küllmann, J. Notholt, S. Godin-Beekmann, O. P. Tripathi and G. Nikulin: Arctic ozone depletion in 2002–2003 measured by ASUR and comparison with POAM observations, J. Geophys. Res., 116, doi:10.1029/2011JD016020, 2011.

8. **Kuttippurath, J.**, A. Kleinböhl, H. Bremer, H. Küllmann, J. Notholt, B.-M. Sinnhuber, W. Feng and M. Chipperfield: Aircraft measurements and model simulations of stratospheric ozone and N_2O: Implications for chemistry and transport processes in the models, J. Atmos. Chem., doi:10.1007/s10874-011-9191-4, 2011.

9. **Kuttippurath, J.**, S. Godin-Beekmann, F. Lefèvre and F. Goutail: Spatial, temporal, and vertical variability of polar stratospheric ozone loss in the Arctic winters 2004/2005–2009/2010, Atmos. Chem. Phys., 10, doi:10.5194/acp-10-9915-2010, 9915–9930, 2010.

10. **Kuttippurath, J.**, F. Goutail, J.-P. Pommereau, F. Lefèvre, H. K. Roscoe, A. Pazmiño, W. Feng and M. P. Chipperfield: Estimation of Antarctic ozone loss from Ground-based total column measurements, Atmos. Chem. Phys., 10, doi:10.5194/acp-10-6569-2010, 6569–6581, 2010.

11. **Kuttippurath, J.**, S. Godin-Beekmann, F. Lefèvre and A. Pazmiño: Ozone depletion in the Arctic winter 2007/08, Int. J Remote Sens., 30, doi:10.1080/01431160902821965, 4071–4082, 2009.

12. Dupuy, E., K. A. Walker, J. Kar, (including **J. Kuttippurath**) et al.: Validation of ozone measurements from the Atmospheric Chemistry Experiment (ACE), Atmos. Chem. Phys., 9, doi:10.5194/acp-9-287-2009, 287–343, 2009.

13. Lott, F., **J. Kuttippurath** and F. Vial: A Climatology of the gravest waves in the equatorial lower and middle stratosphere: Method and results for the ERA-40 re-analysis and the LMDz GCM, J. Atmos. Sci., 66, doi:10.1175/2008JAS2880.1, 1327–1346, 2009.

14. Payan, S., C. Camy-Peyret, H. Oelhaf, (including **J. Kuttippurath**) et al.: Validation of version-4.61 methane and nitrous oxide observed by MIPAS, Atmos. Chem. Phys., 9, doi:10.5194/acp-9-413-2009,

413–442, 2009.

15. Santee, M., A. Lambert, W. Read, (including **J. Kuttippurath**) et al.: Validation of the Aura Microwave Limb Sounder ClO Measurements, J. Geophys. Res., 113, doi:10.1029/2007JD008762, 2009.

16. Solomon, S. J., G.W. Schade, **J. Kuttippurath**, A. Ladstätter-Weissenmayer and J. P. Burrows: VOC Concentrations in an Indoor Workplace Environment of a University Building, Indoor and Built Environ., 17, 260–268, doi:10.1177/1420326X08090822, 2008.

17. Strong, K., M. A. Wolff, T. E. Kerzenmacher, (including **J. Kuttippurath**) et al.: Validation of ACE-FTS N_2O measurements, Atmos. Chem. Phys., 8, doi:10.5194/acp-8-4759-2008, 4759–4786, 2008.

18. Wolff, M. A., T. Kerzenmacher, K. Strong, (including **J. Kuttippurath**) et al.: Validation of HNO_3, $ClONO_2$, and N_2O_5 from the Atmospheric Chemistry Experiment Fourier Transform Spectrometer (ACE-FTS), Atmos. Chem. Phys., 8, doi:10.5194/acp-8-3529-2008, 3529–3562, 2008.

19. **Kuttippurath, J.**, H. Bremer, J. Burrows, A. Kleinböhl, H. Küllmann, K. Künzi, J. Notholt, M. Sinnhuber, C. von Savigny, N. Lautiè, D. Murtagh, J. Urban, M. Milz, G. P. Stiller, S. Petelina, J. de La Noé, E.Le Flochmoén and P. Ricaud: Intercomparison of ozone profile measurements from ASUR, SCIAMACHY, MIPAS, OSIRIS, and SMR, J. Geophys. Res., 112, doi:10.1029/2006JD007830, 2007.

20. Cortesi, U., J. C. Lambert, C. De Clercq, (including **J. Kuttippurath**) et al.: Geophysical validation of MIPAS-ENVISAT operational ozone data, Atmos. Chem. Phys., 7, doi:10.5194/acp-7-4807-2007, 4807–4867, 2007.

21. Wang, D., M. Höpfner, C. E. Blom, (including **J. Kuttippurath**) et al.: Validation of MIPAS HNO_3 operational data, Atmos. Chem. Phys., 7, doi:10.5194/acp-7-4905-2007, 4905–4934, 2007.

22. Fix, A., G. Ehret, H. Flentje, G. Poberaj, M. Gottwald, H. Finkenzeller, H. Bremer, M. Bruns, J. P. Burrows, A. Kleinböhl, H. Küllmann, **J. Kuttippurath**, A. Richter, P. Wang, K.-P. Heue, U. Platt, I. Pundt and T. Wagner: SCIAMACHY validation by aircraft remote sensing: design, execution, and first measurement results of the SCIA–VALUE mission, Atmos. Chem. Phys., 5, doi:10.5194/acp-5-1273-2005, 1273–1290, 2005.

23. Kleinböhl, A., **J. Kuttippurath**, M. Sinnhuber, B.-M. Sinnhuber, H. Küllmann, K. Künzi and J. Notholt: Rapid meridional transport of tropical airmasses to the Arctic during the major stratospheric warming in January 2003, Atmos. Chem. Phys., 5, doi:10.5194/acp-5-1291-2005, 1291–1299, 2005.

24. Kleinböhl, A., H. Bremer, H. Küllmann, **J. Kuttippurath**, E. V. Browell, T. Canty, R. J. Salawitch, G. C. Toon and J. Notholt: Denitrification in the Arctic mid-winter 2004/2005 observed by airborne submillimeter radiometry, Geophys. Res. Lett., 32, doi:10.1029/2005GL023408, 2005.

25. Urban, J., N. Lautié, E. Le Flochmoën, (including **J. Kuttippurath**) et al.: Odin/SMR limb observations of stratospheric trace gases: Validation of N_2O, J. Geophys. Res., 110, doi:10.1029/2004JD005394, 2005.

Reviewed Extended Abstracts

1. **Kuttippurath, J.**, H. Bremer, A. Kleinböhl, H. Küllmann, J. Notholt and K. Künzi: Seasonal and latitudinal distribution of stratospheric ozone: Observations and model calculations, Proc. of Quadrennial Ozone Symposium, 107 pp, 2004.

2. **Kuttippurath, J.**, A. Kleinböhl, H. Bremer, H. Küllmann and J. Notholt: Validation of SCIAMACHY ozone limb profiles by ASUR, Proc. of the 2^{nd} Workshop on the Atmospheric Chemistry Validation of ENVISAT (ESA-ESRIN, Frascati, Italy), ESA special publication: 562 (CD-ROM), D. Danesy (ed.), 17.1–17.13, 3–7 May 2004.

3. Cortesi, U., C. E. Blom, C. Camy-Peyret, K. Chance, J. Davies, F. Goutail, **J. Kuttippurath**, C.T. McElroy, F. Mencaraglia, H. Ölhaf, A. Petritoli, M. Pirre, J.-P. Pommereau, F. Ravegnani, J. B. Renard and K. Strong: MIPAS ozone validation by stratospheric balloon and aircraft measurements, Proc. of the

2^{nd} Workshop on the Atmospheric Chemistry Validation of ENVISAT (ESA-ESRIN, Frascati, Italy), ESA special publication: 562 (CD-ROM), D. Danesy (ed.), 17.1–17.13, 3–7 May 2004

4. Kleinböhl, A., **J. Kuttippurath**, H. Bremer, M. Sinnhuber, H. Küllmann and K. Künzi: Retrieval of mesospheric ozone profiles from airborne submillimeter measurements, Proc. of MICRORAD, 24–27 February 2004.

5. Küllmann, H., A. Kleinböhl, H. Bremer, **J. Kuttippurath**, M. Sinnhuber, J. Notholt and K. Künzi: Radiometry of atmospheric chemical composition from SOFIA, Proc. of SOFIA Upper Deck Science Opportunities Workshop, NASA Ames Research Center, Moffett Field, CA, 22–23 June 2004.

6. Küllmann, H., **J. Kuttippurath**, H. Bremer, A. Kleinböhl, C. von Savigny, J. Notholt and K. Künzi: Submillimeter measurements of O_3 and N_2O and a first Comparison with SCIAMACHY Ozone Profiles, Proc. of 5^{th} GSVT meeting, Bremen, Germany, 7–9 December 2004.

7. **Kuttippurath, J.**, A. Kleinböhl, H. Bremer, H. Küllmann, M. von König and K. Künzi: Stratospheric trace gas measurements by the Airborne Submillimeter Radiometer ASUR during SCIA–VALUE 2002, Proc. of IEEE International Geoscience and Remote Sensing Symposium, Vol. 4, doi:10.1109/IGARSS.2003.1294423, 2305–2307, 2003.

Conference Communications

1. **Kuttippurath, J.**, F. Goutail, F. Lefèvre, J.-P Pommereau, A. Pazmiño and H. K. Roscoe: Probing the Antarctic ozone hole with NDACC total ozone column observations in 1989–2010, Symposium on 20^{th} Anniversary of NDAAC, Reunion Island, 6–10 November 2011.

2. **Kuttippurath, J.**, S. Godin-Beekmann and A. Pazmiño: Signatures of the Antarctic ozone loss saturation in the late 1980s, Geophysical Research Abstracts, Vol. 13, EGU 2011-9341, 2011.

3. Godin-Beekmann, S., **J. Kuttippurath**, F. Lefèvre, M. L. Santee and L. Froidevaux: Record-breaking ozone loss during the Arctic winter 2010/2011: Comparison with the Arctic winter 1996/1997, AGU Fall meeting, San Francisco, USA, December, 2011.

4. Goutail, F. Lefèvre, A. Pazmiño, J.-P. Pommereau, **J. Kuttippurath**, M. Van Roozendael, M. Chipperfield, W. Feng, E. Kyro, P. Ericksen, K. Stebel, V. Dorokhov, C. Adams, X. Zhao, K. Walker and K. Strong: Arctic O_3 loss 2010/2011, EGU General Assembly, Vienna, Austria, 3–8 April 2011.

5. Goutail, F., A. Pazmiño, **J. Kuttippurath**, F. Lefèvre, J.-P. Pommereau, M. Chipperfield and W. Feng: Interannual variability of ozone loss in the Arctic and Antarctic polar vortex using 20 years of NDACC ozone measurements, NDAAC symposium, Reunion Island, 6–10 November 2011.

6. Goutail, F., J.-P. Pommereau, F. Lefèvre, A. Pazmiño, **J. Kuttippurath**, M. Chipperfield, W. Feng, M. Van Roozendael, P. Eriksen, K. Stebel, V. Dorokhov, E. Kyro and K. Strong: Record total ozone depletion in the Arctic vortex in 2011, AGU Fall Meeting, San Francisco, California, USA, 5–9 December 2011.

7. **Kuttippurath, J.**, S. Godin-Beekmann, F. Lefèvre and G. Nikulin: Dynamics of the exceptional warming events during the Arctic winters 2003/04, 2005/06 and 2008/09, Geophysical Research Abstracts, Vol. 12, EGU2010-5499, 2010.

8. Goutail , F., F. Lefèvre, **J. Kuttippurath** , J.-P. Pommereau, A. Pazmiño , M. Chipperfield, W. Feng , M. Van Roozendael, P. Eriksen, K. Stebel, V. Dorokhov, E. Kyro, C. Adams and K. Strong: Total ozone loss during the 2009/10 Arctic winter and comparison to previous years, Geophysical Research Abstracts, Vol. 12, EGU2010-3725-2, 2010.

9. **Kuttippurath, J.**, S. Godin-Beekmann, F. Lefèvre, and A. Pazmiño: Numerical simulation of ozone loss in the Antarctic winters 2005–2008: Comparison with MLS measurements, Geophysical Research Abstracts, Vol. 11, EGU 2009-9672, 2009.

10. **Kuttippurath, J.**, F. Goutail, F. Lefèvre, J.-P Pommereau, A. Pazmiño, W. Feng and M. Chipperfield: Antarctic Ozone loss 1988–2008 History at Dumont d'Urville (67S, 140E), Geophysical

Research Abstracts, Vol. 11, EGU 2009-10750, 2009.

11. Pazmiño, A., F. Goutail, **J. Kuttippurath**, J.-P. Pommereau: Evaluation de la perte d'ozone polaire à partir des mesures SAOZ, 6^{me} Journées Scientifiques CNFRA, Paris, France, 1–2 October 2009.

12. **Kuttippurath, J.**, S. Godin-Beekmann, F. Lefèvre and A. Pazmiño: Simulations of ozone loss for the recent Arctic and Antarctic winters, Quadrennial Ozone Symposium, QOS–2008, Tormso, Norway, 29 June–5 July 2008.

13. **Kuttippurath, J.**, F. Goutail, F. Lefèvre, A. Pazmiño, J. P Pommereau, W. Feng and M. Chipperfield: Measurements of ozone loss in the Antarctic winter 2006 and 2007 and comparison to previous winters, Quadrennial Ozone Symposium, Tromso, Norway, 29 June–5 July 2008.

14. Lott, F., **J. Kuttippurath** and F. Vial: Equatorial wave packets in the LMDz stratospheric model and ERA-40 reanalysis, 4^{th} SPARC General Assembly, Bolgana, Italy, 31 August–5 September 2008.

15. **Kuttippurath, J.**, F. Lott and F. Vial: Equatorial waves in the stratospheric version of LMDz model and in the NCEP reanalysis, AGU Chapman Conference on Stratosphere in Climate and Climate Change, Santorini, Greece, 24–28 September 2007.

16. Solomon, S. J., J. Burrows, **J. Kuttippurath**, A. Ladstätter-Wissenmayer and G. Schade: Evaluation of occupational exposure to VOC concentrations in an indoor workplace environment, ACCENT Symposium, Urbino, Italy, 11–16 September 2007.

17. **Kuttippurath, J.** and F. Lott: Tropical waves in the LMDz stratospheric model and in the ERA 40 reanalysis, Geophysical Research Abstracts, Vol. 8, 03023, 2006.

18. Cortesi, U., C. Blom, T. Blumenstock , and et al. (including **J. Kuttippurath**): Co-ordinated validation activity and quality assessment of MIPAS-ENVISAT ozone data, Proc. ESA 1^{st} Atmospheric Science Conference, H. Lacoste (ed.), ESA special publication: 628, ISBN:92-9092-939-1, ISSN-1609-042X, 8–12 May 2006.

19. Payan, S., K. Grunow, J. Bureau, G. Wetzel, M. Pirre, **J. Kuttippurath**, V. Payne, A. Bracher, N. Glatthor, G. Stiller, U. Cortesi, P. Raspollini, C. Vigouroux, A. Engel, C. Piccolo, C. M. Volk, A. Butz and M. De Mazière: Validation and data characteristics of methane and nitrous oxide profiles observed by MIPAS and processed with Version 6.1 algorithm, 3^{rd} Workshop on the Atmospheric Chemistry Validation of Envisat, ESA ESRIN Frascati, Italy, 4–7 December 2006.

20. Solomon, S. J., **J. Kuttippurath**, A. Ladstätter Wiessenmayer and J. Burrows: Exposure assessment of VOCs in an indoor workplace environment of a university building in Germany, Geophysical Research Abstracts, Vol. 8, 09266, 2006.

21. Bremer, H., A. Kleinböhl, M. Palm, H. Küllmann, **J. Kuttippurath**, M. Sinnhuber, and J. Notholt: Observations of stratospheric trace gases during the PAVE mission by ASUR, EOS Aura Validation Workshop, Lanham-Seabrook, MD, USA, 19–23 September 2005.

22. Kleinböhl, A., H. Bremer, **J. Kuttippurath**, H. Küllmann, J. Notholt and K. Künzi: Stratospheric trace gas measurements by ASUR during PAVE, EOS Aura Science Team Meeting, Pasadena Convention Center, CA, USA, 28 February–3 March 2005.

23. Kleinböhl, A., H. Bremer, H. Küllmann, **J. Kuttippurath**, E. V. Browell, T. Canty, R. J. Salawitch, G. C. Toon and J. Notholt: Airborne submillimeter measurements in the Arctic mid-winter 2004/2005 – Evidence for chlorine activation and denitrification, AGU Fall Meeting, San Francisco, California, USA, 5–9 December 2005.

24. **Kuttippurath, J.**, H. Bremer, A. Kleinböhl, H. Küllmann and K. Künzi: Airborne microwave observations of stratospheric trace gases during SCIAMACHY validation campaigns, Deutschen Physikalischen Gesellschaft (DPG), Munich, Ref. No: UP 17.7, 22–26 March 2004.

25. **Kuttippurath, J.**, A. Kleinböhl, H. Bremer, H. Küllmann, C. von Savigny and K. Künzi: SCIAMACHY Ozone limb profiles: First validation by ASUR, European Geosciences Union, 1^{st} General Assembly, Nice, France, EGU04-A-04222, 25–30 April 2004.

26. **Kuttippurath, J.**, A. Kleinböhl, H. Bremer, K. Küllmann, J. Notholt and K. Künzi: Measurements and model calculations of Nitrous oxide: Implications for stratospheric transport, SPARC 3^{rd} General Assembly, Victoria, British Columbia, Canada, Ref. No: 10097, 1–6 August 2004.

27. Bremer, H., A. Kleinböhl, **J. Kuttippurath**, M. Sinnhuber, H. Küllmann and K. Künzi.: Denitrification and increase of middle Stratospheric Ozone and N_2O in the Arctic Winter 2002/03, Nice, France, Geophysical Research Abstracts, Vol. 6, EGU04-A-03704, 2004.

28. Bremer, H., A. Kleinböhl, **J. Kuttippurath**, H. Küllmann and K. Künzi: Measurements of HCN, NO, and Ozone during the LEONID MAC CAMPAIGN 2002, 35^{th} COSPAR Scientific Assembly, Paris, France, Abstract No: 02835, 18–25 July 2004.

29. Heue, K., U. Platt, I. Pundt, T. Wagner, A. Fix, H. Flentje, G. Ehret, H. Küllmann, H. Bremer, A. Kleinböhl, **Jayanarayanan. K.**, J. Notholt, K. Künzi, M. Bruns, P. Wang, A. Richter and J. Burrows: SCIAMACHY Validation with the DLR Falcon, 16^{th} ESA Symposium on European Rocket and Balloon Programmes and Related Research (St. Gallen, Switzerland), B. Warmbein (ed.), ESA special publication: 530, ISBN:92-9092-840-9, 2–5 June 2003.

30. Kleinböhl, A., **J. Kuttippurath**, M. von König, H. Küllmann and K. Künzi: Preliminary results of stratospheric trace gas measurements by ASUR in Arctic winter and spring 2002/2003, Geophysical Research Abstracts, Vol. 5, 1607-7962/gra/EAE03-A-02916, 2003.

31. Kleinböhl, A., H. Bremer, **J. Kuttippurath**, M. von König, H. Küllmann and K. Künzi: Results of stratospheric trace gas measurements by ASUR in Arctic winter and spring 2002/2003, SOLVE II / VINTERSOL, Joint Science Team meeting, Orlando, USA, 21–24 October 2003.

32. Küllmann, H., H. Bremer, A. Kleinböhl, **J. Kuttippurath**, A. Rozanov and K. Künzi: Airborne microwave observations during SCIAMACHY validation campaigns: first results, Geophysical Research Abstracts, Vol. 5, 1607–7962/gra/EAE03-A- 11750, 2003.

33. Fix, A., H. Flentje, G. Ehret, H. Küllmann, H. Bremer, A. Kleinböhl, **Jayanarayanan. K.**, J. Notholt, K. Künzi, M. Bruns, P. Wang, A. Richter, W. Gurlit, K. Gerilowski, J. Burrows, K. Heue, U. Platt, I. Pundt and T. Wagner: SCIAMACHY and MIPAS Validation with the DLR Falcon Aircraft, Envisat Validation Workshop, ESRIN, Frascati, Italy, 9–13 December 2002.

34. Küllmann, H., H. Bremer, J. Burrows, A. Kleinböhl, K. Künzi and **J. Kuttippurath**: Validation of SCIAMACHY Ozone Profiles and other Gases with the ASUR Airborne Sensor: Instrument Status and Method, 6^{th} European symposium on stratospheric ozone, Göteborg, Sweden, 2–6 September 2002.

Research project reports

1. David, C. and S. Godin-Beekmann, S. (**J. Kuttippurath**, Contributor): Ozone layer and UV radiation in a changing climate Evaluated during the IPY: ORACLE–FRANCE, ANR-06-BLAN-0246, 2011.

2. Solomon, S., **J. Kuttippurath**, A. Ladstaetter-Wissenmayer and J. Burrows: Surface-atmosphere flux measurements of soil methanol and NO_x from a managed cropland ecosystem: comparison with EC and chamber methods, ACCENT–BIAFLUX, 2009.

3. Harris, N. R. P. et al.: The Northern Hemisphere Stratosphere in the 2004/05 Winter, Report for 2005, SCOUT–O_3 Integrated Project, IUP, University of Bremen (**J. Kuttippurath**, Contributor), 2006.

4. Küllmann, H., **J. Kuttippurath**, H. Bremer, A. Kleinböhl, M. Sinnhuber, J. Notholt, K. Künzi and J. Burrows: Validation von SCIAMACHY LEVEL-2 Datenprodukten mit Hilfe des ASUR-Sensors von Bord des FALCON-Flugzeugs, FKZ 50EE0022, University of Bremen, 2005.

Abstract

Ozone is one of the key constituents in the atmosphere, although present only in trace amounts. The stratospheric ozone plays a pivotal role in regulating the incidence of harmful ultra-violet radiation (400–100 nm) and radiative balance of the earth, and thus influences the global climate. This thesis deals with the spatial, temporal and vertical evolution of polar stratospheric ozone and its interactions with climate change over 1979–2012, with an emphasis on the winters of 2000s.

Analysis of the dynamical situation in the Arctic winters reveals that there is an increase in the occurrence of major warmings (MWs) in recent years (1998/1999–2009/2010), as there were 13 MWs in the 12 winters (∼11 MWs/decade), although the long-term average (1957/1958–2009/2010) of the frequency stays around its historical value (∼7 MWs/decade). A study of the chemical ozone loss in the past 17 winters (1993/1994–2009/2010) suggests that the loss is inversely proportional to the intensity and timing of MWs in each winter, where early (December–January) MWs lead to limited loss. This high frequency of the MWs has significant implications for stratospheric ozone trends and hence, the Arctic and global climate.

A detailed assessment of the Arctic winters 1996/1997 and 2002/2003–2010/2011 shows that the winter 2002/2003 had a MW and three minor warmings. However, the winter still had a cumulative ozone loss of ∼1.5 ppmv at 450–500 K or 65 DU over 400–550 K by the end of March, apart from the record loss of ∼0.7 ppmv in December–January, as no other winter had such a large loss during the early winter over 1988/1989–2010/2011. In contrast, the largest ozone loss ever observed was in 2010/2011, about 2.5 ppmv at 400–550 K or 140 DU over 350–550 K. Our study shows that the loss in 2010/2011 was close to that found in some Antarctic winters, for the first time in the observed history. The prolonged strong chlorine activation and denitrification during the winter triggered this record loss. The loss in other winters was between 0.7 and 1.6 ppmv at around 475 K or 40 and 115 DU over 350–550 K, in which the smallest loss was estimated in the warm winter 2005/2006.

In order to make a long-term ozone loss time series for Antarctica, a method is introduced and applied to ground-based and space-borne total column ozone observations for the 1989–2012 period. The vortex-averaged ozone loss in the Antarctic is shown to be about 33–50% during 1989–1992 in agreement with the increase in halogens during that period, and then stayed at around 48% due to saturation of the loss. The loss in warmer winters (e.g. 2002 and 2004) is slightly smaller (37–46%) and the loss in very cold winters (e.g. 2003 and 2006) is relatively larger (52–55%). The maximum loss in the Antarctic is observed from mid-September to mid-October, and the peak loss rate is found in the August–early September period, with an average of about 0.5%/day. Furthermore, analysis with high resolution ozone profile measurements and simulations for the Antarctic winters 2004–2010 also showed the largest ozone loss in the colder winters of 2005 and 2006 with about 3.5 ppmv at 450–550 K or around 170 DU over 350–850 K, and the smallest loss in the warmer winters of 2004 and 2010 with about 2.5 ppmv at 450–550 K or around 140 DU over 350–850 K. The peak ozone loss altitude in Antarctica is around 500 K. However, the very cold winters show a higher and warmer winters show a lower shift in the peak loss altitudes (about 25 K), exhibiting a clear distinction between various winters in terms of the altitude of maximum loss. The study further indicates that the comparatively smaller Antarctic ozone loss and ozone holes in the recent winters (2004–2010) were due to the effect of a number of minor warmings during the period.

Our study for a range of Arctic and Antarctic winters shows that the Arctic ozone loss contributed by the halogen cycles (ClO–ClO and ClO–BrO) account for about 85% of the total loss below 550 K. There is an average contribution of about 19±7 DU from the NO_x cycle above 550 K to the total column loss in the Arctic, as analysed from the winters 2004/2005–2010/2011. Whereas in Antarctica, the ozone loss has a broad spread over 350–650 K, for which the lower stratospheric loss below 550 K is dominated by the halogens, but the loss above that level is dominated by NO_x with a contribution of about 75%, as in the Arctic. On average, the column ozone loss above 550 K is about 50±5 DU as estimated from the Antarctic winters 2004–2010 using the modelled and measured data. These findings imply that about one-third of the total column loss (50 DU out of 150–180 DU) in the Antarctic is contributed by the NO_x cycle, which is nearly three times larger than that in the Arctic.

To estimate the long-term trends, a regression model that explains the ozone variability by various climatic indices (planetary wave drive, solar cycle, quasi-biennial oscillation, etc.) and stratospheric chlorine is developed and applied to the ground-based and satellite ozone observations. Our study reveals that the Antarctic ozone recovery is well on course, as the diagnosis shows a trend of about −45 DU/decade in 1980–1999 and about +10 DU/decade in 2000–2010 in agreement with the levels of ozone depleting substances in each period, and both trends are significant at the 99% confidence intervals. The significant positive trends during the latter period indicates that the implementation of the Montreal Protocol is a great success. Therefore, this thesis offers a number of significant references for future ozone evolution, and thus for the regional and global climate change studies.

Résumé

L'ozone est un constituant important dans la chimie de l'atmosphère, cela malgré sa faible concentration. L'ozone stratoshérique joue un rôle essentiel à la fois dans la régulation des radiations ultraviolettes du soleil connues pour être dangereuses aux différentes formes de vie sur Terre et également dans l'équilibre radiatif influençant le climat global. Cette thèse est consacrée à l'étude de l'évolution temporelle et spatiale de l'ozone stratosphérique polaire entre 1979 et 2012, ainsi qu'à son interaction avec le changement climatique, avec une attention particulière pour les années après 2000.

L'analyse de la dynamique des hivers arctiques révèle une augmentation des évènements de forts réchauffements (EFR) ces dernières années (comparaisons faites entre les hivers 1998/99 et 2009/10). Alors qu'on compte 13 EFRs lors des 12 derniers hivers (soit 11EFR/décennie), le nombre moyen entre les hivers 1957/58 et 2009/10 s'élève à 7 EFR/décennie. Une étude chimique de la destruction de l'ozone lors des 17 derniers hivers (1993/94–2009/10) montre que celle-ci est inversement proportionnelle à l'intensité des EFRs. De même, il semble que, pour chaque hiver, plus l'EFR se produit tôt dans l'année (Décembre-Janvier), plus la perte d'ozone enregistrée est faible. Ainsi la fréquence des EFRs lors des récents hivers arctiques joue un rôle significatif sur la concentration moyenne d'ozone stratospherique dans l'hémisphère Nord et par conséquent également sur le climat arctique et global.

Une analyse détaillée de la destruction d'ozone lors des hivers arctiques 1996/97 et 2002/03–2010/11 montre que l'hiver 2002/03 a subit un EFR et trois réchauffements mineurs. Pourtant, lors de cet hiver, une grande quantité d'ozone a été détruites à la fin du mois de mars. Environ 1.5 ppmv détruit entre 450 et 500 K, ou 65 DU entre 400 et 550 K qui s'ajoutent aux 0.7 ppmv détruit au mois de décembre (il s'agit de la plus forte perte d'ozone enregistrée au mois de décembre entre les hivers 1988/89 et 2010/11). La plus forte perte d'ozone enregistrée sur un hiver entier lors de cette décennie a été observée en 2010/11 (soit environ 2.5 ppmv entre 400–500 K ou 140 DU entre 350–550 K). L'étude montre également que, pour la première fois depuis que nous observons l'ozone, la quantité d'ozone détruite lors de cet hiver est comparable à celle détruite lors de certains hivers en Antarctique. Nous montrons que cette destruction d'ozone record est due à une activation des chlorines et une denitrification importante et prolongée lors de cet hiver. La perte d'ozone lors des autres hivers est de l'ordre de 0.7 à 1.6 ppmv autour de 475 K ou 40 à 115 DU entre 350 et 550 K (la plus petite destruction d'ozone ayant été mesurée lors de l'hiver 2005/06, particulièrement chaud).

Pour l'Antarctique, une méthode est proposée pour estimer la tendance à long terme de la destruction chimique de l'ozone. Cette méthode est utilisée sur la période 1989–2012 pour estimer, en colonne totale, les tendances d'ozone à partir d'observations au sol et satellitaires. A l'interieur du vortex polaire, nous montrons que la perte moyenne d'ozone se situe entre 33–50% pendant la période 1989–1992. Cette valeur est en accord avec l'augmentation de la concentration d'halogène lors de cette même période. Après cette periode, la perte moyenne d'ozone semble atteindre une valeur de saturation aux alentours de 48%. La destruction d'ozone lors des hivers les plus chauds (e.g. 2002 et 2004) est légèrement inférieure (37–46%) et celle des hivers les plus froids (e.g. 2003 et 2006), légèrement supérieure (52–55%). La perte maximum d'ozone en Antarctique est observée entre le milieu du mois de septembre et le milieu du mois d'octobre, et la plus forte valeur de perte d'ozone est observée entre fin août et début septembre, atteignant en moyenne 0.5%/jr. Des analyses basées à la fois sur des profils d'ozone simulés grâce à un modèle haute résolution et sur des profils observés par instrument satellitaire lors des 7 hivers antarctiques entre 2004 et 2010, montrent également que les plus fortes pertes d'ozone coincident avec les hivers les plus froids de 2005 et 2006. Lors de ces deux hivers, la perte d'ozone a atteint 3.5 ppmv entre 450 et 550 K, ou 180 DU entre 350 et 850 K. Les deux hivers les plus chauds (2004 et 2010) ont connu les plus faibles pertes d'ozone (environ 2.5 ppmv entre 450 et 550 K, ou 160 DU entre 350 et 850 K). En Antarctique, l'altitude du maximum de destruction d'ozone est 500 K, cependant, pendant les hivers les plus froids et les hivers les plus chauds, ce maximum est 25 K plus haut (respectivement plus bas). Ce déplacement du maximum de perte permettant ainsi clairement de distinguer les hivers froids des hivers chauds. Cette étude montre également que la relative faible perte d'ozone ainsi que le trou d'ozone des récents hivers antarctiques (2004–2010) sont due à des phénomènes de réchauffement moindre.

L'étude à la fois des hivers arctiques et antarctiques, montre que la perte d'ozone en Arctique en dessous de 550 K est due aux cycles halogènes (ClO–ClO et BrO–BrO) à hauteur de 85%. L'étude des hivers 2004/05–2010/11 montre que la contribution moyenne du cycle des NO_x à la diminution de la colonne totale Arctique s'élève à 19±7 DU en dessous de 550 K, alors qu'en Antarctique, la perte d'ozone s'étale entre 350–650 K. Dans les deux cas la perte d'ozone en basse stratopshère (en dessous de 550 K) est contrôlée par les halogènes. En Antarctique cependant, la perte d'ozone au dessus de 550 K est quant à elle dominée par le cycle des NO_x qui y contribuent pour 75%. En moyenne entre 2004 et 2010, les données modèles et mesurées montrent que la perte d'ozone au dessus de 550 K est d'environ 50±5DU. En Antarctique, cela implique qu'environ un tiers de la perte d'ozone en colonne totale (50 sur 150–180 DU) est imputable aux cycles des NO_x, alors que c'est environ trois fois plus en Arctique.

Un modèle de regression est développé pour expliquer cette variablité de l'ozone grâce à differents indices climatiques (ondes planétaires, cycle solaire, oscillation quasi-biennale, etc) ainsi que grâce à la chlorine stratosphérique. Ce modèle est appliqué sur les données sol ainsi que sur les données satellitaires afin d'extraire des tendances d'ozone à long terme. Cette étude révèle une reconstitution significative et progressive de la couverture d'ozone en Antarctique. En effet, la tendance montre une augmentation de $-45\,\mathrm{DU}$/décennie entre 1980 et 1999, et environ $+10\,\mathrm{DU}$/décennie entre 2000 et 2010. Ces résultats étant en accord avec les variations des espèces chimiques liées à la destruction d'ozone lors des mêmes periodes et ces tendances étant testées avec des intervalles de confiance à 95%. Les tendances mesurées ces dernières années démontrent le rôle positif du protocole de Montreal. Finalement, cette thèse énumère un nombre important de références pour la poursuite de l'étude de l'évolution de l'ozone polaire ainsi que pour l'étude du changement climatique et ses effets autant locaux que globaux.

"To the Philosopher, the Physician, the Meteorologist and the Chemist, there is perhaps no subject more attractive than that of Ozone".

Cornelius Benjamin Fox (British Chemist)

Ozone and Antozone (1873).

Motivation

Ozone and climate: The climate of the earth is controlled by a number of chemical, radiative and dynamical processes. The chemistry and climate interaction in the bottom 100 km is key in this regard (e.g. SPARC, 2010). The tropospheric convection, pollution, air-sea exchange, boundary layer process, stratospheric ozone, radiative changes, and mesospheric ion chemistry are very important in linking the chemistry with climate (e.g. WMO, 2011). Stratospheric ozone is one of the important constituents in determining the changes in radiative balance of the region and the ozone abundance determines the amount of incident harmful ultra-violet (UV) radiations on the surface (e.g. WMO, 2007). Therefore, monitoring stratospheric ozone layer has a great significance in tracking the climate change.

There are still some uncertainties in quantifying the increase in green-house gases (GHGs) and their modification of the climate (Plummer et al., 2010). For instance, the stratospheric water vapour (H_2O) and its impact on the climate is highly unpredictable. The climate models predict an increase in the tropospheric H_2O in the coming decades, which suggests enhanced stratospheric H_2O. This would trigger higher polar stratospheric clouds (PSCs) and hence, larger ozone loss (SPARC, 2010). Another potential component of stratospheric H_2O is the methane (CH_4). If there are increased levels of CH_4 from permafrost thawing, rice cultivation or live stock farming, these would add substantial volume of H_2O. Since CH_4 is a GHG, enhanced levels of CH_4 is a climate change concern, which has also a direct influence on stratospheric ozone levels. Increase in CH_4 particularly affects ozone in the upper stratosphere and mesosphere, where HO_x produced from H_2O is efficient in destroying ozone (WMO, 2011). A schematic view of this chemistry–climate interaction is presented in Fig. 1.

Changes in the abundances of nitrogen dioxide (N_2O) from natural and anthropogenic sources affect the nitrous oxide (NO_2) concentrations in the stratosphere. Since N_2O is transported from the troposphere, its concentration in the troposphere decides its abundance in the stratosphere, apart from changes in the speed of the Brewer-Dobson (BD) circulation (Cagnazzo et al., 2006; Jonsson et al., 2009). This implies that the tropospheric N_2O regulates the stratospheric NO_2, which has a direct relationship with the ozone loss cycles in the middle and upper stratosphere (e.g. Eyring et al., 2010; Kuttippurath et al., 2010a). So the increase in N_2O is likely to cause additional ozone loss in the middle and upper stratosphere (Eyring et al., 2010). Therefore, reductions in N_2O may result in a relatively rapid recovery of the stratospheric ozone layer.

An important process that can affect the stratospheric ozone levels is the stratosphere–troposphere exchange or the interactions between upper troposphere and lower stratosphere (UTLS) and these processes are graphically outlined in Fig. 2. Ozone transport from the troposphere to stratosphere is significant in this context, which is about 550 megaton $O_3\,yr^{-1}$, about 140% of the net ozone production in the troposphere. Therefore, reduced ozone transport and lower ozone concentrations in the stratosphere will leak higher UV radiation to the lower altitudes and thus, make

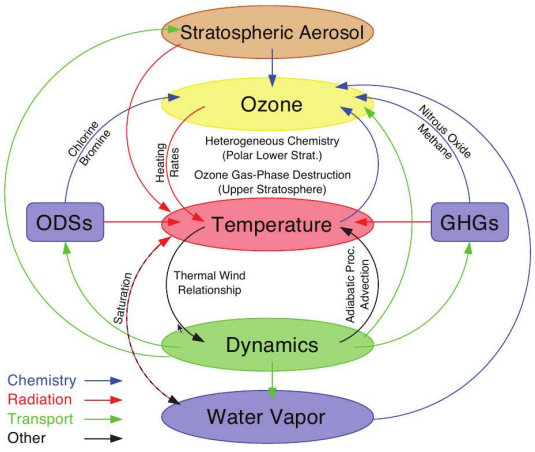

Figure 1: A schematic presentation of chemistry and climate interactions (WMO, 2011).

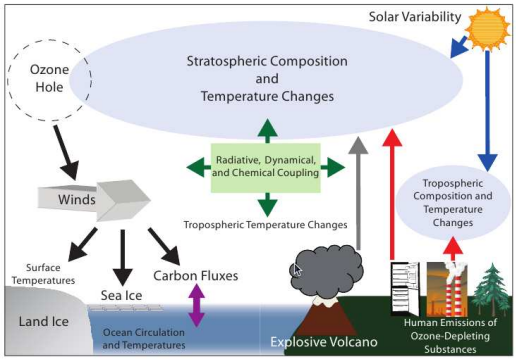

Figure 2: A schematic presentation of stratospheric temperature, ozone, surface processes, stratosphere–troposphere exchange and climate interactions (WMO, 2011).

serious health issues (WMO, 2011).

It is evident that the chemistry and natural variability such as the solar radiation affect the ozone layer (Gray et al., 2010). The BD circulation and its changes also significantly influence the ozone transport and its distribution (Cagnazzo et al., 2006; Butchart et al., 2010). The photochemical production and loss, homogeneous and heterogeneous reactions, and changes in the circulation are important in this context. Our understanding on the tropospheric convection is very limited and hence, its parameterisation in the models is far from complete. Therefore, how the convection evolves with time is another concern and that currently relies on some incomplete statistical speculations in the models. Any alterations in the convection will change the H_2O levels in the UTLS region and will increasingly influence the ozone generation, formation of cirrus clouds and radiation (SPARC, 2010). Also, changes in the convection can induce changes in the lightning and NO_x formation through lightning, and thus the ozone production and its chemistry there.

Another major threat to stratospheric ozone is the stratospheric cooling due to increased carbon dioxide (CO_2) concentrations (Mahfouf et al., 1994; Jonsson et al., 2009; Gillett et al., 2011). Lower temperatures form more PSCs and trigger more ozone loss through heterogeneous chemistry. Therefore, even if the stratospheric halogens are decreasing (Montzka et al., 1999), the lower temperatures might mask the effect of the reduction in halogens for few years and hence, the recovery of the stratospheric ozone can be delayed. Alternatively, the lower temperatures reduce the amount of atomic oxygen, which increases the amount of ozone. It has to be noted that the atomic oxygen drives many ozone loss cycles in the middle and upper stratosphere (Kuttippurath et al., 2010a). Therefore, in the upper stratosphere the increase in CO_2 levels has mitigated ozone loss through temperature dependent chemistry there. Note also that the uncertainties of bromine budget in the stratosphere is associated with the delivery of reactive brominated hydrocarbons to the stratosphere (WMO, 2011). In summary, the stratospheric ozone has a greater role in the climate system through its chemistry-climate feedback, and hence, this challenging science still motivates.

Ozone trends: The first observational evidence of Antarctic ozone loss was found in the early 1980s (Farman et al., 1985; Solomon et al., 1986) and nearly half a decade later in its Arctic counterpart (Hofmann et al., 1989). The ozone loss was also found to be spread to the adjacent mid-latitudes in both hemispheres (e.g. Cariolle et al., 1990), mainly due to the heterogeneous chemistry on volcanic aerosols (Bekki et al., 1993; Solomon, 1999) and transport of vortex air-masses during the displacements or splitting of polar vortex (Roscoe et al., 2006) due to major stratospheric warmings (e.g. Kuttippurath and Nikulin, 2012). The analysis with both observations and multi-model simulations exhibits a clear negative trend in global ozone, with the largest negative trends in the polar regions (Eyring et al., 2010). The loss in the southern polar region started in the early 1980s, intensified in the late 1980s, saturated in the 1990s (Jiang et al., 1996) and stayed at this level thereafter (WMO, 2007). Studies reveal that the northern middle and high latitude ozone trends are of the order of -2 to $-3\%\,\mathrm{decade}^{-1}$ with respect to the 1980 ozone. The trends in the southern mid-latitudes are about $-6\%\,\mathrm{decade}^{-1}$, whereas it is about $-1\%\,\mathrm{decade}^{-1}$ in the tropical region. The decreasing trends in ozone during the period 1980–1996 are attributed to the increase in ozone depleting substances (ODSs) during the period, and the ozone plateau thereafter coincides with the decrease in ODS levels since 1997 in the middle and low latitudes and 2000 in the high

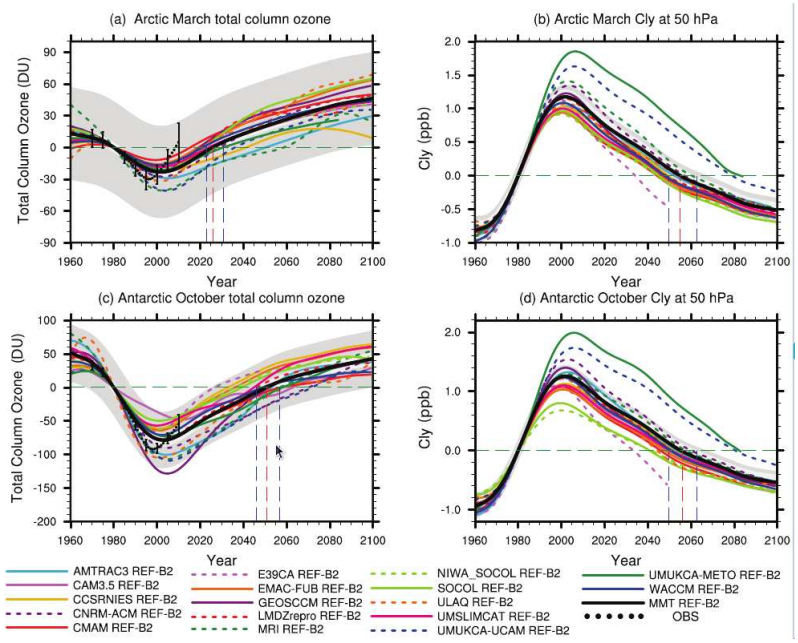

Figure 3: Multi-model simulations and projections of stratospheric ozone and Cl_y from the recent chemistry-climate model validation exercise (SPARC, 2010). Each model result is represented by different line styles and colour codes, the average of the model results is noted by MMT, and the observations are represented by OBS.

latitudes (SPARC, 2010; WMO, 2011; Nair et al., 2013).

Figure 3 shows the observed and predicted ozone trends from various chemistry climate models and observations (Eyring et al., 2010). The model projections suggests the ozone recovery to the 1980 level by 2050–2060 in the Antarctic and by about a decade earlier in the Arctic. The model results differ largely in the ozone recovery predictions, as most of them struggle to get an agreement with the observed Cl_y in the stratosphere. This points out that there is large uncertainty in the ozone recovery date predictions by the models due to the differences in their input (SPARC, 2010). In addition, the chemistry of stratospheric ozone in the models is inter-linked to other parameters, such as temperature, chemistry of related specie, accuracy of meteorological data, tropospheric boundary conditions and radiation schemes. Nevertheless, there is a consensus among the models in simulating the general evolution of ozone in the stratosphere.

Since studies have already suggested that the Cl_y levels are decreasing in the stratosphere, we expect a corresponding change in ozone, i.e. an increasing trend of ozone. However, the decrease in Cl_y levels or ODS components during 2000–2010 is relatively slower than their increase during 1980–1999 (WMO, 2011). Therefore, the ozone recovery trends will be much smaller than the Cl_y decreasing trends and thus it is necessary to analyse the evolution of stratospheric ozone in the coming years to detect its clear recovery signal. This thesis discusses these aspects of stratospheric ozone and assesses the link between ozone and climate change.

This thesis has three sections followed by the introduction in Chapter 1, where the basic physics and chemistry related to this study are presented. Section I deals with chemistry and dynamics of the Arctic stratosphere, Section II assesses the chemistry and physics related to Antarctic ozone and Section III presents the trends in polar ozone. In Section I, Chapter 2 assesses the dynamics of the Arctic winters, as the inter-annual variability of Arctic winters is dominated by stratospheric warmings. A detailed analysis of the Arctic winter 2002/03 is presented in Chapter 3 and the chemistry and dynamics of the Arctic winters 2004/05–2009/10 are discussed in Chapter 4. The chemistry and dynamics of the winters 1996/97 and 2010/11 are presented in Chapter 5. In Section II, a method is introduced to estimate Antarctic total column ozone loss in Chapter 6 and its application to the winters 1989–2010 is given in Chapter 7. The vertical variability of Antarctic ozone loss during the winters over 2004–2010 is given in Chapter 8. In Section III, Chapter 9, polar ozone trends are presented from the perspective of ozone recovery and climate change.

List of Figures

List of Tables

Chapter 1
Introduction

Contents

1.1 Background

The Earth's atmosphere can be divided vertically into different layers based on temperature distribution with altitude, as shown in Fig. 1.1. The bottom layer with a height of about 8–16 km is called the troposphere and its top most region is the tropopause. The height of the troposphere depends on seasons and latitudes. Generally, the tropical tropopause has a maximum height of about 16–18 km and the tropopause height decreases with increasing latitude with about 12–14 km in the middle latitudes and 8–10 km in the high latitudes. The temperature decreases with altitude in the troposphere, with an average rate of 6.5 K km^{-1} and the lowest temperatures of around 195 K are found at the tropical tropopause. There are different definitions for the tropopause based on temperature, ozone, potential temperature, water vapor or combinations of all these. However, it can generally be defined as the lowest level where the temperature gradient is 2 K km^{-1} or smaller such that the region is characterised by high static stability. The rate at which tropospheric source gases enter the stratosphere is decided here (Andrews et al., 1987). Almost all atmospheric water vapor is found in the troposphere and all weather phenomena occur there. This dynamically unstable layer, owing to its negative temperature gradient, triggers rapid mixing with a speed of about 1–2 months.

A region above the tropopause to about 50 km is called stratosphere, the name derived from the Greek word *stratus* that means "layered". The discovery of this region of scientific interest dates back to 1902. Léon Teisserenc de Bort, a French scientist at the observatory of Trappes (near Paris in France) observed from meteorological balloon soundings that there is a 10 km wide isothermal layer above 10 km and called the region as stratosphere (Müller, 2009; Brasseur, 2008). Unlike in the troposphere, temperature increases in the stratosphere and thus the layer is dynamically stable. Due to its stability, the very slow vertical transport time scales of the order of 3–5 years provide large lifetime for the constituents those solely removed in the stratosphere, such as Chloro-Flouro Carbons (CFCs). Other notable features related to the stratosphere are that it is very dry, density is very low and the tropical stratosphere is always warmer than the poles. The top of this atmospheric layer is called stratopause, which is characterised by a temperature maximum of about -3° C (Brasseur and Solomon, 2005). The region above stratopause is seldom discussed in this thesis and hence, will not be described.

The stratosphere or the atmosphere can be further divided into the tropics (30° N–30° S), mid-latitude surf zone with turbulent mixing (30°–60° N/S) and high latitudes (60°–90° N/S). In the lowermost stratosphere, a mixture of tropospheric and stratospheric air is observed, at around 385 K (Holton et al., 1995). The winds are easterly in the summer hemisphere, westerly in the winter hemisphere and they shift their direction at the end of the winter to establish the summer circulation (e.g. Waugh et al., 1999).

1.1.1 Dynamics

In the atmosphere, there are four different forces acting on an air parcel: gravitational, pressure gradient, Coriolis, and frictional. The first two forces can be excreted on a static/moving air

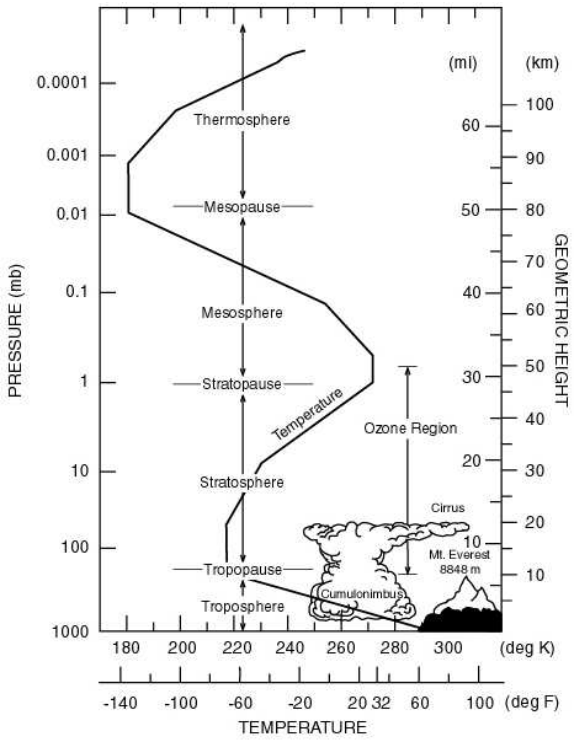

Figure 1.1: The vertical structure of the standard atmosphere. The stratospheric region is also called the ozone region (image courtesy: Oxford University Press).

molecule, but the latter two are excreted only when the parcel is moving. The gravitational force, the force per volume acting on an air parcel, is the gravitational acceleration times the mass of the air parcel. That is,

$$F_{gravity} = \rho g \tag{1.1}$$

where ρ is the density of air and g is the gravitational acceleration (g=9.8 m s^{-2}). To account for the variations of gravity with altitude and latitude, a new scale of geopotential is introduced,

$$F_{geopotential} = -\rho \nabla \Phi \tag{1.2}$$

where Φ is gravitational potential.

Since atmospheric motions are generally related to the pressure gradient forces explained by the hydrostatic equilibrium between pressure gradient force and gravity, the pressure gradient force can be expressed as,

$$\frac{\partial p}{\partial z} = -\rho g; \tag{1.3}$$

where p is pressure and z is altitude.

Pressure is used as a vertical coordinate in the atmospheric science and in numerical models where mass is conserved (see Kasahara, 1974 for a detailed review of various vertical coordinate systems). Similarly, potential temperature (Θ) is considered as another vertical co-ordinate in the scientific analyses and in the models. It is a conserved quantity in the stratosphere for a few days and therefore it is often used in stratospheric transport studies. The Θ is defined as the temperature that an air parcel (at pressure P) would acquire if it adiabatically brought to the surface pressure P_0 (usually 1000 hPa). That is,

$$\Theta = T \left(\frac{P_0}{P} \right)^k \tag{1.4}$$

where T is the temperature in Kelvin, $k = \frac{R}{C_p} = \frac{2}{7}$, R is the universal gas constant and C_p is the specific heat capacity of air at constant pressure. Isentropes are the surfaces of constant potential temperatures.

Any moving body, in a rotational frame, experiences an inertial force perpendicular to both its direction of the movement and axis of rotation, which is called the Coriolis force. However, only the horizontal component is relevant in the atmosphere. The Coriolis force can be defined as a fictitious

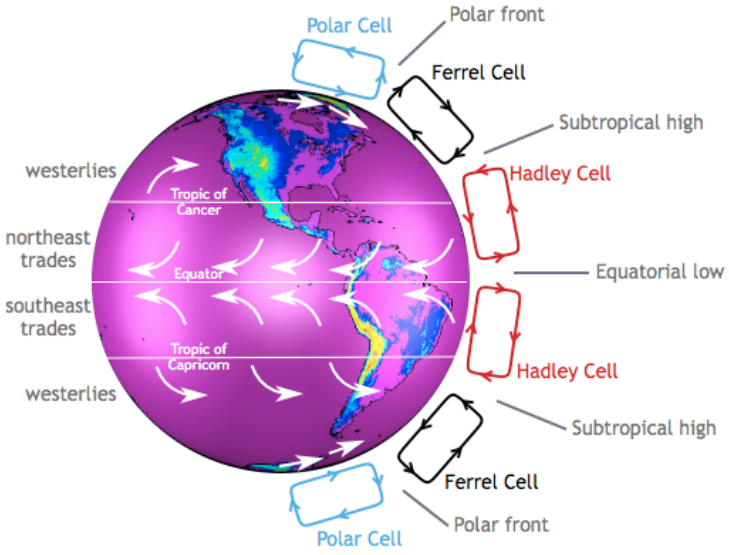

Figure 1.2: The Hadley, Ferrel and Polar cells, and tropospheric circulation patterns (image courtesy: www.cmmap.org)

force excreted on an air parcel when it is moving in a rotating frame. The Coriolis parameter is defined as,

$$f = 2\Omega sin\phi \tag{1.5}$$

where Ω is the angular velocity of the Earth (7.292×10^{-5}rad s^{-1}) and ϕ is latitude. Therefore, the Coriolis force (i.e. fv, where v is velocity) is maximum at the poles and zero at the equator.

The frictional force is the force excreted on an air parcel when it travels opposite to other air parcels with different velocities.

The motions in the atmosphere can also be viewed in two different angles. (i) The atmosphere is a collection of air parcels in which all particles move with individual velocities with respect to time, termed as the Lagrangian motion of the particles. (ii) On the other hand, the movement of air can be pictured in a fixed coordinate and hence, the air parcels can be defined as a function of their location and time. This is called the Eulerian motion of the air particles, where the viewer is fixed. The Lagrangian motion is adopted in most chemical transport models (CTMs) and the Eulerian approach is generally employed in the large scale atmospheric and ocean general circulation models (GCMs).

1.1.1.1 Stratospheric transport

In 1735, George Hadley suggested that the differences in the intensity of sunlight between the polar regions (down to 100 Wm^{-2}) and middle latitudes (up to 300 Wm^{-2}) drive the temperature and energy contrasts and those create a thermal circulation consisting of a large convection cell over each hemisphere. In the 1920s a three cell model, the Hadley, Ferrel and Polar cells, as illustrated in Fig. 1.2, was introduced. However, the discovery of barocilinic instability in the 20th century drastically improved our understanding on general circulation of the atmosphere and thus the stratosphere.

Initially, it was thought that the temperature of the polar stratosphere was controlled by the changes in the solar declination from the winter to summer solstice and by the distribution of radiatively active trace gases CO_2, H_2O and O_3. Nevertheless, the polar lower stratosphere in winter was always warmer than that would be expected from a pure radiative transfer calculation. Later, Alan Brewer discovered that there is a circulation consisting of large scale ascent in the tropics (i.e. tropical upwelling) and a wave driven poleward and downward transport in the mid-latitudes (Brewer, 1949). Therefore, the additional warming in the polar winters is due to the non-linear wave breaking and polar descent. In sum, the westerly zonal flow driven by wave breaking results into a poleward drift and this meridional drift leads to upwelling in the low latitudes and downwelling in the high latitudes by the law of mass continuity (Randel et al., 1993). In addition, there is an exchange between stratosphere and troposphere in the lowermost stratosphere of around 385 K, with high descent in the polar region (Holton et al., 1995).

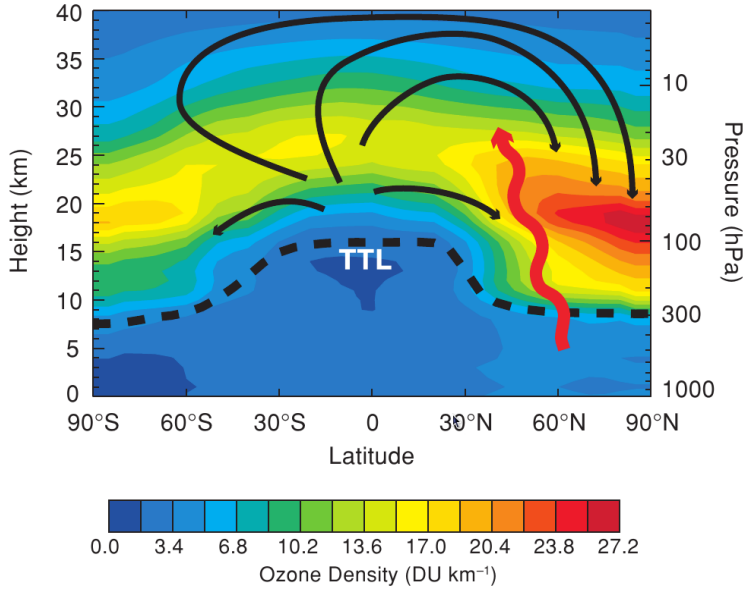

Figure 1.3: The ozone climatology from Fortuin and Kelder (1998). The black arrows show the Brewer-Dobson circulation and the red arrow shows the planetary wave propagation to the stratosphere. TTL is the tropical tropopause layer (IPCC, 2007).

The findings of Brewer (1949) using water vapour measurements were subsequently corroborated with ozone measurements by Dobson (1956). The summer circulation is very weak compared to winter hemispheric circulation as the easterly mean flow in the stratosphere inhibits the propagation of waves into the stratosphere in summer. These transport of air masses is called Brewer-Dobson circulation, to honor the findings of the pioneering scientists Brewer and Dobson, who discovered the mechanism. The theoretical explanation is that the primary driver of the BD circulation is the momentum deposited by the wave breaking at the tropopause, for which the planetary scale waves originate in the troposphere (Haynes et al., 1991; Randel et al., 1993; Plumb, 1996; Haynes, 2005). Most stratospheric trace gases connected to ozone chemistry are originating from the troposphere and enter the stratosphere through the tropical tropopause by the tropical upwelling (Holton et al., 1995). A schematic diagram showing the stratospheric circulation (black contours) superimposed on an ozone climatology (colour contours) is given in Fig. 1.3.

1.1.1.2 Polar vortex

In polar winters, the incidence of sunlight in the stratosphere diminishes considerably and the emission of thermal radiation leads to radiative cooling of the upper stratosphere. Therefore, the polar air mass descends down which results into a low pressure region in the upper stratosphere. However, the stratospheric air is warmer and pressure is higher in the sunlit parts of the middle and low latitudes. This makes a meridional pressure gradient between the high and middle latitudes and hence, the air mass flows from the high to low pressure region. This air mass transport deflects to the right in the NH and to the left in the SH due to the action of Coriolis force. This particular movement of air masses produces a circumpolar motion of westerly (blowing from west to east) winds and is termed as the polar (night) jet or polar vortex (e.g. Waugh et al., 1999). The location of polar jet is normally found close to the latitude separating day and night during the polar winter and thus acts as a boundary region of the spinning vortex. The strong westerlies effectively separate mid-latitude air from those within the polar vortex, and thus act as the dynamical barrier between these two latitude regions. A three-dimensional view of the polar vortex in the Arctic winter 2003/04 is shown in Fig. 1.4. As depicted in the figure, the structure, breadth and strength of the polar vortex are different at different altitude levels and in different winters, as they depend on the meteorological situation of each winter (e.g. Thiéblemont et al., 2011; Kuttippurath et al., 2010a; Harvey et al., 2002).

The temperature inside the vortex is much lower than that of the middle latitudes (or outside the vortex) (e.g. Waugh et al., 1999; Claud et al., 1996). Therefore, chemistry and dynamics of the vortex are different from its adjacent mid-latitude regions. The vortex area is usually divided into the vortex core and vortex edge region, where the edge region is the outer ring of the vortex

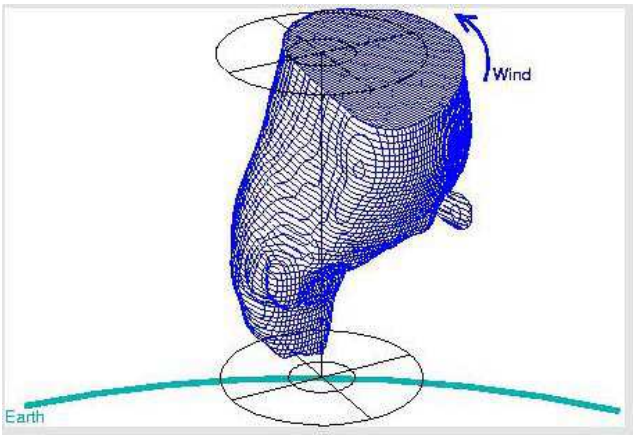

Figure 1.4: A three dimensional view of the Arctic vortex in the 2003/04 winter (image courtesy: JPL/NASA).

core with a breadth of about 15° as analysed from the measurements (Roscoe et al., 2012). Since the land-ocean contrast is very large in the NH compared to that in the SH, the planetary wave activity is higher in the Arctic and hence, the polar vortex is less stable there (Manney et al., 2005; Kuttippurath and Nikulin, 2012). On the other hand, Antarctica is isolated from the continents and hence, the wave activity is suppressed there. Therefore, the Antarctic vortex temperature is about 10 K lower than that in the Arctic. For the same reason, the polar vortex in the SH is more stable, stronger and persists longer than (normally from May to November in the SH and from December to March in the NH) that observed in the Arctic.

In this study we use the Nash et al. (1996) criterion to separate vortex air from the mid-latitude air. By applying this method, we classify the vortex core and edge region or the mid-latitude air using the Potential Vorticity (PV) values, which is calculated as:

$$P = (\xi_p + f)g\frac{\delta\theta}{\delta p} \tag{1.6}$$

where ξ_p is angular velocity. As long as the adiabatic processes are concerned, PV is a conserved quantity and can be used as a tracer for air motions (1 pvu [PV unit] is $10^{-6}\,\mathrm{Km^2\,kg^{-1}\,s^{-1}}$). Therefore, it can be used to differentiate various kinds of air masses in the stratosphere, e.g. tropical and polar vortex air masses from the mid-latitude air masses (e.g. Hoskins et al., 1985).

Another coordinate derived from the PV values is the equivalent latitude (EqL) and is a Lagrangian coordinate (Butchart and Remsberg, 1986; Müller et al., 2008; Kuttippurath et al., 2009). Equivalent latitude is calculated as:

$$\phi = sin^{-1}\left(\frac{A}{2\pi a^2} - 1\right) \tag{1.7}$$

where A is the area enclosed to the South/North ($A = 0$ corresponds to the equivalent South/North Pole) and a is the radius of the Earth. This method produces a mapping that is as continuous as the data permit in contrast to the binning that makes a coarse-gridded mapping. Each isoline in an EqL map behaves like an atmospheric tracer and encircles the same area as the latitude line of equivalent value, hence the "equivalent latitude". The PV and EqL values are positive in the NH and negative in the SH, and their maximum values are found at the centre of the vortex.

1.1.1.3 Sudden stratospheric warmings

Sudden stratospheric warmings (SSWs) are winter stratospheric phenomena, where an abrupt increase in stratospheric temperature (at least 25°) is observed in a short period of time (in a week or less). The first observational evidence for this stratospheric event was reported by Scherhag (1952) and its first theoretical explanation was given by Matsuno (1971). There are three different types of warmings: major, minor and Canadian. By the definition of WMO (1978), a major mid-winter SSW happens when the zonal mean westerlies at 60°N turn easterly and the temperature gradient between 60°N and 90°N reverses at 10 hPa or below during the November–February period (McInturff, 1978). If the warming does not follow the wind reversal then it is a minor warming. The

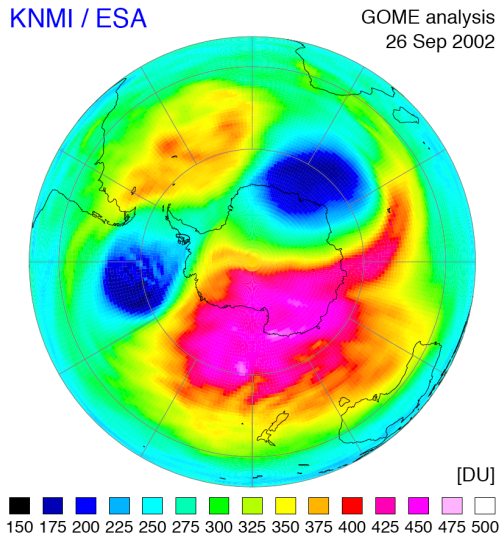

Figure 1.5: The total ozone distribution on 26 September 2002 from the Global Ozone Monitoring Experiment. The image also shows the only vortex split event observed in the Antarctic (image courtesy: KNMI/ESA).

Canadian warmings are the early winter minor warmings which take place during mid-November through early December (Labitzke and Naujokat, 2000). Therefore, there is no Antarctic counterpart for the Canadian warmings. Although minor warmings are normally observed (e.g. 2004, 2010 and 2012), the occurrence of major SSWs in the Antarctic stratosphere are extremely rare, as in the case of the warming in 2002 (e.g. Roscoe et al., 2006; Grooß et al., 2005b).

As characterised by various dynamical features, the warmings are differentiated with respect to vortex split or vortex displacement types (Charlton and Polvani, 2007; Kuttippurath and Nikulin, 2012). Most major SSWs are vortex displacement types during which the vortex shifts its location off the pole. In contrast, if a warming splits the vortex into two separate vortices of considerable size at 10 hPa on the central date – the date on which the westerlies change to easterlies at 10 hPa/60° – then the event is termed as a vortex split major SSW. Note that the vortex split events occur only in major SSW episodes. Figure 1.5 shows the only vortex split major SSW observed in the Antarctic, as analysed from the Global Ozone Monitoring Experiment (GOME) total column ozone data. Similarly the warmings are also classified as wave-1 or wave-2 events depending on which zonal wavenumber was prominent for the poleward eddy heat transport leading to those warmings (Kuttippurath and Nikulin, 2012; Bancalá et al., 2012; Cohen and Jones, 2011). For instance, the strongest warming in the Arctic winter stratosphere was observed in January 2009 (winter 2008/09) and this was a vortex split event, triggered by an intense wave-2 forcing (i.e. wave-2 warming). On the other hand, the major SSW during January 2006 (winter 2005/06) was forced by a strong wave 1 amplification (i.e. wave-1 warming) and was a vortex displacement event (e.g. Harada et al., 2010; Kuttippurath and Nikulin, 2012; Manney et al., 2008). Additional information on SSWs can be found from Holton (1980) and Schoeberl (1978).

1.1.1.4 Quasi-biennial oscillation

The quasi-biennial oscillation (QBO) is a kind of oscillation found in the stratosphere that discovered in 1950s (Reed et al., 1961). It is a quasi-periodic oscillation of the equatorial zonal winds between easterlies and westerlies in the tropical stratosphere at 15°N–15°S with an average frequency of 20–36 months, as shown in Fig.1.6. This shifting wind regimes develop at the top of the lower stratosphere and descend at a rate of about 1 km per month from 10 to 100 hPa until they are dissipated at the tropical tropopause (Andrews et al., 1987). Downward motion of the easterlies is generally more discontinuous than that of the westerlies. The amplitude of the easterlies is about twice as strong as the westerlies. At the top of the vertical QBO domain, easterlies dominate, while the westerlies appear normally at the bottom layers (Baldwin et al., 2001a). The theory of QBO is not completely understood and hence, its representation in the models is not fully developed yet (e.g. SPARC, 2010). A general concept about the QBO is that the equatorial Kelvin waves produce the westerly and Rossby-waves induce the easterly momentum for the oscillation (e.g. Lott et al.,

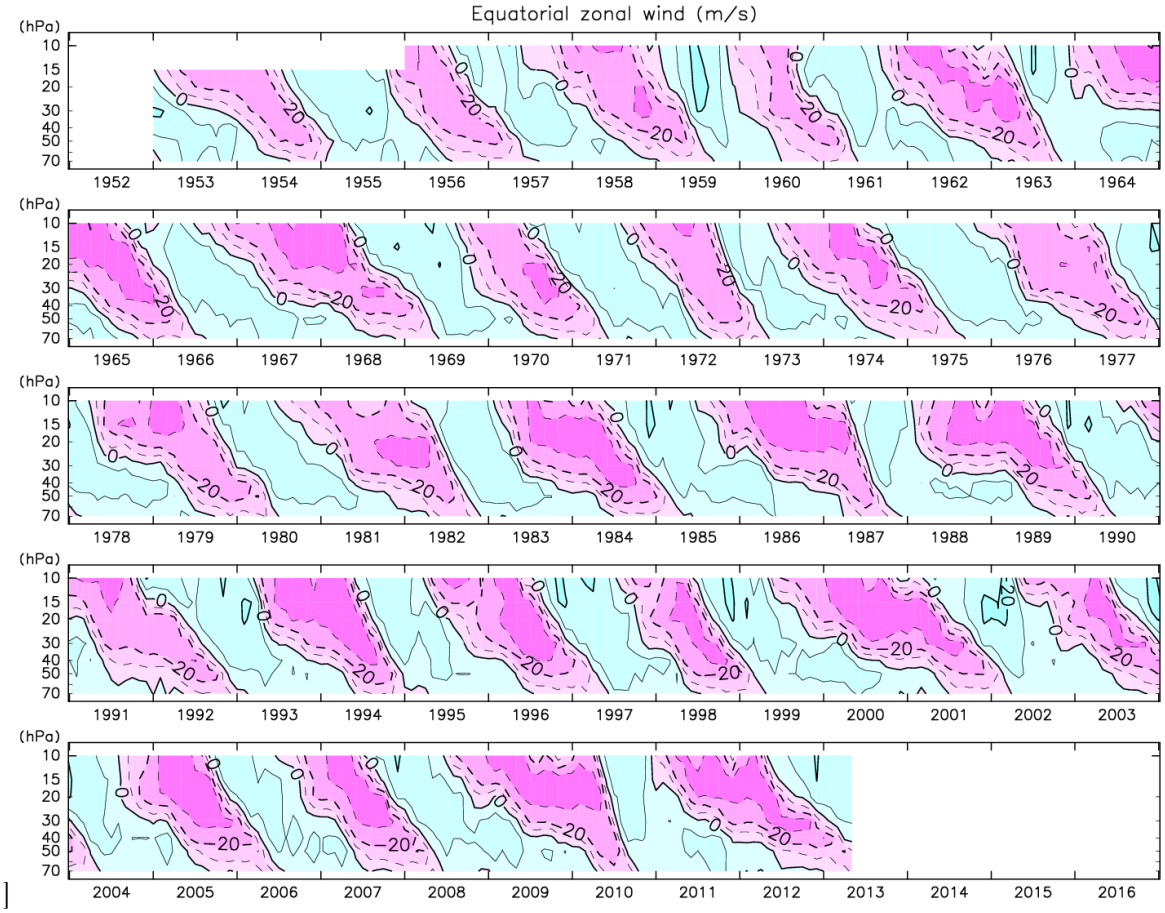

Figure 1.6: The time-height (year against pressure) section of equatorial zonal wind in the lower stratosphere. The shaded regions represent easterlies and the other regions denote westerlies. The plot is produced using the meteorological analyses of Freie Universität Berlin (image courtesy: http://www-mete.kugi.kyoto-u.ac.jp/mete/J/benkyo/QBO/).

2009). Nevertheless, QBO has far reaching consequences in the stratosphere as it also affects the hurricane frequencies (e.g. lower for easterly QBO), El Niño-Southern Oscillation (ENSO), monsoon and major SSWs.

1.1.2 Chemistry

The atmosphere is filled with different gases with about 78% of nitrogen (N_2) and 20% of oxygen (O_2). Most of these constituents are stable in concentrations. $\zeta\varepsilon\iota\nu$, this Greek word spells "ozone" and that means "to smell". Ozone is "very rare" and is present only about 0.0003% of the total constituents in the atmosphere. It was first produced in the laboratory by Christian F. Schönbein in 1839 and was discovered in the air by André Houzeau in 1858 (Müller, 2009; Brasseur, 2008). The ozone concentrations vary rapidly in space and time (WMO, 2011).

The trace gases are quantified in their number density or volume mixing ratios (VMRs), depending on the characteristics of the measuring instruments. The number density is the number of molecules per volume and VMR is the ratio of the number of molecules to the total number of molecules in the atmosphere. The number density can be calculated from the VMR, i.e.

$$\mu = \frac{\eta k_B T}{p} \tag{1.8}$$

where μ is VMR (in parts per million by volume – ppmv or parts per billion by volume – ppbv), η is number density of the molecule, k_B is Boltzmann's constant ($1.38\times10^{-23}\mathrm{JK}^{-1}$). Since the VMR is expressed in relative concentration, it is conserved in all atmospheric motions and is used in most

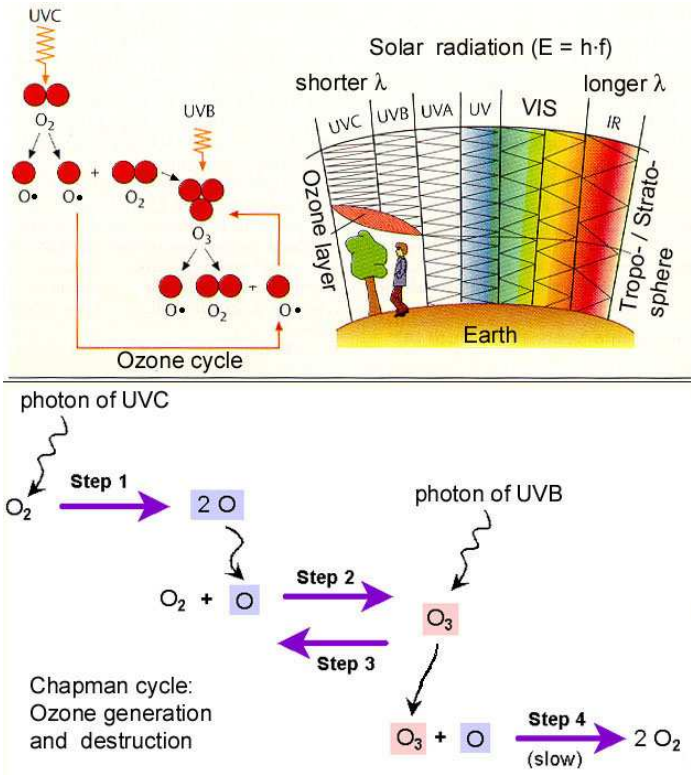

Figure 1.7: A graphical representation of the production and destruction of ozone through the Chapman cycle (image courtesy: http://biophysics.sbg.ac.at).

analyses and transport studies. The vertical integral of the number density is called the column of the trace gas. The ozone column is expressed in Dobson unit (DU) (after Gourdon Miller Bourne Dobson, who built the first instrument to measure total column ozone from the ground and is called the Dobson spectrometer, 1 DU = 2.69×10^{16} molecules cm^{-2}). That is, 1 DU corresponds to a layer of ozone that would be 10 μm thick under standard pressure and temperature conditions, and the ozone column (i.e. DU) is particularly important to assess the UV radiation input on the earth surface.

1.1.2.1 Production and photolysis of ozone

Production of ozone occurs through the photolysis of O_2 by UV radiation of wavelength <242 nm that can penetrate to about 30 km altitude, followed by the recombination of an O atom with an O_2 molecule.

$$O_2 + h\nu \rightarrow O + O \tag{1.9}$$

$$O + O_2 \xrightarrow{M} O_3 \tag{1.10}$$

where M is nitrogen or oxygen molecule needed for the conservation of momentum, hν is the photon energy where h is the Planck's constant 6.626×10^{-34} J s and ν is the frequency. This is a fast reaction of the order of a fraction of a second in the stratosphere and releases energy of about 24 kCal mol^{-1}. Therefore, this reaction is responsible for the positive temperature gradient of the stratosphere.

The production of ozone is most prominent in the tropical stratosphere as the solar radiation is sufficiently intense to dissociate the molecular oxygen continuously there. However, the ozone column is found to be lowest in the tropics and highest in the high latitudes. Also, the total column at the middle and high latitudes does not correlate to the amount of sunlight available for the production of ozone in the region. This is due to the stratospheric transport, by which the trace gases are transported from the tropics to the high latitudes. Note that the BD circulation is comparatively stronger in winter/spring months than in summer/autumn. Therefore, the maximum ozone at the high latitudes is observed in spring and the minimum in autumn. These transport processes are more important in the lower stratosphere (below 25 km) as the photochemical lifetime

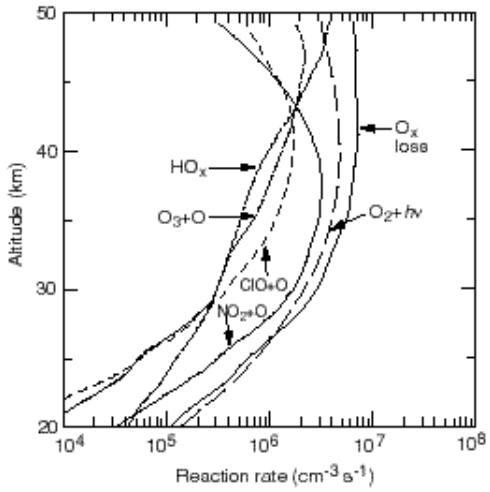

Figure 1.8: Daily mean of the Ox production and loss rates computed with a gas-phase chemistry model constrained with simultaneous measurements of O_3, H_2O, CH_4, NO_y and Cl_y from the space shuttle (McElroy and Salawitch, 1989).

of ozone is longer there. Above 40 km, the photochemistry determines the abundances of ozone because of its shorter lifetime there. The ozone levels in the 30–40 km region are controlled by both transport and photochemistry. Note that, ozone is destroyed at higher wavelengths through:

$$O_3 + h\nu \rightarrow O_2 + O(^3P) \qquad \lambda < 1100 \ nm \tag{1.11}$$

$$O_3 + h\nu \rightarrow O_2 + O(^1D) \qquad \lambda < 310 \ nm \tag{1.12}$$

The oxygen atom in the excited state $O(^1D)$ can relax to its ground state $O(^3P)$ by collision with other atmospheric constituents (e.g. O_2 or N_2).

1.1.2.2 The Chapman mechanism

In 1930, Chapman proposed a theory regarding the photochemical balance between the production and destruction of ozone (Chapman, 1930) in which ozone is destroyed by:

$$O + O_3 \rightarrow O_2 + O_2 \tag{1.13}$$

$$O + O \xrightarrow{M} O_2 \tag{1.14}$$

The rate limiting step of this cycle is the reaction O+O_3. A schematic presentation of this chemical cycle is shown in Fig. 1.7. However, these slow reactions could not completely explain the real balance between the photochemical production and photolytic destruction of ozone, as the actual concentration of ozone in the atmosphere was lower than (underestimated by a factor of two) that was predicted by the Chapman cycle. Therefore, other ozone loss cycles initiated by the catalysts were put forward later and are described below. These ozone loss cycles are faster than the Chapman cycle and require atomic oxygen and hence, they are more effective above 30 km, where O atoms are sufficient. The catalytic cycles that do not require O are responsible for the ozone loss in the lower stratosphere.

1.1.2.3 Hydrogen cycle

In 1950, it was found that ozone can be removed from the atmosphere through a catalytic cycle involving OH produced by the oxidation of hydrogenated compounds like, H_2O, methane (CH_4) and H_2 transported from the troposphere (Bates and Nicolet, 1950). These OH radicals react rapidly

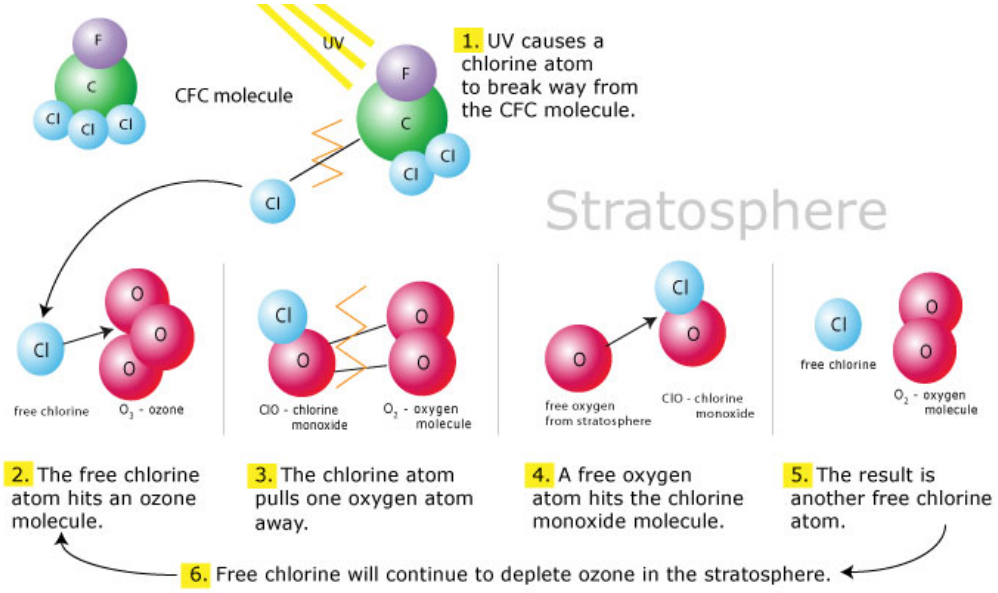

Figure 1.9: A schematic of the ozone loss caused by anthropogenic compounds such as CFCs (image courtesy: www.learner.org).

with O_3 producing hydroperoxyl radical (HO_2). The HO_x cycle is:

$$H_2O + O(^1D) \rightarrow 2OH \quad (1.15)$$
$$O + OH \rightarrow O_2 + H \quad (1.16)$$
$$H + O_2 \xrightarrow{M} HO_2 \quad (1.17)$$
$$O + HO_2 \rightarrow O_2 + OH \quad (1.18)$$
$$O + O \xrightarrow{M} O_2 \quad (1.19)$$
$$OH + O_3 \rightarrow HO_2 + O_2 \quad (1.20)$$
$$HO_2 + O \rightarrow OH + O_2 \quad (1.21)$$
$$O_3 + O \rightarrow 2O_2 \quad (1.22)$$

The rate limiting step of this reaction is $HO_2 + O$ and thus the efficiency of this cycle is controlled by the availability of O atoms. Therefore, the removal of ozone through the HO_x cycle is relevant above 30 km while ozone is destroyed through its direct reaction with HO_2 without involving O atom below 30 km and hence, the importance of the hydroxyl radical is two fold. In both cases, HO_2 is produced, which in turn destroys ozone. For instance, below 30 km,

$$OH + O_3 \rightarrow HO_2 + O_2 \quad (1.23)$$
$$HO_2 + O_3 \rightarrow OH + 2O_2 \quad (1.24)$$
$$2O_3 \rightarrow 3O_2 \quad (1.25)$$

The reaction between HO_2 and O_3 is the rate limiting step of this cycle. In addition to these cycles, hydrogen radicals also involve in other minor ozone destroying cycles. Therefore, the interaction of HO_x family with other atmospheric constituents has also to be considered for an accurate evaluation of the impact of HO_x on ozone (e.g. $HO_2 + NO \rightarrow OH + NO_2$ in the lower stratosphere).

1.1.2.4 Nitrogen cycle

In 1970, Crutzen (1970, 1971) discovered that the destruction of ozone is also possible by the oxides of nitrogen. The major source of NO_x is the oxidation of N_2O with $O(^1D)$. N_2O is emitted at the surface by the biological processes and also by the emission from the combustion of engines of

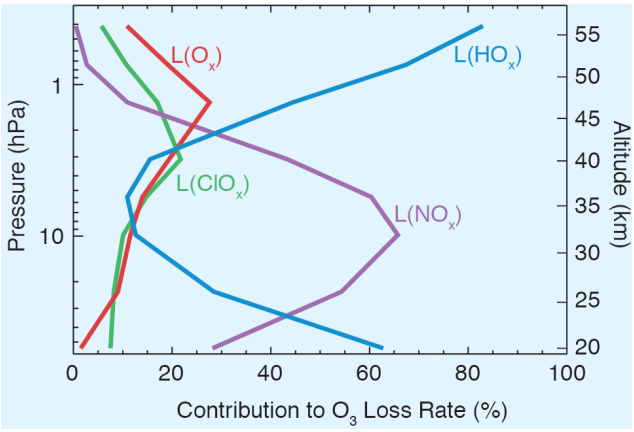

Figure 1.10: Model simulations of the photochemical removal rates of ozone by various chemical cycles (Müller, 2009; IPCC, 2007).

aircrafts. Since N_2O has a lifetime of ∼130 years, it is well-mixed in the troposphere, and enters stratosphere and produces NO. That is:

$$NO + O_3 \rightarrow NO_2 + O_2 \quad (1.26)$$
$$O + NO_2 \rightarrow NO + O_2 \quad (1.27)$$
$$O + O_3 \rightarrow 2O_2 \quad (1.28)$$

This is a fast reaction and the rate limiting step is the reaction $O + NO_2$ as the resulting NO quickly converts to NO_2 by reacting with O_3. The NO_x cycle is predominant in the middle and upper stratosphere as its potency is determined by the abundance of O atoms. The NO_x cycle will continue to remove ozone until the NO_x is sequestrated in the long-lived reservoirs such as HNO_3, $ClONO_2$ or $BrONO_2$. Similar to hydrogen radicals, nitrogen oxides interact with other chemical compounds. For instance, the HNO_3 molecule is formed by a three body process involving OH, NO_2 and a molecule M. The formation of HNO_3 provides a sink for NO and OH catalysts. However, HNO_3 is photolysed to release NO_x and it in turn participates in the ozone loss catalytic cycle. Since the photolysis of HNO_3 is very slow, it acts as a reservoir for NO_x and thus the latter is effectively removed from the catalytic cycle through the formation of HNO_3. The daily mean of the O_x production and loss rates computed with a gas-phase chemistry model constrained with measurements is given in Fig.1.8. It shows that ozone loss in the middle and upper stratosphere (above 25 km) is controlled by the NO_x cycle.

1.1.2.5 Chlorine and Bromine cycles

The other important ozone loss catalytic cycles are the ones involving halogen species of chlorine–Cl (Molina and Rowland, 1974) and bromine–Br (McElroy et al., 1986). The natural source of stratospheric Cl is the destruction of chlorinated organic compounds, i.e. the long-lived chlorinated compounds like methyl chloride (CH_3Cl), emitted in the troposphere are transported to the stratosphere, where they are photolysed to produce Cl atoms. Similarly, the industrial source of stratospheric Cl is the photolysis of the industrial by-product, CFCs, in the stratosphere. The CFCs have long lifetime (∼50 years) and are inactive in the troposphere. The Cl atoms produced in these pathways are treated as inorganic Cl. These Cl atoms react immediately with O_3 reforming ClO. The efficiency of this cycle is determined by the reaction rate of ClO and O, and hence, the availability of O atoms. Therefore, the rate limiting step is the reaction O+ClO. At about 40 km, the ClO radical and atomic oxygen are abundant and hence, the Cl cycle is dominant there. A schematic of the ozone loss process involving anthropogenic compounds such as CFCs is presented in Fig.1.9.

Similarly, stratospheric Br is produced by the photolysis or oxidation of brominated compounds such as methyl bromide (CH_3Br) and halons. Due to the long lifetime of brominated compounds emitted in the troposphere through natural or industrial processes and their inactivity, they are transported to the stratosphere, where they undergo dissociation and produce Br atoms. The ozone

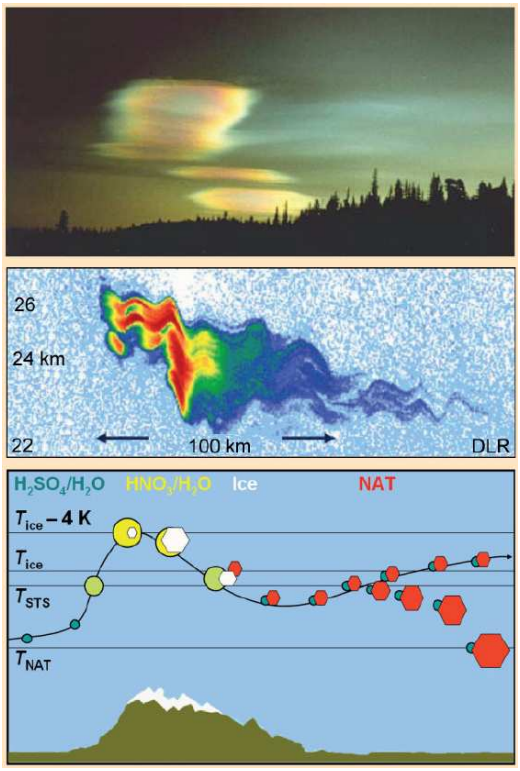

Figure 1.11: An image of a PSC event over Kiruna/Sweden, PSC measurement by an air-borne lidar and analysis of possible PSC composition (Dameris et al., 2007).

loss through these cycles are shown below:

$$Cl + O_3 \rightarrow ClO + O_2 \quad (1.29)$$
$$O + ClO \rightarrow Cl + O_2 \quad (1.30)$$
$$O + O_3 \rightarrow 2O_2 \quad (1.31)$$

$$Br + O_3 \rightarrow BrO + O_2 \quad (1.32)$$
$$O + BrO \rightarrow Br + O_2 \quad (1.33)$$
$$O + O_3 \rightarrow 2O_2 \quad (1.34)$$

Most of the inorganic Cl is kept in the long-lived reservoirs such as HCl or $ClONO_2$. However, compared to the amount of Cl in ClO, about half of the stratospheric Br is present in the form of more reactive BrO radicals than in the long-lived reservoirs (HBr or $BrONO_2$). Therefore, the ozone depleting potential of Br is higher than that of Cl on a per atom basis, about 45–130 times, depending on season and latitude (WMO, 2011). Additionally, the catalytic cycles involving reaction of reactive Br and BrO with ClO, NO_2 and HO_2 do not require O atom to destroy ozone. So these reactions can take place in the lower stratosphere where only a few O atoms are available. Nevertheless, note that the abundance of anthropogenic bromine is about 300 times lower than that of chlorine and the abundance of stratospheric inorganic chlorine is nearly 170 times that of bromine.

The ozone loss rates by these catalytic cycles are different at different altitude levels in the stratosphere, as illustrated in Fig. 1.10. From the figure, it is evident that the NO_x cycle is dominant in the removal of ozone in the middle and upper stratosphere. However, ozone loss in the polar spring remained a mystery for the above-mentioned chemical cycles and were later explained with several heterogeneous reactions (Solomon et al., 1986; Solomon, 1999), and are described below.

1.1.2.6 PSC, Heterogeneous chemistry and Polar ozone loss

The nacreous clouds found in winter polar stratosphere were named as PSCs by McCormick et al. (1982). These clouds were usually found at 15–26 km altitude region when the temperatures are

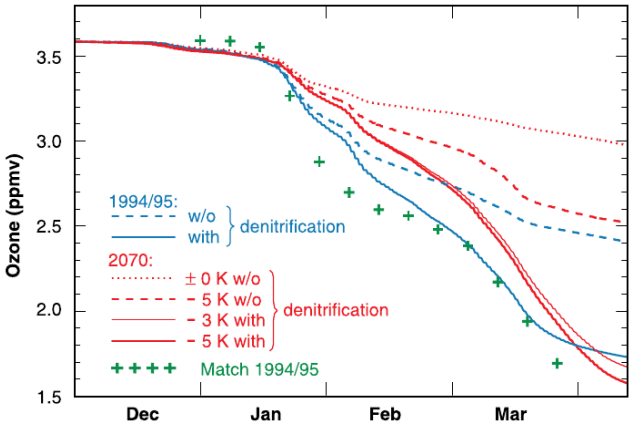

Figure 1.12: Box model simulations of ozone loss due to denitrification in the Arctic winter 1994/95. The ozone loss derived from ozonesonde measurements is also shown (Rex et al., 2004). Projections of ozone loss due to various scenarios for the winter 2070 is also depicted (Waibel et al., 1999).

below 195 K during the periods from June to September in Antarctica and January–mid-March in the Arctic (Pitts et al., 2009, 2007; Peter, 1997).

Although the normal ozone loss cycles are common to all latitudes, the situation during the polar night provides a different scenario for additional ozone loss. During that period, when the polar temperatures are below 195 K in the 15–26 km altitude region the background aerosols take up HNO_3 and H_2O, leading to the formation of supercooled ternary $HNO_3/H_2SO_4/H_2O$ droplets, referred to as PSCs. A picture showing the glowing PSCs in the Arctic stratosphere is shown in Fig. 1.11. These clouds are classified as Type I (1 μm) and Type II (5 μm). Type I has been further subdivided into Type Ia and Type Ib. Type Ia PSCs are made up of crystals of Nitric Acid Trihydrate [NAT - (HNO_3. $3H_2O$)] and Type Ib consists of supercooled ternary solutions (STS) of $HNO_3/H_2SO_4/H_2O$. Type II PSCs are frozen water ice non-spherical crystalline particles as shown by the analyses in the figure.

During the polar winters, the following heterogeneous reactions take place on PSC surfaces, which facilitate the Cl and Br reservoirs (HCl, $ClONO_2$ and $BrONO_2$) to convert into their active forms and hence, produce rapid ozone loss (Solomon et al., 1986):

$$ClONO_2 + HCl \rightarrow HNO_3 + Cl_2 \quad (1.35)$$
$$BrONO_2 + HCl \rightarrow HNO_3 + BrCl \quad (1.36)$$
$$ClONO_2 + H_2O \rightarrow HNO_3 + HOCl \quad (1.37)$$
$$BrONO_2 + H_2O \rightarrow HNO_3 + HOBr \quad (1.38)$$
$$HOCl + HCl \rightarrow H_2O + Cl_2 \quad (1.39)$$
$$HOBr + HCl \rightarrow H_2O + BrCl \quad (1.40)$$

When sunlight returns in the polar lower stratosphere in spring, these active Cl_2 and HOCl are photolysed to form Cl atoms, which swiftly convert to ClO. At high concentrations, ClO undergoes a self reaction forming ClO dimers. Catalytic reactions involving these ClO dimers (the ClO–ClO cycle or Molina–Molina cycle) are mainly responsible for the significant reduction of ozone in the polar lower stratosphere (Molina and Molina, 1987). This cycle is effective only under cold conditions. When temperatures increase, ClO dimer becomes thermally unstable and converts to 2ClO. That is;

$$ClO + ClO \xrightarrow{M} Cl_2O_2 \quad (1.41)$$
$$Cl_2O_2 + h\nu \rightarrow Cl + ClO_2 \quad (1.42)$$
$$ClO_2 \xrightarrow{M} Cl + O_2 \quad (1.43)$$
$$2[Cl + O_3 \rightarrow ClO + O_2] \quad (1.44)$$
$$net: 2O_3 \rightarrow 3O_2 \quad (1.45)$$

Likewise, Br radicals participate in very similar kinds of catalytic reactions resulting in large ozone loss (McElroy et al., 1986). Most of the inorganic Br is present in the form of chemically

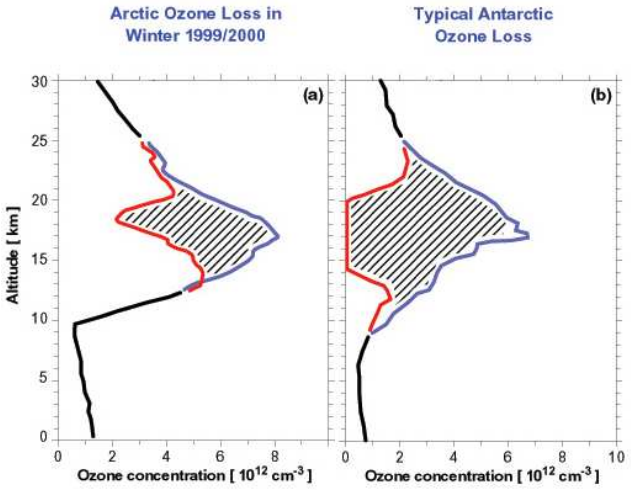

Figure 1.13: The ozone loss in the Arctic winter 1999/00 compared to the typical Antarctic scenario. The measurements are taken from balloon sondes (SPARC, 2002).

active BrO throughout the stratosphere. The BrO undergoes two types of ozone destroying cycles as given below:

$$BrO + ClO \rightarrow BrCl + O_2 \quad (1.46)$$
$$BrCl + h\nu \rightarrow Cl + Br \quad (1.47)$$

$$BrO + ClO \rightarrow Br + ClO_2 \quad (1.48)$$
$$ClO_2 \xrightarrow{M} Cl + O_2 \quad (1.49)$$

$$Cl + O_3 \rightarrow ClO + O_2 \quad (1.50)$$
$$Br + O_3 \rightarrow BrO + O_2 \quad (1.51)$$
$$net : 2O_3 \rightarrow 3O_2 \quad (1.52)$$

The catalytic cycles (both the Cl and Br cycles) occur in the lower stratosphere and hence, account for most of the lower stratospheric polar ozone loss in spring. These cycles are more effective in the Antarctic region than in the Arctic because of several reasons. For instance, the vortex is stronger and cold conditions sufficient for the formation of PSCs are more prevalent in the Antarctic and hence, Cl and Br atoms are more abundant there, whereas the Arctic stratosphere is relatively warm and thus restricts the formation of PSCs and related heterogeneous ozone loss.

1.1.2.7 Denitrification

Most of the heterogeneous reactions those take place on the surfaces of PSCs produce a large fraction of HNO_3 (e.g. Eqns.1.35). In addition, the hydrolysis of N_2O_5 on the sulfate aerosols and PSC surfaces acts as a major source of HNO_3. That is:

$$N_2O_5 + H_2O \rightarrow 2HNO_3 \quad (1.53)$$
$$N_2O_5 + HCl \rightarrow ClNO_2 + HNO_3 \quad (1.54)$$

If the lower temperatures (<195 K) in the polar regions persist for several months, then HNO_3 condensed to NAT particles could grow to large sizes of $> 10\mu\,m$. This process results into gravitational settling of HNO_3 and hence, removes it from the regions of ozone layer. This irreversible removal of HNO_3 is called denitrification. The photolysis of HNO_3 in polar spring releases NO_2, which deactivates Cl:

$$HNO_3 + h\nu \rightarrow OH + NO_2 \quad (1.55)$$
$$ClO + NO_2 \xrightarrow{M} ClNO_3 \quad (1.56)$$

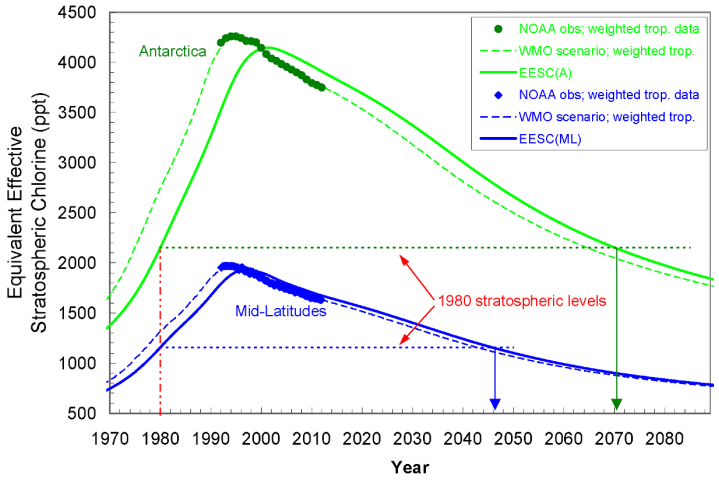

Figure 1.14: The temporal evolution of Equivalent Effective Stratospheric Chlorine (EESC) in the polar and mid-latitude regions (image courtesy: NOAA Earth System Research Laboratory).

Hence, the removal of HNO_3 slows down the deactivation of Cl. Therefore, a denitrified environment prolongs the activation of Cl and Br and thereby enhances the destruction of ozone (Fahey et al., 1990). The ozone loss due to denitrification is more common in the Antarctic stratosphere because of the colder and more stable vortex conditions there (e.g. Santee et al., 1995). Several Arctic winters such as 1999/00 (e.g. Kleinböhl et al., 2002; Santee et al., 2000) and 2004/05 (e.g. Kleinböhl et al., 2005b) were also experienced severe denitrification and hence, large loss in ozone. For instance, Fig. 1.12 illustrates the effect of ozone loss in the Arctic winter 1994/95 as analysed from a suite of box model simulations (Waibel et al., 1999).

1.1.2.8 The ozone hole

Owing to the special physical and chemical scenarios mentioned earlier, the Antarctic ozone experiences significant destruction during winter and spring seasons (Farman et al., 1985). Due to the increased halogen loading in the stratosphere this ozone loss has increased dramatically during 1985–1990 and saturated thereafter (Jiang et al., 1996). Therefore, since early 1990s ozone soundings in the Antarctic showed a complete or near-complete removal of ozone (i.e. saturation of ozone loss) in the 15–21 km altitude region (Solomon et al., 2005) and this feature is observed since then in all winters, as shown in Fig.1.13. The total column ozone observations from ground-based and satellite instruments also showed equivalent characteristics of ozone loss saturation, where the measured ozone column values were often below 220 DU. This ozone value is conventionally taken as the limit of the thickness of the ozone layer to be called an "ozone hole" (Stolarski, 1988), implying that the thinning of the polar stratospheric ozone layer has eventually lead to a "hole" (i.e. a depression) in that layer. Note that ozone column values of less than 220 DU were not observed in the historic measurements in Antarctica prior to 1979. In addition, as observed from direct measurements, an ozone column of less than 220 DU is a result of the ozone destruction from the halogens (alone) in Antarctica. Although ozone loss in the Arctic polar stratosphere is also a regular feature in winter and spring for many decades, an Arctic ozone hole has not been observed yet. Nevertheless, the ozone loss during the winter 2010/11 was record-breaking, which showed signs of an Arctic ozone hole (Kuttippurath et al., 2012a; Manney et al., 2011; Sinnhuber et al., 2011).

1.1.2.9 Ozone depleting substances

Ozone depleting substances (ODSs) are those compounds which destroy ozone (Montzka et al., 1999). They are commonly used in air-conditioners, refrigerators, electronic equipment, fire extinguishers, in dry cleaning, and as agricultural fumigants. The primary ODSs are Chlorofluorocarbons (CFCs), Halon, Carbon tetrachloride (CCl_4), Methyl chloroform (CH_3CCl_3), Hydrobromofluorocarbons (HBFCs), Methyl bromide (CH_3Br) and Bromochloromethane (CH_2BrCl), and are generally designated by the term halocarbons. The ODSs are very effective in ozone destruction processes mainly for two reasons: (i) they are not destroyed in the lower atmosphere and hence, they have

long lifetime in the atmosphere/stratosphere (20–120 yr depending on the specie), and are not washed-out back to the surface of the Earth as for most gases. (ii) Secondly, they release bromine and/or chlorine by UV photolysis in the stratosphere and thus, participate actively in the ozone loss processes.

Equivalent effective stratospheric chlorine (EESC) is an estimate of the total effective amount of chlorine and bromine in the stratosphere (Newman et al., 2007). It is computed from emissions of chlorofluorocarbon and related halogenated compounds into the troposphere, weighted by their efficiency in ozone depletion (ozone depletion potential, ODP), and by making assumptions on transport times into the stratosphere (Waugh and Hall, 2002). This parameter (i.e. EESC) is applied to quantify man-made ozone depletion and its changes with time. It is computed as;

$$EESC = Cl_y + \alpha Br_y \tag{1.57}$$

where Cl_y and Br_y are total inorganic Cl and Br, respectively, and α is the time constant (i.e. age of air).

This formulation provides quantitative estimates of EESC that can be directly connected to inorganic chlorine and bromine throughout the stratosphere. Figure 1.14 shows the model simulations of past and future projections together with the measurements of EESC in the Antarctic and mid-latitude regions. It indicates that the EESC peaked by 1997 in the mid-latitudes and by 2000–2001 in the polar regions. There is a gradual decrease in the concentrations of EESC thereafter due to the control and phasing out of ODSs, by the Montreal Protocol and its amendments and adjustments (Velders et al., 2007). Therefore, ozone recovery is anticipated from these reductions in the atmospheric burden of ODSs and will be discussed in detail in Chapter 9.

1.2 Summary

A concise description of the stratospheric chemistry and dynamics is presented here. A special emphasis is given to the physical and chemical processes that govern changes in the distribution of stratospheric ozone. Any additional information on these topics can be found from standard text books (e.g. Andrews et al., 1987; Brasseur and Solomon, 2005; Mohankumar, 2008; Müller, 2011) or from the review articles by Solomon (1999); Plumb (2002); Haynes (2005); Holton et al. (1995); Schneider (2006); McConnell and Jin (2008) and Shepherd (2008), as a detailed description of all atmospheric processes in the stratosphere is beyond the scope of this thesis [e.g. changes in ozone abundances due to the effects of the North Atlantic Oscillation (NAO) (Wanner et al., 2001), ENSO (Enfield, 1989; Turner, 2004) and solar activity (Gray et al., 2010)]. Although chemistry and climate modelling is a key subject of this thesis, detailed descriptions of the modelling is not presented here. Fundamental of atmospheric modelling can be found in Jacobson (2005) and additional information on climate and chemical transport modelling can be found in the references given in the respective chapters, and in Donner and Large (2008) and SPARC (2010). A thorough description of the mathematical modelling of atmospheric chemistry, by G. P. Brasseur and D. J. Jacob, is also presented on `http://acmg.seas.harvard.edu/education/brasseur_jacob/index.html`. Therefore, the primary concepts about force acting on air parcels, transport of air masses, stratospheric circulation features, the formation and evolution of polar vortices, the Chapman cycles and polar heterogeneous chemistry of ozone loss are presented.

SECTION I

ARCTIC STRATOSPHERE

Chapter 2

Dynamics of Arctic winters *

Contents

One of the interesting phenomena in climate science is the large inter-annual variability of Arctic stratospheric winters, characterised by extremely warm and very cold winters. This year-to-year variability is dominated by SSWs during which the polar temperature rises and the zonal flow weakens or reverses (Scherhag, 1952). There are different definitions for a SSW to be called major or minor. According to the World Meteorological Organisation (WMO) a SSW can be said to be *major* if at 10 hPa or lower altitudes the latitudinal mean temperature increases abruptly poleward from 60° latitude with an associated circulation reversal in a short period of time. If the reversal of temperature gradient does not follow the zonal-mean wind reversal, then it is a *minor* SSW (e.g. WMO, 1978, item 9.4, 35–36; Andrews et al., 1987; Labitzke and Naujokat, 2000). In some cases the increase in temperature near the pole can be up to 40–60 K in a week at 10 hPa (Limpasuvan et al., 2004; Andrews et al., 1987). The followed zonal wind reversal displaces or splits the polar vortex towards mid-latitudes (e.g. Kuttippurath et al., 2010a; Charlton and Polvani, 2007). Since the WMO definition considers the major SSWs (hereafter major warmings–MWs) from November to February, studies have slightly modified this criterion to account for the warmings from October through May (e.g. Charlton and Polvani, 2007; Bancalá et al., 2012). Also, there is an ambiguity regarding the temperature gradient criterion of the WMO definition (e.g. the difference between Limpasuvan et al., 2004 and Krüger et al., 2005). Apart from these, classifications of MWs based on the northern annular mode (Baldwin and Dunkerton, 2001b) and external atmospheric forcings (Blume et al., 2012) are also being proposed.

Although studies use different definitions for MWs, there is a general agreement on the poleward temperature increase from 60° N. Some studies are critical about the timing of wind reversal that it must last for 5 days (e.g. Limpasuvan et al., 2004), but no strict time condition is followed by some others (e.g. Labitzke, 1981; McInturff, 1978). Regarding the wind reversal, the latter two use a circulation reversal poleward of 60° N, whereas Charlton and Polvani (2007) consider that the winds must reverse at 60° N. Nevertheless, Limpasuvan et al. (2004) applied the same condition of temperature increase and wind reversal with a slight difference in latitude, 65° N instead of 60° N.

The meridional transport in the winter stratosphere is largely controlled by large amplitude planetary waves. The most important of them are quasi-stationary Rossby waves those propagate upward from the troposphere and are quite strong and variable in winter (Andrews et al., 1987).

*This chapter is partly based on: Kuttippurath, J. and G. Nikulin: A comparative study of the major sudden stratospheric warmings in the Arctic winters 2003/2004–2009/2010, Atmos. Chem. Phys., 12, doi:10.5194/acp-12-8115-2012, 8115–8129, 2012.

Other planetary waves are the traveling normal modes and they do not transport much momentum, but can interact with other waves or with zonal mean flow. The interaction of planetary waves and the zonal mean flow is known to be the major driver of winter stratospheric dynamics. The key process in a MW is the growth and interaction of upward propagating transient planetary waves (Matsuno, 1971). The breaking and dissipation of westward propagating planetary waves relative to the zonal flow in the stratosphere decelerate or even reverse the prevailing eastward flow of the polar stratosphere and induce heat by adiabatic processes, which often result in a MW. Alternatively, there can be an upward circulation in the mesosphere that makes adiabatic cooling in that region (e.g. Siskind et al., 2010).

The dynamical activity in recent winters reveals that the frequency of MWs in the Arctic is increasing (e.g. Charlton-Perez et al., 2008). Studies showed that there were 5 MWs in 6 winters over 1967/68–1972/73 (e.g. Bancalá et al., 2012; Cohen and Jones, 2011; Labitzke and Naujokat, 2000; Andrews et al., 1987). Similarly, there were 5 MWs in 6 winters from 1983/84 to 1988/89 (e.g. Butler and Polvani, 2011; Harada et al., 2010; Manney et al., 2008). On average, during 1957/58–1990/91, MWs occurred only once every two Arctic winters (e.g Bancalá et al., 2012; Cohen and Jones, 2011; Andrews et al., 1987). Conversely, no MW occurred in 9 consecutive winters from 1989/90 to 1997/98, except a minor warming in early February 1990 (Manney et al., 2005). However, there were 7 MWs in 5 out of the 6 winters from 1998/99 to 2003/04 (e.g. Kuttippurath et al., 2011; Kleinböhl et al., 2005a; Manney et al., 2005; Liu et al., 2009; Naujokat et al., 2002). The winter 1999/00 was unusually cold but each other winter was prone to MWs. Furthermore, two MWs were observed in 1998/99 and 2001/02 (e.g. Charlton and Polvani, 2007). This warming sequence continued and there were 5 MWs in 5 winters again in 2005/06–2009/10 (Ayarzagüena et al., 2011; Harada et al., 2010; Orsolini et al., 2010; Coy et al., 2009; Labitzke and Kunze, 2009; Manney et al., 2009, 2008; Hirooka et al., 2007). Many of the MWs in recent years have been atypically early (December/early January) compared to those found before 1990s, which were observed mostly in February (e.g. Bancalá et al., 2012; Charlton and Polvani, 2007). Climate model simulations also predict similar MW events and their evenly distributed occurrences throughout the winter (December–March) for the 2010–2100 period (Mitchell et al., 2012). However, note that the unusual frequency of MWs in recent years has not translated into early final warmings in most cases (e.g. Manney et al., 2005). These results are consistent with the findings of Waugh et al. (1999), who found no significant relation between the vortex characteristics and its long-term persistence.

It is a very difficult task to understand the variability of Arctic winters and to predict the influence of the stratosphere on the troposphere. The large inter-annual variability makes the detection of trends in the Arctic extremely difficult (Manney et al., 2005). Studies on the evolution of stratospheric warmings can provide further insights on these issues. While the winters before 2003/04 are relatively well studied (e.g. Manney et al., 2005), detailed comparisons are not available on the winters thereafter. Therefore, in this study, (i) we characterise the MWs of the Arctic winters 2003/04–2009/10. In addition to this objective, we also (ii) examine the frequency of MWs in recent Arctic winters and (iii) assess the impact of MWs on the polar ozone.

2.1 Data and methods

In order to discuss the dynamical evolution, we have derived heat, momentum, EP and wave EP fluxes, and EP flux divergence in each winter using the European Centre for Medium-Range Weather Forecasts (ECMWF) operational data. These data have 2.5° horizontal resolution on 14 pressure levels between 1000 and 1 hPa. The impact of the MWs on the threshold of PSCs is analysed with area of PSC (A_{PSC}), which was calculated using 4.5 ppmv of H_2O and a HNO_3 climatology (Kleinböhl et al., 2002), as computed in Rex et al. (2004) and Kuttippurath et al. (2010a).

There are several definitions for MWs, therefore, to classify the warming events. Therefore, we use McInturff (1978) by which a warming is said to be a MW, if at 10 hPa or below the latitudinal mean temperature increases rapidly poleward from 60° N and is followed by the zonal wind reversal in a short period of time. A warming is called *minor* for a significant temperature increase at any stratospheric level in any area of the wintertime hemisphere, provided the criterion for a MW is not met.

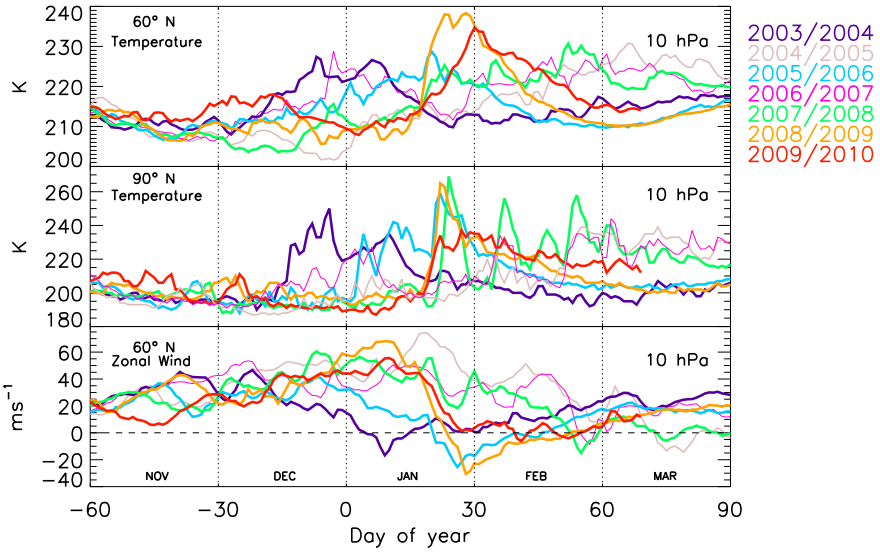

Figure 2.1: Temporal evolution of the zonally averaged temperature and zonal wind in the ECMWF operational analysis for the Arctic winters 2003/04–2009/10. The dashed horizontal line represents 0 ms^{-1} and the dotted vertical lines separate each month.

We only briefly explain the physical and dynamical terms used here. For a detailed discussion on these, the readers are requested to refer to Andrews et al. (1987). In order to estimate the aforementioned fluxes, we have calculated the zonal-means and their fluctuations from the zonal-means (eddies). Throughout this section we denote the zonal-mean with an *over-bar* and eddies with a *prime* symbol. The intensity of the dynamical processes in a MW can be diagnosed by the fluxes and we derive the heat and momentum fluxes as:

$$F_{\mathrm{heat}} = \overline{T'v'} \quad ; \quad F_{\mathrm{momentum}} = \overline{v'u'}$$

where v', T' and u' are the eddies of meridional wind, temperature and zonal wind, respectively. To describe the motions, which can be of synoptic to planetary scale, the amplitude of planetary waves is derived using Fourier analysis of geopotential data. Since the observed waves in the stratosphere are usually of zonal wave numbers 1–3, we calculate the amplitudes of waves 1 and 2. The quasi-geostrophic version of the EP flux ($\vec{F}$) are:

$$F_z = \rho_0 f a \cos\phi \quad \frac{R}{HN^2} \quad \overline{T'v'} \quad ; \quad F_\phi = -\rho_0 a \cos\phi \quad \overline{v'u'}$$

where ρ_0 is air density, a is radius of the Earth, f is Coriolis parameter, H is scale height, R is the gas constant and N is the buoyancy frequency. These EP flux equations show that the meridional component (F_ϕ) is proportional to the momentum flux and the vertical component (F_z) is proportional to the heat flux.

2.2 Evolution of the winters: 2003/04–2009/10

We first examine the time evolution of zonally averaged temperature and zonal wind at 60° N and 10 hPa to identify the warmings. The 90° N/10 hPa temperatures are also checked to probe the intensity of the warmings. The temporal evolution of the vertical distribution of temperature and zonal winds, propagation and amplitude of the planetary waves, and impact of MWs on the structure and stability of polar vortex during the winters are discussed in the succeeding sections.

2.2.1 Temperature and zonal winds

2.2.1.1 MWs during the winters

Figure 2.1 shows the time series of zonally averaged temperature at 60° and 90° N, and zonal wind at 60° N for 10 hPa in the Arctic winters 2003/04–2009/10. The warming in 2009/10 was severe,

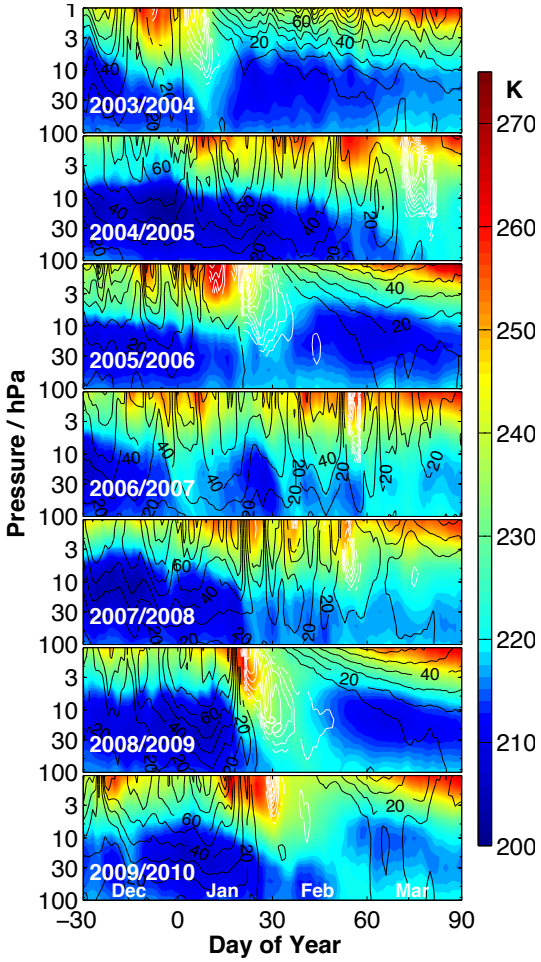

Figure 2.2: Temporal evolution of the vertical distribution of zonal-mean temperatures (color contours) in the ECMWF operational analysis for the Arctic winters 2003/04–2009/10. The overlaid white contours illustrate the position and propagation of the zonal-mean easterlies and the black overlaid contours are the zonal-mean westerlies.

where a rapid increase of temperature from 207 K in early January to 235 K in late January was observed at 60° N. However, the largest increment of temperature at 60° N was experienced in 2008/09, during which temperatures of about ∼207 K were found in November–December and they rose to 239 K by late January. In winters 2003/04, 2005/06 and 2006/07 there was an increase of about 25 K (from 205 K to 230 K) from late November to late December, mid-January, and late December, respectively, and thus, a prolonged warming (from day of year −8 to 45) is evident in 2005/06 at 60° N. Note that a similar duration of warming is also found in 2003/04 as it spans from early December to late January (day of year −26 to 24), as also observed by Manney et al. (2008, 2005) and Orsolini et al. (2010). There were two short warming episodes in 2006/07; in late December and early February at the same latitude region. In 2007/08, the temperature in early December was ∼202 K and it slowly increased to 232 K by late February at 60° N, with three short warming events in late December, late January, and late February.

The temperature at 90° N exhibits a similar time evolution in all winters, but with significantly higher values. The striking feature found at 90° N is the rise in temperature in late January 2007/08, which is equal to that of the warmest winter 2008/09. Unlike in other winters, there were three minor warmings in 2007/08; in late January, early February and mid-February, and these peaks are more pronounced at 90° N; as the easterly jet was stronger towards the high latitudes and the polar vortex was shifted off the pole during these periods in 2007/08. Further characteristics of the temperature distributions in each winter will be discussed in Sect. 2.2.1.2.

In all winters the maximum temperature is followed by a reversal of the zonal wind with a couple of days lag at 60° N. In 2009/10, the MW criterion was accomplished on 9 February and the winds reversed at least twice before the final warming. The wind reversal in 2009/10 was comparatively short and weak, with easterlies of the order of 1–5 ms^{-1}, and was identical to that in 2003/04, 2006/07 and 2007/08. The MWs in the latter three winters were observed on 5 January, 24 February, and 22 February, respectively. These winters show short (<10 days) and weak (5–15 ms^{-1}) easterlies

at this latitude/altitude level. On the other hand, in 2005/06 and 2008/09 the MW criterion was met by 21 January and 24 January, respectively, and the associated easterlies prevailed for about 30 days with a maximum speed of about 30–35 ms^{-1}. In 2004/05, the temperature was relatively lower (e.g. 2003/04, 2005/06 and 2006/07) in November–January at both latitudes and there was no MW, but the final warming was in mid-March. Although the westerlies appeared again by the end of March, their speed was less than 5 ms^{-1} and hence, we consider the warming by 14 March 2005 as the final warming (e.g. Bancalá et al., 2012).

2.2.1.2 Vertical development of the MWs

Figure 2.2 displays the seasonal march of the vertical distribution of zonal-mean temperature (color contours) and zonal winds (westerlies in black and easterlies in white overlaid contours) for the Arctic winters 2003/04–2009/10. The winter 2009/10 exhibits high temperatures in the upper stratosphere in early January, which slowly extended down to 10 hPa by mid-January. The westerlies turned to easterlies by late January and they moved down to 10 hPa for a period of about 10 days.

When compared to the warming in 2009/10, the rise in temperatures was observed in mid-December in 2003/04, early January in 2005/06, and mid-January in 2008/09 in the upper stratosphere. Subsequently, the easterlies were also appeared by mid-December, early January, and mid-January, respectively, in each winter. The easterlies were comparatively stronger and extended down to 75 hPa in 2008/09 and to 30 hPa in 2005/06, and thus the MWs are stronger in these two winters. In 2009/10, although the temperatures above 10 hPa were higher than those of other winters, the wind reversal was weaker and restricted to the upper stratosphere. In contrast, a late MW with weak easterlies that seldom propagated down to 20 hPa was observed in 2007/08. A similar progression in the vertical and temporal distribution of temperature and zonal wind is also found in 2006/07. Nevertheless, below 10 hPa, although the temperatures were slightly lower in 2007/08 than in 2006/07, the presence of easterlies was limited to four days only in 2006/07. On the other hand, 2004/05 was the coldest among the studied winters, in which the temperature from early December to early March was continuously lower than 220 K over 100–10 hPa. These results are consistent with those of Orsolini et al. (2010), who present a similar analysis using satellite observations for these winters. In 2003/04, relatively lower temperatures in the upper stratosphere and the temperatures similar to those found before the MW in the middle stratosphere were observed in late January and early February, as also mentioned by Manney et al. (2005). Note that some studies recommend the presence of at least 5 days of easterlies for a warming to be called *major* (e.g. Limpasuvan et al., 2004). Therefore, we have excluded 2006/07 and the cold winter 2004/05 (without MW) in the following discussion (Sects. 2.2.2, 2.2.3 and 2.3) on MW winters.

2.2.2 Fluxes and waves

Since wave interaction is a key phenomenon in MWs, it is necessary to look at the nature of waves present during the MW periods to elucidate the events. The wave activity analysis is also necessary to interpret the temporal and vertical development of polar vortex. In general, the shape, strength, and persistence of polar vortices will be different in each winter and they very much depend on the dynamical activity in the winters. Therefore, we now discuss the evolution of planetary waves in this section and the impact of wave activity on the polar vortices during the winters in the next section. In Fig. 2.3 the temporal evolution of wave amplitudes, heat flux, momentum flux, and EP flux divergence for the warm winters of 2003/04–2009/10 at 60° N/10 hPa is depicted.

In 2009/10, large heat flux of about 300 $m\,K\,s^{-1}$ and the largest momentum flux (500 $m^2\,s^{-2}$) among the winters are estimated during the MW period. Enhanced wave 1 amplitude of about 110 $m^2\,s^{-2}$ and wave 1 EP flux of 1.5×10^5 $kg\,s^{-2}$ are also calculated for the period. Note that the large EP flux convergence suggests the westward zonal force exerted by eddies on the atmosphere, i.e. negative (positive) EP flux divergence implies suppressed westerlies or the reversal of the winds (enhanced westerlies). Another interesting feature to note is the minor warming initiated by a strong wave 2 event with significant heat flux ($\sim$200 $m\,K\,s^{-1}$), and momentum flux (250–400 $m^2\,s^{-2}$) in early to mid-December.

In agreement with the higher temperatures and longer duration of easterlies, large heat flux (up to 750 $m\,K\,s^{-1}$), momentum flux (up to 425 $m^2\,s^{-2}$) and the largest EP flux convergence (up to

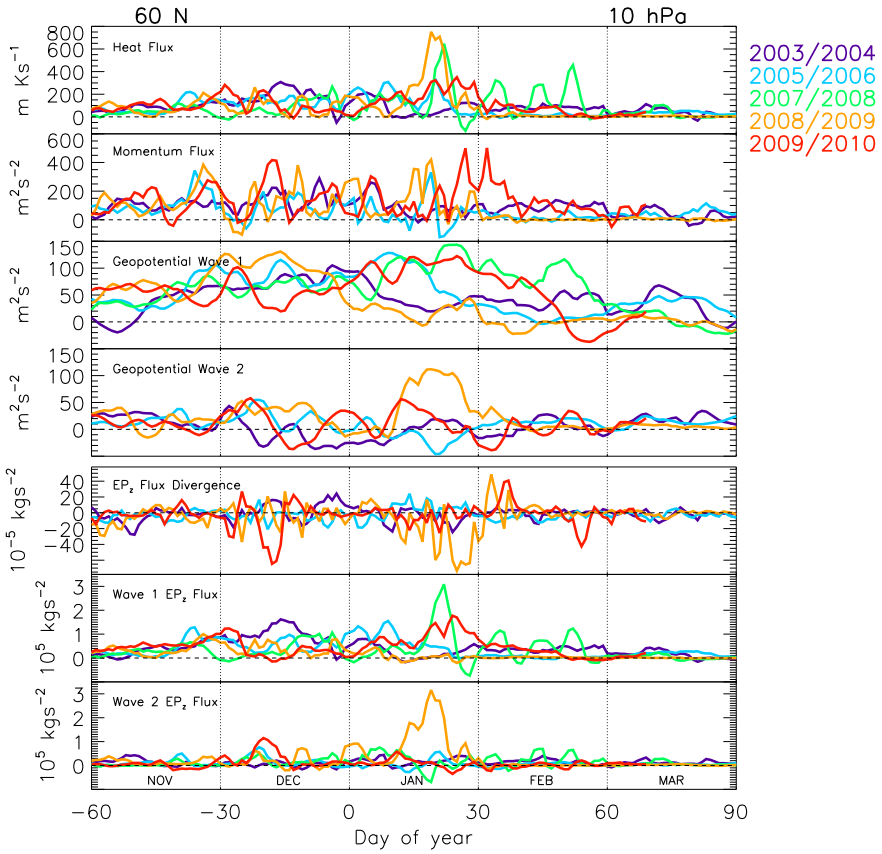

Figure 2.3: Temporal evolution of various zonally averaged derived quantities for selected Arctic winters at 10 hPa and 60° N. The quantity zero is marked with dashed horizontal lines. Since the warming was not severe in 2007/08, some entities are not shown for this winter for clarity reasons. The dotted vertical lines represent the month boundaries.

$-65\times10^{-5}\,\mathrm{kg\,s^{-2}}$) are estimated during the MW in 2008/09. The amplitude of wave 2 and its EP flux in this period are also the largest among the winters, with a maximum of about $110\,\mathrm{m^2\,s^{-2}}$ and $3\times10^5\,\mathrm{kg\,s^{-2}}$, respectively. It is noteworthy that the difference between the maximum heat flux at the time of MW in 2008/09 and 2009/10 is $\sim400\,\mathrm{m\,K\,s^{-1}}$. Furthermore, the wave 2 amplitude is twice that of other winters, indicating the intensity of the MW in 2008/09. Note also that the EP flux convergence during the minor warming in mid-December 2009/10 have matching values to those found during the strongest MW in January 2008/09, suggesting profound wave activity in both winters. The wave amplitudes derived for 2008/09 is in very good agreement with those estimated by Labitzke and Kunze (2009) and Manney et al. (2009).

Another prominent feature to note is the minor warming due to a strong wave 1 amplification during late January in 2007/08. Large heat flux ($\sim600\,\mathrm{m\,K\,s^{-1}}$), and the largest wave 1 amplitude ($\sim145\,\mathrm{m^2\,s^{-2}}$) and its EP flux among the winters ($\sim3\times10^5\,\mathrm{kg\,s^{-2}}$) are calculated for this period. The other winters also show significant heat flux, momentum flux, and wave 1 amplitude during their MW periods, but in relatively smaller magnitudes.

It is interesting to note the large momentum flux and both types of waves in the form of large pulses prior to the MWs in all winters. For instance: the winters 2008/09 and 2009/10 exhibit enormous momentum fluxes of about 200–$400\,\mathrm{m^2\,s^{-2}}$ associated with a number of bursts from November through January. These intermittent pulses normally build momentum for the forthcoming MWs (e.g. Coy et al., 2009; Polvani and Waugh, 2004; this will be discussed in detail in Sect. 2.3). The magnitude of momentum flux estimated during the MW periods in 2009/10 and 2008/09 is about $200\,\mathrm{m^2\,s^{-2}}$ and $100\,\mathrm{m^2\,s^{-2}}$ larger than that of other winters, reiterating the strength of MWs in these winters.

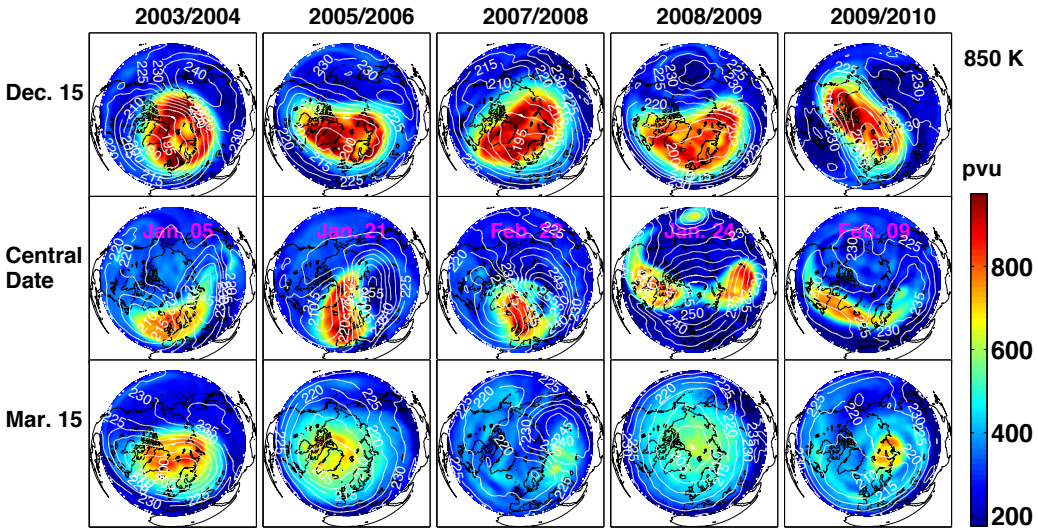

Figure 2.4: Maps of potential vorticity at 850 K (∼ 10 hPa/30 km) for selected Arctic winters on 15 December, 15 March and on the central date (as noted on the maps), the day on which the westerlies changed to easterlies at 60° N/10 hPa. The overlaid white contours show temperature in Kelvin.

2.2.3 PV diagnostics

We now discuss the development, movement, and dissipation of polar vortices during the warm winters to further characterise the MWs. To perform this, we analyse the PV fields (e.g. Hauchecorne et al., 2002) calculated from the ECMWF operational analysis at two representative altitudes in the middle (850 K or ∼ 10 hPa/30 km) and lower (475 K or ∼ 85 hPa/18 km) stratosphere. Figures 2.4 and 2.5 illustrate the status of polar vortices on selected days at 850 K and 475 K, respectively. Two common dates along with the central date, the date on which the westerlies change their direction at 60° N/10 hPa (e.g. Charlton and Polvani, 2007), are selected for this discussion. The common dates, 15 December and 15 March, fairly represent the day before and after the MW, respectively, in each winter.

In 2009/10, the vortex was stable and strong from December through January in the middle stratosphere, at 850 K. The temperature started to increase by mid-January and the wave disturbances pushed the vortex to the adjacent mid-latitudes. The vortex was still relatively large, strong, and nearly concentric until early February. However, strong wave 1 activity pushed the vortex to the Atlantic and then split into two parts with a large, strong, and near-concentric vortex over the Atlantic and a small patch of vortex air above Russia, around 5 February, at 850 K. The separated vortices merged in a few days and the redeveloped vortex transformed to an elongated structure on the central date, and it started to dissipate thereafter, as shown by the map on 15 March. In contrast, at 475 K, a minor warming due to a wave 2 event split the vortex into two independent lobes, as displayed on 15 December. Vortices of considerable size with one over the North America and another over Russia were found for a few days after the split. Yet, the vortex bulbs merged again to form a large vortex and it stayed near the pole, but the center of the vortex was over Siberia until early February. The vortex was unstable and was a crescent shaped patch of air on the central date. Nevertheless, the vortex split again during the MW period due to strong wave 1 activity and the separated vortices sustained intact until early March at 475 K. Our vortex analyses with high resolution PV maps are consistent with those discussed with various data sets by Dörnbrack et al. (2012) and Khosrawi et al. (2011) for this winter.

In 2008/09 and 2005/06, large and strong vortices were present in December at 850 K. The temperatures began to increase by mid-January and the vortices shrunk and moved to mid-latitudes as severe wave activity led to the MWs by late January in both winters. The vortices started to collapse thereafter, as shown by the PV maps on 15 March. At 475 K, the wave disturbances started early and thus two nearly-split vortices were found on 15 December in both winters. Although relatively stronger vortices were observed on the central dates, they dissipated thereafter. Note that wave 1 disturbances led to the MW of 2005/06, but wave 2 activity was pivotal in triggering

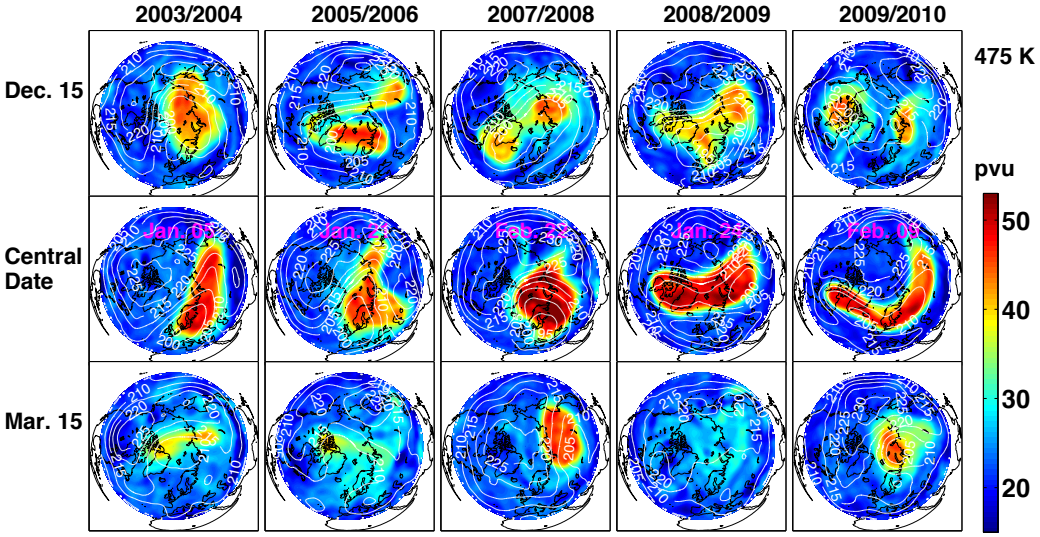

Figure 2.5: Same as Fig. 2.4, but for 475 K (∼ 85 hPa/18 km).

the MW of 2008/09. Also, in 2008/09, the vortex split on the central date at 10 hPa and hence, the MW was a vortex split event, as also analysed by Harada et al. (2010) and Manney et al. (2009).

The penetration of easterlies down to the lower stratosphere was not effective in 2007/08 as illustrated in Fig. 2.2. At 850 K, due to strong wave disturbances, the vortex shifted off the pole in the warming period. The vortex began to dissipate and there was no solid vortex in March. At 475 K, however, there was significant wave activity in the early winter, which split the vortex around mid-December. The vortices merged and the redeveloped vortex remained unscathed until late March in agreement with the lower temperatures there.

In 2003/04 at 850 K, the vortex was very large and concentric until late December and then it weakened and displaced to mid-latitudes due to wave 1 disturbances and subsequent MW in early January. The temperature became very low again in March, and therefore, a strong and concentric vortex was reestablished after nearly two months of intense and continuous disturbance. As a result, a well shaped large vortex was formed around 15 March at 850 K and sustained intact until late April. At 475 K, a similar situation is replicated, where even stronger but smaller vortex was found throughout March. Note that the MWs of 2003/04, 2005/06, 2007/08 and 2009/10 were primarily driven by wave 1 amplification and were vortex displacement events, as the associated vortex split was not evident at 10 hPa on the central date of the respective MWs (e.g. also see Harada et al., 2010; Manney et al., 2009, 2008). Further information about the MWs in these winters is given in Table 2.1.

2.3 Tropospheric wave forcing

Stratospheric warmings usually initiate in the troposphere from where the planetary scale disturbances propagate into the stratosphere and break there (e.g. Bancalá et al., 2012; Butler and Polvani, 2011; Cohen and Jones, 2011; Kolstad and Charlton-Perez, 2011; Manney et al., 2009; Charney and Drazin, 1961). The MW periods normally preceded by high wave activity at the tropopause, in which more than one planetary wave (generally waves 1 and 2) will be present. The EP flux/heat flux derived at 100 hPa is often regarded as a measure of wave activity entering the stratosphere (e.g. Naujokat et al., 2002; Newman et al., 2001; Pawson and Naujokat, 1999; Coy et al., 1997) and hence, it can well describe the wave forcing for the MWs. Therefore, Fig. 2.6 examines the time evolution of zonal-mean EP flux, wave EP flux and wave amplitudes for the winters at 100 hPa averaged over 45–75° N.

Elevated EP fluxes and wave 1 amplitudes are estimated just before the MW in 2009/10 and are about 4×10^5 kg s^{-2}, implying a profound wave forcing during the period. The EP flux values

Table 2.1: Features of the MWs in recent Arctic winters. Central date (the day on which the westerlies changed to easterlies at 60° N/10 hPa), whether the MW is vortex displacement/split event and prominent wave forcing are listed (data: the ECMWF operational analysis).

Arctic winter	Central date	Warming event	Prominent wave
2003/04	5 January	vortex displacement	wave number 1
2005/06	21 January	vortex displacement	wave number 1
2006/07	24 February	vortex displacement	wave number 1
2007/08	22 February	vortex displacement	wave number 1
2008/09	24 January	vortex split	wave number 2
2009/10	9 February	vortex displacement	wave number 1

are even comparable to those found during the severe MW in 2008/09, where they are around $4.1\times10^5\,\mathrm{kg\,s^{-2}}$. Wave 2 with a peak amplitude of about $30\,\mathrm{m^2\,s^{-2}}$ in January was the key in driving the MW of 2008/09. In 2005/06, a constant EP flux of around $1.5\times10^5\,\mathrm{kg\,s^{-2}}$ and wave 1 EP flux of around $1\times10^5\,\mathrm{kg\,s^{-2}}$ are observed for about 45 continuous days in January–February. In 2007/08, although the MW in late February was mainly forced by a wave 1 event, the minor warming in mid-February was triggered by a strong wave 2 episode with an amplitude of about $32\,\mathrm{m^2\,s^{-2}}$. The other winters also show their peak EP flux (2–$2.5\times10^5\,\mathrm{kg\,s^{-2}}$) and wave 1 amplitude ($12\,\mathrm{m^2\,s^{-2}}$) just before the MW, but in smaller magnitudes than those found in 2009/10. More importantly, the winters display short wave bursts prior to the MWs, indicating the preconditioning or tropospheric forcing (e.g. Coy et al., 2009). These features are perhaps best described by the wave EP fluxes, which show an advance shift of about 7 days with the peak wave amplitude episodes. Also, the largest wave 1 EP flux of about $4\times10^5\,\mathrm{kg\,s^{-2}}$ for 2009/10 and wave 2 EP flux of about $5\times10^5\,\mathrm{kg\,s^{-2}}$ for 2008/09 are estimated shortly before the MW, consistent with the intensity of the MWs in these winters. It should be noted that a similar feature of heat flux emergence prior to weak vortex events was also shown by some earlier investigators (e.g. Polvani and Waugh, 2004; Newman et al., 2001). In sum, the winters show significant wave activity and considerable EP flux and momentum flux (not shown) at the tropopause shortly before and during the MWs, suggesting a strong connection between tropospheric wave forcing and MWs.

Our wave activity analyses are also in concert with the findings of other studies using geopotential heights in the troposphere. For instance: Hirooka et al. (2007) report a tropospheric ridge over Alaska around early January, which was instrumental in driving the MW in 2003/04. Similarly, Coy et al. (2009) show a sudden increase in the geopotential heights over the Northern Atlantic at 360 K in mid-January, in which the accompanied wave breaking in the upper troposphere triggered the MW in 2005/06. Thurairajah et al. (2010) show a strong anticyclone around mid-February that weakened and displaced the vortex off the pole, leading to the MW in 2007/08. Harada et al. (2010) observe a remarkable upper tropospheric ridge over Alaska during 10–13 January, which played prominent roles in the upward propagation of waves from Alaska/Siberia during the first/second development stages of the MW in 2008/09. Ayarzagüena et al. (2011) find that the amplification of the upward wave propagation for the MW in 2009/10 was initiated by anomalous Rossby wave trains and their interaction with climatological waves in the troposphere in late January. Further details about these tropospheric processes and preconditioning can be found in the respective references.

2.4 MWs and ozone loss

We have already seen that MWs have a great impact on the temperature structure, and thus on the temporal and vertical evolution of polar vortex in the Arctic winters. As the occurrence of a MW is associated with increase in polar temperatures, it restricts the formation of PSCs. In the polar stratosphere, the ozone loss occurs through heterogeneous chlorine activation on PSC surfaces when the sunlight returns over the region. Therefore, we now look at the connection between A_{PSC} and chemical ozone loss together with other dynamical entities in the Arctic winters. In order to make a better statistical analysis, we use data for the seventeen winters during 1993/94–2009/10.

Figure 2.7 shows time series of the cumulative ozone loss estimated from the ground-based ultraviolet-visible (UV-VIS) total column ozone measurements (Kuttippurath et al., 2010a; WMO,

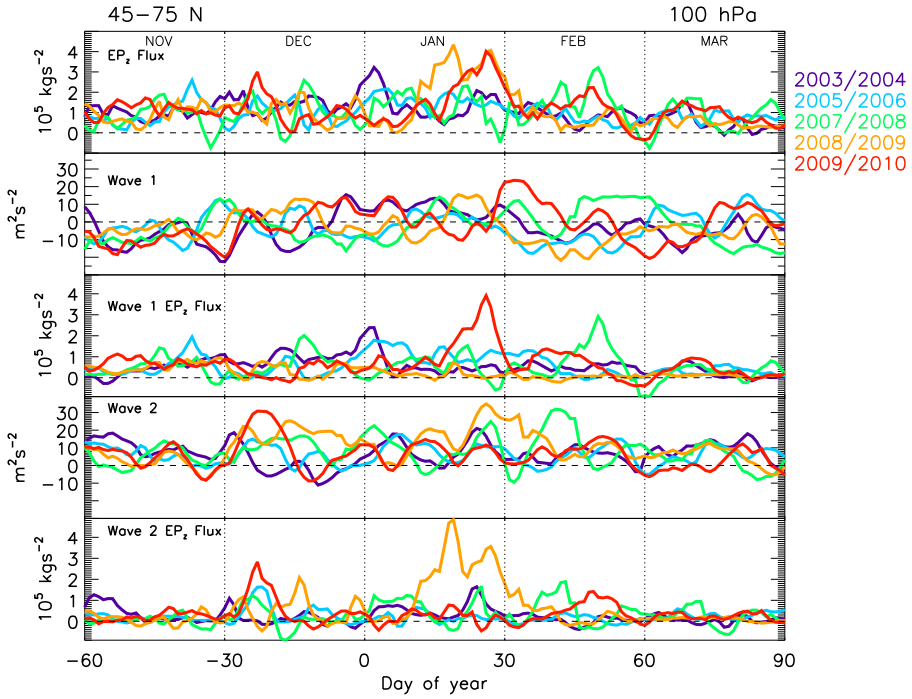

Figure 2.6: Temporal evolution of various zonally averaged quantities for selected Arctic winters at 45–75° N/100 hPa. The quantity zero is marked with dashed horizontal lines and the dotted vertical lines separate each month.

2007; Goutail et al., 2005) and December–March mean of A_{PSC} at 475 K, and January average of the zonal-mean temperatures, zonal winds, and geopotential heights at 50 hPa averaged over 60–90° N in the Arctic for the 1993/94–2009/10 period. The ozone loss is the maximum loss determined at the end of each winter. It is computed as the difference between the measured ozone and the passive tracer [i.e. 100×(passive tracer–ozone)/passive tracer)] simulated by the REPROBUS (REactive PRocesses ruling the Ozone BUdget in the Stratosphere) chemical transport model (Lefèvre et al., 1998), for which the model was initialised on 1 December (1 November for 2002/03 to account for early ozone loss in this winter) from the ECMWF ozone data for each winter (i.e. no ozone loss until the initialization day). Additional information about these calculations can be found in Goutail et al. (2005) and Kuttippurath et al. (2010a).

There were no MW over 1993/94–1997/98 and therefore, temperatures were lower, areas of PSCs were larger, westerlies were stronger, and geopotential heights were comparatively lower and hence, large loss of ozone is estimated in these winters. Although there was no MW in 1993/94, the January average of temperature was higher and A_{PSC} was smaller in this winter. However, the loss in ozone was comparable to other cold winters. This mismatch is due to the unusual cold spell and associated ozone loss during late February–early March 1994 (Manney et al., 1995). The situation was entirely different during 1998/99–2002/03, which experienced 6 MWs and therefore, the winters except 1999/00 show warmer temperatures, smaller PSC areas, and weaker westerlies. The warmings in 1998/99 and 2001/02 were very severe as there were two MWs in each winter, for which the lowest A_{PSC} (nearly zero) in the seventeen years is deduced in 1998/99. Consequently, the ozone loss in these winters was the smallest among the winters, about 7–10 %. The winter 1999/00 was very cold, where the lowest geopotential height in the 17-year period is also registered and thus, large loss in ozone is estimated. A similar situation is replicated in 2004/05, a cold winter surrounded by 2 warm winters. The largest A_{PSC} among the winters and significant ozone loss are estimated for that winter. It suggests that the late MW in 1999/00 (20 March 2000) or the early final warming in 2004/05 (14 March 2005) did not inhibit the ozone loss in these cold winters. The winters from 2003/04 to 2009/10 had 6 MWs, where 2003/04 and 2005/06 show relatively higher temperatures, smaller A_{PSC}, and thus minimal ozone loss.

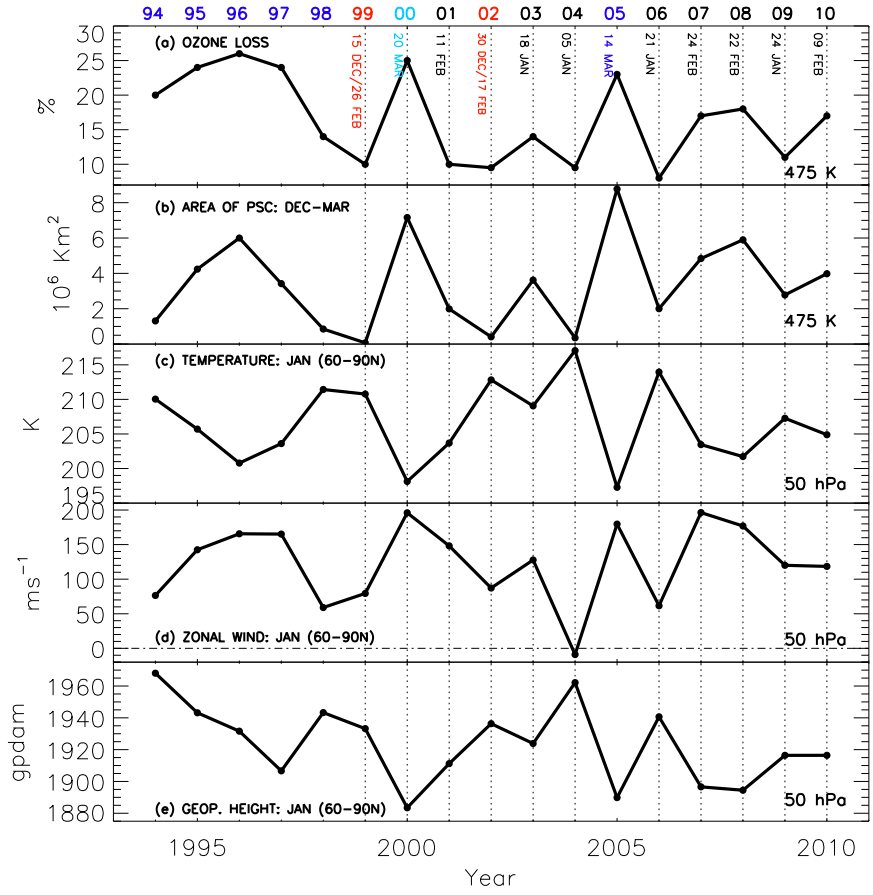

Figure 2.7: (a) The cumulative total column ozone loss at the end of each winter (late March or early April and 20 February for 2009/10), **(b)** the average area of PSCs in December–March at 475 K, **(c)** the zonal-mean temperatures, **(d)** zonal winds and **(e)** geopotential heights averaged over 60–90° N in January at 50 hPa for the Arctic winters 1993/94–2009/10. The UV-visible ozone loss estimate for each year is taken from Goutail et al. (2005), WMO (2007) and Kuttippurath et al. (2010a). The winters with MW are marked with dotted vertical lines and the zero-wind line is marked with a dash-dotted line. The central date for each MW is also noted on the top panel **(a)**. The winters 1998/99 and 2001/02 had 2 MWs and the MW in 1999/00 was in late March.

2.4.1 Correlation between temperature/zonal wind and ozone loss

It is well-known that there is a good relation between the partial column ozone loss and volume of PSCs in the Arctic stratosphere (Rex et al., 2004). We also find a strong correlation between the relative ozone loss (%) and the December–March average of A_{PSC}, zonal-mean January temperature and zonal winds at 60–90° N. Nevertheless, we have also performed a detailed analysis of the correlation between the ozone loss (%) and the dynamical parameters (temperature, zonal wind and geopotential height) for various months and altitudes, i.e. we keep the ozone loss unchanged, but switch the dynamical entities averaged for various months and altitudes for these tests. The analysis shows that the correlation of these parameters (averages in January) with ozone loss (in %) is 0.71–0.78 at 50 hPa. Correlations of ozone loss with the parameters averaged at other altitudes (100 and 30 hPa) are weak (r = 0.45–0.65), but comparable for 70 hPa (around r = 0.8). Our diagnosis for other months (or combination of months) reveals that the correlations are weak for December, February and March, and for the December–January or December–February average. Although the correlations are slightly better for the December–March average (r = 0.81–0.88), they do not relate in the same way as for the January average, i.e. the near one-to-one correlation as illustrated in Fig. 2.7. Furthermore, the higher correlations during December–March are weighted by the higher temperatures or weaker westerlies in February/March due to the MWs in January/February of late 1990s and 2000s, as there was only one winter with a MW in March (1999/2000) during the period. Since the timing of MWs is different in each winter, the data averaged in a particular month may not always reflect the exact intensity of MWs. For instance, the MW was very strong in 2008/09

but the zonal wind shows a speed of 120 ms^{-1} against $-5\,ms^{-1}$ in 2003/04. Therefore, care must be taken to delineate various parameters and their correlation in a particular time period. In this context it is also worth mentioning that there is a well established relation between spring time heat flux and ozone in the northern high latitudes (e.g. Weber et al., 2011).

2.4.2 Timing of MWs and ozone loss

To investigate the impact of timing of MWs on the ozone loss, we use the central dates derived from the ECMWF operational analyses (shown in Fig. 2.7a). Note that there can be slight differences in the MW central dates when they are deduced from a different meteorological data set (e.g. Harada et al., 2010; Charlton and Polvani, 2007; these will be discussed in detail in Sect. 2.5.1). As emphasized earlier, there were no MWs in the 1993/94–1997/98 period and thus these winters experienced large loss in ozone. However, the MWs in 1998/99 and 2001/02 were in December (e.g. Butler and Polvani, 2011) and hence, the ozone loss in these winters was very small. Likewise, the MWs of 2002/03, 2003/04, 2005/06 and 2008/09 were in January, (e.g. Cohen and Jones, 2011; Kuttippurath et al., 2011; Kleinböhl et al., 2005a) and consequently the ozone loss during the winters was also very small. The MWs of other winters were in February or March (e.g. Harada et al., 2010; Orsolini et al., 2010) and therefore, the ozone loss was severe in those winters (e.g. the MW in 1999/00 was on 20 March 2000). It suggests that there is a good relation between the timing of MW and the amount of ozone loss in each winter, where early (December–January) MW leads to nominal ozone loss. This is due to the fact that, in the Arctic, very low temperatures (<195 K) in December–January is important for the formation of PSCs and subsequent chlorine activation on them. Therefore, MWs in these months limit the formation of PSCs and hence, restrict the ozone loss. In addition, note also that a prolonged appearance of a cold stable vortex is a necessary requirement for the sustained ozone loss, but the warmings greatly disturb the stability of a vortex.

2.5 Discussions and conclusions

2.5.1 MWs of the Arctic winters

We have characterised various dynamical processes in the Arctic winters 2003/04–2009/10. In 2009/10, the warming began with strong wave 2 disturbances around mid-December and that split the vortex in the lower stratosphere. The vortex redeveloped afterwards, but later wave 1 episodes built momentum for the MW in early February. All winters, except 2008/09 show wave 1 amplification that led to the MWs. In contrast, wave 2 activity was pivotal in driving the MW in 2008/09, which rarely happens. Previous wave 2 MW event occurred in 1988/89 and such events occur only in La Nina conditions, except for the winter 1978/79 (e.g. Butler and Polvani, 2011; Charlton and Polvani, 2007). In 2008/09, the EP flux estimated for wave 2 during the MW period is reportedly the largest since 1978/79 (Harada et al., 2010). In 2008/09, the wave forcing at the tropopause was unusually large before and during the MW, which triggered the atypical MW, confirming the findings of Harada et al. (2010). Among the winters, 2003/04 had the earliest MW as it was in early January. However, the MWs in 2006/07 and 2007/08 were in late February, as for a typical pre-1990 MW (e.g. Cohen and Jones, 2011; Andrews et al., 1987).

The MW in 2008/09 was a vortex split event, but the MWs in other winters (during 2003/04–2009/10) were vortex displacement events. Note that if the vortex splits at 10 hPa on the central date, then the MW is a vortex split event. Nevertheless, it also depends on the meteorological data (e.g. ECMWF) and time (e.g. 12 h) considered for the diagnosis, as the central date can be different for different data sets. For instance, the central date of 2003/04 is 5 January in our analysis with the ECMWF operational data, whereas it is 7 January in Cohen and Jones (2011) and Butler and Polvani (2011), who used the National Center for Environmental Prediction-National Center for Atmospheric Research (NCEP-NCAR) reanalysis for their studies. Such differences in the central dates calculated for several MWs using the ECMWF 40-yr reanalysis (ERA-40) and NCEP–NCAR data over 1957–2002 can also be found in Charlton and Polvani (2007). In addition, possibly due to the differences in central dates, Cohen and Jones (2011) classify the MWs of 2003/04, 2005/06 and 2009/10 as vortex split events, in contrast to our results and to those of Harada et al. (2010) and

Manney et al. (2009, 2008, 2005). Therefore, attention must be paid when interpreting a MW as a vortex split or displacement event. Our analysis also shows that the wave 1 MWs (e.g. Kuttippurath et al., 2011; Kleinböhl et al., 2005a; Manney et al., 2005; Liu et al., 2009) usually end up with vortex displacement events, while the wave 2 MWs (e.g. Harada et al., 2010; Manney et al., 2009) generally lead to vortex split events, consistent with the findings of previous studies (e.g. Bancalá et al., 2012; Cohen and Jones, 2011).

Exact reasons for the occurrence of stratospheric warmings are still not fully understood. A study by Taguchi (2008) using a 49-yr reanalysis data did not show any significant correlation between MWs and tropospheric blocking events. In contrast, a recent study by Martius et al. (2009) shows a clear connection between them. The analyses of Taguchi (2008) are mostly at 500 hPa, while the study of Martius et al. (2009) exhibits that the signals are more apparent at 200 hPa or above. Similarly, the most recent studies using various meteorological fields (e.g. ERA-40 and NCEP-NCAR) for about 52 Arctic winters also show evidence for the connection between MWs and tropospheric blockings (Bancalá et al., 2012; Castanheira and Barriopedro, 2010; Woollings et al., 2010). In agreement with the findings of Martius et al. (2009), the aforesaid studies also observe that the (wave 1/2) MWs can be preceded by tropospheric blocking activity (in the Euro-Atlantic/Pacific region) within a few weeks or days prior to the central date of MWs. In this study we diagnosed the wave forcing at 100 hPa and demonstrated a clear connection between tropospheric forcing and MWs. It is manifested more clearly with the wave 1 and wave 2 EP fluxes, which show an advance shift in time (around 7 days) with the central dates, suggesting a strong preconditioning or wave forcing. It has to be reminded that the occurrence of MWs is also strongly affected by several external factors such as QBO, solar cycle and sea surface temperature anomalies, e.g. MWs tend to happen more frequently during solar maximum in the westerly phase of QBO (e.g. Blume et al., 2012). However, a detailed account on these issues are beyond the scope of this study. Nonetheless, it has to be kept in mind that all MWs are not necessarily preceded by tropospheric blocking activity (e.g. Bancalá et al., 2012; Taguchi, 2008).

2.5.2 Impact of MWs on ozone

Polar ozone loss during 1993/94–2009/10 shows a high correlation with the December–March average of A_{PSC} at 475 K, and zonal-mean temperature and zonal wind at 50 hPa averaged over 60–90° N in January. There are studies showing a good correlation between the ozone loss and volume of PSCs in the Arctic (Rex et al., 2004). The interesting aspect of our results is that we use entirely different data sets (ground-based chemical ozone loss in percent), time period (maximum ozone loss vs. December–March A_{PSC} and January zonal-mean temperature, zonal winds and geopotential heights averaged over 60–90° N) for these comparisons, and hence, these analyses are different and new. Therefore, this study further attests the robustness of the correlation between ozone loss and PSC or temperature in the Arctic winter stratosphere and hence, the local climate.

Our analysis shows an increase in the frequency of MWs in recent years as there were 13 MWs during 1998/99–2009/10, in which six of them were over 2003/04–2009/10. This is in agreement with the number of MWs identified using other data sets for this period. For instance, studies using the 6-hourly Japan Meteorological Agency Climate Data Assimilation System and the Japanese 25-yr Reanalysis (Harada et al., 2010), the NCEP– NCAR data (Butler and Polvani, 2011; Cohen and Jones, 2011), the ERA-40 reanalysis (Bancalá et al., 2012) and the ECMWF operational analyses (Ayarzagüena et al., 2011) also report a similar number of MW events during the period. Therefore, our analysis confirms the results of previous studies on the frequency of MWs in recent Arctic winters (Mitchell et al., 2012; Ayarzagüena et al., 2011; Charlton-Perez et al., 2008; Manney et al., 2005).

It is clear that there is a significant increase in the occurrence of MWs in recent Arctic winters and these MWs have a strong impact on the trace gas distribution in that region. However, ozone variations in the polar stratosphere are tightly related to the changes in the levels of anthropogenic halogenated ODSs (e.g. Shepherd, 2008), GHGs (e.g. Eyring et al., 2010; Plummer et al., 2010), temperature (e.g. Gillett et al., 2011; Shepherd, 2008), and planetary wave drive (e.g. Austin et al., 2003). So changes in the polar stratospheric ozone are interconnected with key chemical and dynamical processes, such as the cooling of the upper stratosphere by increased CO_2 levels in the past has mitigated the ozone loss through the temperature dependence of ozone chemistry

there (e.g. Eyring et al., 2010; Jonsson et al., 2009) and hence, its continued increase in future is likely to contribute to the upper stratospheric ozone recovery from the declining levels of ODS. The GHG-driven changes in the residual circulation also affect the spatial and temporal distribution of ozone and long-lived tracers (e.g. Waugh et al., 2009; Salby and Callaghan, 2002). Studies have already shown that the long-term increases in the poleward transient Rossby wave episodes in the subtropical lower stratosphere have significantly contributed to the trends in the mid-latitude ozone (e.g. WMO, 2007; Hood and Soukharev, 2005). The expected changes of the concentration fields in stratospheric N_2O, CH_4 and H_2O, due to increased BD circulation, are very important in this context (e.g. Butchart et al., 2010), as they are connected to the NO_x and HO_x driven ozone loss in the stratosphere (e.g. Eyring et al., 2010; Kuttippurath et al., 2010a). Therefore, attribution of ozone trends to a particular chemical or dynamical process is very challenging. Note, however, that earlier investigators have already pointed out reduction in the ODSs and subsequent positive changes in the abundances of stratospheric ozone, irrespective of latitudes (e.g. WMO, 2011, 2007 and references therein). Yet, as the frequency of MWs over 1998/99–2009/10 (∼1.1 MWs/winter) is nearly twice that during 1957/58–1997/98 (∼0.6 MWs/winter), the higher polar temperatures resulted from increased dynamical activity could have masked the PSC-related ozone loss due to anthropogenic halogen emissions. The study by de Laat and van Weele (2011) also suggests that the minor warmings of the Antarctic winters 2004 and 2010 have contributed to the reduced Antarctic ozone loss in those winters. Therefore, our study indicates that the positive ozone trends estimated during 1998/99–2009/10 are likely to be affected by these events of higher ozone abundances due to MWs and hence, care should be taken when estimating and interpreting the (ozone) trends in the polar stratosphere.

Characterisation of a warming event is important for the diagnosis of possible change in the dynamical activity, and its representation in chemistry climate models needs to be improved (Mitchell et al., 2012; SPARC, 2010). Models with temperature sensitive radiation schemes show a jump in tracer values after MWs (e.g. Kuttippurath et al., 2010a). So the diagnosis of warming events with respect to time is necessary to enhance the performance of the models. Furthermore, trend studies on periods with MWs occurring in the beginning or at the end of the period make trend detection difficult and often confusing, as also noted by Manney et al. (2005). This is particularly important in the context that there is an increase in the occurrence of MWs in recent Arctic winters, as there were 13 MWs in 11 out of the 12 winters over 1998/99–2009/10. The only winter without having a MW in this period is 2004/05. Yet, the final warming of this winter was relatively early for a cold winter, on 14 March 2005 (note that this warming was taken as a MW by Harada et al., 2010, but not in our study; Butler and Polvani, 2011; and in Cohen and Jones, 2011). Note, however, that the frequency of MWs over 1993/94–2009/10 (which includes 5 consecutive winters without MWs) is ∼0.76 and is comparable to the findings of other studies on the frequency of MWs (0.6 ±0.1 MWs/winter) over the 1957/58–2009/10 period (Charlton and Polvani, 2007; Blume et al., 2012). It implies that, although there is an increase in the occurrence of MWs in recent years, their long-term average is likely to stay around the historical value (∼0.7 MWs/winter). To this end, it should be kept in mind that the climate model simulations also predict a similar number of MWs (0.7–0.78 MWs/winter) for the 2010–2100 period (Mitchell et al., 2012). Therefore, studies on the frequency and variability of warm winters, as presented here, have a great importance in diagnosing trends in the winter stratospheric conditions and thus tracking climate change in the polar regions.

Chapter 3

Arctic ozone loss: 2002/2003 *

Contents

Stratospheric ozone loss in the Arctic was first observed in 1989 (Hofmann et al., 1989) and significant reduction in ozone has been measured since then in each cold winter (e.g. WMO, 2007). The difference in ozone loss from one winter to the other is found to be extremely large and is controlled by temperature history of the winters. The meteorology of Arctic winters is characterised by intermittent SSWs (Kuttippurath and Nikulin, 2012; Charlton and Polvani, 2007). Therefore, the extent of ozone loss in an Arctic winter is determined by the dynamics of the region. This is clearly manifested with the range of ozone depletion observed over the years, with 5–7% or <40 DU in warm winters and 25–30% or >60 DU in cold winters (Müller et al., 1997; Andersen and Knudsen, 2002; Harris et al., 2002; Rex et al., 2002, 2004; Goutail et al., 2005; Tilmes et al., 2006; WMO, 2007; Müller et al., 2007; Blumenstock et al., 2009; Kuttippurath et al., 2010a). Another important feature observed is the spread in the ozone loss derived by different measurement techniques in each year. For instance, Newman et al. (2002) list a deviation from 0.7 to 2.1 ppmv for the Arctic winter 1999/00 and Kuttippurath et al. (2010a) find a similar range in the ozone loss for the Arctic winter 2004/05 by various methods. However, this high spread to a large extent is due to the differences in the sampling and estimation method. Therefore, a reasonable agreement among various ozone loss estimates can be reached by selecting a common criterion for the loss estimates, such as similar vortex sampling, vortex edge criterion, time period, and the same method of loss computation, as demonstrated by Harris et al. (2002). The large inter-annual variability and the differences in estimated ozone losses still attest the necessity to assess ozone loss in each winter by different methods. It is also essential to diagnose the evolution of ozone in each winter to assist the interpretation and prediction of its future development in a perspective of ozone recovery. Therefore, in this chapter we present the ozone loss determined using airborne measurements and satellite observations for the Arctic winter 2002/03 and compare the inferred loss with other available results for this winter and other Arctic winters.

The Arctic winter 2002/03 was exceptional as it was unusually cold in the first half and was subjected to a MW in the second half. Two major field campaigns were conducted to probe the evolution of ozone, PSCs, and ozone loss by various instruments in this winter. The campaigns were executed

*This chapter is partly based on: J. Kuttippurath, A. Kleinböhl, M. Sinnhuber, H. Bremer, H. Küllmann, J. Notholt, S. Godin-Beekmann, O. P. Tripathi and G. Nikulin: Arctic ozone depletion in 2002–2003 measured by ASUR and comparison with POAM observations, J. Geophys. Res., 116, doi:10.1029/2011JD016020, 2011.

Table 3.1: The flight route of the Falcon-20 research aircraft during the EuPLEx 2003 and SCIA-VALUE 2003 campaigns in the Arctic winter 2002/03.

Flight date	Flight track
EuPLEx	
14-01-2003	Munich - Kiruna
15-01-2003	Kiruna local flight
19-01-2003	Kiruna local flight
23-01-2003	Kiruna local flight
26-01-2003	Kiruna local flight
07-02-2003	Kiruna local flight
08-02-2003	Kiruna local flight
09-02-2003	Kiruna local flight
12-02-2003	Kiruna - Munich
SCIA–VALUE	
10-03-2003	Munich - Kiruna
12-03-2003	Kiruna - Nylesund - Kiruna
13-03-2003	Kiruna - Keflavik
14-03-2003	Keflavik - Kangerlussuaq
15-03-2003	Kangerlussuaq - Keflavik
17-03-2003	Keflavik - Munich
19-03-2003	Munich local flight

in the framework of the European Polar Lee-wave Experiment (EuPLEx) in January–February 2003 (Kleinböhl et al., 2005a) and the SCIAMACHY –SCanning Imaging Absorption spectroMeter for Atmospheric CHartographY– validation and utilization experiment (SCIA–VALUE) in March 2003 (Fix et al., 2005; Kuttippurath et al., 2007). A suite of instruments participated in the campaign and performed ground-based, airborne and in situ measurements (Christensen et al., 2005; Goutail et al., 2005; Raffalski et al., 2005; Streibel et al., 2006; Kuttippurath et al., 2007). The airborne sub-millimeter radiometer (ASUR) was onboard the German Falcon-20 aircraft to perform measurements as a part of these campaigns. Both surveys provided a good set of ASUR trace gas measurements, including ozone and ClO. We investigate the ozone loss features of the winter using the ASUR observations and compare with the results from other studies (Tilmes et al., 2003; Urban et al., 2004; Christensen et al., 2005; Feng et al., 2005b; Goutail et al., 2005; Grooß et al., 2005b; Raffalski et al., 2005; Singleton et al., 2005; Streibel et al., 2006; Tripathi et al., 2006; Konopka et al., 2007; Müller et al., 2007; El Amraoui et al., 2008a; Ryskin and Kulikov, 2008; Sonkaew et al., 2013). Here we analyse the meteorological situation, evolution of ozone and chemical ozone loss with the ASUR measurements, which have hitherto not been used for the study of Arctic ozone loss in 2002/03. To get the complete evolution of ozone and ozone loss during the winter, we complement the ASUR measurements with Polar Ozone and Aerosol Measurement (POAM)-III observations. The passive tracer method is applied to compute ozone loss from the measurements (e.g. Kuttippurath et al., 2010a), for which the passive tracer needed is simulated by the MIMOSA-CHIM CTM (e.g. Kuttippurath et al., 2009). Therefore, the ozone loss determined from the measurements is also compared to the simulated loss.

3.1 Data and methods

3.1.1 Air-borne measurements

The ASUR measurements taken during the EuPLEx and SCIA–VALUE 2003 campaigns are used here. The campaigns and observations are described in detail by Kuttippurath et al. (2010); Kuttippurath (2005) and Kleinböhl et al. (2005a). A total of 12 flights, between 13 January 2003 and 20 March 2003, was carried out with more than 70 flight hours of measurements for various stratospheric trace gases. Both campaigns surveyed similar latitudes between 50° and 80°N with a focus on the polar vortex. Therefore, a large number of measurements were taken inside the vortex to allow a reasonable analysis of the polar processing and ozone loss. Further details of these measurements are given in the above-said references and in Table 3.1 and Section 3.3.1.1.

ASUR is a passive heterodyne receiver operating in a frequency range at 604.3–662.3 GHz. The receiver has two spectrometers; an acousto optical spectrometer (AOS) and a chirp transform spectrometer. We use the stratospheric measurements performed with the AOS, which has a bandwidth of 1.5 GHz and a resolution of 1.27 MHz. The observations are performed onboard a research aircraft to avoid signal absorption by tropospheric water vapor. The sensor observes upward at a constant zenith angle of 78° and measures thermal emissions from the rotational states of the observed species. Vertical profiles of ozone and ClO are retrieved in an equidistant altitude grid of 2 km spacing using the method of Rodgers (1976). An in-house radiative transfer model is applied to invert the measurement spectra for a non-scattering atmosphere, for which the *a priori* profile was taken from Bremer et al. (2002). The altitude range of ASUR ozone and ClO is 15–50 km and the vertical resolution of both measurements is about 6–25 km, where the resolution decreases with altitude from the lower to the upper stratosphere. Horizontal resolution of the measurements is 18 km and 40 km for ozone and ClO, respectively, and the accuracy of measurements is about 12–15% (Kuttippurath et al., 2007, 2010).

3.1.2 Space-based observations

POAM–III, a United States Naval Research Laboratory space experiment, was launched on the French Système Probatoire d'Observation de la Terre–4 satellite in March 1998 into a polar, sun-synchronous orbit. In this orbit 14 occultations are obtained per day around a circle of latitude in each hemisphere, with consecutive observations separated by ∼25° longitude. The latitude range is 63°–88° in the SH, and 55°–71° in the NH. The NH measurements are carried out during the spacecraft sunrise that corresponds to local sunset. The instrument operated in its nominal auto mode and measured atmospheric slant path transmission in 9 channels at 354–1018 nm. Inversion of the optical depth data yields vertical profiles of ozone in the altitude range of 13–60 km with a vertical resolution of about 1 km and an accuracy of ±5% (Randall et al., 2003).

3.2 The MIMOSA-CHIM model simulations

The MIMOSA-CHIM (Modélisation Isentrope du transport Méso-échelle de lÓzone Stratosphérique par Advection – Chimie) CTM has been successfully used for the diagnosis of polar ozone loss in previous winters (Kuttippurath et al., 2010a, 2009; Tripathi et al., 2007, 2006) and is described in detail by Tripathi et al. (2006). The model combines the MIMOSA advection code (Hauchecorne et al., 2002) with the REPROBUS chemistry scheme (Lefèvre et al., 1994). The spatial domain of the model is 30°–90°N with 1°×1° horizontal resolution. There are 16 isentropic vertical levels between 350 and 950 K with a resolution of 1.5–2 km. The model is forced by ECMWF analyses. The chemical fields are initialised from the 3-D CTM REPROBUS output (Lefèvre et al., 1998) and it uses the MIDRAD radiation scheme (Shine, 1987). Climatological H_2O, CO_2 and interactive O_3 fields are used for the calculation of heating rates. The kinetic data are taken from Sander et al. (2003), but the Cl_2O_2 photolysis cross-sections from Burkholder et al. (1990), with a log-linear extrapolation up to 450 nm (Stimpfle et al., 2004). These are in very good agreement with the Cl_2O_2 spectrum measurements by Papanastasiou et al. (2009). Note that these new measurements form the basis of the JPL 2011 recommendation. A detailed sensitivity study using different Cl_2O_2 scenarios in the model with respect to various Arctic winters, including 2002/03, has already been presented in Tripathi et al. (2006, 2007). The studies show a difference of about 2% in the estimated ozone loss among the tests. Therefore, to compare with other model results for this winter we have used Burkholder et al. (1990) for this model run. The model includes the chemical scheme of REPROBUS that contains 55 species and 160 reactions including gas phase, heterogeneous, and photolytic reactions (Lefèvre et al., 1998). The Br_y in the model is based on a correlation with CFC-11 that considered supply of bromine from CH_3Br, halons, as well as CH_2Br_2 and CH_2BrCl (Wamsley et al., 1998).

The model has a detailed scheme of PSC formation and growth. The saturation vapor pressure given by Hanson and Mauersberger (1998) is used to assume the existence of NAT particles and the one given by Murray (1967) is considered for ice particles. Equilibrium composition and volume of binary (H_2SO_4–H_2O) and ternary (HNO_3–H_2SO_4–H_2O) droplets are computed using an analytic

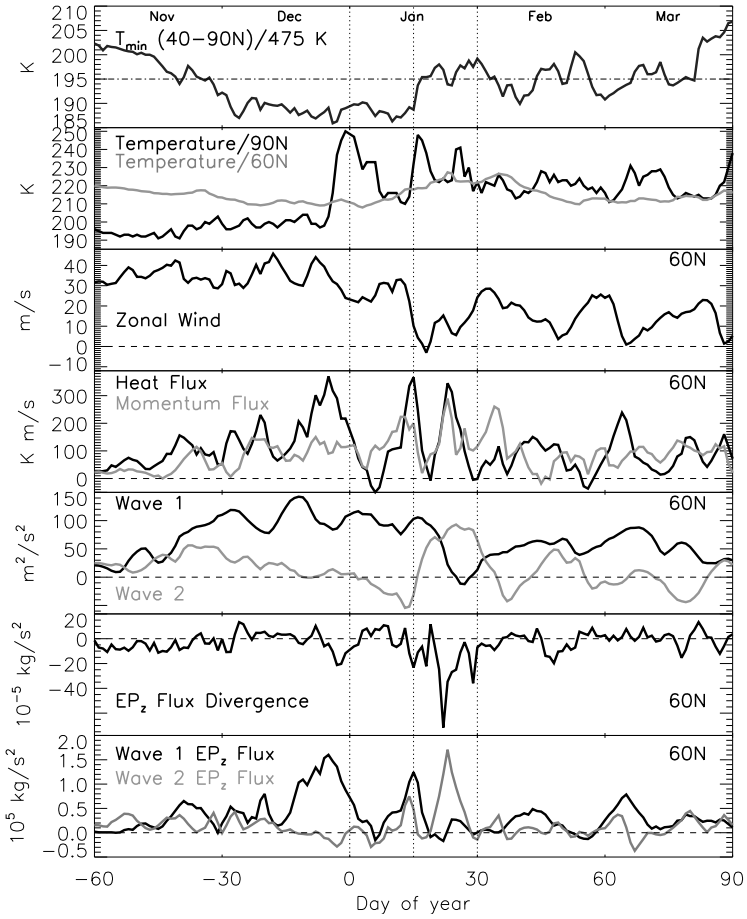

Figure 3.1: Meteorological situation of the Arctic winter 2002/03. Minimum temperature extracted from the ECMWF operational data in 40°–90°N at 475 K (top panel), temperature at 60°N and 90°N at 10 hPa, and zonal wind together with other dynamical entities at 60°N and 10 hPa, where the major warming criterion is defined. The dotted vertical lines represent day 1, 15 and 30 of January 2003, the dashed lines mark 0, and the dash-dotted line demarcates 195 K.

expression provided by Luo et al. (1995). Liquid supercooled sulphuric acid aerosols, NAT, and ice particles are considered in equilibrium with the gas phase (Lefèvre et al., 1998). For NAT and ice particles, the number density is set to 5×10^{-3}cm^{-3} and the particle diameter is calculated within the scheme, from available volume of HNO_3 and water. A denitrification scheme is incorporated to account for the sedimentation of HNO_3 containing particles where the NAT particles are assumed to be in equilibrium with gas phase HNO_3. All the three types of particles – NAT, ice and liquid aerosols – are considered in the sedimentation module and the sedimentation speed of the particles is calculated according to Pruppacher and Klett (1997). Nevertheless, recent studies indicate that PSCs do not frequently exist at NAT temperatures (WMO, 2011; Pitts et al., 2009, 2007) and liquid aerosols often dominate heterogeneous halogen processing (Portmann et al., 1996). Therefore, care must be taken when comparing these results with studies using a different PSC scheme.

3.3 Results and discussions

3.3.1 Synoptic evolution of the winter

Figure 3.1 presents the temperature, zonal wind and heat flux together with other dynamical entities at 60°N/10 hPa to assess the meteorological situation of the winter. Note that a detailed discussion of the evolution of polar vortex during this winter has been presented in Günther et al. (2008). Therefore, a similar analysis will not be presented. The minimum temperature extracted from ECMWF analyses at 40°–90°N for the winter shows very low values, below 195 K, from mid-November to mid-January. Furthermore, the temperatures show exceptionally low values and hence, the winter was unusually cold in December and early January. Though there was a warming in late January, the temperatures were again set to cold scales of <195 K, in early and late February. A minor warming in mid-February and early March is also apparent. In short, the winter was remarkably cold in the first half and very warm with three occasional warmings in the second half.

In order to investigate whether the warming was major or not, we now look at the temperatures at 90° and 60°N (second panel) together with zonal wind at 60°N and 10 hPa (third panel), where the criterion of a MW is generally examined (McInturff, 1978; WMO, 1978). As shown by the minimum temperature distributions (top panel), very cold temperatures are evident in November, December and early February at both latitudes (second panel). However, an abrupt increase in temperature was found in late December, from 198 to 252 K, within a few days time at 90°N, apart from two minor warmings in mid-February and early March. The warming at 60°N was comparatively slow, where it showed an increment of 18 K in a couple of weeks; from 208 K in early January to 226 K by late January. In conjunction with the high temperatures, the zonal wind reversed on 18 January 2003 and thus fulfilled the condition for a MW. However, the easterlies lasted for a single day only, although relatively diminished amplitudes of westerlies were present thereafter.

To scale the intensity of the warmings, we now derive various fluxes and wave amplitudes (the four bottom panels). As depicted in the figure, large heat and momentum fluxes are found in the MW period. The heat flux follows the temperature distributions of the winter, as expected, and shows large fluxes of about 380 K $\mathrm{m\,s^{-1}}$ in late December, mid- and late January in accordance with the increase in temperature. The EP flux divergence shows strikingly higher values of around $-65\times10^{-5}\mathrm{kg\,s^{-2}}$ during the warming periods, indicating the source of profound wave activity. The waves extracted from geopotential heights also show the presence of wave 1 before and during the MW, and both wave 1 and 2 after the MW with comparatively large amplitudes of around $90\,\mathrm{m^2s^2}$. The evolution of planetary waves and their estimated amplitudes are in very good agreement with those of Günther et al. (2008), although the scale of the amplitudes is different in both studies. The EP flux calculated for the waves exhibits very large values of $1.7\times10^{5}\mathrm{kg\,s^{-2}}$ for wave 1 in late December and mid-January, just before the MW. The momentum flux and wave EP flux also show an advanced shift in time with the warming periods, indicating considerable wave forcing prior to the MW (e.g. Kuttippurath and Nikulin, 2012). This is also shown with the wave 1 amplitude, where a peak amplitude of $150\,\mathrm{m^2s^2}$ was estimated a few days prior to the MW. Though wave 1 amplitudes are small, wave 2 amplitudes are larger in late January and those triggered the minor warming in late January. It is interesting to note that the wave 2 EP flux during this minor warming is equal to or higher than that found for wave 1 during the MW. However, it is clear that the wave 1 amplification led to the MW in mid-January and the minor warmings in mid-February and early March.

We now analyse how this particular meteorological situation affected the temporal evolution of the polar vortex in the lower stratosphere as our aim is to calculate the ozone loss inside the vortex. Fig. 3.2 shows the PV maps at 475 K constructed from the ECMWF data for selected days of the winter. It shows that the vortex has already formed in November and strengthened by December, consistent with the very low temperatures. A strong concentric vortex was formed in early January and it slightly elongated by 10 January 2003 as the wave 1 got amplified. Subsequently, the vortex split on 20 January 2003, just after the MW with the reversal of westerlies. Since the easterlies were not strong and did not prevail more than a day, the warming did not dissipate the vortex. Kleinböhl et al. (2005a) also report that although there was an event of rapid meridional transport of tropical air into the Arctic during this period, the low latitude air did not mix with the vortex air. So the vortex merged again by early February as the winds were westerlies and temperatures were lower. Nevertheless, the lower stratospheric vortex split again in mid-February due to a wave 1 event. The separated vortices, however, joined again to form a pole centered strong vortex by early March and sustained intact until the end of March, consistent with the discussion of polar vortex evolution presented in Günther et al. (2008).

3.3.1.1 Meteorology during the measurement period

The ASUR observations of the polar vortex in 2002/03 are limited to 16 days with about 180 ozone profile measurements. Though measurements are sampled between 50° and 79°N (65°–90°N EqL) these are mostly around a few longitudes (60°E–60°W). Therefore, the general evolution of the polar processes and vortex situations discussed in the previous section might not be applicable for all days of the ASUR flights. So in this section we discuss the situation of the polar vortex during the specific days of ASUR sampling. The ASUR measurements started on 14 January 2003, on which

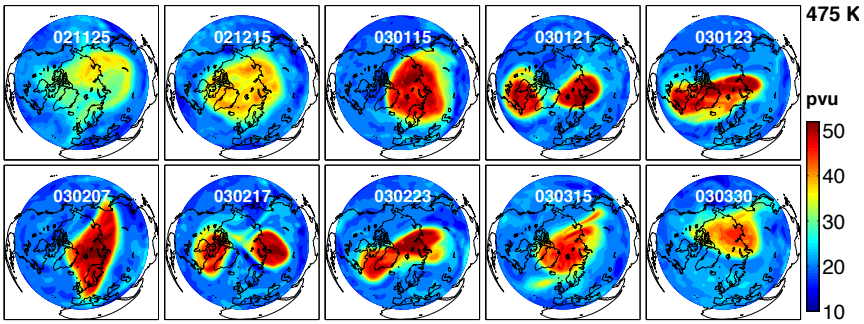

Figure 3.2: Temporal evolution of the polar vortex in the Arctic winter 2002/03 at 475 K. The dates are selected by analysing the complete record of the winter from November through the end of March.

the vortex and the cold pool was on the same axis of the flight (similar to the one shown for 15 January 2003 in Fig. 3.2, but tilted to the left) and therefore, a large number of measurements were performed in the vortex. However, the outside edge of the vortex was sampled on the following day, 15 January 2003, and thus no measurement was found inside the vortex. The vortex disturbances started by 17 January 2003 and the vortex modified like a dumb-bell in the east–west direction (similar to the one shown in Fig. 3.2 for 21 January 2003), and therefore, only a part of the vortex was sampled on 19 January 2003. The warming intensified and the vortex moved up towards the pole and merged afterwards and hence, the measurements during 23–26 January 2003 sampled the vortex air near to the center of the pole only. The vortex became cold and near-concentric again and began to stabilise, as depicted in Fig. 3.2 for 3 February 2003. Consequently, the measurements taken during 7–9 February 2003 were mostly inside the vortex. The vortex shrunk by 12 February 2003 due to the severe warming and hence, no measurement was found inside the vortex during the transit flights on 12 February and 10 March 2003.

Even if the vortex split on 17 February 2003, it had strengthened again by merging its parts during the second leg of the flights (SCIA-VALUE 2003). So relatively large, strong and concentric vortices were observed for the following days of the flights. Therefore, a majority of the measurements were inside the vortex during the period 13–19 March 2003, except for the longitudinal flight on 14 March, where no vortex sampling was found at 475 K, although some measurements were found inside the vortex at higher altitudes. This indicates that the vortex was tilted up, and was not symmetric with altitude. For instance at 450–550 K, there were 13 days (out of 16) of vortex sampling with more than 100 (out of ∼180) ozone measurements.

The POAM measurements, however, have global coverage between 51° and 71°N (65°–90°N EqL) and thus the general meteorological situation described (Sect. 3.3.1) is fairly applicable to those observations. Despite limited to 71°N, as far as the nature of the winter and the Arctic vortex are concerned, this sampling pattern is sufficient to make a reasonable analysis of ozone loss, as the vortex was often displaced to mid-latitude regions due to the frequent warmings. Consequently, a large number of ozone measurements were found inside the vortex, i.e. around 550 out of ∼1500 measurements. The sampling pattern of these vortex observations can be found in Figure 3 of Singleton et al. (2005). Furthermore, these are also the best vortex-sampled satellite measurements available for this winter as compared to other satellite observations.

3.3.2 PSC and chlorine activation

We now look at the distribution of PSCs in the Arctic winter 2002/03. In this study, the A_{PSC} is defined as the area characterised by temperatures less than the NAT formation, T_{NAT}. The T_{NAT} calculation is performed by using the formula of Hanson and Mauersberger (1998), for which the temperature and pressure data are taken from ECMWF operational analyses, with a constant value of 4.5 ppmv of H_2O and a HNO_3 climatology for the Arctic winter stratosphere (Kleinböhl et al., 2002). The resulting calculation is displayed in Fig. 3.3.

In line with colder temperatures, large areas of PSCs are found in December and January. The maximum areas of these PSCs are found in the second half of December with values of 1.4–

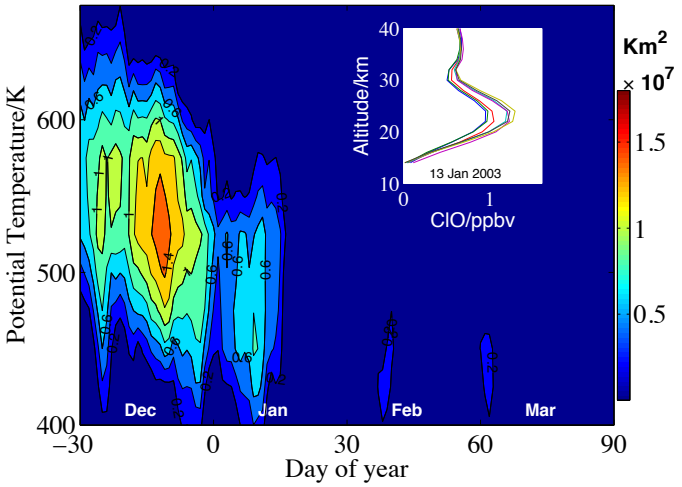

Figure 3.3: Area of PSCs as defined by the area below the T_{NAT}, which were calculated by using the method of Hanson and Mauersberger (1998) using ECMWF meteorological analyses with 4.5 ppmv of H_2O and climatological profiles of HNO_3 for the Arctic winter 2002/03. Inset: The ASUR ClO measurements taken inside the vortex (Nash et al., 1996) with SZA <89° on 13 January 2003. The ClO measurements were separated by a few minutes as illustrated with different colors. Though ASUR has ClO measurements on other flight days, profiles with the highest ClO VMRs (activated profiles) are displayed here.

1.7×10^7 km^2. The area of PSCs cover a large vertical extent of 450–625 K. As the temperatures began to increase by early January, the A_{PSC} is reduced considerably and shrunk to a small area at 450–525 K with peak values of about 0.7×10^7 km^2. After the MW, small areas of occasional PSCs are found in mid-February and early March for a few days below 475 K.

The ASUR ClO mixing ratio profiles observed inside the vortex (with solar zenith angle [SZA] <89°) on 13 January 2003 are presented in the inset of Fig. 3.3. The measured profiles with activated ClO are shown here. In agreement with the PSC calculations, the ASUR ClO measurements show activated chlorine/ClO of about 1.3 ppbv at around 22 km. These results are in good agreement with the findings of Tilmes et al. (2003) and Urban et al. (2004), who report high chlorine activation in early and mid-January in tune with the large areas of PSC in the early winter. Furthermore, Tripathi et al. (2006) also find a similar amount of ClO, about 1.2 ppbv at around 450 K, in the HALOX (HALogen OXide monitor) measurements (von Hobe et al., 2005; Günther et al., 2008) and MIMOSA-CHIM simulations on 15 January 2003.

3.3.3 Ozone and ozone loss

To derive ozone loss from the ASUR measurements, the passive tracer technique is applied and a detailed description of the method can be found in Chapter 6 and Kuttippurath et al. (2009). As the ASUR measurements are discontinuous and start in early January, we use the POAM ozone observations to get the complete evolution of the ozone and ozone loss from November through the end of March. This gives an opportunity to compare ozone and ozone loss from ASUR with those of POAM and the model. Our analysis with ASUR concentrates on the lower stratospheric isentropes of 450, 475, 500 and 550 K, where most of the loss occurs in the majority of Arctic winters (Rex et al., 2004; Kuttippurath et al., 2010a). The model ozone and tracer profiles are interpolated to the ASUR and POAM measurement locations. The comparisons are performed for each profile measurement and then averaged for each day if the measurements are inside the vortex (Nash et al., 1996). In order to compare the ASUR and model ozone, and to compute ozone loss from the ASUR measurements, the model ozone and tracer profiles are convolved with ASUR ozone averaging kernels to account for the lower vertical resolution of the ASUR measurements (Kuttippurath, 2005; Kuttippurath et al., 2007, 2010).

Figure 3.4 (left panel) illustrates the distribution of ozone from ASUR, POAM and the model, and the ozone loss computed from the ASUR, POAM and MIMOSA-CHIM data at 450–550 K for the Arctic winter 2002/03. The ASUR ozone and ozone loss at POAM overpass points, within 200 km, are also shown for comparison. However, since both ASUR data sets (all ASUR measurements and ASUR at POAM overpass measurements) show very similar values for ozone, the ASUR observations irrespective of POAM overpass (shown in blue) are discussed throughout this chapter. Instead of average values, all individual ASUR measurements close to the POAM locations inside the vortex are shown here to demonstrate the spread of ASUR measurements around the POAM data locations.

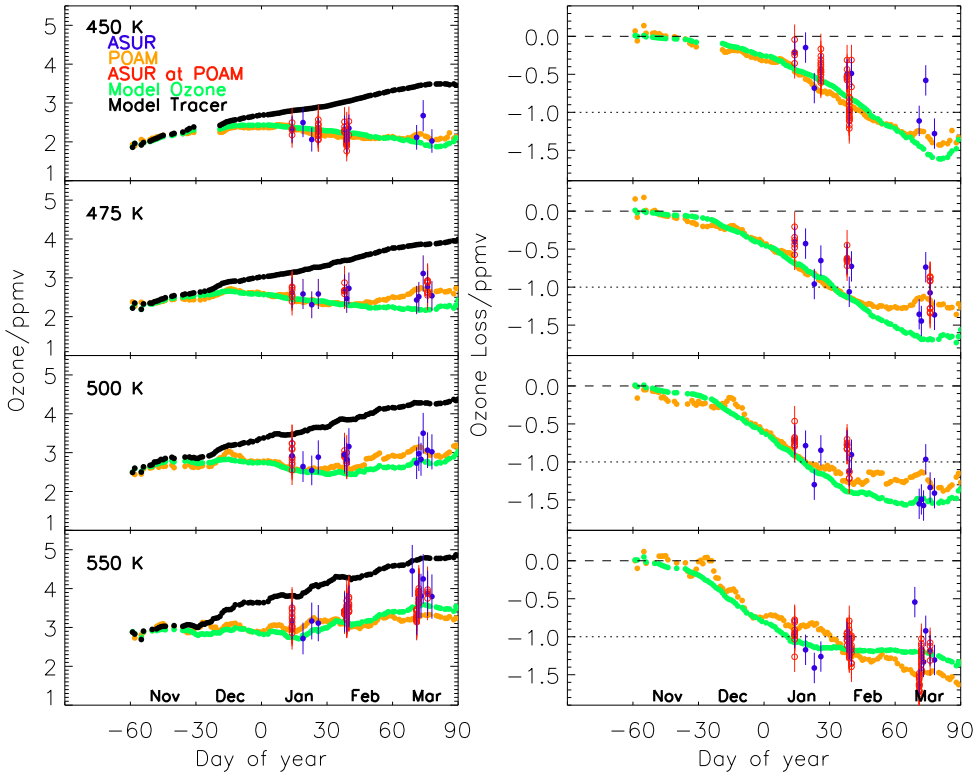

Figure 3.4: Vortex averaged ozone (left panel) and ozone loss (right panel) from ASUR compared to that of POAM and MIMOSA-CHIM CTM for the Arctic winter 2002/03. The ozone loss is computed as ASUR ozone-tracer at ASUR locations, POAM ozone-tracer at POAM locations, and modelled ozone-tracer at POAM overpass for each measurement inside the vortex, and then averaged for each day. The ASUR ozone observations sampled near to POAM measurements, within 200 km, and the corresponding ozone loss estimated using the model tracer are also shown (red points: ASUR at POAM). The modelled ozone and tracer are the interpolated data at the POAM overpass locations. The horizontal dotted lines (right panel) represent 1 ppmv of ozone loss. The data shown are smoothed for 7 days, except for ASUR.

This also illustrates the inhomogeneity of the ozone distribution inside the vortex.

The ozone data from ASUR and POAM and the model agree quite well at all altitudes in November through mid-February. However, the model underestimates the measured ozone by about 0.5±0.2 ppmv in March at 475 and 500 K. The model also overestimates the POAM and underestimates ASUR ozone by about 0.3±0.2 ppmv in March at 550 K.

Figure 3.4 (right panel) delineates the ASUR, POAM and MIMOSA-CHIM ozone loss at various lower stratospheric altitudes for the Arctic winter 2002/03. The ASUR ozone loss shows 0.7±0.2, 1±0.2, 1.2±0.2 and 0.9±0.2 ppmv at 450, 475, 500 and 550 K, respectively, by late January. Tripathi et al. (2006) and Streibel et al. (2006) aslo report correspondingly large ozone loss rates of around 4 ppbv sh^{-1} (parts per billion in volume/sunlit hour) and 6 ppbv sh^{-1} at 475 K and 500 K, respectively, by the end of January. This much ozone loss in mid-winter is uncommon in the Arctic (e.g. Newman et al., 2002; Goutail et al., 2005; Kuttippurath et al., 2010a). The loss rates are also higher than that found in other Arctic winters during this period of the winter (e.g. Rex et al., 2004; Kuttippurath et al., 2010a). The large areas of PSC occurrence and high chlorine activation at those parts of the vortex displaced into sunlight triggered this unusual ozone loss. The loss continued to occur at 450 K and reached a maximum of 1.3±0.2 ppmv by late March, in conjunction with cold temperatures found at this level, as shown in Fig. 3.3. However, further loss in ozone was mitigated by relatively higher temperatures and the absence of PSCs at higher altitudes. Therefore, the maximum loss was limited to 1.4–1.5±0.2 ppmv at 475–550 K. This excludes a single day measurement that showed a loss of about 1.6±0.2 ppmv by late January at 550 K.

The POAM observations find almost the same value of ozone loss for the ASUR measurement days at 450–500 K. In agreement with the lower ozone, the ozone loss is slightly higher in POAM at

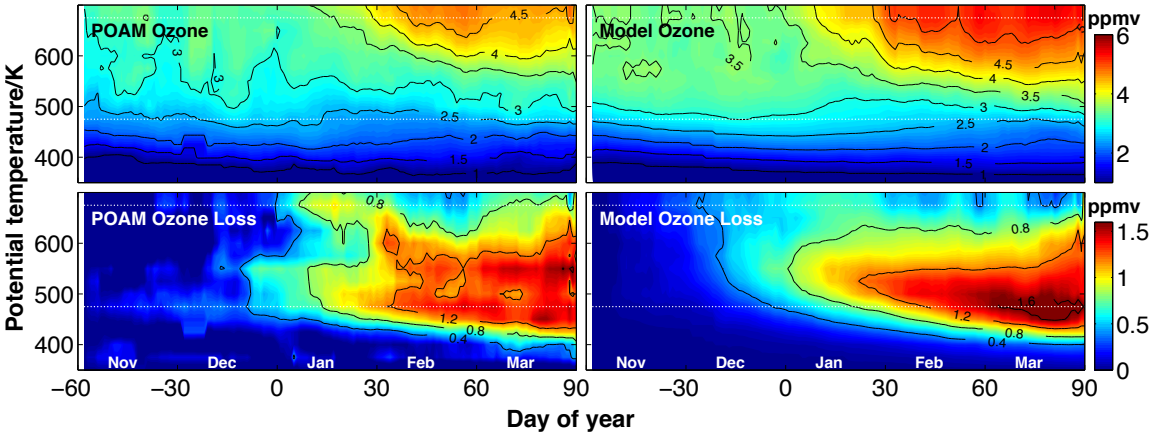

Figure 3.5: Temporal evolution of the vertical distribution of ozone and ozone loss in POAM and MIMOSA-CHIM CTM in the Arctic winter 2002/03. The loss is estimated inside the vortex using the Nash et al. (1996) criterion for each altitude and is smoothed for 7 days. The dotted horizontal lines represent 475 and 675 K.

550 K in March. The ASUR ozone loss is in good agreement with modelled loss for the respective days, except for March at 475 and 500 K, where the model overestimates both the ASUR and POAM ozone loss. POAM and MIMOSA-CHIM, however, exhibit slightly higher loss at some altitudes as the analysis extends to the end of March. Therefore, the ozone loss reaches 1.5±0.2 ppmv at 550 K in POAM and 1.6±0.2 ppmv at 475/550 K in MIMOSA-CHIM by the end of March, which are still in the error bounds of ASUR ozone, even though the model underestimates the measured ozone at 475 K. In general, the ozone loss estimated from ASUR data is in good agreement with that of POAM and MIMOSA-CHIM.

It has to be noted that the ozone loss in December is unusually large as it reaches about 0.5±0.2 ppmv at 450–550 K in both POAM and MIMOSA-CHIM. Feng et al. (2005b) report high chlorine activation down to 400 K in early December and as shown by the PV maps the vortex was very cold and elongated, which allowed vortex air to be frequently exposed to sunlight. Grooß et al. (2005b) too observe that the vortex spent more time at the sunlit parts of the mid-latitudes during this period compared to that of other Arctic winters. Therefore, the unusually cold temperatures initiated large areas of PSCs and subsequent chlorine activation, and the vortex excursions to sunlit parts of the mid-latitudes led to this large loss in ozone.

3.3.4 Vertical distribution of ozone and ozone loss

Apart from the inter-annual variability of ozone loss and the difference in ozone loss estimated by various techniques, there is also a spread in the altitude of maximum loss estimated by different instruments/methods for the same winter, as discussed in Kuttippurath et al. (2010a). In this study we have seen that ASUR, POAM and MIMOSA-CHIM show similar altitudes of maximum ozone loss. In order to study the vertical distribution of ozone loss closely, we use POAM measurements as ASUR observations are rather sporadic.

Figure 3.5 illustrates the resulting ozone (upper panel) and ozone loss (lower panel) evolution during the winter with respect to potential temperature. The model results are interpolated to each POAM overpass measurement and are sorted inside the vortex with respect to each altitude. The measurements show relatively small values (<2 ppmv) in the lower stratosphere in November–January. After the vortex split during the MW, the split vortices in the mid-latitudes constituted little higher ozone in February–March for the same altitudes. Nevertheless, these polar processes did not affect the vortex chemistry greatly as discussed earlier and hence, the change in ozone was not significant. The simulations show comparable values below 600 K, where the deviations are mostly within ±0.2 ppmv, but slightly larger above that altitude level.

Regarding the ozone loss, POAM and MIMOSA-CHIM follow similar timing and vertical extent in ozone loss distribution. The loss started by early December and intensified with the pres-

ence of large areas of PSCs by January around 475 K. As stated previously, the high ozone loss (0.7±0.2 ppmv) in the early winter is unusual compared to the previous (Goutail et al., 2005) and following winters (Kuttippurath et al., 2010a), and this makes the winter very distinct. The ozone loss in January–March is vertically spread at 425–650 K, and both POAM and MIMOSA-CHIM show the peak loss in late March. This highly vertically spread ozone loss coincides with the timing and location of the area of PSCs and chlorine activation. Studies with MIMOSA-CHIM (Tripathi et al., 2006) have already shown that there was significant denitrification in the vortex in 450–650 K in this winter. Since denitrification enhances accumulated ozone loss by removing HNO_3, which otherwise deactivates ClO into its reservoirs (Waibel et al., 1999), the contribution of denitrification to the additional ozone loss was estimated to be about 11–17% around 475 K in this winter (Tripathi et al., 2006; Grooß et al., 2005b). It indicates that, in addition to the chlorine activation, substantial denitrification was also found to be responsible for this large ozone loss.

Significant ozone loss is also observed at higher altitudes, especially above 600 K in January. This is due to the NO_x catalysed ozone destruction (Grooß et al., 2005b; Kuttippurath et al., 2010a), as large NO_x-rich air descended into the polar vortex from the mesosphere (Konopka et al., 2007; Huret et al., 2006) and subtropical air was transported to the Arctic (Kleinböhl et al., 2005a) during the period. Note that, in the PSC free stratosphere over 600–900 K, most loss occurs through the NO_x catalytic cycle with a rate limiting step between NO_2 and O (Kuttippurath et al., 2010a). The box model calculations of Konopka et al. (2007) also confirm that ∼76% of ozone loss at this altitude range was contributed by the NO_x cycle. This ozone loss estimated from POAM is reasonably reproduced by the MIMOSA-CHIM simulations. Apparently all data sets show the maximum loss of 1.3–1.5±0.2 ppmv in the 450–500 K altitude range. A recent study by Kuttippurath et al. (2010a) notes that the altitude of maximum ozone loss of Arctic warm winters is slightly higher than that of the cold winters. This feature is found in this warm winter too, which is also reported by Tripathi et al. (2006), but was in comparison with the cold Arctic winter of 1999/2000.

3.3.5 Column ozone loss

In order to get a comprehensive overview of ozone loss in this winter, we now compute the partial column ozone loss from the measurements and simulations inside the vortex. As most ozone loss occurs in the lower stratosphere, and to compare with other loss estimates, we have derived ozone loss in the column range of 400–550 K. The partial column ozone loss calculated from the available ASUR measurements shows 61±4 DU over 400–550 K in late March. The maximum loss estimated from the POAM measurements shows 63±4 DU, and the modelled ozone loss at the POAM overpass points shows 65±4 DU at the aforesaid column range for the same period. All data show a similar evolution of column ozone loss, such that they exhibit a loss of around 12±1 DU in December, 20–30±2 DU in January, 30–50±3 DU in February and 50–65±4 DU in March over 400–550 K. These exclude a single day POAM measurement that shows about 71±4 DU of ozone loss in mid-March in the same altitude range. The large loss in December, as discussed in Sect. 3.3.3, is also shown by the column values. Consistent with the good agreement in ozone and ozone loss comparison in VMRs, the ASUR and POAM measurements show similar column ozone loss. The slight difference between the ozone measurements is also reflected in their column ozone loss values, but are still within the error bars. Even if there are some differences in sampling patterns of both instruments, the sampled vortex air between 50° and 75°N shows similar loss. The modelled ozone loss at the observed points is in excellent agreement with the column loss estimated from the respective measurements.

3.3.6 Uncertainty of the estimated ozone loss

The first and foremost factor that can significantly affect the computation is the initialisation of the model runs for the tracer calculations. The model should be initialised with respect to the status of vortex in the early winter, i.e. in order to catch the early ozone loss as in the present case, the model run has to be initialised sufficiently early. Additionally, the passive method relies on the assumption that the ozone loss until the initial day is zero. So if there is an offset between the measured ozone and modelled tracer, the tracer/model ozone should be corrected with respect to the measured ozone. Otherwise, the ozone loss offset will be propagated and the derived loss will

Table 3.2: Vortex averaged (Nash et al., 1996) ozone loss estimated (by late March) from the ASUR, POAM and MIMOSA-CHIM data compared to different studies for the Arctic winter 2002/03. The passive tracer method is denoted by PS, tracer correlation method is marked by TC and the vortex averaged/profile descent method is denoted by VAO. The analyses based on station measurements (e.g. Kiruna) are denoted by §, model simulations are marked with ∗, analyses based on N_2O levels instead of altitude levels are marked with ‡ and estimates with total column measurements are shown with †.

Study	Method	Loss/ppmv	Peak altitude	Period	Data
Ozone Loss in VMR					
This study	PS	1.3–1.5±0.2	450–475 K	Jan–Mar	ASUR
This study	PS	1.3–1.5±0.2	500–550 K	Nov–Mar	POAM
Streibel et al. (2006)	Match	1.6±0.2	407 K	Dec–15 Mar	Match
Singleton et al. (2005)	PS	1.2±0.3	435 K	Dec–Mar	POAM
Christensen et al. (2005)	VAO	1.3±0.1	435 K	10 Dec–10 Mar	ozonesondes
Tilmes et al. (2003)	TC	1.5±0.0	440 K	16 Dec–Feb	HALOE
Ryskin and Kulikov (2008)	VAO	1.86±0.33	530 K	Dec–5 Mar	MWR§
El Amraoui et al. (2008a)	VAO	1.1±0.2	25ppbv/N_2O	15 Nov–15 Jan	SMR‡
Raffalski et al. (2005)	VAO	1.1±0.1	150ppbv/N_2O	mid/Dec–mid/Feb	MWR‡§
Sonkaew et al. (2013)	VAO	0.7±0.3	450–475 K	Dec–Mar	SCIAMACHY
Singleton et al. (2005)	PS	1.2±0.3	425–450 K	Dec–15 Mar	SLIMCAT∗
Grooß et al. (2005b)	PS	1.3±0.1	460 K	Dec–Mar	CLaMS∗
Tripathi et al. (2006)	PS	1.3–1.5±0.2	450–475 K	Nov–Mar	MIMOSA-CHIM∗
This study	PS	1.3–1.5±0.2	450–475 K	Nov–Mar	MIMOSA-CHIM @ POAM ∗
Ozone Loss in column		Loss/DU			
This study	PS	61±4	400–550 K	Jan–Mar	ASUR
This study	PS	63±4	400–550 K	Nov-Mar	POAM
Streibel et al. (2006)	Match	56±4	407–501 K	Dec–15 Mar	Match
Christensen et al. (2005)	VAO	68±7	380–525 K	10 Dec–10 Mar	ozonesondes
Tilmes et al. (2003)	TC	48±4	416–510 K	16 Dec–Feb	HALOE
Müller et al. (2007)	TC	43–47±6	380–550 K	Dec–22 Feb	HALOE/ILAS
Goutail et al. (2005)	PS	90±5	Total Col.	Dec–10 Mar	SAOZ†
Grooß et al. (2005b)	PS	46	380–550 K	Dec–15 Mar	CLaMS∗
Feng et al. (2005b)	PS	65	345–670 K	Dec–Mar	SLIMCAT∗
Tripathi et al. (2006)	PS	63±4	400–550 K	Nov–Mar	MIMOSA-CHIM∗
This study	PS	65±4	400–550 K	Nov–Mar	MIMOSA-CHIM @ POAM ∗

be corrupted. Another important factor to be considered is the proper selection of a vortex edge, as it is necessary to isolate the vortex from mid-latitude air. In this study we have tested three different criteria (above 65°N EqL, the vortex edge and vortex core), which all yield very similar results (not shown). The accuracy of the measurements (about 5–12%) is also to be accounted for. Therefore, to compute the uncertainty of the estimated ozone loss, we consider all the above-mentioned parameters, i.e. the accuracies of the ASUR and POAM, the mean difference between model and ASUR/POAM ozone, the average difference among the ozone loss computed by different vortex criteria, and the initial offset in ozone loss that used to correct the inferred ozone loss, and take root square sum (RSS) of them. The RSS of these quantities show about 0.17 ppmv or 3.5–5.1% at the studied altitudes, and can be considered as the accuracy of the loss estimated from ASUR and POAM observations.

3.4 Comparison with other estimates

There are several published results available for comparison with the ozone loss estimated in this study, which are listed in Table 3.2. The ASUR ozone loss of 1.3±0.2 ppmv at 400–500 K by late March is in good agreement with that of Singleton et al. (2005); Christensen et al. (2005); Grooß et al. (2005b) and Tilmes et al. (2003), as they show the maximum loss within 1.2–1.5 ppmv between 400 and 450 K. Furthermore, as found with the ASUR observations, El Amraoui et al. (2008a) also estimate the same ozone loss of 1.1±0.2 ppmv by mid-January at 475 K from the measurements of the Sub-millimeter Radiometer (SMR) on the Odin satellite. The loss estimated, 1.6±0.2 ppmv at 435 K by mid-March, from ozonesonde measurements by the Match method (Streibel et al., 2006) is close to the ozone loss estimated from ASUR observations. The ozone loss deduced from SCIAMACHY measurements, i.e. 0.7 ppmv at 425–475 K in late March, shows the lowest loss among the various estimates for this winter. This can be due to the sampling limitation of the sensor, as it cannot observe high latitudes in early winter (Sonkaew et al., 2013). As expected, the loss

determined from local measurements – Kiruna and Kola peninsula – (Raffalski et al., 2005; Ryskin and Kulikov, 2008) departs slightly from our loss estimates because of the uneven or undersampling of the vortex over a single station, as they essentially delineates the developments of the polar vortex over those stations only. Since the loss estimated from POAM and MIMOSA-CHIM data are similar to that of ASUR, the above-mentioned comparisons hold good for POAM and MIMOSA-CHIM too. Nevertheless, note that the model underestimates the measured ozone at 450–500 K and overestimates at 550 K. In agreement with the ASUR ozone loss, the maximum loss is estimated in the lower stratosphere by other methods too, with slight differences in the peak ozone loss altitudes (±25 K). Such discrepancies in the maximum loss altitudes were also reported by Grooß et al. (2005b) for this winter and Kuttippurath et al. (2010a) for 2004/05. It is interesting to note that the POAM measurements with the SLIMCAT passive tracer also infer a similar ozone loss of 1.2–1.5±0.3 ppmv by late March over 425–450 K (Singleton et al., 2005), as found in this study. These results corroborate the strength and consistency of the loss computation method and POAM data.

The column ozone loss computed from the ASUR observations is generally in good agreement with that from other techniques. For instance, the column loss calculated using ozonesonde measurements over 400–550 K around mid-March by Christensen et al. (2005) is in excellent agreement with those estimated from ASUR, POAM and MIMOSA-CHIM as they show a loss of 68±7 DU for the same period and altitude range. The ozone loss calculated by Feng et al. (2005b) and Tripathi et al. (2006) too find a similar loss of 65–67±4 DU over 400–550 K in late March. The loss estimate of Müller et al. (2007), 43–47±6 DU over 400–500 K, from the Halogen Occultation Experiment (HALOE) and the Improved Limb Atmospheric Spectrometer (ILAS)–II satellite measurements is in excellent agreement with our estimate of 45±3 DU over 400–500 K, around 22 February 2003. Their ozone loss estimate of 55±6 DU in 380–550 K by 22 March 2003 is close to our estimate for the same period, i.e. 60±3 DU over 400–550 K. The ASUR/POAM ozone loss estimates of 55±3 DU over 400–500 K by late March is in very good agreement with that inferred from the Match method, about 56±4 DU over 407–501 K in mid-March (Streibel et al., 2006). Nevertheless, the loss estimated by Tilmes et al. (2003), i.e. 48±4 DU over 416–510 K in mid-April, is lower than the above-mentioned loss estimates. The difference between our estimates in mid-March (55±3 DU) and the estimates of Grooß et al. (2005b) (about 46 DU) is also beyond the error bars of the compared data sets, but could be due to the differences in the loss estimation methods and data used for the analyses. In short, except these two loss values (i.e. Tilmes et al., 2003; Grooß et al., 2005b) all partial column estimates agree very well, and they show an average loss of 65±5 DU in 400–550 K in the Arctic winter 2002/03.

When our partial column estimates are compared to the total column estimates of Goutail et al. (2005), i.e. 90±5 DU, there is a difference of 25–30 DU. That total column loss equals to the loss usually estimated for a cold or moderately cold winter (Kuttippurath et al., 2010a; Harris et al., 2010; WMO, 2011). A recent study by Kuttippurath et al. (2010a) reports an average difference of 19±7 DU between the partial column loss calculated below and above 550 K. Apparently, this also demonstrates the difference between the ozone loss contributed by halogens in the lower stratosphere and NO_x in the middle stratosphere. In the Arctic winter 2002/03, the halogen dominated loss in the lower stratosphere is about 60–65 DU at 400–550 K. The difference between this partial column loss to the total column loss (i.e. 25–30 DU) is much larger than the expected average loss (19±7 DU) above 550 K. This hints at the special dynamics of the winter, as there was large mesospheric descent of NO_x-rich air masses and rapid meridional transport of subtropical air masses (Kleinböhl et al., 2005a), which offered a conducive atmosphere for ozone loss by the NO_x chemical cycle at higher altitudes. The study by Konopka et al. (2007) also confirms this ozone loss feature as they compute ∼27–30 DU (or 76%) column loss by the NO_x cycle, from satellite measurements above 550 K. Their column ozone loss (27–30 DU) matches exactly the difference computed between the partial column loss from our study and total column loss from Goutail et al. (2005) (i.e. 25–30 DU), and thus it suggests that the large loss above 550 K was due to the NO_x chemistry activated on a NO_x-rich air influx from the mesosphere and sub-tropics. To check this additional loss above 550 K, we computed the loss at 350–950 K (to the topmost level of the model) from the POAM and MIMOSA-CHIM data and it yielded 86±5 DU and 70±4 DU, respectively. These estimates are very close to the total column estimate of 90±5 DU by Goutail et al. (2005). Since the model overestimates the POAM ozone above 550 K and there is no upper stratosphere and mesosphere in the model, the

deficit in the simulated column loss is reasonably justified. This additional ozone loss above 550 K further manifests that the winter was very special in various aspects of stratospheric dynamics and chemistry.

3.5 Comparison with other Arctic winters

The Arctic winter stratosphere intermittently experiences major and minor warmings, which make large inter-annual variability in the ozone loss. Ozone loss estimates in the Arctic is available from various measurement sources for each winter since 1988/89 (Hofmann et al., 1989; Goutail et al., 2005; Tilmes et al., 2006; Harris et al., 2010; Kuttippurath et al., 2010a; WMO, 2011). Among these winters, 1994/95, 1995/96, 1999/00 and 2004/05 were very cold (Müller et al., 1997; WMO, 2007) and hence, the total column loss calculated from ground-based total ozone measurements showed >80–90 DU (Goutail et al., 2005; Kuttippurath et al., 2010a). The winters 1991/92, 1993/94, 1996/97, 1997/98, 2006/07 and 2007/08 were moderately cold and thus the total column loss was in an average scale of around 60 DU (Andersen and Knudsen, 2002; Goutail et al., 2005; Kuttippurath et al., 2010a). On the other hand, the winters 2000/01, 2003/04, 2005/06 and 2008/09 were subjected to minor and major warming events with subsequent break in the long persistence of polar vortex. Therefore, ozone loss computed in these warm winters showed the lowest values of around 25–30 DU (Goutail et al., 2005; Kuttippurath et al., 2010a). In addition to the total column, similar amounts of ozone loss were also estimated in the partial column range of 380–550 K from ozonesonde measurements for all winters (Rex et al., 2004; Harris et al., 2010) and hence, they also express analogous features of ozone loss. Although the loss estimated from satellite measurements (Tilmes et al., 2006) show slightly lower values than those estimated from the ground-based/Match (Goutail et al., 2005; Rex et al., 2004) measurements for individual years, those analyses still show a corresponding difference between the loss derived in the warm and cold winters (Andersen and Knudsen, 2002), as discussed for the total column measurements.

When comparing the ozone loss of 65±5 DU in 400–550 K in this winter, as analysed from the ASUR, POAM and MIMOSA-CHIM results together with other published works, to the loss estimated in the Arctic winters since 1989, the estimated loss in 2002/03 is close to the estimates for the moderately cold winters. Furthermore, in line with the column ozone loss, the loss found in mixing ratio also exposes a distinct difference between the range of ozone loss observed in the cold and warm winters, with a loss of ∼1.5–2.1 ppmv in cold (Rex et al., 2004; Kuttippurath et al., 2010a) and about 0.5–0.7 ppmv in warm winters (Manney et al., 2003; Rex et al., 2004; Kuttippurath et al., 2010a; Sonkaew et al., 2013). Therefore, the ozone loss computed in 2002/03, i.e. 1.5±0.3 ppmv, stays between these cold and warm winter estimates. Apart from the significant ozone loss in December (0.5±0.2 ppmv at 450–500 K or 12±1 DU in 400–550 K), such large loss in a winter with three minor and a major warming is exceptional, and is occurred for the first time in the Arctic over 1989–2010, and this makes the Arctic winter 2002/03 unique.

3.6 Conclusions

The Arctic winter 2002/03 was remarkable as it was characterised by an unusual cold spell in the first half and a MW in the second half. Therefore, large areas of PSCs are found at 450–625 K from December through mid-January. A wave 1 event led to the MW around 18 January 2003 and thus the high temperatures inhibited the formation of PSCs afterwards. However, the easterlies did not prevail, though only diminished amplitudes of westerlies were present in the later part of the winter. In addition to the MW in mid-January, there were three minor warmings in mid-December, mid-February and early March. Though the vortex split during the MW in mid-January and during the minor warming in mid-February, it did not disappear until early April. Since the vortex split was confined mostly to the lower stratosphere and was not observed at 10 hPa on the central date, the MW can be classified as a vortex displacement event.

The ozone loss determined with the ASUR measurements taken during the EuPLEx and SCIA–VALUE 2003 airborne campaigns shows large values in the mid-winter. The ASUR measurements show the maximum ozone loss of 1.3±0.2 ppmv at 450–500 K, from the available measurements

until late March. The partial column loss calculated from ASUR observations over 400–550 K shows about 61±4 DU in the same period. These ozone loss estimates, both in mixing ratios and partial column, are in very good agreement with those derived from POAM, MIMOSA-CHIM CTM and other available published results for this winter. The POAM/MIMOSA-CHIM loss amounts to 0.5±0.2 ppmv at 450–550 K or 12±1 DU in 400–550 K in December, which is uncharacteristically large during this period in the Arctic winter stratosphere. The uncommon ozone loss in the early winter was due to very low temperatures, large areas of PSCs, significant vortex wide denitrification and strong chlorine activation, as the vortex moved to sunlit parts of the adjacent mid-latitude regions.

In this chapter we have presented both the dynamical processes in the minor and major warmings, and the chemical ozone loss during the Arctic winter 2002/03. The ASUR measurements used for the diagnosis of ozone loss have not hitherto been used for the study of this winter. The heat flux, momentum flux, EP flux, EP flux divergence and PV maps were used for the description of the dynamical situation, which were not presented together to characterise this winter before. On average, in conjunction with all published results, this winter was experienced with a maximum ozone loss of 1.5±0.3 ppmv at 450–550 K or 65±5 DU in 400–550 K by late March. Interestingly, the values inferred from a number of estimates rightly coincide with those derived in our study (1.3±0.2 ppmv or 63±4 DU at the same altitude ranges). When compared to other Arctic winters, as analysed from this work, this winter has a unique feature of three minor warmings, a MW and large ozone loss that usually observed in a moderately cold winter, in addition to its unusually large ozone loss in December–January.

Chapter 4

Arctic ozone loss: 2004/2005–2009/2010 *

Contents

Compelling improvements have been made in understanding the chemistry of ozone loss in the polar lower stratosphere in the last decade (WMO, 2007). As described in Chapter 1, very low temperatures (<195 K) initiate the formation of PSCs, and chlorine activation on these PSCs triggers the ozone loss when the sun returns over the Arctic in spring. The halogen cycles ClO–ClO and ClO–BrO contribute about 80–90% of ozone loss in this region through the above-said processes (WMO, 2007). However, ozone loss at higher altitudes is driven by different chemical cycles than those discussed in the lower stratosphere. A detailed study on the ozone loss process at higher altitudes (above 550 K) is still lacking. The available studies deal with specific issues of mid-winter warming and concomitant mid-latitude ozone loss (e.g. Grooß et al., 2005b; Vogel et al., 2008). None of these studies perform a detailed analysis of the winter stratosphere in different conditions to diagnose the contribution of relevant cycles to the ozone loss in a concluding manner. Although the study by Konopka et al. (2007) deal with more than one winter, it is limited to a box model rather than a full-chemistry 3-D model. Therefore, a comprehensive study is warranted to characterise the contribution of various chemical cycles to the ozone loss in the polar stratosphere in different meteorological conditions. The recent six winters were entirely different in this regard, which provide a perfect scenario to perform such a study. So in this chapter, we examine the ozone loss and its driving chemical cycles for the recent winters 2004/05–2009/10 and assess the variability of ozone loss in a quantitative perspective using simulations and measurements.

4.1 Data and methods

An improved version of the MIMOSA-CHIM CTM is used for this study (Kuttippurath et al., 2009). The model spatial domain is now extend from 10°S to 90°N in the NH and from 90°S to 10°N in the SH. Also, the vertical levels are increased from 16 to 25 isentropical levels and are finely resolved with a spacing of 5 K (between 425 and 500 K) in the lower stratosphere. Although other model specifications and input are unchanged as described in the previous chapter 3, absorption cross-sections and kinetics data are based on Sander et al. (2006). The absorption cross-sections of Cl_2O_2 are taken from Burkholder et al. (1990) and are extrapolated to 450 nm. Monthly varying H_2SO_4 fields leading to the formation of liquid aerosols in the CTM are computed from the output of a 2-D-model long-term simulation, which considers the impacts of volcanic eruptions. Cl_y and Br_y are explicitly calculated from their long-lived sources at the surface and are therefore, time

*This chapter is partly based on: Kuttippurath, J., S. Godin-Beekmann, F. Lefèvre and F. Goutail: Spatial, temporal, and vertical variability of polar stratospheric ozone loss in the Arctic winters 2004/2005–2009/2010, Atmos. Chem. Phys., 10, doi:10.5194/acp-10-9915-2010, 9915–9930, 2010.

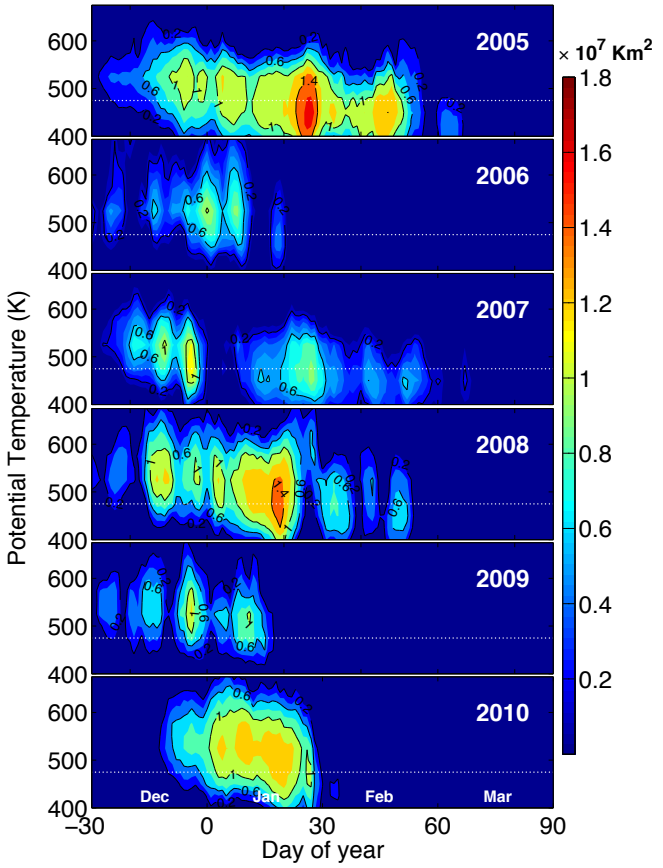

Figure 4.1: The area (km^2) covered by PSCs (between 400 and 675 K) estimated from the ECMWF temperature data for the Arctic winters 2004/05–2009/10. PSCs are assumed to form at the NAT frost point. The dotted line represents 475 K and the topmost boundary stands for 675 K.

dependent. An additional 6 pptv of bromine in the form of CH_2Br_2 is added to Br_y to represent the contribution of brominated short lived species reaching the stratosphere (WMO, 2007). For each Arctic winter considered here, the model was run from 1 December to 31 March. Initialisation of ozone on 1 December was provided by the ECMWF operational analyses. Other species in MIMOSA-CHIM were initialised from a long-term simulation of the REPROBUS CTM driven from ECMWF meteorological analyses.

Ozone and ClO observations (v 2.2) from the Microwave Limb Sounder (MLS) on Aura are used to compare with the simulations. The retrieved ozone profiles have a vertical range of 215–0.02 hPa and a vertical resolution of ∼3 km, while the horizontal resolution of a profile is ∼200 km. The vertical range of ClO is 100–0.1 hPa and the vertical resolution is 3–3.5 km, whereas the horizontal resolution ranges from 350 to 500 km. The estimated accuracy is 5–10% for ozone and 10–20% for ClO depending on altitude (Froidevaux et al., 2006; Santee et al., 2008).

4.2 Temperature distribution during the winters

Figure 4.1 shows the A_{PSC} calculated from the ECMWF temperature and pressure data for the last six winters. PSCs are assumed here to form at the NAT frost point according to Hanson and Mauersberger (1998) and are calculated using climatological values of HNO_3 and H_2O, as described in the previous chapters. Winter 2004/05 shows the largest PSC area with a maximum of 1.7×10^7 km^2 in late January. Considerable area of PSC is also found in December–January 2008, with a maximum of 1.4×10^7 km^2 in mid-January. Due to a vortex split occurrence in mid-December at 475 K and a major warming in February 2010, Apsc during the winter is reduced and it shows a maximum of 1.2×10^7 km^2 in mid-January. The warm winters 2005/06 and 2008/09 show much smaller PSC area, limited to the late December–early January period with a peak area of about 0.8×10^7 km^2. In winter 2006/07, the largest area of PSCs, 1×10^7 km^2, are observed in late December.

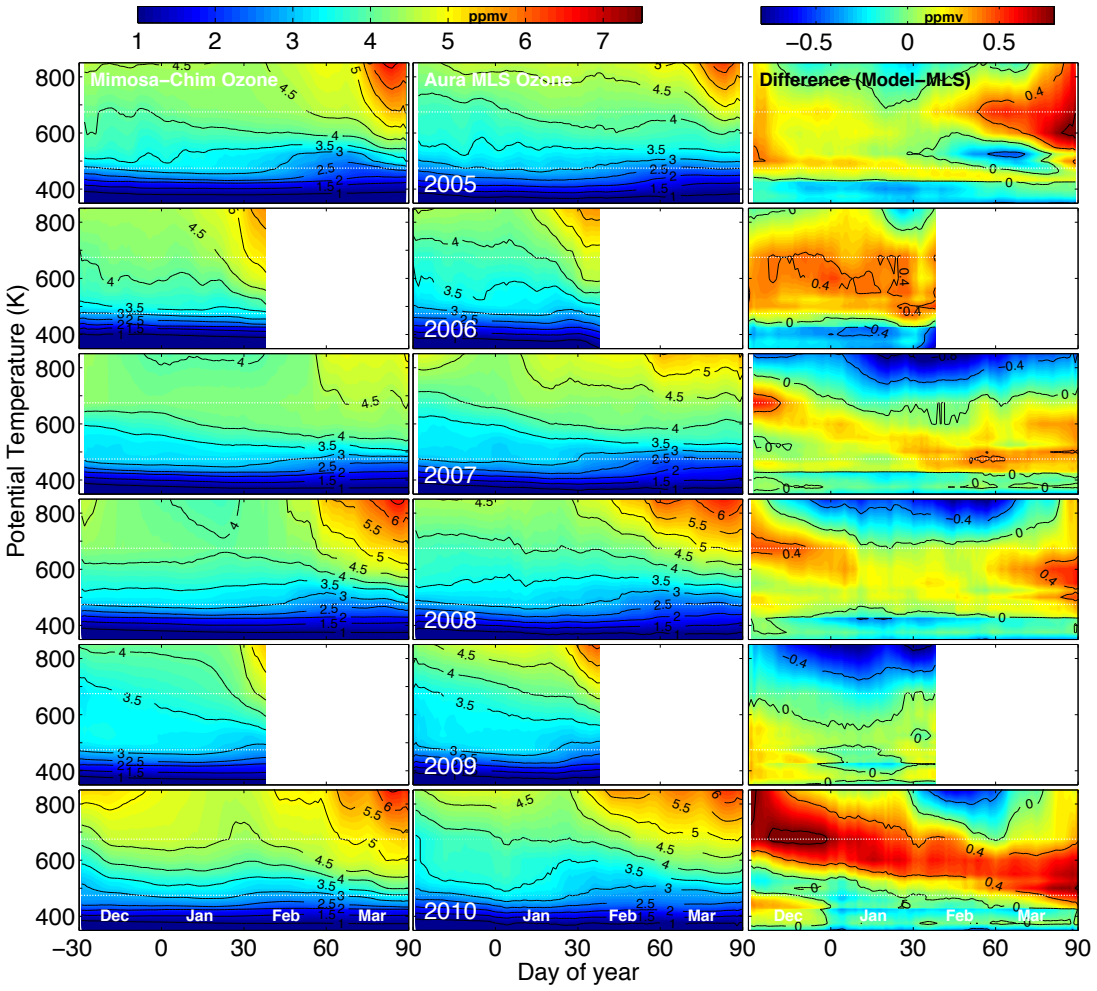

Figure 4.2: Temporal evolution of the vertical distribution (350–850 K) of vortex averaged (≥65° EqL) ozone (ppmv) for the Arctic winters 2004/05–2009/10. Left: MIMOSA-CHIM calculations, Middle: MLS measurements and Right: The difference between modelled and measured ozone. The model fields are sampled at location of the MLS observations. Due to early vortex dissipation caused by major SSWs, the analysis does not extend beyond 10 February in 2006 and 2009. Both model results and data are smoothed for seven days. The white dotted lines represent the study altitudes 475 and 675 K.

4.3 Results

We look into the details of ozone loss process of the recent winters in this section. Since the passive method used for the loss diagnosis depends on tracer simulations, the quality of the model simulations has to be checked. Therefore, we compare the ozone calculations with MLS observations, as the instrument provides measurements of a number of compounds linked to polar ozone loss.

4.3.1 Ozone: simulation and comparison with MLS

Figure 4.2 displays the vertical distribution of the MIMOSA-CHIM and MLS ozone together with their difference, sampled at the same time and location of the satellite observations. The results are averaged inside the polar vortex defined as the area enclosed inside 65° N of EqL (see Müller et al., 2008 for further discussions on definition of polar vortex). Due to early final warming (since there was no strong or well-defined polar vortex, we take the major warming in late January/early February 2006 and 2009 as the final warming), the data beyond these events are not considered in this study.

Both simulations and measurements show similar maximum and exhibit a rather good agreement, with differences within ±0.5 ppmv depending on isentropic level and time. In general, the

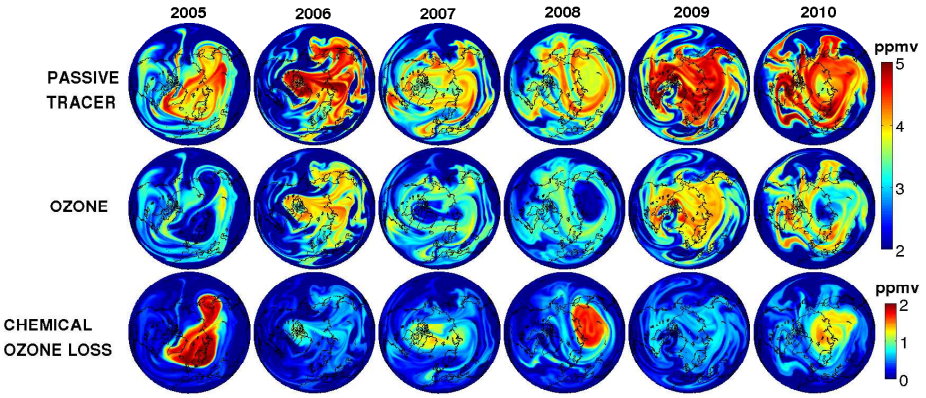

Figure 4.3: Maps of passive tracer, ozone and chemical ozone loss (passive tracer-ozone) calculated by MIMOSA-CHIM at 475 K on 15 March 2004/05–2009/10.

comparison yields good agreement in the lower stratosphere, below 500 K in particular. The calculations are in good agreement with the observations in the winters 2006/07, 2007/08 and 2008/09. The model captures well the ozone enhancement during the SSWs, specifically at higher altitudes, in January–February 2006 and 2009. The simulated middle stratospheric ozone levels during these periods are higher than those of other winters in accordance with the observations. In February 2010, the higher ozone values due to meridional transport of ozone rich air masses from low latitudes, associated with a major SSW, can also be seen in both data sets. Inter-annual variability in the evolution of ozone with altitude is apparent in the figure. For instance, the winter 2004/05 shows low ozone values in the lower stratosphere up to 600 K and the ozone maximum in the winter 2006/07 is comparatively smaller than that of other winters. Nevertheless, as displayed in Fig. 4.2, the simulations systematically overestimate (up to 0.7 ppmv) the observations in early December and March above 600 K in all winters, due to differences in subsidence. This difference is found to be largest in March 2005, and in December and March 2010. In 2005/06, the model shows higher values of around 0.25 ppmv from December to February at 500–800 K. Conversely, the calculations underestimate (up to 0.5 ppmv) the measurements in January–February below 450 K and above 675 K in most winters. Among the winters the smallest differences are found in 2007/08 and the largest in 2009/10.

4.3.2 Ozone loss

4.3.2.1 Model simulations

Fig. 4.3 shows the passive tracer, ozone, and the difference (chemical ozone loss) calculated at 475 K on 15 March for each winter. In the figure, polar vortices with high ozone mixing ratios of around 4.5 ppmv corresponding to warm winters and reduced mixing ratios of around 3 ppmv corresponding to cold winters, are clearly shown.

Since the winter 2004/05 was one of the coldest, a vast vortex and large reduction in ozone is simulated, suggesting sustained and large ozone loss in that winter. Although not as large as observed in 2004/05, a significant area of low ozone levels off the pole is visible in 2007/08. Due to a strong SSW in mid-January, there was no vortex afterwards and hence, high ozone is simulated in 2005/06 and 2008/09. In 2006/07, the vortex was seemingly smaller and therefore, the ozone loss is reduced. In 2009/10, even though there was a major SSW in late January forced by a wave 1 event, the vortex split during the period and then merged again afterwards. Therefore, a small dissipated vortex, displaced to the mid-latitudes, with moderate ozone loss is simulated in that period. The maps displayed in Fig. 4.3 clearly illustrate the strong inter-annual variability in the meteorology and ozone loss in the Arctic, with large loss (2 ppmv) diagnosed inside the vortex in 2004/05 and 2007/08, more limited loss in 2006/07 and 2009/10 (0.8–1 ppmv), and the absence of vortex, as of 15 March, in 2005/06 and 2008/09. Thus as discussed previously, the most recent Arctic winters show a wide variety of polar processing, quite in line with previous northern winters (WMO, 2007).

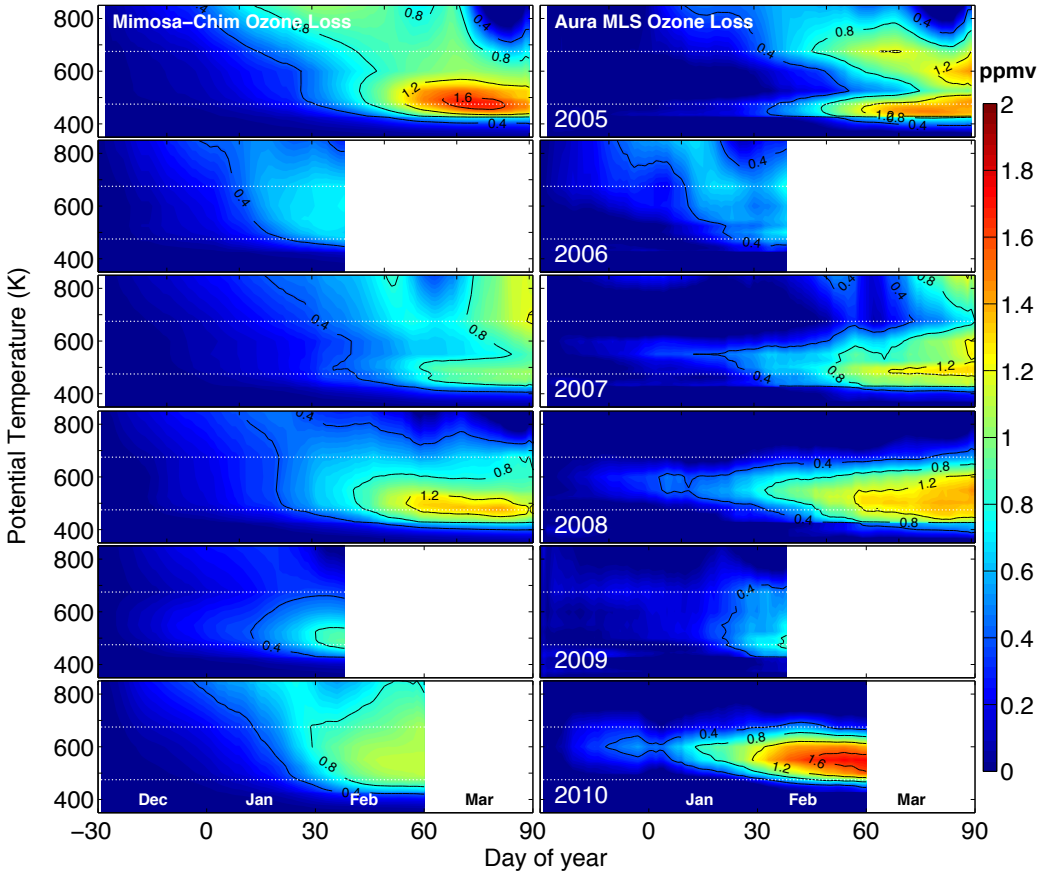

Figure 4.4: Temporal evolution of the vertical distribution (350–850 K) of vortex averaged (≥65° EqL) ozone loss (ppmv) estimated for the Arctic winters 2004/05–2009/10. Left: the ozone loss derived from the difference between the passive tracer and the chemically integrated ozone by MIMOSA-CHIM. Right: the ozone loss derived from the difference between the MIMOSA-CHIM passive tracer and the ozone measured by MLS. The model fields are sampled at location of the MLS observations. Due to early vortex dissipation caused by the major SSWs, the analysis does not extend beyond 10 February in 2006 and 2009, and 28 February in 2010. Both model results and measurements are smoothed for seven days. The white dotted lines represent 475 and 675 K.

4.3.2.2 Comparison with MLS

Figure 4.4 (left panel) displays the vertical structure of the accumulated chemical ozone loss computed from the simulations for the winters 2004/05–2009/10. The vortex averaged ozone loss computed from the model grids and at the MLS sampling points show rather small differences. Therefore, we present the ozone loss computed at the MLS footprints inside the vortex for each winter for comparison purpose.

Among the winters, 2004/05 exhibits the largest ozone loss with a maximum of 1.7 ppmv in March around 475 K. The loss is spread vertically between 450 and 850 K in January–February, reaching 1.5 ppmv above 600 K in late February. In March, most of the loss is confined between 400 and 600 K. Comparatively large losses are also found in the cold winters 2006/07 and 2007/08. In 2006/07, the ozone loss shows a double peak feature with a maximum of 1.3 ppmv at 675 K. In 2007/08, the loss is delimited between 450 and 600 K with a peak loss of 1.4 ppmv around 475 K. Little loss is computed above the 650 K level in this winter. Due to major SSWs, the winters 2005/06 and 2008/09 show restricted ozone loss, about 0.8 ppmv. The winter 2008/09 presents the smallest vertical extent in the derived ozone loss, which is mainly found below 650 K until the final warming. In 2009/10, a wide spread loss of around 0.9 ppmv from mid-January to February at 450–800 K with a peak loss of about 1.1 ppmv at 600 K is estimated. Ozone loss analysis for this winter is restricted until February due to problems in tracer descent after the warming, as identified from the modelled N_2O isopleths. Additionally, there was no activated chlorine to induce a sustained loss afterwards in March.

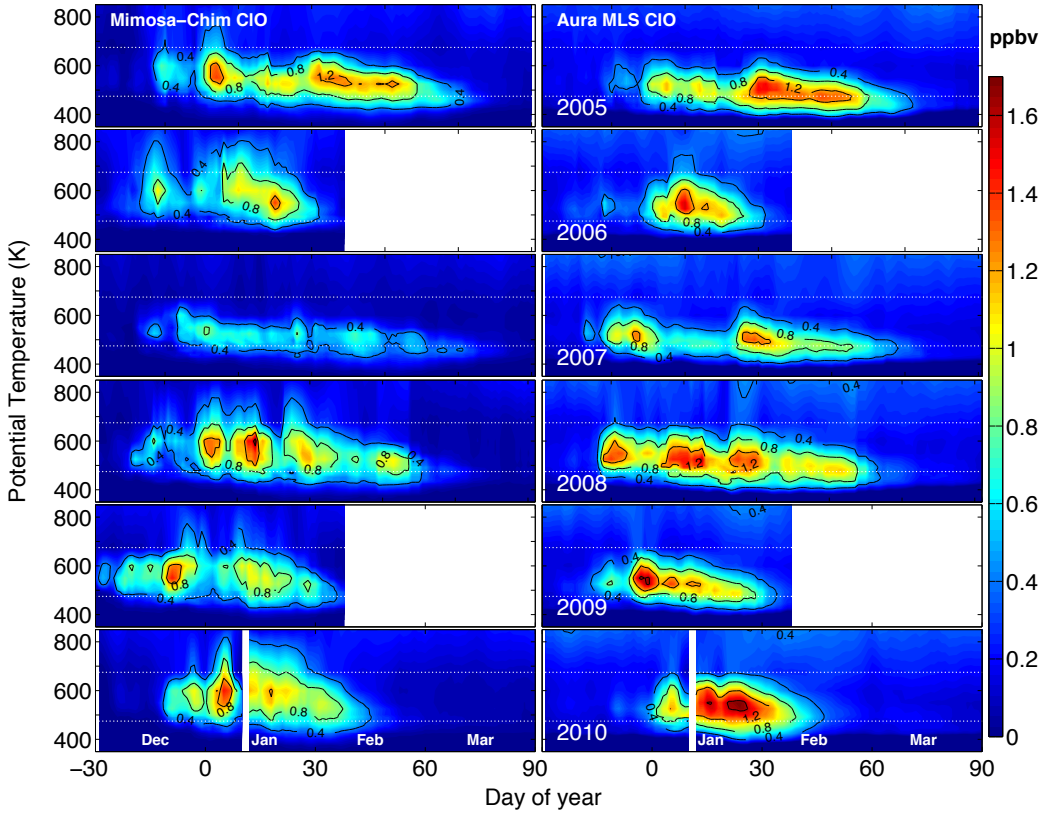

Figure 4.5: Temporal evolution of the vertical distribution (350–850 K) of vortex averaged (≥65° EqL) ClO (ppbv) for the Arctic winters 2004/05–2009/10. Left: MIMOSA-CHIM calculations and Right: MLS measurements. The model and MLS ClO coincident profiles are selected for SZAs <89° and local time between 10 and 16 h. Both simulations and measurements are smoothed for three days.

Figure 4.4 (right panel) illustrates the temporal evolution of the vertical distribution of vortex averaged ozone loss derived from the observations. Ozone loss from the measurements is computed in a similar way as for the simulation. In agreement with the calculations, comparatively large losses are estimated from the measurements in 2004/05 and 2007/08, reaching 1.5 and 1.4 ppmv, respectively. The simulations reproduce quite well the gross features of observed ozone loss in each winter, e.g. its onset in the course of the winter, the altitude of its maximum and its vertical distribution. The agreement between the model and MLS is particularly good in 2005/06, 2006/07, 2007/08 and 2008/09, where the differences are mostly within ±0.2 ppmv. As shown in Fig. 4.2, the modelled ozone in March is comparatively larger and therefore, the maximum ozone loss is slightly smaller in the model depending on altitude. In 2009/10, the computed loss from MLS observations is about 0.5 ppmv larger than that of MIMOSA-CHIM. This difference is due to relatively larger values (0.5–0.8 ppmv) in the simulated ozone throughout the winter at 500–700 K and also because of larger passive tracer values simulated after the SSWs, as compared to previous winters. However, in 2004/05 the model does simulate the second ozone loss maximum observed around 600 K, albeit with a lesser amplitude. In both cases, the results show a large loss in the middle stratosphere, as compared to other winters followed by its strong decrease in March. In addition, both the simulations and observations provide the largest loss above 500 K in 2006/07. To further investigate the causes of differences in the estimated ozone loss, we now analyse the measured chlorine activation and its representation in the model.

4.3.2.3 Comparison: Chlorine activation

Figure 4.5 compares the temporal evolution of vertical distribution of vortex averaged ClO extracted from MLS observations and MIMOSA-CHIM simulations for various winters. As expected from large areas of PSCs, the observations show high chlorine activation in 2004/05, 2007/08 and 2009/10 with

Table 4.1: The vortex averaged (≥65° EqL) ozone loss estimated in VMR (ppmv) from MIMOSA-CHIM and MLS data compared to different studies for the Arctic winter 2004/05. The initial offset in tracer and MIMOSA-CHIM ozone is corrected with respect to MLS ozone to avoid any bias in the loss computations. The passive method is denoted by PT and the vortex averaged/profile descent method is denoted by VAO. The estimates based on assimilated data are indicated by *.

Study	Method	Loss/ppmv	Peak altitude	Period	Measurements
This study	PT	1.5	475 K	Dec/Mar	MLS
Manney et al. (2006)	VAO	1.5	450 K	Jan/10 Mar	MLS
El Amraoui et al. (2008b)	VAO	1.5	425 K	10 Jan/10 Mar	MLS
Singleton et al. (2007)	PT	1.8	450 K	Jan/Mar	MLS
Jin et al. (2006)	Various	1.8–2.3	475–550 K	1–7 Jan/mid-Mar	ACE/FTS
Rex et al. (2006)	Match	1.3–2.1	450–475 K	Jan/25 Mar	Ozonesondes
Tsvetkova et al. (2007)	VAO	1.7	450 K	Jan/25 Mar	SAGE III
Rösevall et al. (2007)	VAO	1.3	450 K	Jan/14 Mar	MLS*
Jackson and Orsolini (2008)	VAO	1.2	450 K	early Jan/early Mar	MLS/SBUV2*
Rösevall et al. (2007)	VAO	0.6–0.9	450 K	Jan/14 Mar	SMR/Odin*
					Simulation
This study	PT	1.7	475 K	Dec/Mar	MIMOSA-CHIM
Grooß and Müller (2007)	PT	1.4±0.3	475 K	Jan/Mar	CLAMS
Singleton et al. (2007)	PT	2.4/2.3	450/475 K	Jan/Mar	SLIMCAT

enhanced ClO values in the lower stratosphere up to about 600 K. In these winters, vortex averaged ClO reach 1.2–1.5 ppbv around 550 K in January. Chlorine activation usually starts in December above 475 K (in late December during the first two winters and a little earlier in the later ones) and then extends lower down in the course of the winter. Both simulated and measured ClO occupy a larger vertical stretch and exhibit higher values in January 2010 when compared to other winters, consistent with larger ozone loss estimated in that period. The simulations generally reproduce the observed ClO and its variability throughout the winter quite well, although some differences are evident. In 2004/05 and 2009/10, a stronger chlorine activation extending up to 650 K is simulated in late December compared to the observations. In 2004/05, later during the winter, higher ClO values are observed in MLS extending up to mid-March. This discrepancy explains the stronger ozone loss derived from the observations at 500–600 K in March (see Fig. 4.4). In 2006/07, MIMOSA-CHIM clearly underestimates the observed chlorine activation. The vortex averaged ClO in MIMOSA-CHIM is lower by about 0.4 ppbv, which explains the reasons for the underestimation of ozone loss in the simulations for that year. In other winters, the simulations show generally a good agreement with the observations at most altitudes. A closer examination of the ozone loss in the lower and middle stratosphere at two representative isentropic levels, 475 and 675 K, is presented in the following sections.

4.3.2.4 Comparison: lower stratosphere

As shown by Fig. 4.4, the simulated ozone loss until January is generally within 0.2 ppmv and it varies in January–March for each year at 475 K. The maximum ozone loss derived from the simulations is 1.7, 0.7, 1.1, 1.3, 0.9 and 0.9 ppmv in 2004/05, 2005/06, 2006/07, 2007/08, 2008/09 and 2009/10, respectively. The corresponding observed losses are in turn 1.5, 0.7, 1.2, 1.4, 0.8 and 0.9 ppmv, and are in very good agreement with the simulated ones, where the differences are within ±0.2 ppmv.

The ozone loss estimated from our study is in general good agreement with those found with other techniques for the winter 2004/05 (WMO, 2007), 2005/06 (Manney et al., 2007) and 2006/07 (Rösevall et al., 2008). Table 4.1 presents the comparison of ozone loss derived from various measurements and model calculations for the winter 2004/05. The maximum loss simulated at 475 K is about 1.7 ppmv (1.5 ppmv from MLS) in 2004/05, which compares well with that of Grooß and Müller (2007). Our loss estimates are also in very good agreement with those of Jackson and Orsolini (2008); Rösevall et al. (2007); Singleton et al. (2007) and Tsvetkova et al. (2007), as we compute comparable values in respective periods. It must be noted that the ozone loss inferred from MLS observations by Manney et al. (2006) and El Amraoui et al. (2008b) also show the same maximum of 1.5 ppmv, which greatly support our ozone loss computation technique. However, the peak ozone

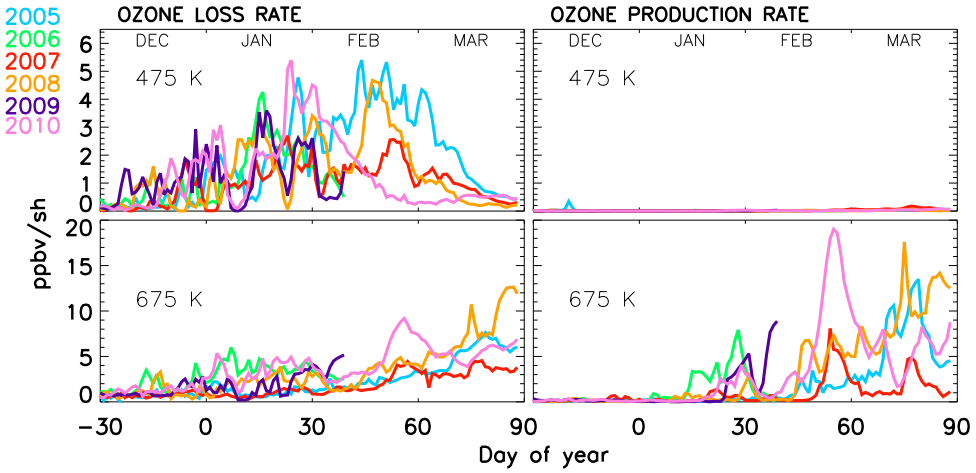

Figure 4.6: Vortex averaged (≥65° EqL) chemical ozone loss and production rates at 475 and 675 K, expressed in ppbv sh^{-1}, for the Arctic winters 2004/05–2009/10. The data are exempted from temporal smoothing to explicitly show the effect of daily movement of vortex and its impact on ozone production and loss rates.

loss altitude shown by some studies are generally about 25 K lower than in our analysis. Such a discrepancy among various techniques was also noted by Grooß et al. (2005b) and Kuttippurath et al. (2011) for the winter 2002/03, as presented in Chapter 3. The only diagnosis that departs considerably from all other evaluation is Rösevall et al. (2007). This could be due to the peculiarity of their method, which is prone to more mixing and dilution in the vortex air. The vertical motion was not represented explicitly but was calculated from N_2O measurements in their analyses. Other details regarding the method can be found from Jackson and Orsolini (2008), who provide a brief comparison of most ozone loss estimation techniques. In agreement with the measured and simulated ozone loss and Apsc, the chlorine activation is predominant in 2004/05 and 2007/08, moderate in 2009/10, and weak in 2006/07 at 475 K. The winters 2005/06 and 2008/09 started off with low temperatures and therefore, subjected to early chlorine activation and ozone loss compared to other winters. Note that a similar range of ozone loss values, from 0.7 to 2.3 ppmv, was also computed for the cold Arctic winter 1999/00 by various methods (Newman et al., 2002).

4.3.2.5 Comparison: middle stratosphere

As evident in Fig. 4.4, the simulated ozone loss at 675 K is around 0.2 ppmv in early January in most winters. The maximum loss reaches 1.1, 0.7, 1.2, 0.8, 0.3 and 0.9 ppmv in 2004/05, 2005/06, 2006/07, 2007/08, 2008/09 and 2009/10, respectively. The loss derived from observations show successively 1.2, 0.6, 0.8, 0.7, 0.5 and 0.7 ppmv for the corresponding winters. The simulated ozone loss shows good agreement with that of observations, within ±0.2 ppmv. The large loss calculated around 675 K in January–February 2005 is also confirmed by other estimates (Jin et al., 2006; Rex et al., 2006; Grooß and Müller, 2007; Tsvetkova et al., 2007; Jackson and Orsolini, 2008). The estimated loss at 675 K is in good agreement with that of Grooß and Müller (2007), who simulate a similar loss at this altitude. The double peak structure is not pronounced in the analysis of Singleton et al. (2007) and thus the measured and simulated ozone loss in their study are considerably smaller (about 0.7 ppmv) than our estimates. There is only a little amount of active chlorine present at 675 K, as most of it is found below 600 K. Therefore, key factors driving ozone loss at 675 K will be discussed in the succeeding sections.

4.4 Discussions

4.4.1 Ozone loss and production rates

To gain further insights into the inter-annual variability of ozone in the Arctic vortex, we have calculated the ozone loss and production rates for the winters 2004/05–2009/10. The following equation was applied to compute the vortex averaged ozone loss and production rates from the model simulations.

$$\overline{\delta \mathrm{O_3}(\theta, j)} \quad (\mathrm{ppbv\,sh^{-1}}) = \frac{\sum_{\lambda_{eq}=65}^{\lambda_{eq}=90} \delta \mathrm{O_3}(\theta, j, \lambda_{eq}) \times \mathrm{sh}(\theta, j, \lambda_{eq})}{\sum_{\lambda_{eq}=65}^{\lambda_{eq}=90} \mathrm{sh}(\theta, j, \lambda_{eq})}$$

where, $\overline{\delta \mathrm{O_3}(\theta, j)}$ is the ozone loss or production averaged within EqL (λ_{eq}) $\geq$65° for each model isentrope (θ) and day (j). $\delta \mathrm{O_3}(\theta, j, \lambda_{eq})$ is the instantaneous ozone loss or production calculated by the model for each grid point defined by latitude (ϕ) and longitude (ψ) for each θ and j. $\mathrm{sh}(\theta, j, \lambda_{eq})$ is the sunlit hour calculated with respect to SZA <95° that varies between 0 and 1 for complete darkness to full illumination. The λ_{eq} is computed for each model grid (θ,ϕ,ψ) and for each day using PV data. Fig. 4.6 shows the vortex averaged instantaneous ozone loss and production rates in ppbv sh^{-1} at 475 (top panel) and 675 K (bottom panel).

4.4.1.1 Lower stratosphere

At 475 K, the winter 2004/05 shows the largest loss rate of around 5 ppbv sh^{-1} in February. In 2009/10, loss rates of 3–5 ppbv sh^{-1} are calculated in mid-January/mid-February, while relatively lower loss rates are found in 2007/08 and 2006/07 during these months. The warm winters 2008/09 and 2005/06 show loss rates up to 3–4 ppbv sh^{-1} in December and mid-January respectively, which are larger than those of the cold winters during the same period. There is hardly any ozone production at this isentropic level.

For the winters discussed here, there are no other studies with which to compare our simulated ozone loss rates. Therefore, we compare the results of previous Arctic winters from Frieler et al. (2006). They derive ozone loss rates (seven/ten day averages) of 5–10 ppbv sh^{-1} at 490 K in 1995, 5–8 ppbv sh^{-1} at 475 K in 1996, 6–7 ppbv sh^{-1} at 500 K in 2000, 4.5–8.5 ppbv sh^{-1} at 475 K in 2001 and 4–5 ppbv sh^{-1} at 475 K in 2003 in January. Since the calculations of Frieler et al. (2006) are based on a box model, the values are not directly comparable. However, our results are generally in good agreement with their analyses. For instance, (i) both observations and our simulations show larger loss rates in late January/early February, (ii) the loss rates in warm winters rarely extend beyond January, but are larger than those for most cold winters for the same period and (iii) cold winters with sustained loss show larger simulated loss rates in January/mid-March, consistent with the measured loss rates.

4.4.1.2 Middle stratosphere

At 675 K, ozone loss and production rates tend to increase with time until February. The largest loss rates are found during February–March 2008, around 12 ppbv sh^{-1}. In 2009/10, elevated loss rates of 4–9 ppbv sh^{-1} are simulated from mid-February to mid-March. A similar evolution of production rates is also found during these two winters, in which the latter shows a large production of 5–19 ppbv sh^{-1}. The large loss of 2–6 ppbv sh^{-1} is masked by enhanced production of 2–14 ppbv sh^{-1} in mid-March 2005. The loss rates dominate over production rates in 2006/07 except in late February, which is consistent with the largest ozone loss found at 675 K in March. The warm winter 2005/06 records the largest loss and production rates from December to January in line with the high chlorine activation and ozone loss during the period.

Figure 4.7 shows the PV maps on 15 March of each year at 675 K. Since ozone production depends solely on sunlight, the movement of vortex to illuminated regions causes its variation. As

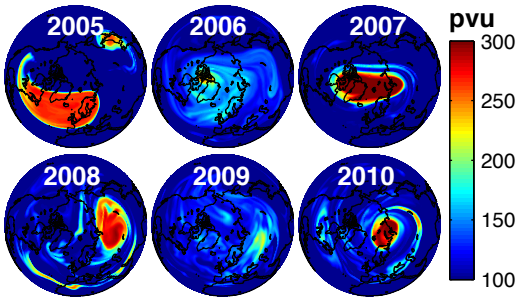

Figure 4.7: Maps of potential vorticity calculated from ECMWF data on 15 March 2004/05–2009/10 at 675 K. The maps also display the strength and position of polar vortex on that date in each winter.

can be seen from the figure, the displacement of the vortex to the mid-latitudes explains the reasons for higher production rates in 2004/05, 2007/08 and 2009/10. This is also seen in the late January–early February period in 2006 and 2009, and from late February to early March 2010, during which the polar vortices were displaced off the pole by major SSW events (Manney et al., 2006; Flury et al., 2009; Kuttippurath and Nikulin, 2012). Furthermore, it is evident from Fig. 4.6 that the production rate in March increases with time, which is well anticipated with the final warming. On the other hand, a pole centered vortex and hence, comparatively diminished production rates are found in 2006/07.

4.4.2 Ozone loss and chemical cycles

To better understand the key chemical cycles driving the ozone loss inside the vortex in the lower and middle stratosphere, we have evaluated contribution of various chemical cycles as a function of time at 475 and 675 K for the winters discussed here. Contribution of each cycle is given in percent of the total contribution from all cycles. This contribution is shown in Fig. 4.8.

4.4.2.1 Lower stratosphere

The importance of halogen cycles in ozone loss process in the polar lower stratosphere is relatively well known (e.g. WMO, 2007) and this study too finds similar results. At 475 K, the ClO–ClO and ClO–BrO cycles represent ∼80–90% of the total loss (e.g. Frieler et al., 2006; Woyke et al., 1999). The ClO–O cycle contributes 10% to the loss throughout the winter at this level, consistent with a previous study at 465 K based on Upper Atmosphere Research Satellite (UARS) MLS measurements in the Arctic and Antarctic winter of 1993 (MacKenzie et al., 1996). The ClO dimer cycle is prominent during January–mid-March (since the ozone loss before January is very small, the contribution before is not shown), with a maximum contribution of ∼50% in the mid-January to mid-February period. Due to its quadratic dependence on ClO, the efficiency of the ClO–ClO cycle to destroy ozone falls very rapidly when active chlorine returns to reservoir forms at the end of the winter. This is not the case for the contribution of ClO–BrO, which decreases not as rapidly in these conditions, and therefore becomes larger than that of the ClO–ClO cycle in early March. When the ClO dimer cycle becomes less important, the contribution from ClO–BrO enhances. A similar result was observed by Butz et al. (2007) in the Arctic winter 1999 from balloon-borne measurements. From early March onwards, as there are no PSCs and chlorine activation the contribution of the HO_x and NO_x cycles grow quickly and become the active ozone depleting cycles in the second half of the month.

Another interesting feature to note is the contribution of the cycles in 2009/10. During this winter temperatures were relatively high and, as stated previously, the vortex was subjected to a major SSW and subsequent split. Therefore, in early February the ClO–ClO contribution fell dramatically and contribution from other cycles (HO_x and ClO–BrO cycles in particular) dominated later during the winter. Contribution from HO_x dominates during warming periods, and is demonstrated by its relatively higher contribution in the vortex dissipation (mid/late March) or major SSW periods (late January 2006 and 2009, and mid-February 2010). Since increase in mixing ratios of H_2O and HNO_3 during warmings are expected (e.g. Flury et al., 2009) and are the sources of HO_x, contribution from this cycle outweighs others in these periods.

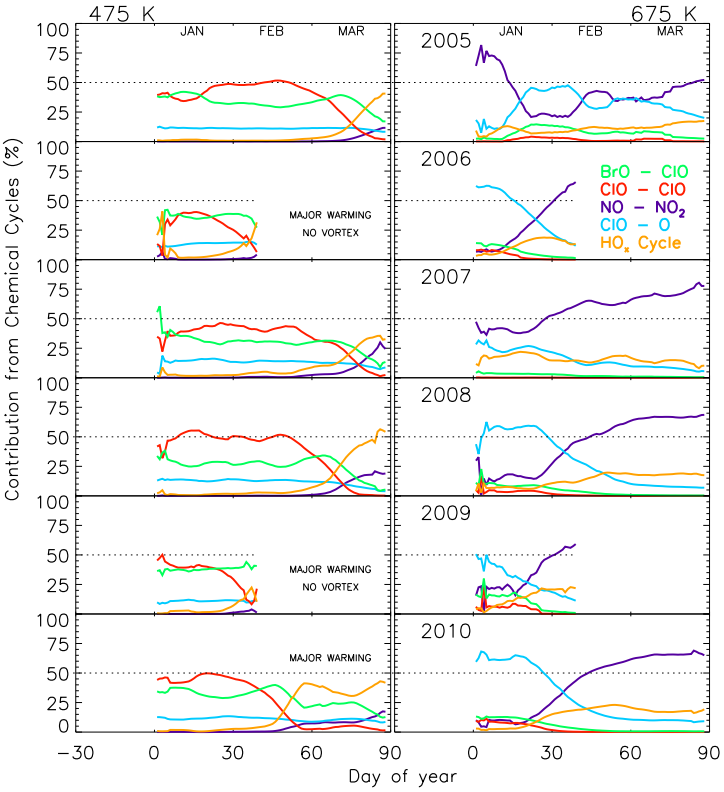

Figure 4.8: Vortex averaged (≥65° EqL) relative contribution of selected ozone depleting chemical cycles to the total chemical ozone loss at 475 (left panel) and 675 K (right panel) in the Arctic winters 2004/05–2009/10. The data are smoothed for ten-days. The dotted lines represent 50% and the top lines of each plot represent 100% contribution.

The maximum contribution of the ClO–ClO cycle to the total loss varies from ∼50% in cold winters to ∼40% in warm winters. In contrast, the contribution from ClO–BrO equals that of ClO–ClO in warm winters and decreases to ∼25–30% in cold winters. The larger difference in the contribution of both cycles, during the period of sustained ozone loss, is found in the winter 2007/08 from January to late February.

Our results on the contribution of halogens to the total loss are consistent with those found in Frieler et al. (2006). Using a photochemical box model, they also show a contribution of 50% from the ClO dimer, ∼27–48% from ClO–BrO and 5–10% from ClO–O to the total loss in the Arctic winters 1994/95, 1995/96, 1999/00 and 2000/01, and in the Antarctic winter 2003 in the lower stratosphere. They also find that the efficiency of the ClO–BrO cycle increases with faster photolysis rate of ClO dimer. Studies using UARS MLS measurements for the Antarctic winters 1992–1994 also point out that these two cycles account nearly for 90% of the total loss in the lower stratosphere (Wu and Dessler, 2001). Therefore, our study confirms the fact that the odd oxygen loss in the polar winter lower stratosphere is dominated by the ClO dimer and ClO–BrO catalytic cycles, which is quite in line with our current theoretical understanding and the findings of previous studies (e.g. WMO, 2011).

4.4.2.2 Middle stratosphere

In contrast to what is found at 475 K, the halogen catalysed cycles play comparatively a small role in the Arctic ozone loss at 675 K, as demonstrated in Fig. 4.8 (right panel). At this level, the loss is essentially due to the NO–NO_2 cycle, which represents 50–75% of the total loss during February–March, complemented by the ClO–O cycle that contributes about 10–20% to the total loss in that period. The ClO–O contribution is found to be as large as 20–55% in January. However, ozone loss at this altitude during the period is very small (0–0.3 ppmv). The contribution of HO_x cycle, which is about 10–20% in January, increases during the course of the winter to become equal to or larger than that of ClO–O in late winter. The rate limiting step in all these cycles is the combination of the oxygen atom with a specific molecule (e.g. HO_2+O for HO_x, and ClO+O for ClO_x). In sum, the availability of O-atoms mainly determines the efficiency and duration of these cycles and thus the accumulated ozone loss.

Table 4.2: The vortex averaged (≥65° EqL) column ozone loss (DU) estimated at 350–850 and 350–550 K from the MLS sampling inside the vortex and corresponding MIMOSA-CHIM simulations interpolated to the observed points for each winter (121 Days from December to March). The SAOZ total column loss computations for the winters are compared to MIMOSA-CHIM and MLS loss estimates in 350–850 K. The calculations for the warm winters 2005/06 and 2008/09 are performed for 72 days (from 1 December to 10 February), and 2009/10 for 90 days (from 1 December to end of February). The maximum loss is found (shown below) around 23–25 March in the cold winters.

350–850 K	2004/2005	2005/2006	2006/2007	2007/2008	2008/2009	2009/2010
MIMOSA-CHIM	109	42	80	98	53	79
MLS	115	26	84	112	38	60
SAOZ	103	58	99	115	56	120
350–550 K						
MIMOSA-CHIM	91	27	57	80	43	55
MLS	81	14	62	90	28	42

The inter-annual variability is relatively strong for ClO–O and NO–NO_2 cycles, markedly in January. The variability of ClO–O contribution is linked to the formation of PSCs. The NO–NO_2 cycle contributes 10–20% in 2009/10, 2008/09, 2007/08 and 2005/06, but 30–45% in 2005 and 2007 in January. The maximum ozone loss simulated around 675 K in 2006/07 is in agreement with the relatively large contribution of NO–NO_2 during the winter. However, similar contribution of this cycle in other winters is compensated by large ozone production, as discussed in Sect. 4.4.1.

Unlike for lower stratosphere, only a few studies are performed on the aspects of contribution of different chemical cycles to the total loss above 550 K. Moreover, the available studies on previous winters address contribution of the cycles in some specific issues such as ozone loss due to additional NO_x loading during solar proton events or warming events (Grooß et al., 2005b; Vogel et al., 2008). For instance, box model calculations by Konopka et al. (2007) noted the efficiency of NO_x, HO_x, ClO–ClO and ClO–BrO cycles as 76, 12.5, 3.5 and 1% respectively at 600–900 K during the warm Arctic winter 2003. Interestingly, large loss of ozone at higher altitudes with a double peak structure (as found in 2004/05) was simulated in that winter too (Grooß et al., 2005b). Simulated ozone loss for the winter is comparable to that of 2004/05, with a maximum of around 1.4 ppmv at 475 and 675 K. They also linked the larger loss above 600 K to the exposure of vortex air to sunlight (Grooß et al., 2005a). These results are in agreement with our analysis for the warm winters, during which the contribution from NO_x is larger than that of the cold winters, making larger ozone loss above 600 K. Therefore, in PSC-free polar stratosphere at 600–850 K, the NO–NO_2 cycle plays a major role in ozone loss.

4.4.3 Column ozone loss

To complement our ozone loss analysis based on mixing ratios, we have computed the column ozone loss for each winter from both the MIMOSA-CHIM simulations and MLS observations. For the integration, the model ozone and tracer profiles were interpolated to the MLS sampling points inside the vortex (≥65°EqL). The MLS profiles were then interpolated to the vertical levels of the model in order to have the same column computation procedure for both data sets. Most studies concentrate the column ozone loss in the lower stratosphere, and therefore we have calculated the loss in the 350–550 K column range. In order to analyse the contribution from middle stratosphere by cycles like NO_x, as discussed in the previous section, we have computed the column loss for the whole 350–850 K range. Except for the warm winters 2005/06, 2008/09 and 2009/10, the accumulated column ozone loss are estimated from December through the end of March. Calculations for the warm winters are done until 10 February for 2005/06 and 2008/09, and 28 February for 2009/10, consistent with our previous discussion. The daily average ozone and tracer data are used for these column ozone loss calculations. The resulting column losses in 350–550 and 350–850 K for each winter are given in Table 4.2.

For the 350–850 K partial column, the largest loss is found in 2004/05 and the lowest loss in 2005/06, in agreement with our discussion on the vertical distribution of ozone loss. In 2004/05 and 2007/08, the column loss simulated by the model is respectively 109 and 98 DU while that derived from the MLS observations amounts to respectively 112 and 115 DU. In the warm winters 2005/06 and 2008/09, a limited loss reaching 53 DU (in 2008/09) is simulated. The warm winter 2009/10

Table 4.3: The vortex averaged (≥65° EqL) partial column ozone loss (DU) computed from MIMOSA-CHIM and MLS data over 350–550 and 350–675 K are compared to various results for the Arctic winter 2004/05. Individual vortex definition is used in other published results. The error estimation provided by the respective studies are given together with the ozone loss values. Here, the column title "Period" represents the time line of individual studies and "Max. Loss" indicates the day on which the maximum ozone loss is estimated. The column range used for the loss computations are relatively small for the estimates given in *italics*.

Study	Data	Column	Period	Max. Loss	Loss (DU)
This study	MLS	350–675 K	December–March	March end	109
–	MLS	350–550 K	December–March	March end	81
Singleton et al. (2007)	Satellites	*400–550 K*	January/March	March end	90±15
Tsvetkova et al. (2007)	SAGE III	350–625 K	January/25 March	25 March	116±10
Jin et al. (2006)	ACE-FTS	375–650 K	1–7 January/mid-March	15 March	116
Rex et al. (2006)	Match	350–550 K	January/25 March	25 March	127±21
von Hobe et al. (2006)	in-situ	*344–460 K*	7 March	7 March	62^{+8}_{-17}
	Simulations				
This study	MIMOSA-CHIM	350–675 K	December–March	March end	107
–	MIMOSA-CHIM	350–550 K	December–March	March end	91
Grooß and Müller (2007)	CLAMS	380–580 K	January–March	23 March	69±20
Feng et al. (2007a)	SLIMCAT	380–550 K	December–March	March end	∼140

is characterised by a moderate loss of 79 DU by the end of February. The column loss calculated by the model overestimates the measured loss in all three warm winters (2005/06, 2008/09 and 2009/10) by 16–19 DU. These ozone loss estimates from MIMOSA-CHIM and MLS data compare reasonably well with those derived from the ground-based total column observations of UV-visible SAOZ (Systeme d'Analyse par Observation Zenithale) network in the Arctic (Goutail et al., 2005, 2010). As shown by the simulations, large loss in cold and relatively small loss in warm winters are computed from the SAOZ measurements. The SAOZ data based ozone loss estimations are generally in good agreement with those of MIMOSA-CHIM/MLS, within 20 DU. In 2009/10, the difference is much larger, reaching 40 and 60 DU with the simulations and MLS observations, respectively. This offset between SAOZ and MIMOSA-CHIM/MLS ozone loss can be due to differences in the vortex limit criteria and vortex sampling. That is, the ground-based estimations depend on seven stations in the vortex, while the MLS sampling covers relatively quite well the polar region. Additionally, the ground-based analysis uses slightly different vortex criterion and the column measurements do not sample vortex air at all altitudes, whereas only vortex air is considered in our analysis.

The ozone loss in the lower stratosphere, over 350–550 K, shows similar characteristics as noted in the 350–850 K column range. Namely, (i) cold and warm winters exhibit, respectively, larger and smaller column ozone loss, (ii) the ozone loss estimated from MLS is larger than that from the model alone (except in 2004/05 in 350–550 K) and (iii) the modelled loss is larger by about 10–20 DU than the measured loss in warm winters.

In a study using Match ozonesonde measurements in the Arctic, Harris et al. (2010) derive an accumulated ozone column loss of 72 DU in 2006/07 and 65 DU in 2007/08 over 380–550 K. Both MIMOSA-CHIM and MLS ozone loss estimates underestimate the Match results in 2006/07 by 10–15 DU and overestimate them in 2007/08 by 15–25 DU. In contrast, our analyses provide comparatively larger loss in the cold winter 2007/08. The simulated loss in 2005/06 is in good agreement with that of Feng et al. (2007a), who calculate a loss of about 32 DU in early February at 380–550 K. The comparison of column ozone loss estimates for the Arctic winter 2004/05 is presented in a separate section as there are several published results available for a detailed discussion.

The difference between the partial column loss estimated over 350–550 and 350–850 K (i.e. Δ Loss=$\text{Loss}_{350-850\,\text{K}}$–$\text{Loss}_{350-550\,\text{K}}$) averaged over the studied winters is equal to 18±5.2 and 19.7±8.6 DU for the MLS observations and MIMOSA-CHIM simulations, respectively. Such a difference, mainly due to the contribution of NO_x chemistry in the middle stratosphere, has to be taken into account when comparing polar ozone loss computed from total ozone observations with that derived from ozone profile measurements/simulations.

4.4.3.1 Column ozone loss in 2004/05

Since the winter 2004/05 was one of the coldest in the decade, a number of ozone loss estimations based on measurements and simulations have been published. Table 4.3 compiles the vortex averaged column ozone loss calculated from various data sets. For a better comparison with other results we have also estimated the loss at 350–675 K from both MIMOSA-CHIM simulations and MLS observations. As shown in the table the loss estimated by different studies generate different results. The MIMOSA-CHIM analysis shows a good agreement with Singleton et al. (2007), who also compute a similar loss from MLS observations. The MIMOSA-CHIM/MLS ozone loss over 350–675 K show a good agreement with those from Jin et al. (2006) and Tsvetkova et al. (2007). The larger loss simulated in Feng et al. (2007a) is due to the higher vortex descent and accompanied increase in chlorine loading in the lower stratosphere of their model. The ozone loss computation from von Hobe et al. (2006) shows the lowest value among these analyses while that of Rex et al. (2006) provides the largest estimate. The accumulated loss in von Hobe et al. (2006) was estimated on 7 March, which is much earlier than in other studies (around 25 March) and there was a strong vortex and sustained loss thereafter. Also, the loss was estimated only up to 460 K, which is much lower than the column upper limit considered in other studies. Such a discrepancy in the altitude range used for the analyses is one of the reasons for the spread in the results. Another possible reason for the difference is that most works use their own vortex criterion for the column ozone loss estimate.

Regarding the ozone loss derived from various model results, the simulations by Grooß and Müller (2007) show the lowest estimate. This offset can be due to a different sampling of the vortex by the model grid, as compared to the satellite observations. In order to check this, we averaged the simulated loss over all the model grid points (not only at the footprint of MLS observations) using the same vortex criterion of Grooß and Müller (2007) and obtained a loss of 73 DU for the 350–550 K range (our model vertical levels are different). This estimate is in very good agreement with the calculation of Grooß and Müller (2007). Another important fact to note is the sampling of the vortex by the MLS sensor, which is limited to 82°. In contrast, the model grid spans to the full 90° including the pole. Therefore, the average calculated from the model results can cover the area inside the vortex from this additional latitude region of 8° (i.e. 83° to 90° N) too, and hence, this average can slightly differ from the mean loss estimated at the satellite footprints. In short, the differences in vortex sampling, altitude range, time period and vortex definition of the analyses have to be taken into account when comparing different ozone loss estimates.

4.5 Conclusions

The evaluation of vortex averaged ozone loss from the model and satellite observations shows large variability in the Arctic winters 2004/05–2009/10, in accordance with analyses performed for previous northern winters. The cold winters 2004/05 and 2007/08 record the largest loss with peak ozone loss around 475 K. In 2006/07, the maximum loss is estimated at a higher altitude, around 650 K. The smallest loss among the winters is estimated in the warm winters 2005/06 and 2008/09. At 475 K, the cumulative ozone loss ranges from 0.7 ppmv in 2005/06 to 1.5–1.7 ppmv in 2004/05. At 675 K the loss ranges from 0.3–0.5 ppmv in 2008/09 to 1.3 ppmv in 2004/05. In general, the ozone loss values derived from the MIMOSA-CHIM simulations and MLS observations, combined with the model passive tracer, are in good agreement and the differences are mostly within the estimated accuracy of the observations. It has to be noted that, since there is a large variability in peak ozone loss altitude from one year to the next, analysis or comparison of ozone loss at specific altitudes is neither complete nor well-represented as far as the variability of Arctic winters is concerned. Therefore, care has to be taken while interpreting the ozone loss estimated at specific altitudes to characterise or compare different winters.

Our analyses suggest that the halogen cycles; ClO–ClO contributes ∼40–50% and ClO–BrO contributes ∼30–40% to the total loss during December–February at 475 K. These cycles depend on temperatures in the lower stratosphere, PSCs, heterogeneous reactions on PSCs and thus the Arctic meteorology. The NO–NO_2 cycle is the key mechanism that depletes about 60–75% of ozone in the middle stratosphere, which is essentially predominant in the January–March period.

The partial column ozone loss estimated over 350–850 K from MIMOSA-CHIM calculations at the MLS footprints inside the vortex shows about 109, 42, 80, 98, 53 and 79 DU in 2004/05, 2005/06, 2006/07, 2007/08, 2008/09 and 2009/10, respectively, and are in good agreement with those of the MLS and SAOZ observations. There is a significant difference ($\sim$19$\pm$7 DU) in the column ozone loss estimated between the ranges 350–850 and 350–550 K. The additional loss above 550 K is mainly due to the NO_x cycle and should be accounted for when deriving the column ozone loss from ozone profile measurements/simulations. This is particularly important in cold winters with vertically spread ozone loss (e.g. 2004/05) and warm winters with peak ozone loss above 550 K (e.g. 2008/09).

Chapter 5

Arctic ozone loss: 2010/2011 *

Contents

The longest vortex persistence in the Arctic was found in 1996/97, in which the wave activity was considerably suppressed, and therefore, the vortex was sustained until early May (Lefèvre et al., 1998; Coy et al., 1997). Nevertheless, the ozone loss in 1996/97 was lower than that of other cold winters such as 1994/95, 1999/00 and 2004/05 due to relatively higher temperatures in December–February 1996/97, when chlorine activation plays a key role in determining the magnitude of ozone loss (Manney et al., 2003; Santee et al., 1997). In contrast, very low temperatures were observed in March–April due to a high tropopause associated with a tropospheric blocking during the 1996/97 Arctic winter (Coy et al., 1997). A similar evolution in temperature and vortex persistence was also observed in spring 2011 (Hurwitz et al., 2011; Manney et al., 2011), during which the stratospheric halogen loading was very similar to that in 1996/97. Note that long persistence of a cold vortex is a necessary requirement for the sustained ozone loss. Studies have already shown prolonged appearance of very low temperatures and exceptional ozone loss in 2010/11 (Balis et al., 2011; Manney et al., 2011; Sinnhuber et al., 2011). Persistence of very low temperatures and strong vortices for a record period of time, and very late final warmings were the common features of the Arctic winters 1996/97 and 2010/11. The vortex in 1996/97 was even stronger and the final warming was later than in 2010/11. However, the chemical processing and ozone loss were different in these winters. Therefore, the situations in both winters merit a close examination to diagnose the similarities and differences between the polar processing of the winters and to find possible reasons for them. In this chapter, the winters are analysed with high resolution CTM simulations and satellite measurements to further elucidate the ozone loss processes.

5.1 Data and methods

We use the same high resolution Mimosa CTM that discussed in the previous chapter for this study. The kinetic data are taken from Sander et al. (2006), but the Cl_2O_2 cross-sections are from Burkholder et al. (1990), with a log-linear extrapolation up to 450 nm as suggested by Stimpfle et al. (2004). Although there are new measurements for Cl_2O_2 (Papanastasiou et al., 2009), the differences in the simulated ozone loss among various sensitivity runs are very small (2%). The model has detailed PSC and sedimentation schemes. As we use the same model, further details of the model runs can be found in the previous chapters and Kuttippurath et al. (2010a). For the winters considered here, the model was run from 1 December to 30 April. We use the passive tracer method (WMO, 2007 and references therein) to derive ozone depletion.

*This chapter is partly based on: Kuttippurath, J., S. Godin-Beekmann, F. Lefèvre, M. L. Santee and L. Froidevaux: Record-breaking ozone loss in the Arctic winter 2010/2011: comparison with 1996/1997, Atmos. Chem. Phys., 12, doi:10.5194/acp-12-7073-2012, 7073–7085, 2012.

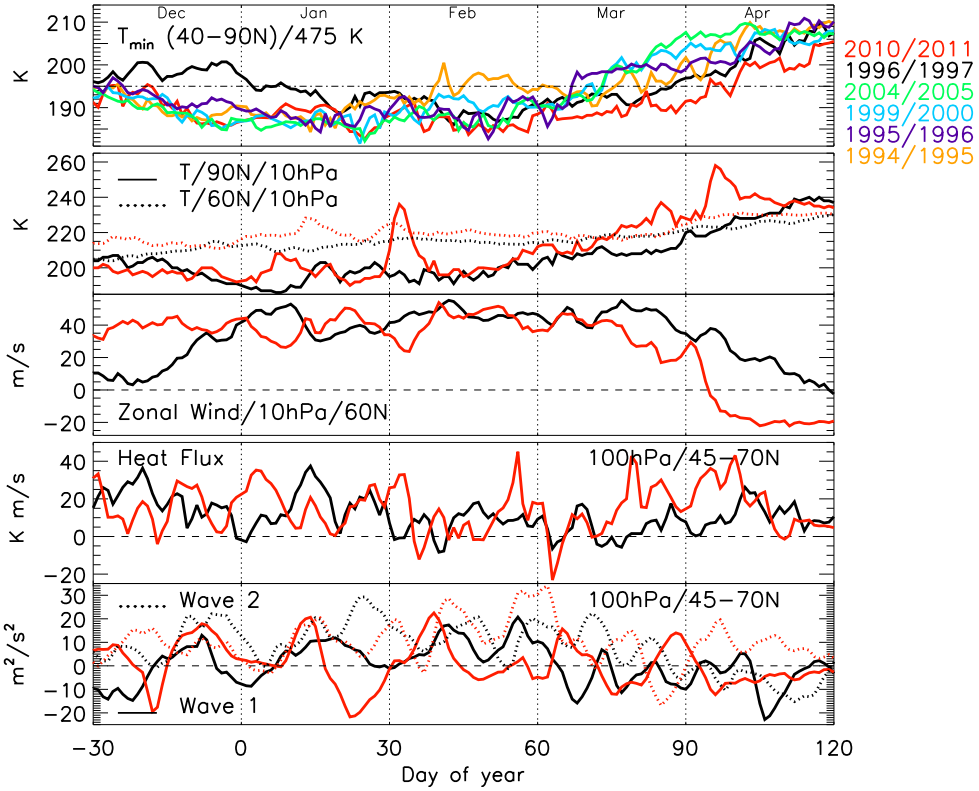

Figure 5.1: Temporal evolution of minimum temperature at 475 K, temperature at 60° and 90° N at 10 hPa, zonal wind at 60° N/10 hPa, heat flux, and planetary wave amplitudes for the Arctic winters 1996/97 and 2010/11. The heat flux and wave amplitudes are averaged between 45° and 70° N at 100 hPa. The minimum temperatures during the cold Arctic winters 1994/95, 1995/96, 1999/00 and 2004/05 are also shown. The dash-dotted line represents 195 K temperature, the dashed lines mark the zero-wind line, zero heat flux or zero wave amplitude in the respective plots, and dotted vertical lines differentiate the approximate boundaries of each month.

To compare with the simulations, we use measurements of O_3 and ClO from the UARS MLS version (v)5 for the winter 1996/97 and the Aura MLS v3.3 for the winter 2010/11. The UARS MLS O_3 profiles have a vertical range of about 15–60 km and a vertical resolution of ∼3–4 km. The uncertainty of a typical O_3 measurement is 6–15% over 16–60 km. The Aura MLS O_3 measurements have a vertical range of about 12–73 km with a vertical resolution of 2.5–3 km and an uncertainty of 5–10% between 68 and 0.2 hPa. The vertical range of UARS MLS ClO profiles is 100–1 hPa, with a vertical resolution of 4–5 km and an uncertainty of 20% at 46 hPa, whereas the Aura MLS ClO has a vertical resolution of 3–3.5 km and a vertical range of 100–0.1 hPa. The uncertainty of Aura MLS ClO retrievals is about 10–20%, depending on altitude. In order to screen the UARS MLS data we have used the guidelines provided by Livesey et al. (2003), with only profiles with positive precision values, Quality values (= 4), and "MMAF_STAT" flags with "G", "t" or "T" being considered. We have also subtracted altitude dependent known biases identified in the UARS ClO profiles prior to their interpolation to specific potential temperature levels. The selection of Aura MLS profiles are based on their Convergence, Quality, Status and Precision values as recommend by Livesey et al. (2011) for each molecule. In addition, latitude-dependent biases at 146, 100 and 68 hPa are subtracted from the ClO profiles before their vertical interpolation. Further details about the data and data screening procedures can be found in Livesey et al. (2003) for UARS MLS and, Froidevaux et al. (2008), Santee et al. (2008), and Livesey et al. (2011) for Aura MLS.

We use the ECMWF operational meteorological analyses to calculate the minimum temperature, PV, heat flux, planetary waves and vortex edge, as for the previous studies. The ECMWF data archived at the Norwegian Institute for Air Research (NILU) data base are used in this study. These analyses have a horizontal resolution of 2.5×2.5° and are available at 1000, 700, 500, 300, 200, 150, 100, 70, 50, 30 and 10 hPa pressure levels (e.g. Woods, 2006).

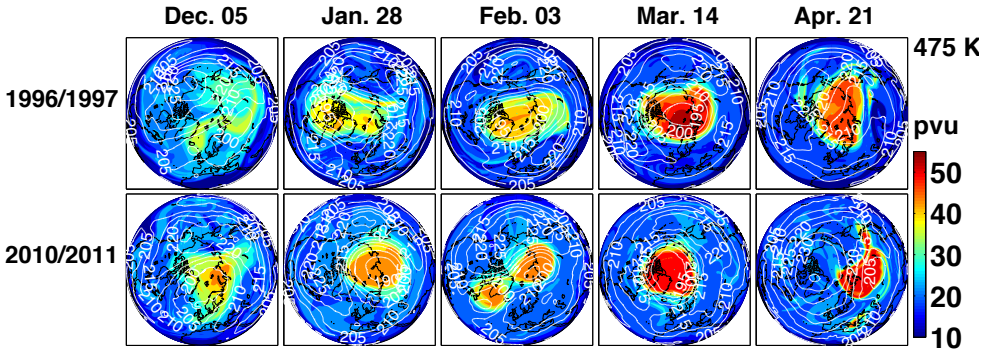

Figure 5.2: Temporal evolution of the polar vortex during selected days of the Arctic winters 1996/97 and 2010/11 at 475 K. The overlaid white contours are temperature in Kelvin.

5.2 Results and discussions

5.2.1 Synoptic evolution of the winters

Figure 5.1 shows the minimum temperature extracted north of 40° N, zonal wind, heat flux and the wave 1 and 2 calculated from geopotential fields for the Arctic winters 1996/97 and 2010/11. In 1996/97, the minimum temperatures show values above and below 195 K in December and January–March, respectively. On the other hand, temperatures below 195 K from December through early April are observed in 2010/11 (Manney et al., 2011). So the minimum temperature in 2010/11 is consistently lower than in 1996/97 throughout the winter by about 2–10 K. As compared to other cold winters in the Arctic, the temperature in 2010/11 is similar until mid-February, but about 10–20 K lower than that of other winters in March–April, indicating the longest period of low temperatures in the last two decades (Manney et al., 2011; Sinnhuber et al., 2011). The temperature in 1996/97 is also lower than that in 1994/95, 1999/00 and 2004/05 from mid-March to April, but is about 10–20 K higher in December–February than all other winters. It should be recalled that these analyses hold for 475 K only. The winters 1999/00, 2004/05 and 2010/11 exhibit the lowest minimum temperature of about 182 K around 20 January.

To diagnose SSWs, the temperature at 60 ° N/10 hPa and 90 ° N/10 hPa and zonal winds at 60 ° N/10 hPa are analysed. In 1996/97, there were no warmings and the westerlies were strong with a speed of $\sim$40 m s^{-1} in January–April, with the final warming unusually late in early May. In contrast, two minor warmings with a magnitude of about 10 and 40 K at 90° N/10 hPa in early January and early February, respectively, were observed in 2010/11. These warmings lasted for a week, and were due to wave 1 and wave 2 amplifications, with zonal mean heat fluxes of about 34 K m s^{-1}. Nevertheless, strong westerlies with a speed of $\sim$40 m s^{-1} were present from December to the end of March in 2010/11. The temperatures began to increase by the second week of April and the winds turned to easterly, indicating the final warming, which was about two weeks earlier than in 1996/97. The heat flux, EP divergence, and EP flux of the waves 1 and 2 (not shown) show very small or near zero values in February–early April in both winters. This implies that there was no significant wave activity to warm the stratosphere up, and hence, the temperature stayed cold and winds remained westerly to sustain a stable vortex during the period. However, the heat flux in February–April and wave amplitudes in March–April show comparatively smaller amplitude in 1996/97, indicating very weak wave driving during the winter. Therefore, prolonged persistence of lower temperatures, larger zonal wind amplitudes, and thus an exceptionally late final warming are observed in the Arctic winter 1996/97. Further details about the dynamical processes of both winters can be found in Hurwitz et al. (2011).

Figure 5.2 shows PV maps at 475 K on selected days of both winters. In 1996/97 (top panel), the vortex was relatively large, stable and pole-centered for most days until late April. In December the vortex was undisturbed, but a minor warming occurred in early January. The vortex was unusually strong in February through mid-April, during which the vortex was mostly pole-centered and large in size. In contrast, in 2010/11 (bottom panel), the vortex formed in early December with

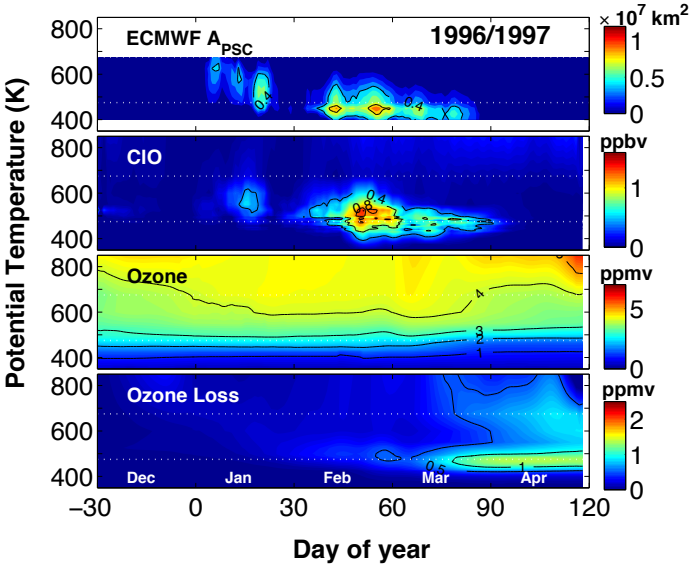

Figure 5.3: Temporal evolution of the vertical distribution of potential PSC areas, and MIMOSA-CHIM simulations of ClO, O_3 and ozone loss inside the vortex for the Arctic winter 1996/97. The ClO profiles are selected at 12 UT and SZAs below 89°. The white dotted lines represent 475 and 675 K.

considerable size. Though the minor warming moved the vortex slightly off the pole in January, the vortex was still strong with PV values of ∼50 pvu. The vortex stayed pole-centered again until the minor warming in early February, during which the vortex nearly split into two parts. Since the warming was short and the westerlies were strong, the vortex merged and regained its strength to form a large pole-centered one after a few days and stayed intact until late April 2011. Note that the vortex was still significantly smaller than that of other cold Arctic winters in February–April, including the winter 1996/97 as shown by the PV maps in Fig. 5.2 and mentioned by Manney et al. (2011). In April, the temperatures began to increase and westerlies started to diminish, and the vortex tilted off the pole and then stayed mostly in the mid-latitudes until the final warming in late April. The vortex evolution was similar at most altitudes between 450 and 850 K, but the vortex dissipation was observed a few days earlier at 850 K in both winters.

5.2.2 PSC, chlorine activation and ozone loss

5.2.2.1 Winter 1996/97

Figure 5.3 shows the potential PSC areas, and the vortex-averaged MIMOSA-CHIM simulations of ClO, O_3 and ozone loss for the Arctic winter 1996/97. The ClO data are filtered with respect to a criterion of 12 UT and SZA less than 89°. In this study A_{PSC} is considered as the area where temperatures are less than T_{NAT} and the calculation is performed as described in the previous chapters.

As the temperatures are above 195 K, no PSCs are found in December. In January, PSCs with areas of $\sim 0.7 \times 10^7$ km^2 are estimated at 500–600 K. Large areas of PSCs with a maximum of about 1.3×10^7 km^2 are found at 400–550 K until mid-March and there were no PSCs afterwards, consistent with the temperatures during the period. So the chlorine activation was moderate, as indicated by the ClO mixing ratios of ∼0.7 ppbv in mid-January, about 1–1.7 ppbv in mid-February and about 0.5 ppbv in March around 475 K. Since the vortex was symmetric and pole-centered, there were no changes in O_3 distributions at most altitudes until late February, but a reduction of 1–1.3 ppmv was found thereafter in the lower stratosphere in the sunlit parts of the vortex. This change in O_3 is evident when following the 3 and 4 ppmv O_3 isopleths. The corresponding ozone loss is about 0.6 ppmv in late February and 1.2 ppmv in late March–April around 475 K. There is also a significant loss of 0.4–0.7 ppmv, by NO_x catalytic chemistry, at altitudes above 550 up to 700 K in April. Since the denitrification in the winter 1996/97 was studied extensively (e.g. Kondo et al., 2000; Santee et al., 1999) and was not severe as in other cold Arctic winters (e.g. Kleinböhl et al., 2005b; Grooß and Müller, 2007), we have excluded discussions on denitrification in this winter.

Figure 5.4 compares the ClO, O_3 and ozone loss simulations with those from the UARS MLS measurements. Here data are selected with respect to the MLS sampling points inside the vortex

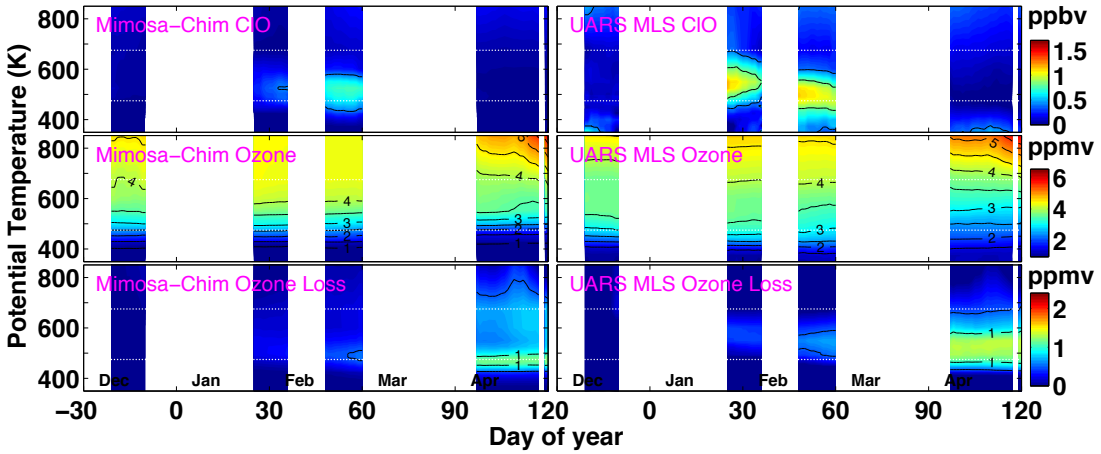

Figure 5.4: Temporal evolution of the vertical distribution of ClO, O_3 and ozone loss from MIMOSA-CHIM and UARS MLS for the Arctic winter 1996/97. The model fields are sampled at the location of MLS observations for each measurement inside the vortex and then averaged for the corresponding day. Both measurements and model data are smoothed for seven days. The model and MLS ClO coincident profiles are selected for SZAs <89° and local time between 10 and 16 h. The MLS ClO profiles are bias corrected. The white dotted lines represent 475 and 675 K.

and hence, these are slightly different from the vortex averages shown in Fig. 5.3. The model results are in reasonable agreement with the observations. The simulated ClO is slightly lower (e.g. Santee et al., 1997) and O_3 is a little higher, and thus, the simulated ozone loss is about 0.1–0.2 ppmv lower than in the observations at 425–550 K. Still the measurements also show a peak loss of about 1.2 ppmv by late April. In addition, our results are in good agreement with those of Manney et al. (2003, 1997) and Knudsen et al. (1998), who estimate a peak ozone loss of about 1.2 ppmv at 465 K and 1.24 ppmv at 475 K by late March from UARS MLS and ozonesonde measurements, respectively. The SLIMCAT model also calculates a similar ozone loss maximum of about 1.1 ppmv at 475 K in late March (Hanson and Chipperfield, 1999).

5.2.2.2 Winter 2010/11

Figure 5.5 presents the modeled and measured ClO, HNO_3, O_3 and ozone loss at the Aura MLS sampling locations inside the vortex, together with the area of PSCs, for the winter 2010/11. Large areas of PSCs with maximum values of about 1.1×10^7 km^2 are estimated from mid-December to late March. Note that the A_{PSC} in 2010/11 is systematically larger than that in 1996/97 both with time and altitude. This suggests that the winter 2010/11 had an unusually long period of PSC appearance in a wide vertical extent between 400 and 600 K compared to any other Arctic winter (Manney et al., 2011; Kuttippurath et al., 2010a).

Consistent with the A_{PSC}, about 0.5–0.7 ppbv of ClO in December and 1–1.8 ppbv of ClO in January–March at 450–600 K are simulated. The ClO simulations show the record maximum of about 1.8 ppbv in mid-January around 475–700 K. Unlike in other Arctic winters (WMO, 2011; Kuttippurath et al., 2010a), the model calculates large ClO values in March at 450–600 K, pointing to an unusually high chlorine activation for an extended period of time. Furthermore, the HNO_3 profiles depict strong denitrification (about 40–50%) as they register about 15 ppbv in December, but are denitrified to 5–8 ppbv in January–March in the lower stratosphere, in agreement with the analyses presented in Manney et al. (2011) and Sinnhuber et al. (2011). In accordance with the high chlorine activation, substantial reduction in O_3 is modelled from late January onwards. The ozone loss started in the sunlit part of the vortex when it moved to the mid-latitudes during the minor warming in early February, with values of about 0.5 ppmv around 550 K. The loss increased to 1.2 ppmv at 475 K by late February and then rapidly reached the maximum loss of 2–2.4 ppmv by the end of March in 450–550 K. Since most Arctic winters show the peak loss in a narrow vertical region, this case in 2010/11 stands in contrast with those. A significant loss of around 1 ppmv is also simulated due to the NO_x chemistry above 550 K in February–March. Such large ozone loss at

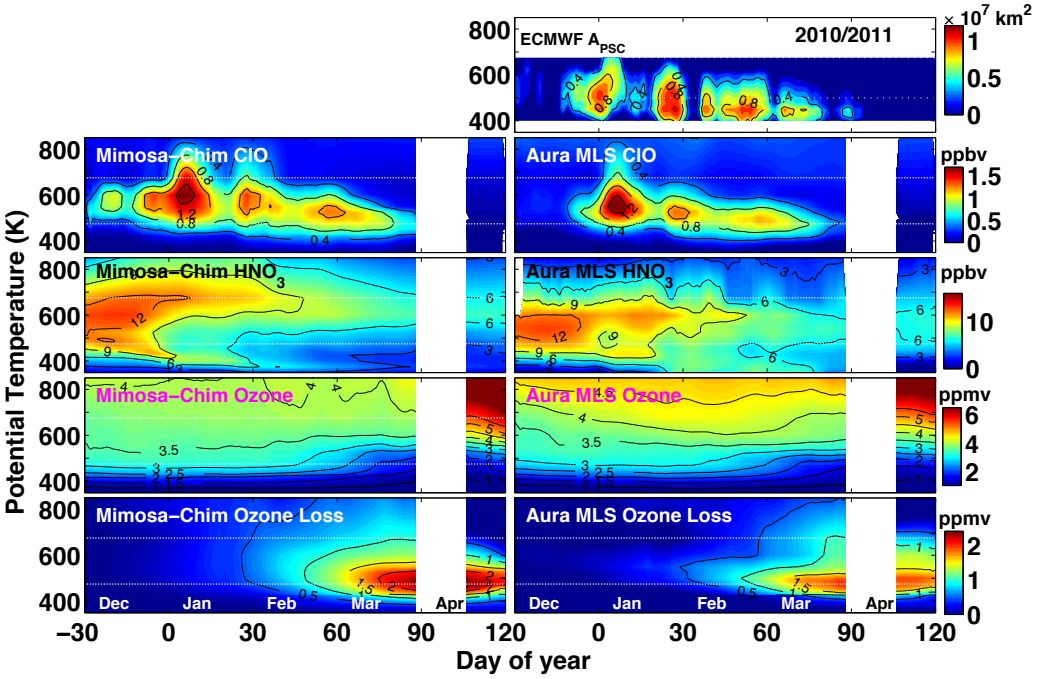

Figure 5.5: Temporal evolution of the vertical distribution of ClO, HNO_3, O_3 and ozone loss from MIMOSA-CHIM and Aura MLS for the Arctic winter 2010/11. The model fields are sampled at the location of MLS observations for each measurement inside the vortex and then averaged for the corresponding day. Both model results and measurements are smoothed for seven days. The model and MLS ClO coincident profiles are selected for SZAs <89° and local time between 10 and 16 h. The MLS ClO profiles are bias corrected (see text). The A_{PSC} computed from the ECMWF operational analyses is also shown (top panel). The white dotted lines represent 475 and 675 K.

higher altitudes is atypical in the Arctic winters (e.g. Kuttippurath et al., 2010a; Rex et al., 2004; Manney et al., 2003).

The model simulations also feature the same ozone loss patterns as the Aura MLS measurements, such as the timing of the onset of loss, the altitude range of loss, and the altitude and timing of the maximum loss and, therefore, exhibit excellent agreement with the observations. Nevertheless, the simulated ozone loss slightly overestimates the Aura MLS observations, as the peak loss is about 0.1–0.2 ppmv lower than that of the observations. This bias is due to the comparatively higher ClO and lower O_3 in the model. The maximum loss found in this study is in good agreement with that estimated from the Aura MLS and Michelson Interferometer for Passive Atmospheric Sounding (MIPAS) observations, about 2.3–2.5 ppmv, by Manney et al. (2011) and Sinnhuber et al. (2011), respectively.

To check the sensitivity to PSCs, we have simulated ozone loss without considering NAT PSCs in the model (e.g. Pitts et al., 2007; WMO, 2011). The test run results give (not shown) a maximum ozone loss of about 1.8 ppmv in 450–550 K when the model considers only the liquid and ice PSCs. As compared to the control run with NAT (plus liquid and ice PSCs) PSCs, the model simulates about 10% less ozone loss at 475 K, but nearly the same ozone loss (about 17–19%) for both runs at 675 K. It confirms that the effect of NAT PSCs on the ozone loss simulations is quite large in the lower stratosphere. This experiment suggests that the contribution of denitrification to the ozone loss of 2.4 ppmv from the control run is about 25% and is the largest among the Arctic winters (e.g. WMO, 2007). Note that this ozone loss (1.8 ppmv simulated with liquid/ice PSCs only) is still larger than that observed in any other Arctic winter, as the previous maximum of 1.6 ppmv was in 2004/05 (Manney et al., 2011; WMO, 2011; Kuttippurath et al., 2010a).

5.2.3 Ozone loss and production rates

Figure 5.6a shows the ozone loss and production rates simulated at 475 and 675 K for selected Arctic winters, including 1996/97 and 2010/11. In 1996/97, the ozone loss was moderate and, therefore,

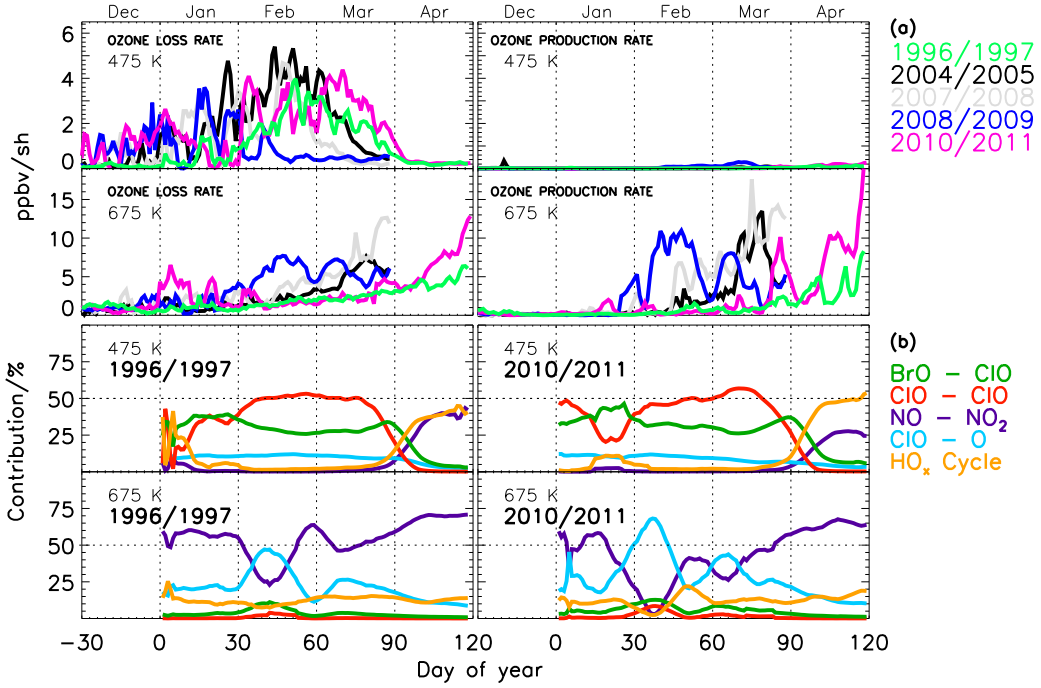

Figure 5.6: a (upper panels): Vortex-averaged (≥65° EqL) instantaneous ozone loss rates (left panel) and production rates (right panel) simulated by MIMOSA-CHIM at 475 and 675 K for the Arctic winter 1996/97 and 2010/11 compared to those of 2004/05, 2007/08 and 2008/09. The data are exempted from temporal smoothing to explicitly show the effect of daily movement of vortex and its impact on ozone production and loss rates. **b (bottom panels)**: Temporal evolution of the vortex-averaged contribution of the ClO–BrO, ClO–ClO, NO–NO_2, ClO–O and HO_x chemical cycles to the ozone loss during the Arctic winter 1996/97 and 2010/11 at 475 and 675 K. The dotted horizontal lines represent 50 % of contribution and the vertical dotted lines mark the approximate boundaries of each month.

loss rates of about 2–3 ppbv sh^{-1} are simulated from mid-February to mid-March at 475 K, as a result of significant ClO enhancements in this time period. In 2010/11, the model simulates an atypical loss rate of 2–4 ppbv sh^{-1} in March and early April. It should be noted that there are high loss rates in December and January 2010/11 in the lower stratosphere at 475 K as a result of enhancement in ClO, as also shown by Manney et al. (2011), which is important for the cumulative ozone loss of the winter. As expected, there is no O_3 production in the lower stratosphere. In the middle stratosphere, at 675 K (Fig. 5.6a), a loss rate of 2–5 ppbv sh^{-1} is simulated in March–April in 1996/97. On the other hand, in 2010/11, large loss rates of about 4–5 ppbv sh^{-1} in January and 13 ppbv sh^{-1} in mid-April are calculated by the model. No significant O_3 production was found until mid-March in both winters, but episodically high production rates of about 5–7 ppbv sh^{-1} in 1996/97 and 10–12 ppbv sh^{-1} in 2010/11 are estimated thereafter.

In most Arctic winters, as depicted in the figure, the loss rates show a maximum of about 3–5 ppbv sh^{-1} in mid-January, mid-February and late February/early March in warm (e.g. 2008/09), moderately cold (e.g. 2007/08) and cold (e.g. 2004/05) winters, respectively, and then suddenly drop to zero loss rate as there is no loss thereafter in the lower stratosphere, at 475 K. Though the loss rates are larger in late February–early March at higher altitudes (e.g. 675 K), O_3 production rates outweigh these high loss rates even in cold winters. In contrast, there are higher ozone loss rates at 475 K in March and early April, and relatively lower O_3 production rates at 675 K in February through mid-March in 2010/11 than in other years. This indicates that the winter 2010/11 was unique in terms of the record ozone loss rates in the lower stratosphere in the March–April period.

We have also evaluated the contribution of various chemical cycles to the ozone loss in the lower and middle stratosphere, as done by Kuttippurath et al. (2010a); results are shown in Fig. 5.6b. The general features and contributions from various chemical cycles in the lower and middle stratosphere are consistent with those of previous studies (Kuttippurath et al., 2010a; Vogel et al., 2008; Butz et al., 2007; Grooß et al., 2005b; Hanson and Chipperfield, 1999; Woyke et al., 1999). However,

in February–March 2011, our analyses show exceptional contributions from the ClO–ClO (30–55%) and ClO–BrO (30–35%) cycles in terms of absolute values in the lower stratosphere at 475 K (although the relative contributions from the various cycles look similar in both winters). The larger contributions of the halogen cycles in 2010/11 are consistent with the prolonged appearance and large amounts of ClO during that period. In April 2011, a remarkable contribution from the HO_x cycle (30–50%) is also calculated in the lower stratosphere. This is linked to relatively higher values of H_2O and HNO_3, the sources of HO_x in spring. In March–April 2011, the model simulates comparatively higher abundances of NO_x at altitudes above 550 K, and hence this cycle dominates (with a 30–70% contribution) the ozone loss there (Fig. 5.6b). The large contributions from these cycles in February–April are consistent with the large loss and loss rates during the period. The contributions of various chemical cycles during the winter 2010/11 thus stand in contrast to those in other Arctic winters (e.g. Kuttippurath et al., 2010a; Hanson and Chipperfield, 1999), as that winter exhibited stronger and more prolonged (February to April) chemical O_3 destruction in comparison to other Arctic winters. Although the relative chemical cycle contributions (see Fig. 5.6b) in 1996/97 are comparable to those in 2010/11, these contributions from all cycles in absolute terms are proportional to the ozone losses that occurred in the respective winters (Kuttippurath et al., 2010a; Butz et al., 2007; Woyke et al., 1999). Further discussions on the contribution of various cycles in the Arctic winter 1996/97 can be found in Hanson and Chipperfield (1999). It should be borne in mind that the rate limiting step of these chemical cycles is the combination of O-atom with the specific molecule. Therefore, the efficiency and duration of the contributions of these cycles and associated ozone loss in the middle stratosphere primarily depend on the available oxygen atoms in this altitude region.

Note that the loss of NO_x happens through photodissociation and thus in the absence of solar radiation during the polar night, it is chemically long-lived. Therefore, its abundance in a particular winter is largely controlled by the prevailing meteorology. When the polar vortex is very strong, large scale diabatic descent in the polar vortex can bring considerable amounts of NO_x from higher altitudes (Solomon et al., 1982). Strong descent of NO_x was also observed during the reformation of polar vortex after its split or displacement due to MWs. As discussed above, since the NO_x catalysed chemistry is very important for the ozone loss at higher altitudes, the winters with larger mesospheric descent during MWs and solar proton events merit a special mention. For instance: studies report large scale NO_x-rich air mass descent during MW of the Arctic winter 2003/04 and 2005/06 (Randall et al., 2009), although the enhancement of stratospheric NO_x in 2003/04 was connected to solar proton events and associated excess production in the mesosphere (Vogel et al., 2008). Nevertheless, both of these winters were prone to additional ozone loss in the middle and upper stratosphere due to higher NO_x abundances as reported by Vogel et al. (2008) and Kuttippurath et al. (2010a). It has to be kept in mind that there were no MWs and large NO_x influx from the mesosphere in 1996/97 and 2010/11, and the contribution of NO_x is discussed with respect to the amount of NO_x present in 2010/11 in comparison to that of 1996/97 only. Therefore, the inter-annual variability of NO_x (and thus the NO_x driven ozone loss) in the stratosphere depends on the dynamics of each winter.

5.2.4 Column ozone loss

To get a complete overview of the ozone loss, we have computed the partial column ozone loss in two potential temperature ranges, 350–850 and 350–550 K, from the MLS measurements inside the

Table 5.1: Vortex-averaged (≥65° EqL) partial column ozone loss (DU) estimated over 350–850 and 350–550 K from the MLS sampling inside the vortex and corresponding MIMOSA-CHIM simulations. The calculations for the moderately cold winter 2009/10 is done from 1 December to 28 February. The maximum loss is found (shown below) around late/mid-March in 2004/05, 2006/07 and 2007/08, and around late/mid-April in 1996/97 and 2010/11.

350–850 K	1996/97	2004/05	2006/07	2007/08	2009/10	2010/11
MIMOSA-CHIM	61	109	80	98	79	160
MLS	60	115	84	112	60	130
350–550 K						
MIMOSA-CHIM	42	91	57	80	55	140
MLS	41	81	62	90	42	115

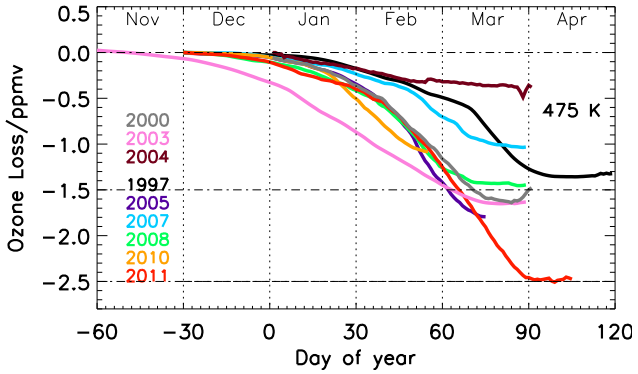

Figure 5.7: Vortex-averaged (≥65° EqL) ozone loss simulated by MIMOSA-CHIM for the Arctic winters 1996/97, 1999/00, 2002/03, 2003/04, 2004/05, 2006/07, 2007/08, 2009/10 and 2010/11 at 475 K. The model initialisation was on first November in 2002/03 to capture early ozone loss in that winter. The dotted vertical lines mark approximate boundaries of each month and the dash-dotted horizontal line is 0 ppmv.

vortex and the corresponding MIMOSA-CHIM simulations (shown in Figs. 5.4 and 5.5). In 1996/97, the MIMOSA-CHIM simulated partial column ozone loss at the UARS MLS sampling points over 350–550 K reaches 7, 17 and 44 DU in late January, late February and late April, respectively. The accumulated ozone loss from the model over 350–850 K by late April shows 62 DU. Identical values are also estimated from the UARS MLS measurements, about 43 DU over 350–550 K and 61 DU over 350–850 K by late April. These estimations are close to the findings of Tilmes et al. (2006) and Harris et al. (2010), who report about 61 ± 20 DU from satellite and 50 ± 20 DU from ozonesonde measurements, respectively, over 380–550 K. The total column ozone loss simulated with REPROBUS, about 50–60 DU (Lefèvre et al., 1998), is also comparable to our estimations. However, these estimations are significantly smaller than the total column ozone loss computed from ozonesonde observations by Knudsen et al. (1998), and Terao et al. (2002), of about 79–96 DU. This offset could be due to the differences in the model simulations, vortex edge criterion, ozone loss estimation method and data used for the loss computations in the respective studies.

In 2010/11, the partial column ozone loss simulated by MIMOSA-CHIM at the Aura MLS footprints reaches about 6, 20, 62 and 112 DU by the end of each month from December through March, and 148 DU in mid-April over 350–550 K. The maximum ozone loss estimated for the 350–850 K altitude range is slightly higher, about 160 DU in mid-April, consistent with the loss simulated above 550 K. The Aura MLS observations show an analogous progression of ozone depletion with time for both column ranges, but the maximum loss is slightly lower than the simulated one, about 115 DU at 350–550 K and 131 DU at 350–850 K. These differences are consistent with the bias found between the measured and modeled ClO and O_3. Nonetheless, these column ozone loss estimations are in good agreement with those estimated by Manney et al. (2011) from the Ozone Monitoring Instrument (OMI) measurements on 26 March 2011 (∼140 DU total column loss) and by Sinnhuber et al. (2011) from the Michelson Interferometer for Passive Atmospheric Sounding (MIPAS) observations by late March (∼120 DU at 380–550 K). The total column ozone loss calculated from the Multi-sensor Reanalysis (MSR) by Balis et al. (2011) is about 95±8 DU and is comparable to our estimations. The slight differences between various ozone loss estimates can be due to the reasons discussed above (for the winter 1996/97). However, the difference with Balis et al. (2011) could be due to the differences in vortex area calculations, as they use a vortex edge criterion of 70°N EqL at 475 K, but we consider the vortex criterion at each altitude. This is particularly important as they use total column ozone data. In addition, their passive tracer simulation is slightly different from that shown in other studies. Note also that model differences or inaccuracies in passive tracer calculations can significantly affect the loss values. For instance: ozone loss calculations based on a pseudo-tracer, in which only chlorine-activating heterogeneous reactions are turned off (Singleton et al., 2005), yield about 10–25% lower loss than that estimated in this study (Balis et al., 2011).

5.2.5 Comparison with other Arctic winters

Table 5.1 shows the partial column ozone loss over two different altitude bounds for the recent cold/moderately cold Arctic winters. Compared to the other Arctic winters, as discussed in 3.5, the loss in 1996/97 is on the scale of a moderately cold winter, i.e. 60–61 DU over 350–850 K. However,

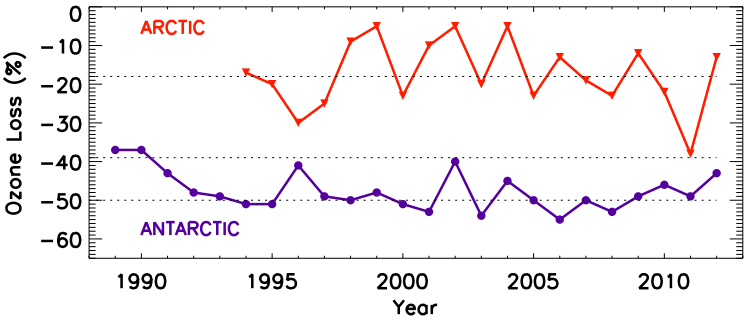

Figure 5.8: Vortex-averaged (Nash et al., 1996) ozone loss estimated from the ground-based total column (SAOZ and UV-visible in the Arctic [data from F. Goutail, CNRS/LATMOS, Paris] and SAOZ, UV-visible, DOAS, Dobson and Brewer in the Antarctic) ozone measurements for the Arctic (1994–2011) and Antarctic (1989–2012) winters.

the loss estimated for 2010/11, 130–160 DU over 350–850 K, is undoubtedly the largest among the Arctic winters, as the previous maximum of 109–115 DU was in 2004/05 (WMO, 2011; Kuttippurath et al., 2010a). Figure 5.7 also shows that the loss in 1996/97 is moderate (1.2 ppmv) and the loss in 2010/11 is the largest (2.4 ppmv) as compared to other winters. The ozone loss in 2004/05 is somewhat larger than that of 2010/11 in February–March, but the additional loss of ∼0.8 ppmv thereafter, in mid-March to mid-April 2011, is exceptional.

5.3 Comparison with the Antarctic winters

Since the ozone loss in the Arctic winter 2010/11 is unprecedented as analysed in this and previous studies (Manney et al., 2011; Sinnhuber et al., 2011), we compare the results with the Antarctic ozone loss. Some additional model runs are performed for a few Antarctic winters and are compared to the Aura MLS observations. Though the main ozone loss processes are alike, the meteorology is entirely different in the two polar regions, giving rise to the difference between the ozone loss observed in the respective polar regions (Solomon et al., 2007; WMO, 2007). On average, our analyses for various winters in 2004–2010 show that peak ozone loss (>2 ppmv) in the Antarctic stratosphere occurs over a broader altitude range of 350–650 K and usually shows its maximum in the late September and early October period (Kuttippurath et al., 2013). The peak ozone loss altitudes hardly change, but the maximum loss usually varies between 2.5 and 3.5 ppmv, depending on the temperature history of each winter. The colder Antarctic winters such as 2006 show a peak loss of about 3.5 ppmv, while the warmer winters, like 2004 and 2009, exhibit a peak loss of about 2.5 ppmv over 450–550 K. In addition, the total column ozone loss in the Antarctic winters, as shown in Fig. 5.8, usually shows about 130–150 DU (35–42%) in the warmer winters and about 160–180 DU (50–55%) in the colder winters (Kuttippurath et al., 2010b). It appears that the maximum column ozone loss estimated for the Arctic winter 2010/11 in this study is close to the loss computed for the early years of Antarctic ozone depletion (1985–1991) (Kuttippurath et al., 2013; WMO, 2007) and the relatively warmer Antarctic winters (e.g. 2002, 2004 and 2009) (Kuttippurath et al., 2013; WMO, 2011, 2007; Kuttippurath et al., 2010b).

Figure 5.9 illustrates the vortex-averaged ClO and ozone loss estimated in the Arctic winter 2010/11 and the mean vortex-averaged ozone loss estimated for the seven Antarctic winters: 2004–2010. We use the same model MIMOSA-CHIM and model set-up, Aura MLS measurements, and the passive method for the ozone loss calculations in the Antarctic to make a fair comparison with those in the Arctic. Note that the Antarctic measurements shown are the Aura MLS O_3 v2.2, but the Arctic observations are v3.3. However, the difference between the vortex-averaged O_3 from v2.2 and v3.3 is negligibly small and thus we can robustly compare these values directly. The ozone loss estimated in these Antarctic winters is about 2.5–3.2 ppmv in the model and 2.4–2.8 ppmv in Aura MLS. The ozone loss estimated in March/April of the Arctic winter 2010/11 is comparable to that of the September average in the Antarctic, as already shown by Manney et al. (2011). Nevertheless, the Arctic ozone loss is marginally smaller than that of the October average that includes three relatively warm (2004, 2009 and 2010) and two very cold (2006 and 2008) Antarctic winters. The altitudes of maximum ozone loss of the 2010/11 Arctic winter, 425–575 K, are also identical to those of the Antarctic winters. Therefore, in addition to the column ozone (Fig. 5.7), the ozone loss profiles in the Arctic winter 2010/11 also show ozone loss features matching those found in

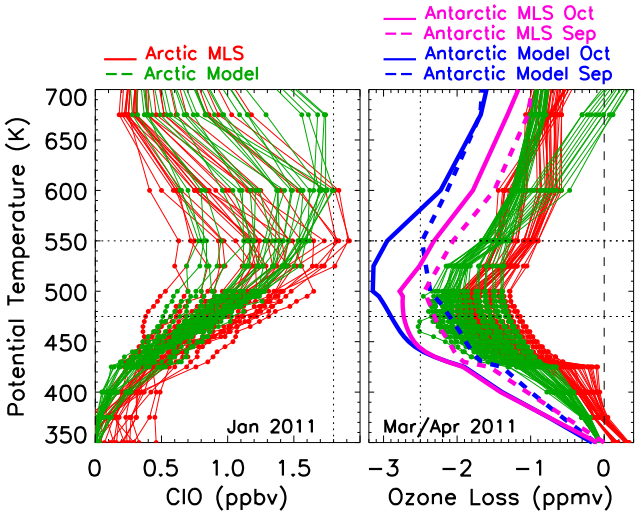

Figure 5.9: ClO (left panel) and ozone loss (right panel) profiles inside the vortex (≥65° EqL) from MIMOSA-CHIM and MLS in the Arctic winter 2010/11, and the mean September and October ozone loss profiles in the Antarctic vortex averaged for seven winters (2004–2010). The dotted vertical line is 1.8 ppbv of ClO or 2.5 ppmv of ozone loss. The dashed vertical line is 0 ppmv. The dotted horizontal lines are 475 and 550 K.

the Antarctic stratosphere. The model simulates relatively lower O_3 than MLS for most Antarctic winters and thus, modeled ozone loss is larger than the loss estimated with the MLS measurements.

In most Arctic winters the peak ozone loss is confined to the lower stratosphere centered around 450 K (e.g. Kuttippurath et al., 2010a; Rex et al., 2004). The loss above 550 K contributes about 19 ± 7 DU to the total column loss, which is mainly driven by NO_x catalysed chemistry in the middle stratosphere (Kuttippurath et al., 2010a). On the other hand, as shown by the ozone loss profiles, ozone loss in the Antarctic stratosphere takes place over a broad altitude range centered around 550 K, and thus nearly half of the loss occurs above this isentropic level. Therefore, the Antarctic partial column (380–550 K) ozone loss (around 130 DU) computed by Tilmes et al. (2006) is not directly comparable to the partial column ozone loss estimated here for the Arctic winter 2010/11. In addition, the sparse sampling of the HALOE in the southern polar vortex region, which does not always cover the maximum ozone loss period of the Antarctic, makes the comparison more difficult.

5.4 Conclusions

A comprehensive analysis of the Arctic winters 1996/97 and 2010/11 is presented with respect to the dynamical and chemical evolution of the winters. Both winters show a prolonged stable vortex from December to late April. However, the winter 1996/97 was moderately cold during December–February and thus, occasional chlorine activation led to a moderate ozone loss of about 1.2 ppmv around 475–550 K or 61 DU over 350–850 K by late March–late April. In contrast, the Arctic winter 2010/11 experienced the largest area and longest period ever of chlorine activation, with ClO values up to 1.8 ppbv around 450–550 K, which translated to the record ozone loss of around 2.4 ppmv at the same altitudes in late March/mid-April. The partial column estimates over 350–850 K also show a correspondingly massive loss of about 130–160 DU in mid-April. The simulated ozone loss rates show large values of 2–4 ppbv sh^{-1} in March–early April at 475 K, which are uncommon in the Arctic at this time of the winter. In tune with these ozone loss features, the ClO–ClO and ClO–BrO cycles show increasingly larger values (∼30–55 and 30–35%, respectively) in late February–March, as does the HO_x cycle in April (about 30–50%) in the lower stratosphere, at 475 K. Additionally, significant ozone loss of about 0.7–1.2 ppmv is also computed at 550–700 K in March–April 2011. As expected, the NO_x cycle dominates the ozone destruction processes in the middle stratosphere, with a contribution of around 30–70% at 675 K.

The ozone loss in the Arctic winter 2010/11 is close to those estimated in the Antarctic winters, as assessed in this study and already shown by Manney et al. (2011). However, it has to be kept in mind that the ozone loss values in the Arctic winter 2010/11 are comparable to those of the relatively warm Antarctic winters only, though September averages of the cold Antarctic winters also show similar magnitude of ozone loss. This is also applicable to total column ozone loss analyses as they show loss ranges (130–140 DU) equivalent to those of the warm Antarctic winters (e.g. 2004 and 2010) and the early years of the Antarctic ozone depletion (1985–1991), as discussed in Sect. 5.3.

The atypically prolonged chlorine activation and strong denitrification triggered this high ozone loss of 2.4 ppmv or 130–160 DU in 2010/11. Furthermore, large loss (1.5 ppmv) over a broader altitude range (400–600 K) similar to that of the Antarctic is observed for the first time in the 2010/11 Arctic winter. Nevertheless, since the halogens are decreasing slowly, the ozone loss in the polar stratosphere is expected to decrease even in cold winters. Yet, as discussed in Sinnhuber et al. (2011), with the predicted rate of stratospheric cooling in a climate changing world, the expected reduction in halogens may not help to cut down the ozone loss rates in very cold winters in the next decade. Therefore, cold winters of this kind with a similar range of ozone loss can be expected in the future (Manney et al., 2011; Sinnhuber et al., 2011).

SECTION II

ANTARCTIC STRATOSPHERE

Chapter 6

Estimation of Antarctic ozone loss *

Contents

Since the discovery of Antarctic ozone hole (Chubachi, 1984; Farman et al., 1985), a string of ground-based and satellite sensors has been dedicated to observe the polar stratospheres in the framework of the international WMO–Global Atmospheric Watch programme (WMO, 1993) and the Network for Detection of Atmospheric Composition Change (NDACC) for the constant monitoring of ozone loss. Although satellites have the advantage of global coverage, they cannot observe at SZA $> 84°$ and thus not during the deep winter months. In addition, i) they have limited lifetime and cannot always be immediately replaced, ii) their measurements usually show progressive degradation and iii) the discontinuity in the observations produce undesirable jumps in the trend analyses when the concatenated data are used. In contrast, although of limited geographical coverage (which is the biggest advantage of space-based measurements as compared to the ground-based observations), ground-based sensors offer the advantage of continuous record and easy repair or replacement if necessary. Additionally, those measuring at visible wavelengths, such as SAOZ spectrometers used in this study, are capable of making reliable measurements until 91° SZA, which is throughout the winter at latitudes around 65°S. Therefore, the maintenance of an independent ground-based capacity is absolutely essential.

The passive tracer method has been successfully applied to the estimation of ozone loss from ground-based total ozone measurements in the Arctic (Goutail et al., 1999). This approach separates the contribution due to transport and photochemical loss in total ozone evolution during the winter. The tracer calculations are performed by CTMs in which photochemistry is deactivated to represent the dynamical evolution of the winter. The objective of the present study is to apply the passive tracer technique to the Antarctic total ozone observations for the yearly evaluation of ozone loss. In order to estimate the loss, we use ground-based measurements from three SAOZ stations in the Antarctic. Fig. 6.1 shows the images of selected ground-based instruments installed in the Antarctic. We use measurements from six Dobsons, two Brewers and a UV-VIS Differential Optical Absorption Spectroscopy (DOAS) spectrometer. Table 6.1 and Fig. 6.2 show details of the stations. We use the REPROBUS and SLIMCAT global three-dimensional (3-D) CTMs for the tracer simulations. The ozone loss derived from the ground-based measurements are compared to that of the space-borne observations of the OMI on Aura and SCIAMACHY on ENVISAT.

*This chapter is partly based on: Kuttippurath, J., F. Goutail, J.-P. Pommereau, F. Lefèvre, H. K. Roscoe, A. Pazmiño, W. Feng, M. P. Chipperfield and S. Godin-Beekmann: Estimation of Antarctic ozone loss from Ground-based total column measurements, Atmos. Chem. Phys., 10, doi:10.5194/acp-10-6569-2010, 6569–6581, 2010.

Figure 6.1: Images of the the Dobson spectrometer at South Pole (image courtesy: http://www.esrl.noaa.gov/gmd/ozwv/dobson/), the Brewer spectrometer at Zhongshan (image courtesy: http://www.theozonehole.com/), the SAOZ instrument at Dumont d'Urville (image courtesy: F. Goutail, CNRS, Paris) and the DOAS instrument at Neumayer (image courtesy: http://www.awi.de/typo3temp/pics/) in Antarctica.

6.1 Ozone column

6.1.1 Ground-based measurements

SAOZ: The zenith sky SAOZ UV-VIS spectrometers (Pommereau and Goutail, 1988) operate at 300–650 nm, looking at sunlight scattered from the zenith sky during twilight. Ozone is measured in the Chappuis band (450–650 nm) at high SZA between 86° and 91° every morning and evening. The main source of uncertainty in the measurements is the air mass factor (AMF) and for instance, the difference in AMF between inside and outside the ozone hole can be up to 10%. The total column measurements in the visible region have a random error of 4.7%, systematic error of 3.6% (Hendrick et al., 2011) and different SAOZ slant column measurements are consistent within ±3% (Roscoe et al., 1999; Van Roozendael et al., 1998).

DOAS: This is a similar instrument to SAOZ but with differences of detail, e.g. light is collected by a small telescope and fed to the spectrograph using two depolarising quartz fiber bundles. The spectrograph consists of a UV and a visible channel. Ozone measurements are performed in 490–555 nm at 84–90° SZA, similar to SAOZ. Ozone slant column densities are converted using AMFs

Table 6.1: Measurement station, latitude, longitude, type of observation (instrument), starting year of observation and period of wintertime measurements for which the ozone loss analyses are performed. The mid-latitude stations denoted with † are not considered for ozone loss analyses for Antarctica, but are used for the diagnosis of inter-annual variations of total ozone in the mid-latitudes.

Station	Latitude	Longitude	Instrument	Starting year	Observation period
South Pole	89.9° S	24.8° W	Dobson	1963	Aug–Nov
Belgrano	77.9° S	34.6° W	Brewer	1982	Sep–Nov
Arrival Heights	77.8° S	166.7° W	Dobson	1988	May–Nov
Halley	75.6° S	26.8° W	Dobson	1958	Aug–Sep
Concordia	75.1° S	123.4° E	SAOZ	2007	May–Nov
Neumayer	70.7° S	8.3° W	DOAS	1992	Aug–Nov
Zhongshan	69.4° S	76.4° E	Brewer	1993	Aug–Nov
Syowa	69.0° S	39.6° E	Dobson	1961	Aug–Nov
Rothera	67.6° S	68.1° W	SAOZ	1996	May–Nov
Dumont d'Urville	66.7° S	140.0° E	SAOZ	1988	May–Nov
Faraday/Vernadsky	65.3° S	64.3° W	Dobson	1957	Aug–Nov
Marambio	64.2° S	56.7° W	Dobson	1987	Aug–Nov
Mid-Lat. stations					
Ushuaia	54.8° S	68.2° W	Dobson	1994	May–Nov
Macquarie Island	54.5° S	159.0° E	Dobson	1957	May–Nov
Rio Gallegos	51.6° S	69.3° W	SAOZ	2008	May–Nov
Kerguelen	49.4° S	70.3° E	SAOZ	1995	May–Nov
Lauder	45.0° S	169.6° E	Dobson	1970	May–Nov
Comodoro Rivadavida†	45.8° S	67.5° W	Dobson	1995	May–Nov
Melbourne †	37.7° S	144.8° E	Dobson	1983	May–Nov
Buenos Aires†	34.6° S	58.5° W	Dobson	1965	May–Nov
Perth †	31.9° S	115.9° E	Dobson	1969	May–Nov

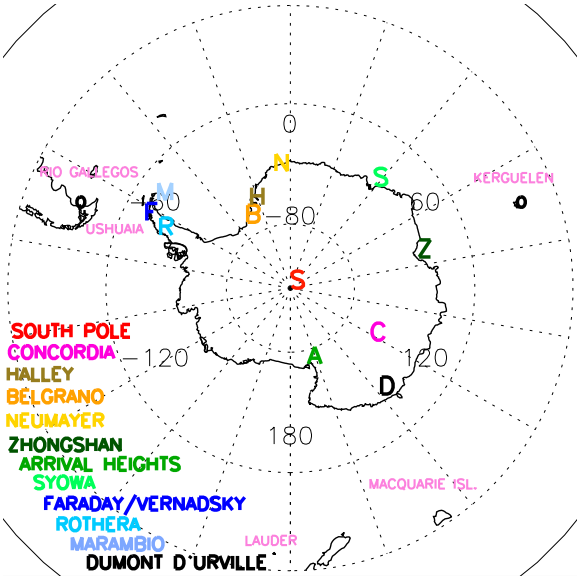

Figure 6.2: Geographical position of the the ground-based stations in Antarctica and southern mid-latitudes considered for the ozone loss analyses in this study. The mid-latitude stations are shown in light pink colour. Positions of the Antarctic stations are marked by the first letter of their names in respective colours (e.g. C is for Concordia).

estimated from AMFTRAN Monte Carlo Radiative Transfer Model. The accuracy of ozone vertical column density retrieved from the Neumayer DOAS is about 2%. The DOAS measurements are described in detail by Frieß et al. (2005).

Dobson spectrophotometer: The instrument consists of a double prism monochromator to measure the differential absorption of ozone in UV (Dobson, 1957). Measurements are performed by looking at the direct sun by clear sky and are averaged to a daily mean. Nevertheless, those measurements are limited to SZA $< 80°$ i.e. after mid-August at the polar circle. As the instrument requires calibration, comparison with the well-calibrated Dobson #83 (Boulder, USA) is carried out. However, calibration with this instrument may not be accurate at the South Pole (because of high latitude and high SZA) and hence, it may slightly affect the accuracy of measurements. The random error of these observations is estimated as 0.5% or 1 DU (Basher, 1982; Scarnato et al., 2010), but is subject to the accuracy of absorption cross-sections and a known significant temperature dependence in the UV and stray light at high SZAs (Hendrick et al., 2011), which were not taken into account for the retrievals used here.

Brewer spectrophotometer: Brewer measurements also make use of differential absorption in the UV region (Brewer, 1973). The determination of total ozone is similar, but sensitivity of the instrument is better than that of the Dobson. As in the case of the Dobson, an empirical relation between simultaneous direct sun and zenith sky has to be established if zenith observations are to be taken. Calibration of the instrument is essential and a well calibrated Brewer direct sun measurement has an error comparable to that of the Dobson. Recent comparisons indicate that the random errors of well-maintained Brewer observations are of the order of 0.15% (Scarnato et al., 2010).

6.1.2 Space-based observations

OMI on Aura: The OMI sensor on the Aura satellite began to operate in 2004 as a successor to the Total Ozone Mapping Spectrometer (TOMS) (Levelt et al., 2006). The nadir viewing UV-VIS spectrometer measures solar light scattered by the atmosphere with a spatial resolution at nadir of 13×24 km. The sun-synchronous orbit of Aura and the wide viewing angle of OMI enable daily global coverage of the sunlit portion of the Earth. The overpass data, spatial averages within 100 km, are retrieved using the TOMS v8 algorithm. The retrieval makes use of two wavelengths: 331.2 and 360 nm for high ozone and at high SZA. However, retrievals from 317.5 and 331.2 nm are used for most conditions. The uncertainty of the ozone column is 2–5% for SZA $< 84°$ (Bhartia and Wellemeyer, 2002).

SCIAMACHY on ENVISAT: SCIAMACHY (hereafter SCIA), an imaging spectrometer on ENVISAT placed into orbit in 2002, utilises nadir, limb and sun/moon occultations for ozone column

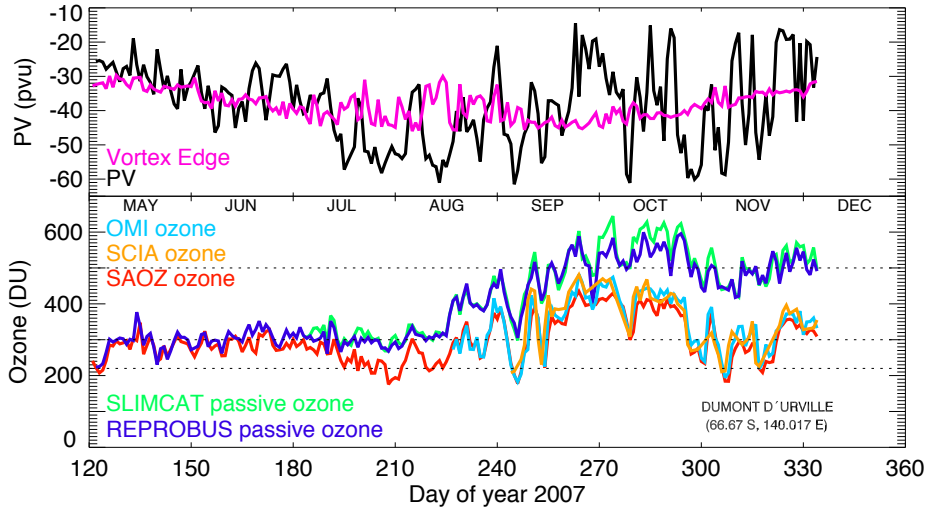

Figure 6.3: Temporal evolution of various parameters used for the computation of ozone loss at Dumont d'Urville in 2007. Top: ECMWF potential vorticity at 475 K, and polar vortex edge. Bottom: SAOZ, OMI and SCIA daily mean total ozone and SLIMCAT and REPROBUS passive ozone (tracer). The horizontal bars represent the 220 DU ozone hole criterion, the 300 DU average pre-ozone hole value and the 500 DU average spring column in the absence of loss.

retrievals (Bovensman et al., 1999). The data are recorded from the transmitted, back scattered and reflected solar radiation from the atmosphere at 240–1700 nm. The instantaneous field of view spans 2.6 km in the vertical and 110 km in the horizontal direction at the tangent point. We consider the total column overpass data calculated from nadir measurements, averaged within 100 km radius above each station, retrieved using the v2 algorithm based on TOSOMI (Total Ozone retrieval scheme for SCIAMACHY based on the OMI DOAS algorithm). The estimated accuracy of the ozone column is about 2–3.3% (Eskes et al., 2005).

6.2 Estimation of ozone loss

To find chemical ozone loss from the measurements by applying the passive technique, tracer calculation by a CTM is required. For this purpose, passive ozone (ozone calculated without interactive chemistry) simulations from REPROBUS for 2006–2009 and SLIMCAT for 2005 are considered, as the data from the former was not available in 2005. We use the diurnal averages of the ozone and tracer column simulations sampled at the location of each station. The details of tracer simulations in the models are given in the following sections and the method is described afterwards.

The REPROBUS 3-D CTM (Lefèvre et al., 1994, 1998) uses a hybrid σ-pressure vertical coordinate for which winds and temperatures are driven by the ECMWF operational data on 60 vertical levels to 0.1 hPa (∼60 km) until February 2006, and then 91 levels to 0.01 hPa (∼90 km) afterwards. Vertical advection is computed directly from the analysed winds. The simulations presented here were integrated on a global grid with a horizontal resolution of $2° \times 2°$. Chemical species are transported by a semi-Lagrangian code (Williamson and Rasch, 1989). The model includes a comprehensive description of stratospheric chemistry. Absorption cross-sections and kinetics data are based on Sander et al. (2006). However, absorption cross sections of Cl_2O_2 are taken from Burkholder et al. (1990) and are extrapolated to 450 nm. Monthly varying H_2SO_4 fields, leading to the formation of liquid aerosols in the CTM, are computed from the outputs of a 2-D-model long-term simulation that consider impacts of volcanic eruptions (e.g. Bekki et al., 1993; Bekki and Pyle, 1994). The model includes reactions on binary and ternary liquid aerosols as well as on water-ice particles. The composition of liquid aerosols is calculated analytically (Luo et al., 1995). The ice particles are assumed to incorporate HNO_3 in the form of NAT (Davies et al., 2002). Cl_y and Br_y are explicitly calculated from their long-lived sources at the surface and are therefore time dependent. An additional 6 pptv of bromine in the form of CH_2Br_2 is added to Br_y to represent the contribution of brominated short lived species reaching the stratosphere (Feng et al., 2007b; WMO,

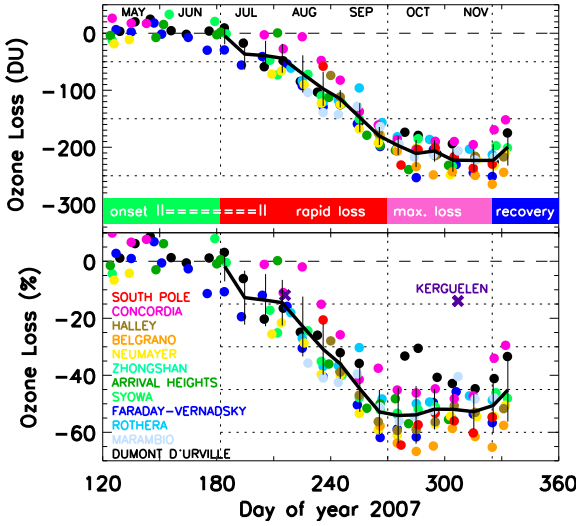

Figure 6.4: Vortex averaged (Nash et al., 1996) individual ozone loss estimated (ten-day mean) at the ground-based stations in the Antarctic using the passive method (top: DU, bottom: percent). The black thick lines represent the mean and the error bars represent the standard deviation from the mean. The observations from Kerguelen, a mid-latitude station, are not included in the average, shown with X marks. The vertical dotted lines represent the different phases of ozone loss process in the Antarctic as marked in the colour shades (see text), while the horizontal dotted lines represent −50, −150 and −250 DU (top), and −15, −30, −45 and −60% (bottom) of ozone loss. Some stations start the wintertime observation in August or September. The ozone loss onset varies with respect to sunlit latitudes and therefore, the onset period depends on co-ordinates of the stations. Thus the onset and rapid loss phases are clustered together with dashed lines in the red and green colour shades.

2007).

SLIMCAT is an off-line 3-D CTM Chipperfield (1999), which uses hybrid σ-θ vertical coordinate and extends from the surface to a top level which depends on the domain of the forcing analyses (Feng et al., 2007a). Here the horizontal winds and temperatures are specified using ECMWF operational data of 60 vertical levels to 0.1 hPa. Vertical advection in the θ-domain (above 350 K) is calculated from diabatic heating rates using the National Center for Atmospheric Research (NCAR) Community Climate Model radiation scheme (Chipperfield, 2006). Chemical tracers are advected by conservation of second-order moments (Prather, 1986). The model describes the main stratospheric chemical species O_x, HO_x, NO_y, Cl_y, Br_y, source gases and a treatment for CH_4 oxidation. It contains a detailed gas-phase stratospheric chemistry scheme. As in REPROBUS, the photochemical data are based on Sander et al. (2006) and the absorption cross sections of Cl_2O_2 are taken from Burkholder et al. (1990), which are extrapolated to 450 nm. The model treats heterogeneous reactions on liquid aerosols, NAT and ice (Chipperfield, 1999), and denitrification schemes (Davies et al., 2002). An extra 6 pptv of bromine reaching the stratosphere from short-lived species is also included in the calculations (Feng et al., 2007b; WMO, 2007).

6.2.1 The passive tracer method

The ozone loss by the passive method is computed by subtracting passive ozone from measured ozone. Large changes in total ozone inside polar vortex are related to convergence or divergence due to changes in tropopause height, planetary wave induced adiabatic motions and diabatic descent due to radiative cooling. To find the ozone loss inside the vortex, the Nash et al. (1996) criterion is applied to find the vortex limit (maximum of the first derivative of PV). A sensitivity test was conducted using the criterion of 35 and 45 pvu. While the low PV criterion adds noise, the high PV criterion makes the data sparse. As expected, though there were differences in number of observations inside the vortex when using different criteria, the final results were similar. Therefore, the Nash et al. (1996) criterion is adopted after exempting some apparent noise in the vortex limit data. The PV data used to differentiate the vortex measurements were generated from the MIMOSA contour advection model (Hauchecorne et al., 2002) forced by the ECMWF operational analyses. The vortex edge calculated at 475 K, where the concentration of ozone has its maximum in spring, is selected for its loss estimation. The ozone loss analysis starts in July and it extends until November.

Figure 6.3 illustrates the basics of the tracer scheme with relevant data at Dumont d'Urville for the winter 2007. The day-to-day variations due to vortex positions are well captured by the measurements and simulations. From July onwards, the ozone values inside the vortex decrease with time while they increase outside. The ozone columns, both measured and calculated, are anti-correlated with the PV values, where the high PV corresponds to the low ozone in the vortex. The SAOZ observations are continuous throughout the winter at Dumont d'Urville, while both OMI and SCIA start in mid-August and thus miss the onset of ozone loss process. Nevertheless, the

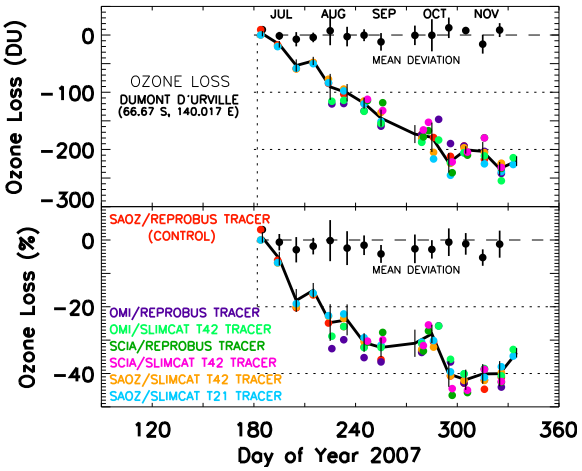

Figure 6.5: Vortex averaged (Nash et al., 1996) ozone loss diagnosed (ten-day mean) using different measurements and various tracer calculations by different model setups at Dumont d'Urville (top: DU and bottom: percent). The black solid lines represent the mean ozone loss from all scenarios and the black filled-circles represent the average deviation from the control (SAOZ/REPROBUS tracer). The error bars represent the standard deviation from the mean. The dotted vertical line represents 1 July. The dotted horizontal lines represent −100 and −200 DU (top), and −20 and −40% (bottom) of ozone loss.

observations from both ground and space are very consistent afterwards.

The chemical ozone loss is then computed by finding the difference between the tracer simulated by the CTM and ozone measured from the ground or space. That is, the observed ozone loss in absolute unit (DU) is estimated as $ozone_{meas} - tracer$ and in relative unit (%) is computed as $100 \times (ozone_{meas} - tracer)/tracer$. This procedure is repeated for each station and then sorted for inside the vortex. The example of 2007 is given in Fig. 6.4. The ozone loss starts at the edge of the vortex in early July, when it is displaced to the sunlit latitudes. So the stations at the edge, such as Dumont d'Urville and Rothera, are subjected to ozone loss early in the winter (e.g. Lee et al., 2000). As the day gets longer and light penetrates deeper inside the continent, the stations Concordia and Arrival Heights followed by Neumayer, Halley, Syowa, Belgrano and South Pole undergo ozone loss (e.g. Chubachi, 2009). Measurements at the latter stations were possible only in late August or September as they require sunlight for making observations. The figure clearly shows the late winter start of ozone loss in the vortex core, Concordia in particular (South Pole measurements start even later, by mid-September, e.g. Solomon et al., 2005). This delayed onset also produces a step like feature in the mean ozone loss curves in the July to mid-August period.

The intensity of ozone loss is also connected to the position of the stations and axis of the vortex. For instance, the sites well inside the vortex experience more loss than those at the edge. Therefore, South Pole or Belgrano observe more severe loss than Dumont d'Urville in each winter. The loss at Concordia is less than that of South Pole and larger than that of Dumont d'Urville due to the strength and longevity of the vortex over the respective locations.

The results delineate three distinct phases of the Antarctic ozone loss as marked with dotted vertical lines and colour shades in Fig. 6.4. The first stage starts in July and ends in late September, where rapid loss occurs with return of the sun over the continent. The loss rate is largest in this period. Starting time of this phase varies from May to July depending on the temperature, the time of vortex formation and its location. If the temperature is relatively low and the vortex appears in early winter that shifted in latitude, there can be some loss in May–June and thus this phase may start in May. The cumulative maximum of the ozone loss is generally observed in early October, afterwards the loss stops when PSCs are no longer forming because of comparatively higher temperatures. This is the second phase of the ozone loss process, where depth of the ozone hole reduces more or less slowly depending on vortex erosion, exchange with mid-latitudes and location of the station. Therefore, the edge stations, i.e. Dumont d'Urville, Marambio and Rothera, recover more rapidly. The ozone hole is not homogeneous. Depending on the location of the station with respect to the vortex, the loss can vary within ±10% (±20 DU). In the third phase, the ozone hole disappears in general by the end of November or early December as in 2006, except in the case of the unprecedented vortex split in 2002. It is during this period (October–November) that vortex pieces or filaments more or less filled-in could be observed at lower latitudes as in Kerguelen at 49° S in present case.

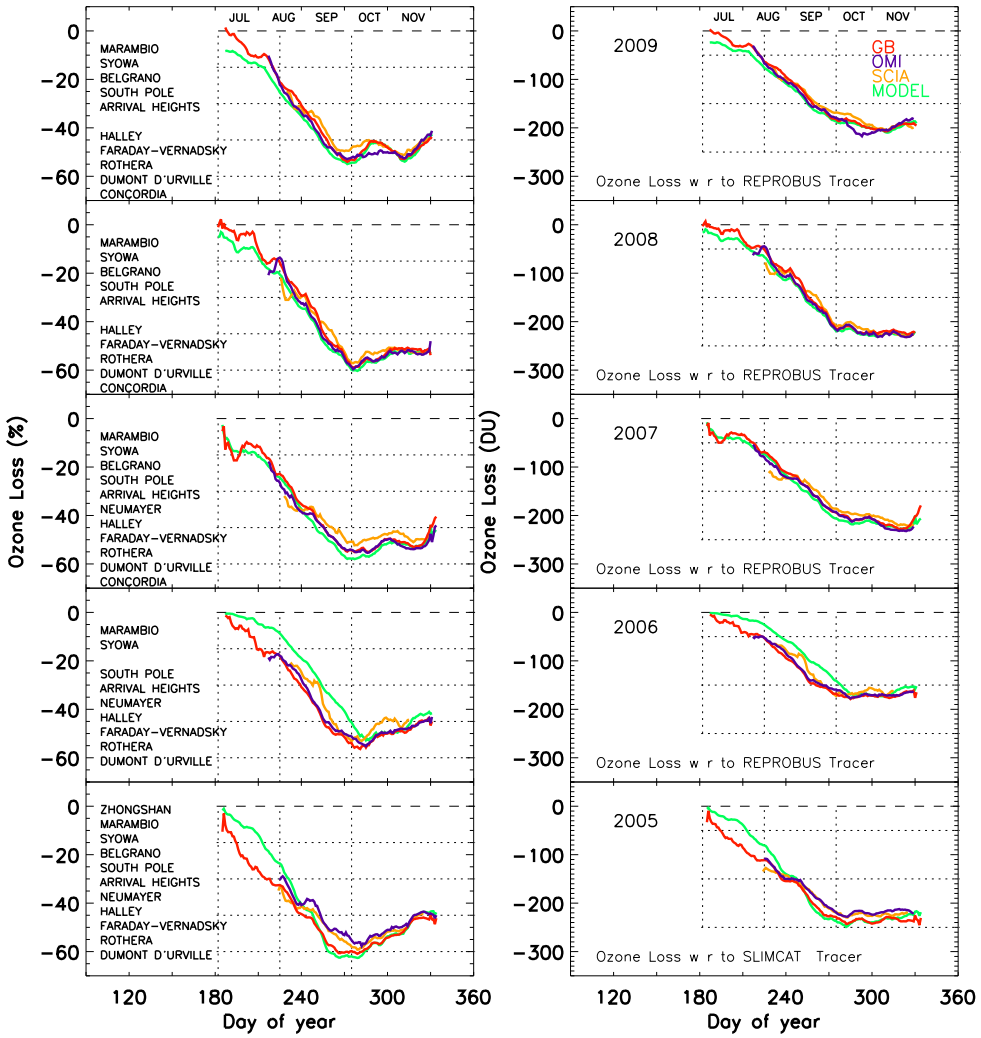

Figure 6.6: Vortex averaged (Nash et al., 1996) ozone loss estimated (ten-day boxcar average) from the ground-based measurements in red, the OMI observations in blue (OMI), the SCIAMACHY measurements in dark yellow (SCIA) and the model simulations by REPROBUS in 2006–2009 and SLIMCAT in 2005 in green (MODEL) for the Antarctic winters 2005–2009 (Left: percent, right: DU). The SCIA average excludes South Pole measurements due to unavailability. The dotted vertical lines represent day 182, 225 and 275, the time window used for the computations of daily ozone loss rates. The horizontal lines represent −15, −30, −45 and −60% (left panel), and −50, −150 and −250 DU (right panel).

6.2.2 Error analysis

In order to investigate the uncertainty of the method, ozone loss under various conditions are analysed. Fig. 6.5 shows the ozone loss estimated with SAOZ, OMI and SCIA using REPROBUS and SLIMCAT (with both T42 and T21 resolution) tracer for Dumont d'Urville in 2007. The stations at the edge region (Lee et al., 2000) show more spread than those inside the vortex (for which Dumont d'Urville shows the largest). We use the SAOZ/ground-based ozone loss analysis with REPROBUS tracer using MIMOSA PV and Nash vortex edge as the control, since simulated results match well with the measurements. To compute the uncertainty, the difference between the control and the ozone loss was estimated with other setups, as shown in the figure. The RSS of all these differences as well as the uncertainties in the measurements yield a deviation up to 4.4% (0–21 DU) depending on day.

The RSS computation includes all main processes that affect the accuracy of the method. Those are: **i)** the systematic differences between the instruments, drop in measured ozone due to presence of PSCs, and difference in AMF profile shapes (considered in the analysis by including the measurement uncertainties of respective instruments), **ii)** differences in simulated profiles with measurements

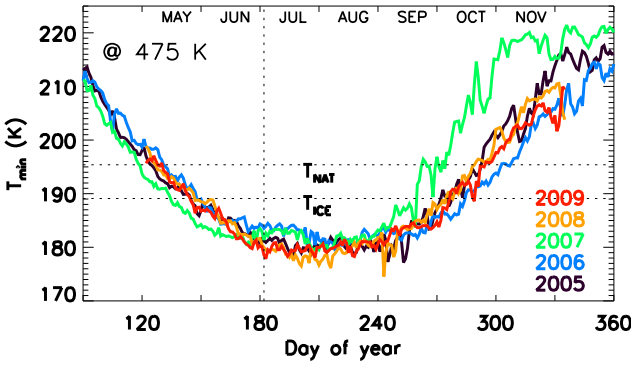

Figure 6.7: ECMWF daily minimum temperatures extracted over 50–90° S at 475 K for 2005–2009. The horizontal lines represent the T_{NAT} and T_{ICE}. The dotted vertical line represents 1 July.

when ozone varies rapidly (considered in the analysis by using tracers from different models of varying horizontal and vertical resolution) and **iii)** shifts in location of estimated vortex edge (considered in the analyses by testing with different vortex edge criteria, PV data sets and horizontal resolution of the models). Since size of the vortex can be smaller above the ozone loss analysis level of 475 K, air outside the vortex cannot be ruled out and was not possible to account for by these experiments.

6.2.3 Accuracy of the method

There are a few parameters that influence the strength of ozone loss evaluation method. The most evident are the realism of the tracer field in the models and the vortex edge calculation from potential vorticity. We tested how the derived ozone loss varies with the expected changes in these parameters. These tests were repeated for the overpass measurements from satellite observations. The RSS of the deviations including measurement accuracies is within 4%. Since accuracy of the measurements is of the order of 3–5% and the total error derived from RSS is ∼4%, the small contribution from other input shows the consistency and potency of the method. In addition, the use of different model setups for the calculations of tracer ensures that the estimation provides consistent results and affirms that the method is sound. The main dispersion of loss computation comes from the inhomogeneous distribution of ozone in the vortex, which ranges from ±2–10% at the beginning when only the edge stations are exposed to sunlight, to ±0–5% at the end when loss has stopped.

6.3 Application of the method

We now apply the passive method to estimate the Antarctic ozone loss and examine the variability of the loss between 2005 and 2009. The loss analyses using SCIA observations exclude South Pole measurements because of their unavailability. The daily ozone loss rates are calculated in a common time window for all data sets, i.e. between day 225 and 275 in each winter. Fig. 6.6 shows the ten-day boxcar average of the vortex mean ozone loss derived from the ground-based, OMI, SCIA and model (REPROBUS for the winters 2006–2009 and SLIMCAT in 2005) data and we begin the discussion with the most recent year. In order to preserve the temporal ozone loss features, instead of finding the vortex averaged loss at each station in every ten days, the average of ozone and tracer data inside the vortex from all stations are considered. Then the observed ozone loss in absolute unit (DU) is estimated as ozone_{avg}-tracer_{avg} and in relative unit (%) is computed as $100\times(\text{ozone}_{avg}\text{-}\text{tracer}_{avg})/\text{tracer}_{avg}$. Here, the ozone_{avg} (tracer_{avg}) represents the mean of the ozone (tracer) data inside the vortex from all stations. The same approach is repeated for the model simulations.

In 2009, the ozone loss started by the first week of July and it peaked to 53% by late September. The satellite observations, both OMI and SCIA, agree well with the ground-based analysis. The ozone loss rate shows 0.62 for ground-based, 0.58 for OMI, 0.54 for SCIA and 0.55% day^{-1} for the model. In 2008, the ground-based measurements find the ozone loss onset in early July and its maximum in early October, about 59%. Similar results are found in the loss computed from satellite and model data, where the differences are within ±2%. The loss rates analysed from the measurements and simulations exhibit similar values of about 0.8% day^{-1}, but slightly less from

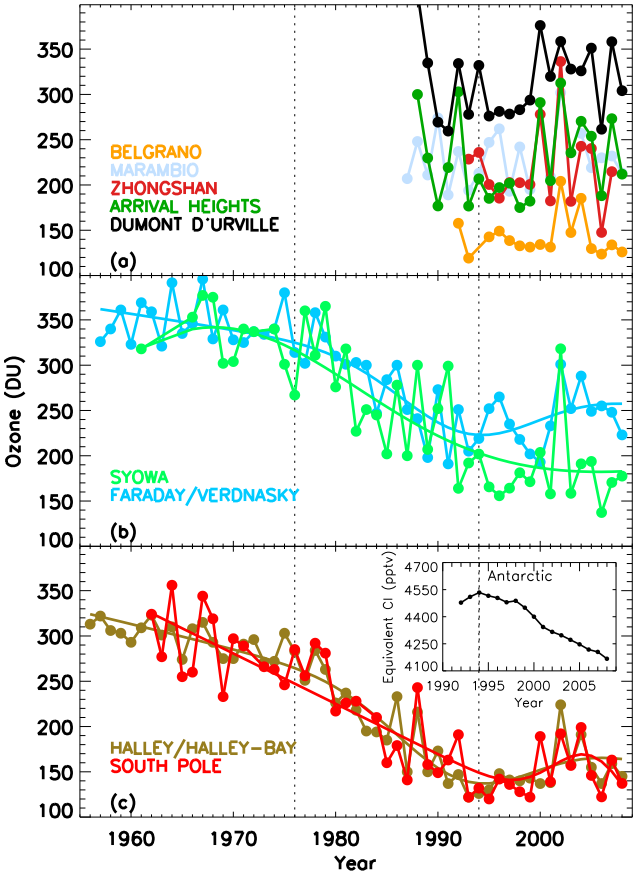

Figure 6.8: Evolution of October mean total ozone in the Antarctic from ground-based observations. **(a)** Stations installed after 1985, **(b)** historical stations Syowa and Faraday, and **(c)** historical stations South Pole and Halley, and the equivalent chlorine in the Antarctic in the inset. The historical data are plotted separately for clarity reasons. The dotted vertical lines represent year 1976 and 1994. A Gaussian fit is shown in the time series of the historical stations.

the SCIA observations. In 2007, as found in other winters, the loss started in July and reached its peak by mid-October. The loss derived from ground-based and OMI observations exhibit a similar maximum of ∼55%, whereas it is 3% less with SCIA and 3% more with the model. The ozone loss rates show 0.62 for ground-based, 0.54 for OMI, 0.47 for SCIA and 0.66% day^{-1} for the model. In 2006, the observed ozone loss shows its onset in early July. The maximum loss derived from ground-based observations shows 56% by early October, consistent with that of OMI measurements. The loss computed from the SCIA and model data show slightly lower values of about 53%. The simulated loss in July–September is slightly smaller than that of the ground-based observations, even if both return similar loss rates of about 0.71% day^{-1}. In 2005, a large loss was measured in early winter and its maximum in early October. The peak loss derived from the ground-based measurements is 61%, whereas it is 1% more from the model calculations. The loss evaluated from satellite observations find agreeable results within ±2–5%. The estimated loss rates are 0.53, 0.5, 0.5 and 0.75% day^{-1} for ground-based, OMI, SCIA and SLIMCAT, respectively.

6.4 Inter-annual variability

The passive method used for the estimation of ozone loss depends largely on tracer simulations in the models. Therefore, a survey with ozone column measurements is necessary to analyse the consistency of the loss evaluation. Since measurements are available for decades, this diagnosis is not restricted to 2005–2009, as in the case of previous discussions.

6.4.1 Antarctic ozone loss

The general behaviour of ozone loss with time and chemistry is alike in all winters. However, the cumulative loss, period of maximum loss and longevity of the ozone hole alter in accordance with the strength of the vortex. In general, as found in previous studies the Antarctic ozone loss starts in early July and stops during the last week of September (Solomon et al., 2005; Tilmes et al., 2006;

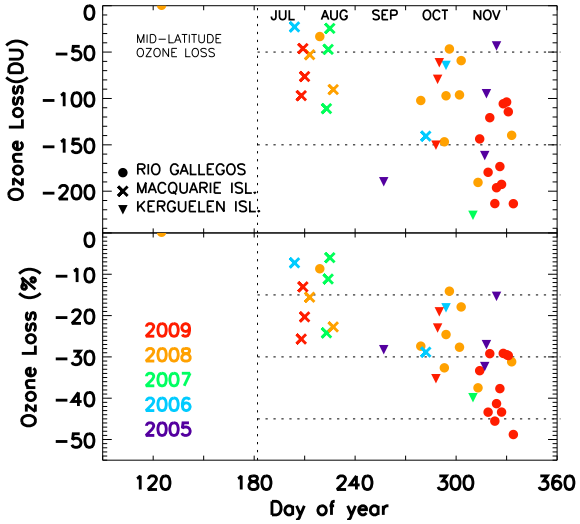

Figure 6.9: Ozone loss estimated during the vortex events (Nash et al., 1996) at selected southern mid-latitude stations for the recent Antarctic winters (Top: DU and bottom: percent). The dotted vertical line represents 1 July, and the horizontal lines show −50 and −150 DU, and −15, −30 and −45% of ozone loss.

Huck et al., 2007) except in 2006 when it extended until the first week of October. In all years the ozone hole could be followed until the 3^{rd} and 4^{th} week of November (Bevilacqua et al., 1997; Solomon et al., 2005).

Figure 6.7 illustrates the daily minimum temperature from ECMWF within 50–90° S at 475 K for 2005–2009. In general, the NAT temperatures are found from mid-May until October. Temperatures below the freezing point of water-ice (T_{ICE}) occur from June to late September. Among the last four winters, 2007 shows the lowest temperatures in May–June, 2008 shows the lowest in mid-July to mid-August and 2006 shows the lowest in mid-September to November. The recent winter 2009 was generally colder than 2008 and 2005, while the winter 2007 had the warmest September–November at 475 K and earliest vortex dissipation. The winter 2006 was one of the coldest, in which the complete breakdown of the vortex was observed in December.

As expected from similar temperatures, the cold winters 2006, 2008 and 2009 show little difference in ozone loss. The maximum ozone loss was found early in 2006 as compared to other winters because of the lower temperatures and well formed early vortex at sunlit parts, whereas the warm winter 2007 shows relatively smaller loss. The ozone loss estimated from the ground and space based observations is very consistent, showing small differences, within ±2%. The model calculations also find similar scales of ozone loss in each winter, where the differences with observations are about ±3–5%. Although the deviations are small, the geographical differences in sampling among the ground-based, satellite and model data could also contribute to this offset. When compared to other winters, the loss calculated with model underestimates the measured loss in 2006. There were no changes in the model input other than the ECMWF meteorological data used in this year as compared to other years. Therefore, the differences could be due to the possible inaccuracies in the temperature data (e.g. Boccara et al., 2008; Pitts et al., 2007), which in turn can affect PSCs, chlorine activation and hence, ozone calculations by the model.

There are no other ozone loss estimations available for the Antarctic winters 2005–2009 to compare with our results. The available studies for the previous winters are not directly comparable as they use either partial columns or a different evaluation method. However, as concluded in WMO (2007) and references therein, it is clear that Antarctic ozone loss has stabilised in the 1995–2005 decade because of its saturation. Therefore, most of the inter-annual variability results more from levels of dynamic forcing than a change in levels of EESC (e.g. Yang et al., 2008). The amplitudes of total loss reported in 1995–2005 are very similar to that derived in 2005–2009. For instance, the partial column loss estimated at 350–600 K from ILAS measurements by applying the tracer correlation approach was 157±17 DU in early October 2003 (Tilmes et al., 2006), which is close to our evaluation for the recent winters during the same period. Our conclusion on the inter-annual variability of ozone loss is also in line with the previous studies (Hofmann et al., 1997; Wu and Dessler, 2001; Bevilacqua et al., 1997; Solomon et al., 2005; Hoppel et al., 2005; Lemmen et al., 2006; Huck et al., 2007). The studies based on ozonesonde observations (e.g. South Pole and Syowa) in the Antarctic have some significance in this context as we have used measurements from these

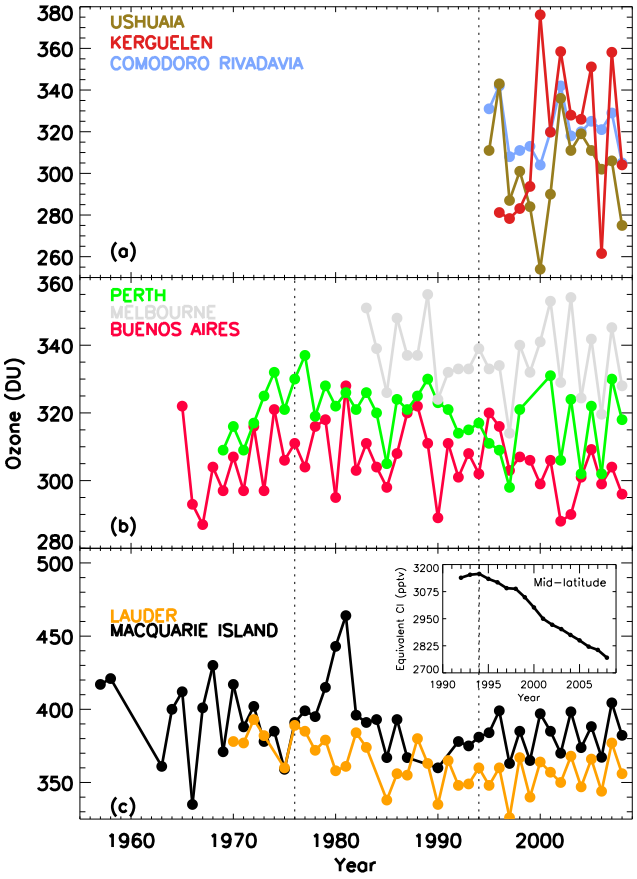

Figure 6.10: Evolution of October mean total ozone at southern mid-latitude ground-based stations: **(a)** stations installed after 1985, **(b)** historical stations at 30–40° S and **(c)** historical stations at 40–60° S with equivalent chlorine in the mid-latitude in the inset. The dotted vertical lines represent year 1976 and 1994.

stations for our evaluations (e.g. Hofmann et al., 1997; Solomon et al., 2005). Additionally, the ozone loss rates in September derived from the South Pole ozone soundings in 1990s (Hofmann et al., 1997) and those estimated from the SLIMCAT simulations in early 2000s (Feng et al., 2005a) are 2–3 and 2.6–3.2 DU day^{-1}, respectively. The loss rates found in our study are also of the same order of magnitude (2–3 DU day^{-1} or 0.6–0.9% day^{-1}), which reinforces the small inter-annual variability of Antarctic ozone loss.

6.4.2 Southern high latitude ozone

Figure 6.8 displays the October mean of total ozone from various stations together with EESC in the Antarctic. The four historic stations Halley, Syowa, South Pole and Faraday have measurements since 1956 and they show large decrease in ozone until early 1990s and saturation of the ozone loss afterwards (Jiang et al., 1996). The little inter-annual variation due to the saturation is clearly evident after mid-nineties. These results are very consistent with previous works on total ozone trends in the Antarctic (Bojkov and Fioletov, 1995; Bojkov et al., 1995; Bodeker et al., 2001; Fioletov et al., 2002; Kane, 2008). The above-mentioned works are especially noteworthy here as we also present similar results for South Pole, Syowa, Halley and Faraday, and thus a very consistent evaluation of inter-annual variation of total ozone in the Antarctic. Even if the current negative trends in EESC sustain in the coming years, studies indicate that it will take several decades to reach ozone recovery (to the 1980 level of ozone) in the Antarctic (e.g. Vyushin et al., 2007; Yang et al., 2008). A detailed trend estimation of the high latitude ozone measurements will be performed in Chapter 9.

6.4.3 Southern mid-latitude ozone

The ozone loss analysis for the Antarctic would not be complete without assessing its impact on mid-latitudes. Therefore, we now examine the ozone loss computed above three stations located at three different regions in southern mid-latitudes. This diagnosis is particularly important since very

low ozone of around 250 DU was observed on some days at these stations during recent winters. Fig. 6.9 shows the ozone loss estimated from Rio Gallegos, Kerguelen and Macquarie Island ozone measurements in 2005–2009. Extension of the vortex to the mid-latitudes was absent in some years, as in 2005 at Macquarie Island and 2008 at Kerguelen. Furthermore, there were no vortex events found over Lauder during these winters.

The analyses expose the vortex overpasses for a few days in October 2008 and November 2009 and show a maximum ozone loss of 40–45% (150–200 DU) at Rio Gallegos. A similar scale (30–50%) of reduction from a higher number of vortex occurrences at Ushuaia is also estimated with the SLIMCAT tracer in September–November 2004–2008 (not shown). Except in 2008, about 30% (50–100 DU) of ozone loss is observed at Kerguelen during the vortex appearance in October–November of the recent winters. Conversely, passage of the vortex over Macquarie Island is found mostly during early winter and the observed loss is about 10–20% (up to 100 DU) in 2006–2009. Note that, this loss is equal to that of the Antarctic during the same period.

In order to analyse the inter-annual variations, the October mean of the total ozone from selected mid-latitude stations are examined in Fig. 6.10. There is a weak signal of ozone reduction (∼50 DU) in 1975–1993 at Lauder and Macquarie Island, in agreement with the studies of Harris et al. (2003) for the former and Chubachi (2009) for the latter stations. The measurements at Perth and Buenos Aires also show some reduction in ozone during the period (Kane, 1991, 2008). These results are consistent with the well established mean 5% loss in the southern mid-latitudes since the pre-ozone hole period (WMO, 2007). Nevertheless, the time series of Melbourne is too short to deduce a significant trend. As expected, the measurements at Ushuaia, Comodoro Rivadavia and Kerguelen exhibit large inter-annual varaibility due to the episodic vortex exposures.

6.5 Conclusions

The passive method is shown to provide ozone loss estimations within an accuracy of about 4% and is applied to evaluate ozone loss from the ground-based measurements in the Antarctic winters 2005–2009. The loss is shown to start at the edge of the vortex by July and each station shows different timing for the onset of ozone loss depending on its exposure to sunlight. The magnitude of loss is also different at each station in line with the temperature, PV, PSCs and prevailing heterogeneous chemistry, which are quite in agreement with our current understanding of polar wintertime chemistry. In accordance with previous studies, the ground-based stations show substantial ozone loss of around 55% since 2005. However, the year-to-year differences in ozone loss are not large in the Antarctic, consistent with earlier studies. The ozone loss and loss rates computed from OMI and SCIA observations compare well with that of the ground-based measurements (within ±2%). The CTMs also imitate well the ozone loss features and reproduce the maximum loss within ±3% difference.

The October average of the total column measurements at the historical ground-based stations do show that the loss started in the late 1970s. The ozone reduction peaked in the early 1990s and stabilised afterwards until present due to its saturation. Another important feature is the effect of extension of ozone hole at southern mid-latitudes. The SAOZ measurements at Kerguelen and Rio Gallegos, the first observations from the latter, reveal severe ozone loss (20–45% or 50–200 DU) episodes, which reiterates the value of observations in southern mid-latitudes.

This study shows that, the maintenance of an efficient ground-based network independent of satellites, particularly UV-visible that are capable of making observations in early winter, is inevitable for monitoring the long term evolution of the ozone hole and its anticipated recovery from the reduced CFC emissions.

Chapter 7

Antarctic ozone loss: 1989–2010

Contents

Stratospheric ozone loss in the Antarctic has been an issue of intense research since its discovery in the early 1980s (Farman et al., 1985). Several estimates of ozone loss are available for Antarctica since then. However, most of them deal with the ozone loss analysis for individual winters, modelled or incomplete due to limitations of the analysed observations (e.g. Austin et al., 2010a; Lemmen et al., 2006; Tilmes et al., 2006; Hoppel et al., 2005), and thus this makes the inter-annual comparison very difficult. For instance, the CCM based studies are mostly exploited for the projection of ozone recovery (e.g. Austin et al., 2010b). Although there are many studies using satellite data, a continuous long-term ozone loss analysis is still not available using these data (Bevilacqua et al., 1997; Hoppel et al., 2005; Tilmes et al., 2006). Therefore, we present a comprehensive ozone loss analysis in the Antarctic using ground-based and satellite measurements for the 1989–2010 period, similar to that in the Arctic (Goutail et al., 2005). Here we use the same model, measurements and method to construct the whole time series, which makes a continuous, coherent and comparable long-term ozone loss analysis. This analysis is also an extension of the study presented in the previous chapter (i..e Chapter 6).

7.1 Data and methods

7.1.1 Ground-based measurements

We use measurements from 12 ground-based stations deployed in and around the continent, such that they cover the entire region to provide a representative analysis for Antarctica, as described in the previous chapter. As the Antarctic vortex is very stable and inter-annual variations in the meteorology are very small compared to those of the Arctic, the estimated ozone loss is less dependent on the selection of the stations, as demonstrated in Kuttippurath et al. (2010b). Nevertheless, the analysis for each year contains data from at least eight stations and hence, assures a reasonable estimate of the Antarctic ozone loss.

7.1.2 Space-based observations

To compare with the ozone loss estimates based on the ground-based observations, v8.5 total column ozone measurements from TOMS onboard Nimbus-7, Meteor-3, and Earth Probe are used (Bhartia and Wellemeyer, 2002). The uncertainty of the TOMS ozone column data is 3.3% and the bias among the TOMS ozone onboard different platforms is 1–2% (Kroon et al., 2008). Since 2005, the OMI data are used as the continuation of the TOMS series. Therefore, a continuous series comparable to that of ground-based is available from TOMS and OMI from 1979 to 2010, with the exception of 1994 and 1995. In addition, we have used a bias corrected reanalysed ozone data set, the Multi Sensor Reanalysis (MSR), compiled from various satellite observations during the period 1979–2008. Our comparisons show a good agreement between the ground-based and satellite/MSR data at all ground-based stations. However, as shown by Hendrick et al. (2011) there is still some bias of the order of 2% between TOMS/OMI and SAOZ observations at Dumount d'Urville, with a strong seasonal dependence. As this bias was random, it was not possible to correct here.

In order to compare the ozone loss estimated with ground-based measurements in early winter, we have calculated ozone columns from the Aura MLS ozone v3.3 profiles, which are averaged within 2×2° around each station. The South Pole data are produced by averaging the four nearest longitude points (0, 90, 180, and 270° E) at 82° S, the southernmost latitude of the MLS observations. The ozone columns from MLS ozone mixing ratio profiles are calculated between 10 and 60 km using the MLS pressure and temperature data. The uncertainty of the MLS ozone profiles is about 5–10% in the stratosphere (Livesey et al., 2011; Froidevaux et al., 2006). Our primary comparisons show a good agreement between the ozone column calculated from the MLS profiles at various Antarctic stations with that of the ground-based measurements. However, there were some systematic offsets between the MLS ozone column and the ground-based data at some stations of the order of 5–10 DU or 2–5% and this deficit has been taken into account for this analysis.

7.1.3 Tracer simulations from REPROBUS

We use the REPROBUS CTM (Lefèvre et al., 1994) discussed by Kuttippurath et al. (2010b) to simulate the passive tracer from 1989 to 2010 for the chemical ozone loss computations. Our new simulations, however, use the ECMWF Reanalysis (ERA) – interrim meteorological data to force the model runs (Dee et al., 2011). The model version used in this work has a horizontal resolution of 2×2° on 60 vertical levels from the surface to 0.1 hPa. We use the passive tracer simulated by the model intialised in 1989, but we reinitialise the tracer fields on every June to match the Antarctic winter period, i.e. the ozone loss on 1 June is set to zero. This implies that there is no ozone loss until the initialisation day. The ECMWF ozone data were used for the initialisation of the model runs. The passive tracer columns used here are the averages within 100 km of each station.

7.1.4 Ozone loss derivation

To find the ozone loss inside the vortex, we select the measurements using the vortex edge criterion of Nash et al. (1996) and apply the passive method (e.g. Kuttippurath et al., 2010b; Goutail et al., 1999) to the selected observations. Note that, although the satellite measurements are available since 1979, the passive tracer simulations start in 1989 and hence, our ozone loss analyses start in the latter year. For instance, Fig. 7.1 illustrates the ozone loss estimated inside the vortex from all ground-based measurements for the Antarctic winter 2006. Generally, each station shows different timings for the onset, progress and maximum in the ozone loss, depending on the history of the exposure of the air parcels observed to contact with PSCs at sunlit parts of the vortex. It should be noted that the transport of ozone depleted air masses over the station can also affect the onset period (Hassler et al., 2011; Kuttippurath et al., 2010b).

There are some variations in ozone distribution inside the vortex with 2 separate air masses - the edge region with a latitudinal extent of about 15° around the perimeter of the vortex as identified by Roscoe et al. (2012) and the vortex core. The behaviour at any one station depends on which air mass is above it, and many stations do not have the same air mass above them throughout the ozone hole period. Faraday-Vernadsky and Rothera are most often in the edge region, with occasional excursions between the edge and core of the vortex. Conversely, Dumont d'Urville is frequently in

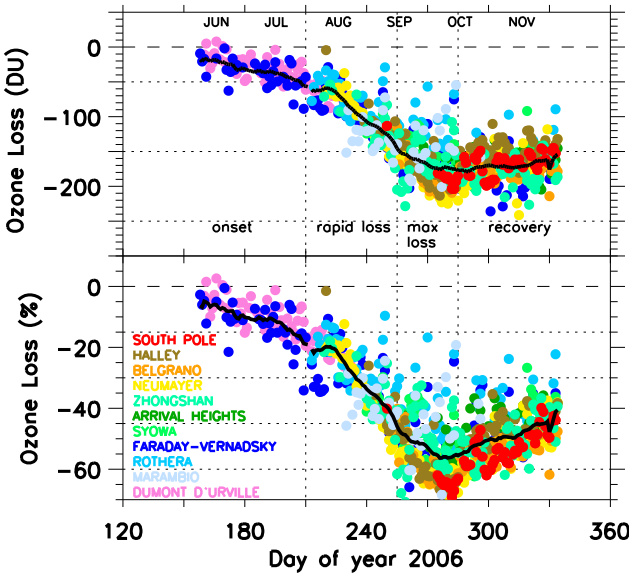

Figure 7.1: Ozone loss estimated from 11 ground-based station observations inside the vortex (Nash et al., 1996) for the Antarctic winter 2006. The ozone loss is estimated as the measured ozone minus the modelled passive tracer, which is initialised on first of June. The average loss estimated from the observations is shown in solid line. The dotted lines represent −50, −150 and −250 DU, and −15, −30, −45 and −60% of ozone loss. The vertical lines represent day 210, 255 and 285.

the edge region, but occasionally inside the vortex core and the stations at 70–90° S are often inside the vortex core. A detailed discussion of the station positions and related observational features can be found in Kuttippurath et al. (2010b). On average (Fig. 7.1 solid line), the ozone loss in the region starts by mid-June and rapidly increases to −160 DU or −52% by the end of September. The maximum ozone loss of −185 DU or −56% was observed at the end of September/early October 2006. The loss stays around the peak loss, or reduces thereafter with respect to the meteorological conditions and vortex persistence. The estimated ozone loss has an uncertainty of about 3–5% (Kuttippurath et al., 2010b).

7.2 Results

7.2.1 Annual ozone minima

The time series of annual ozone minima at a given station usually indicates the amount of maximum ozone loss in the region. In addition, any change in the minimum values and day when the minimum is observed can also indicate the change in ozone trends. Fig. 7.2 presents the minimum ozone observed by various instruments at each site during 1989–2010. Among the stations, South Pole shows the lowest values of about 100 DU, while Dumont d'Urville shows the highest of about 180 DU. These exclude the early years 1989–1992 and the warm winters (2002, 2004, 2007 and 2010), where the vortex dissipated earlier than in other winters due to enhanced wave activity (WMO, 2011; Tully et al., 2011). In 1989–1992, most stations observe a similar minimum of about 140–150 DU, except at Dumont d'Urville, where it is around 200 DU. Similarly, the warm winters of 2002 and 2004 show a comparatively higher minimum at all stations; ∼140 DU at South Pole and ∼175 DU at other stations, excluding Dumont d'Urville. The other stations register the minimum ozone in between these two extremes. For instance, Faraday-Vernadsky, Marambio, Syowa and Zhongshan show values near to 140 DU, but Rothera and Concordia show slightly lower values of about 130 DU. The minimum ozone observed at Belgrano, Halley and Neumayer is comparable with that at the South Pole and is about 110 DU. This suggests that the centre of the vortex is not always at the South Pole (e.g. Hassler et al., 2011; Waugh and Polvani, 2010; Harvey et al., 2002). Among the winters the lowest minimum is observed in 2006 at most stations. However, the minimum observed by the Brewer instrument at Zhongshan was about 85–90 DU in 2001 and is the lowest among the stations/winters. The day when the minimum was measured is between day 260 and 270 at all stations, which falls in the end of September and early October period, indicating the period of maximum ozone loss in the Antarctic, as also mentioned in previous studies (Kuttippurath et al., 2010b; Grooß et al., 2011; Hassler et al., 2011; Newman et al., 2007; Cariolle et al., 1986)

The satellite and MSR data are generally in very good agreement with the ground-based ob-

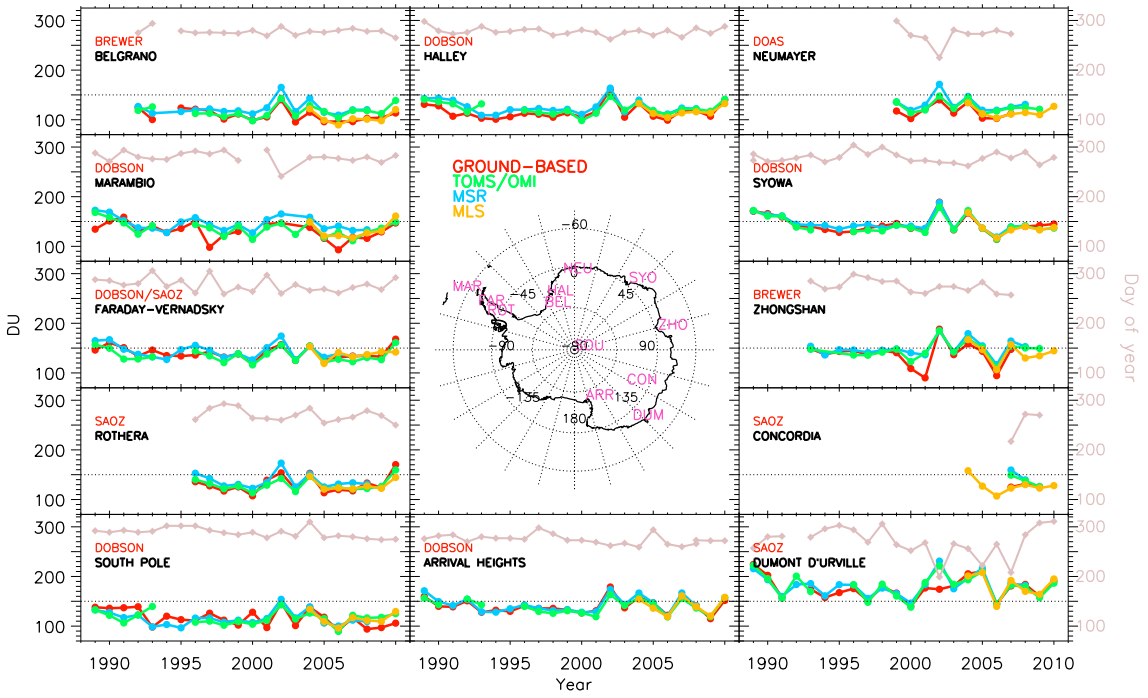

Figure 7.2: Time series of annual ozone minima at the ground-based stations in Antarctica. The corresponding satellite overpass data from TOMS/OMI, MSR and MLS are also shown. Station names on the map are demarcated with the first three letters of the stations (e.g. ROT is for Rothera). The type of ground-based stations (e.g. Dobson at South Pole and SAOZ at Concordia) are also marked on the plots. The SAOZ observation at Faraday/Vernadsky starts in 1996. The pale grey line indicates the day when the minimum is observed by the ground-based sensor (axis on the right). The horizontal dotted lines represent 150 DU of ozone.

servations and their best agreement is found at Halley, Arrival Heights and Dumont d'Urville. Nevertheless, the ground-based instruments measure a comparatively higher minimum at Faraday-Vernadsky and Syowa during 1989–2002. There is a known low bias (∼10%) in the Rothera data related to the uncertainties in the AMF used in the retrievals (Roscoe et al., 1999; Hendrick et al., 2011), which is corrected for this study. The ground-based and satellite differences are mostly within ±5–10 DU, depending on station and winter. Note that these values are extracted from the available measurements by each instrument, as some instruments lack continuous measurements during the August–October period. Therefore, the observational characteristics and measurement gaps could also contribute to the observed differences in the minimum ozone values.

7.2.2 Ozone loss above the stations

Figure 7.3 depicts the ozone (DU) and ozone loss (DU and %) inside the vortex at different Antarctic stations as computed from various data sets averaged from mid-September to mid-October, the minimum ozone period. The average ozone time series show equivalent features that are discussed for each station/winter in Sect. 7.2.1 with corresponding changes in ozone values. Therefore, we now discuss the ozone loss estimated from these ozone measurements for each station. At Arrival Heights, the loss estimated from the ground-based observations is about −32% or −100 DU in 1989 and it rapidly increased to −160 DU or −50% by 1993. The loss gradually reduced to −130 DU or −42% during the next three years and then increased again to −175 DU or −53% by 2001. During the warm winter of 2002, the loss reduced considerably to −135 DU or −34%. Since 2002, there have been two very cold and four relatively warm winters that show extreme values in ozone loss. The largest loss of about −175 DU or −53 to −56% was in the colder winters of 2003 and 2006, and the lowest loss of around −145 DU or −42% was in the warmer winters of 2004, 2005, 2007 and 2010.

The evolution of ozone loss at other ground-based stations is similar, but with slight differences in the ozone loss values. On average, the loss at Syowa and Zhongshan is similar to that of Arrival

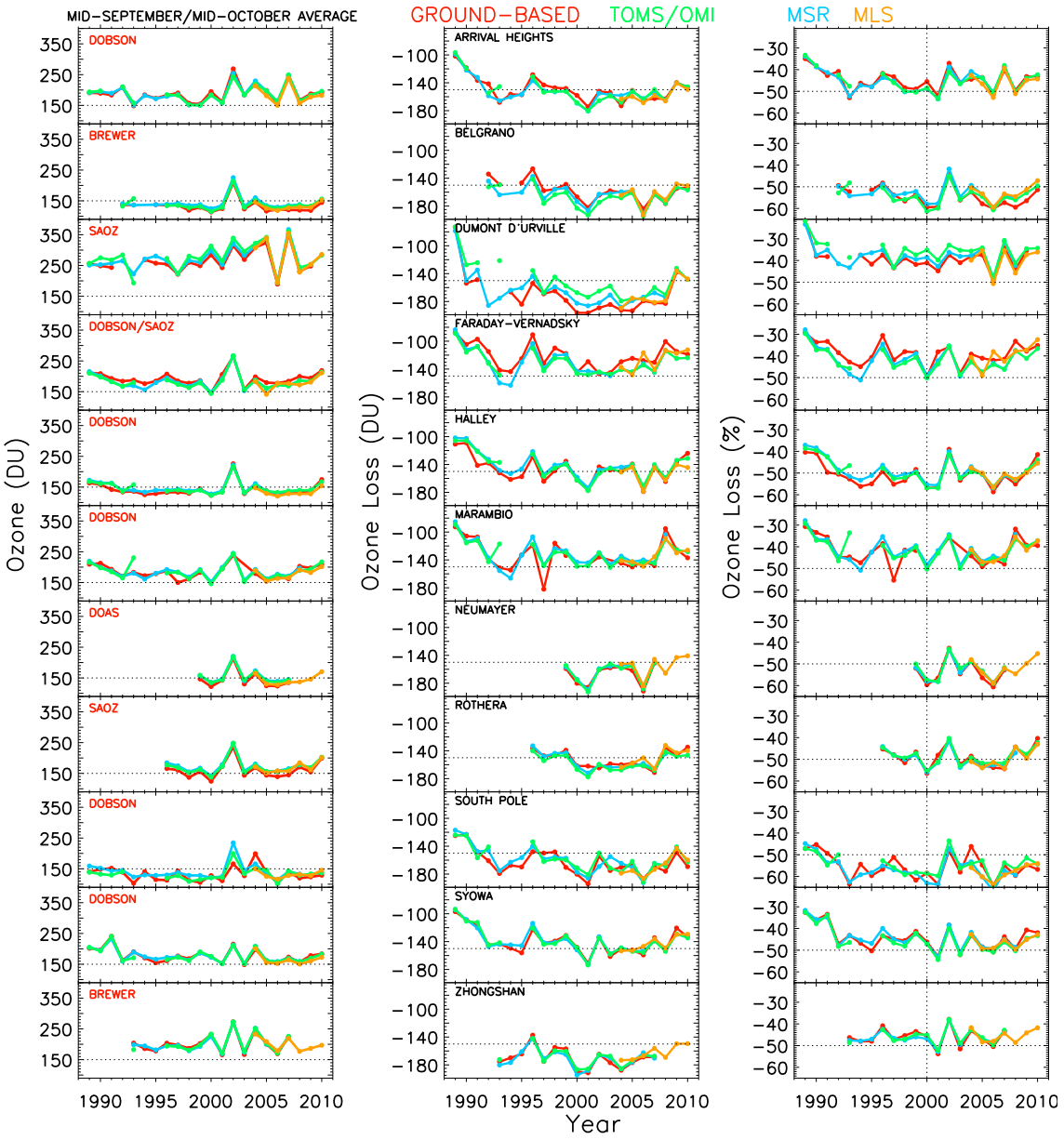

Figure 7.3: The average ozone (left) and ozone loss in DU (middle) and % (right) estimated inside the vortex (Nash et al., 1996) from long-term ground-based measurements at various Antarctic stations during the mid-September to mid-October period of 1989–2010. The corresponding satellite data from TOMS/OMI, MSR and MLS are also shown. The horizontal dotted lines represent 150 DU of ozone (left panel), −150 DU of ozone loss (middle panel) and −50% of ozone loss (right panel).

Heights, about −45%, whilst the loss at Marambio and Faraday-Vernadsky is slightly smaller, about −43%. Halley exhibits larger ozone loss of about −50% and the stations installed inside the vortex core; Belgrano, Neumayer and South Pole, show the highest loss of about −55 to −60%. In contrast, the lowest ozone loss of about −38% is estimated at the edge region station Dumont d'Urville. All stations show the lowest ozone loss in 2002 (about −110 to −140 DU or −35 to −40%) and the highest in 2006, except for Marambio, where it shows the lowest loss in 1997. This discrepancy could be due to the lack of continuous measurements in the late September–early October period in 2006 at Marambio. The edge stations (Marambio, Faraday-Vernadsky and Dumont d'Urville) show comparatively lower ozone loss than the stations inside the vortex core (South Pole, Halley and Belgrano) due to relatively warmer vortex conditions. The analyses based on satellite and MSR data return identical ozone loss values to those of ground-based observations at all stations and the agreement is exceptionally good at Halley, Neumayer, Syowa and Zhongshan, within ±1%.

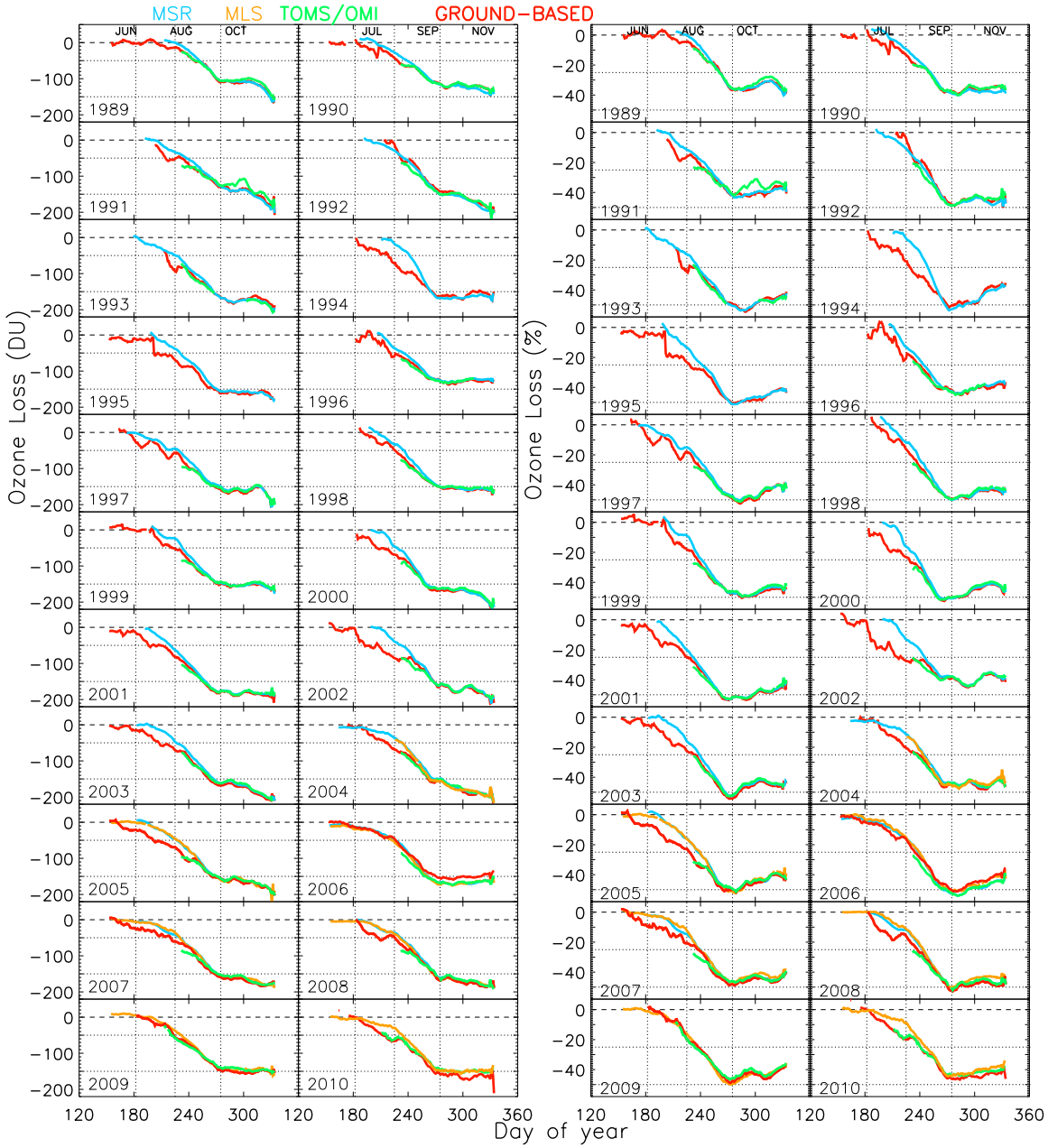

Figure 7.4: Temporal evolution of the ozone loss estimated from ground-based observations (red) inside the vortex (Nash et al., 1996) are compared to that from TOMS/OMI, MSR and MLS in DU (left panels) and % (right panels) in 1989–2010. The MSR and MLS have data for all stations from June onwards (e.g. Dumont d'Urville), while the ground-based average consists of edge stations in the early winter period. The horizontal dotted lines represent −50 and −150 DU of ozone loss (left panels) and −25 and −50% of ozone loss (right panels), while the vertical lines represent day 181, 225 and 275.

However, the differences are slightly larger at Dumont d'Urville in 1998–2004, about ±2–3% or ±5–15 DU.

7.2.3 Ozone loss averaged over all stations

Figure 7.4 shows the average ozone loss estimated for Antarctica from the ground-based, TOMS/OMI and MSR data during 1989–2010. In order to find the average ozone loss for the region, we have found the mean ozone loss inside the vortex of each station for each day from May to November. No special scaling is performed to account for the differences in the position of the

Table 7.1: The vortex-averaged (Nash et al., 1996) ozone loss averaged between 26 September and 5 October (during the maximum ozone loss period). The ozone loss rates estimated between day 13 August and 2 October from ground-based measurements in the Antarctic are also shown. The selection of this time-line depends on the measurement capability of ground-based instruments, where most of them have measurements so that the analyses fairly represent the average of Antarctica. The loss rates are given in DU/day and % day^{-1} in 50 Days. The uncertainty of the estimated ozone loss is about 3–5%.

Year	Loss DU	Loss %	Loss Rate DU day^{-1}	Loss Rate % day^{-1}
1989	-111	-37	1.96	0.61
1990	-112	-37	1.57	0.51
1991	-132	-43	1.57	0.43
1992	-143	-48	2.35	0.80
1993	-158	-49	1.57	0.45
1994	-161	-51	1.67	0.55
1995	-160	-51	1.76	0.53
1996	-122	-41	1.47	0.45
1997	-156	-49	1.96	0.59
1998	-150	-50	1.96	0.67
1999	-152	-48	1.96	0.61
2000	-167	-51	1.86	0.51
2001	-182	-53	1.86	0.53
2002	-167	-40	1.47	0.26
2003	-168	-54	1.86	0.57
2004	-155	-45	1.67	0.47
2005	-154	-50	1.76	0.51
2006	-175	-55	2.05	0.63
2007	-159	-50	1.96	0.55
2008	-168	-53	2.15	0.55
2009	-147	-49	1.76	0.61
2010	-154	-46	1.96	0.57

stations in the vortex, as we are finding the average ozone loss inside the whole vortex. Furthermore, our analysis shows insignificant differences between the loss estimates for various vortex averaged data clustered by different vortex edge criteria (inside vortex, vortex core and over the EqLs 65–90°S), as also mentioned in the previous chapter. In general, the loss starts in mid-June/early July, in agreement with the appearance of PSCs and heterogeneous chlorine activation in the sunlit parts of the vortex (Solomon, 1999; Solomon et al., 1986), except during 1989–1990, where it begins in early August. On the same note, the ozone loss onset in the very cold winters such as in 2003 and 2006 is about a month earlier, in early June. Similarly, the warm winter of 2002 and 1989–1990 show late onset of ozone loss. All years exhibit a higher loss rate during August–September and the peak loss during the end of September and early October period. On average, the maximum loss until mid-October is around −120 DU or −40% in 1989–1990 in agreement with the lower abundances of stratospheric halogens during that period (WMO, 2011) and around −160 DU or −48% thereafter due to saturation of ozone loss (e.g. Jiang et al., 1996; Solomon, 1999; Solomon et al., 2005; WMO, 2011), where the colder winters (2000, 2003 and 2006) show a slightly greater reduction of about −170 DU or −55%. As anticipated, the warmer winters show the opposite pattern of lower ozone loss, as shown by the −40% loss in 2002.

The TOMS/OMI and MSR analyses show a remarkably similar evolution of ozone loss in all winters and the differences among various data sets are mostly within ±5% or ±10 DU. The evolution and maximum ozone loss in the ozone column computed from MLS ozone profiles exhibit a very good agreement with the ground-based estimates, where the differences are within ±2–3% or 5–7 DU. The MLS and MSR data are available from the beginning of each winter for all stations and hence, their average represents data from all stations, in which many of them have different scales of ozone loss in the June–August period. However, the ground-based average contains measurements only from the edge stations (e.g. Dumont d'Urville and Rothera), which gives rise to the difference in the ozone loss estimates of ground-based and MLS observations in June–August. Note also that there is a very good agreement between the ozone loss estimates based on MLS and MSR data during the 2004–2008 period, reinforcing the aforesaid statement. This comparison corroborates

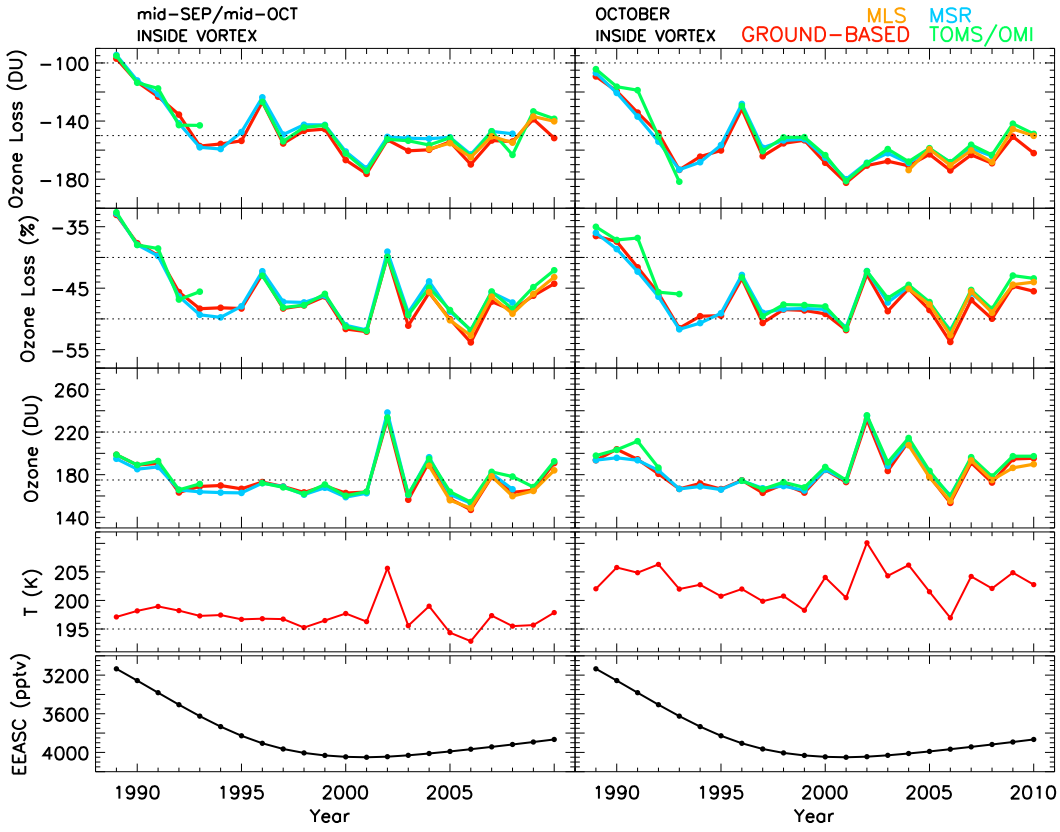

Figure 7.5: The ground-based ozone (in DU) and ozone loss (in DU and %) inside the vortex (Nash et al., 1996) averaged between mid-September and mid-October (left) and in October (right) during the Antarctic winters 1989–2010 compared to those of TOMS/OMI, MSR and MLS. The corresponding vortex averaged temperature at 475 K (in Kelvin – K) from the ECMWF operational analyses is also shown. The EEASC data for the corresponding years are shown in the inverted scale in the bottom panels. The horizontal dotted lines represent −100 and −150 DU of ozone loss (top), −40 and −50% ozone loss (second panel from top), 175 and 220 DU ozone (third panel from top) and 195 K temperature (fourth panel from top) in the respective plots.

the potential and strength of the Aura MLS measurements to be used for total column ozone loss analyses in the polar regions. This is particularly significant as the polar night measurements are not possible by UV-visible instruments.

7.3 Discussion

7.3.1 Inter-annual variability of ozone loss

Figure 7.5 shows the inter-annual variations in vortex averaged ozone loss deduced from different data sets in two different periods. In the Antarctic, the maximum reduction in ozone in each winter is observed by the end of September to early October period and hence, a temporal average of this period is compared to the conventional October average. In the former period, the ground-based estimates show a steep increase of ozone loss from −90 to −155 DU or from −33 to −44% in 1989–1994. There was then a sharp decrease to −125 DU or −42% by 1996, although the loss again slipped gradually to the decadal maximum of −181 DU or −53% in 2001. The warming in 2002 reduced the loss to −151 DU or −40%, but it remained around −160 DU or −48% thereafter, with the highest loss in the coldest winter of 2006, about −53%. These ozone loss estimates mostly follow the amount of halogens in the stratosphere during the respective periods, as the stratospheric chlorine slowly increased from 1989 to 1994, peaked during 1996–2000 and then started to decrease slowly thereafter (e.g. Newman et al., 2007; Jones et al., 2011; WMO, 2011).

The October average also shows a similar ozone loss evolution, but the highest loss is still observed during the mid-September–mid-October period. Therefore, we have derived a ten-day

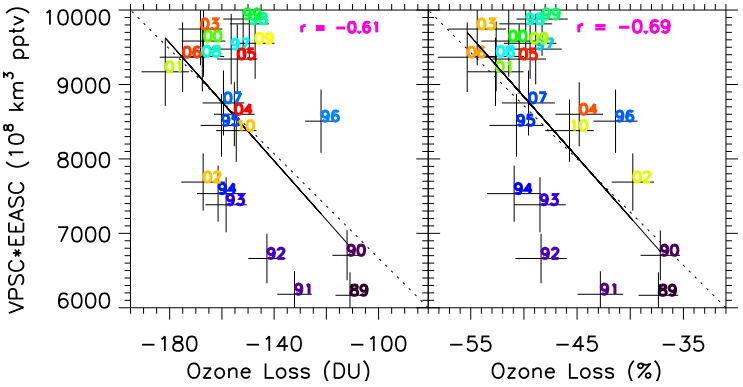

Figure 7.6: The correlation between ozone loss estimated from ground-based measurements (Table 7.1) and the product of V_{PSC} and EEASC. The V_{PSC} are calculated from the ECMWF operational analyses for the period 1989–2010.

ozone loss average during the peak loss period: 26 September to 5 October to find the maximum loss during each winter in 1989–2010 for a reference and these are given in Table 7.1. The ozone loss rates between day 225 (13 August) and 275 (2 October), during which most ground-based instruments have measurements, are also deduced. The ozone loss in this time window is analogous to that discussed for the other season, but as expected, the values are about 2–4% higher. The loss rates also show a similar time evolution, with the largest loss rates (0.63–0.67% day^{-1}) in the coldest winters of 1998 and 2006 and the smallest (0.26% day^{-1}) in the warmest winter of 2002, except for the Pinatubo year 1992 where the loss rates are relatively larger.

In agreement with the ozone loss analyses, the ozone values averaged over the mid-September to mid-October period (Fig. 7.5 left) show a reciprocal evolution in each winter. The ozone evolution during the period is consistent with that discussed in Sect. 7.2.2, but with slight differences in values. The October average shows identical behaviour in ozone time series, but in slightly larger than the aforesaid ones. This confirms that the maximum ozone loss in the Antarctic is observed during the mid-September and mid-October period, which is in agreement with results of previous studies (e.g. Kuttippurath et al., 2010b; Hassler et al., 2011; Solomon, 1999).

The gross features of the October average ozone (Fig. 7.5 right) from ground-based and satellite observations, and MSR data are in excellent agreement with the HALOE and Stratospheric Aerosol and Gas Experiment (SAGE) October average ozone shown by Yang et al. (2008). The ozone and ozone loss values are also well correlated with the time series of average temperature and heat flux during each winter (e.g. Yang et al., 2008; Salby et al., 2011), where the highest temperatures were observed in 2002 and the lowest in 2006. As noted for ozone, the difference in the vortex temperature (at 475 K) averaged from mid-September to mid-October 2002 to that of other winters is ∼10 K, indicating the intensity of the warming in this particular winter.

7.3.2 Ozone loss and V_{PSC}×EEASC

A compact relationship between ozone loss (in DU) and V_{PSC} has been found in the Arctic stratosphere (Rex et al., 2006; Harris et al., 2010). In this study we analyse this relationship in the Antarctic stratosphere. Contrary to the Arctic, where the ozone loss is largely controlled by the inter-annual variability in the meteorology, the Antarctic ozone loss is dictated by the amount of halogens present in the stratosphere. Therefore, we correlate the product of V_{PSC} and EEASC (Newman et al., 2007) against ozone loss in the Antarctic (e.g. Tilmes et al., 2008, 2006, 2004; Huck et al., 2007). Fig. 7.6 delineates the correlation between the ground-based ozone loss and V_{PSC}×EEASC for the 1989–2010 period. Here the ozone loss is the loss averaged between 26 September and 5 October (as shown in Table 7.1), V_{PSC} is averaged from May to November over 350–675 K and EEASC is the annual average for each year. The correlation between the ozone loss and V_{PSC}×EEASC shows about r = 0.61–69 for ozone loss in both relative (%) and absolute (DU) units. However, the correlation between ozone loss (DU) and V_{PSC} is about r = 0.41 in the Antarctic and r∼= 0.94 in the Arctic (Rex et al., 2006; Harris et al., 2010). as the year-to-year variability of ozone loss and temperature in the Antarctic is very weak as shown in Fig. 7.5 and also reported in other studies (e.g WMO, 2011 and references therein). Additionally, studies have already shown that the occurrence of PSCs (Cacciani et al., 1997; Negro et al., 1997) and ozone

loss (Jiang et al., 1996; Solomon et al., 2005; WMO, 2011) have reached the saturation levels in the Antarctic vortex core since early 1990s. Alternatively, in addition to numerous minor warmings, every second winter is subjected to a major warming in the Arctic (e.g. Charlton-Perez et al., 2008; Kuttippurath and Nikulin, 2012) and hence, significant occurrence of PSCs is limited to relatively cold winters there (Manney et al., 2005). Therefore, ozone loss has shown correspondingly large inter-annual variability (WMO, 2011; Kuttippurath et al., 2010a; Harris et al., 2010; Goutail et al., 2005). On the other hand, such warm winters are apparently absent in the Antarctic and thus, there is no one-to-one correlation between ozone loss and V_{PSC} or V_{PSC}×EEASC.

7.3.3 Ozone loss: comparison with other estimates

The total column ozone loss deduced by Huck et al. (2007) shows a peak loss of around −120 DU in most years, with the largest loss of about −130 DU in 2001 and the smallest loss of about −88 DU in 2002. The partial column ozone loss estimated over 380–550 K from the satellite ozone profiles by Tilmes et al. (2006) is about −120 to −145 DU. The peak loss deduced from the available measurements (maximum three ozone profiles) is about −155 DU in 2003 and the smallest of about −115 DU during 1996–1997. Both analyses show lower ozone loss than in our estimates. The differences with the results of Huck et al. (2007) are largely due to the differences in tracer used in the respective calculations. When we use the same tracer to compute the ozone loss from ground-based measurements, we find relatively lower ozone loss values (of up to 50 DU for the maximum loss, depending on year, and 50–120 DU during mid-October through the end of November in all winters) than our original ozone loss estimates with the model tracer. This difference reduces to a large extent when the computations are performed in relative units (%), where the negative bias for the peak ozone loss is about 2–10%. This suggests that the differences and inaccuracies in tracer values induce some uncertainty in the derived ozone loss amounts and hence, it points out the necessity of the ozone loss estimations in both units (in DU and %). The analyses of Tilmes et al. (2006) consider a partial column over 380–550 K, which consists only two-thirds of the ozone loss in the Antarctic stratosphere as the ozone loss occurs over a broad range of altitudes (350–675 K) there (e.g. Kuttippurath et al., 2013; Lemmen et al., 2006; Hoppel et al., 2005, 2003; Bevilacqua et al., 1997). Therefore, the missing ozone loss above 550 K in their study is one of the reasons for the differences with the total column ozone loss analyses presented in this study. Also, the available estimates from Tilmes et al. (2006) use 15 HALOE ozone profiles inside the vortex in each winter (1991–2004), which are limited to the sampling pattern of the satellite. Additionally, temporal coverage of these measurements is confined to spring. Conversely, the ILAS measurements are available mostly in the winter months of each year since 1992, while the maximum loss in the Antarctic is observed in spring. In summary, in addition to the uncertainties of the measurements used in the ozone loss estimations, the differences in tracers and ozone column range also contribute to the offsets in the ozone loss estimates.

7.4 Conclusions

A comprehensive analysis of ozone loss in the Antarctic vortex from 1989 to 2010 is presented using ground-based Brewer, DOAS, Dobson and SAOZ, and space-borne TOMS/OMI and Aura MLS observations. In addition, a bias corrected ozone data (MSR) constructed from various satellite observations during 1989–2008 is also exploited for this purpose. The passive method is applied to find the ozone loss at each station, and then averaged to find the mean loss in the Antarctic. On average, the ozone loss at Arrival heights, Belgrano, Concordia, Dumont d'Urville, Faraday-Vernadsky, Halley, Marambio, Neumayer, Rothera, South Pole, Syowa and Zhongshan shows about −160 to −180 DU or −48%, except for the years 1989–1991 and the extreme winters of 2002 and 2006. The loss in 1989–1991 and 2002 is about −110 to −140 DU or −33 to −40%, and during 1992–2010 (except 2002) is around −160 DU or −48%. The edge region stations (e.g. Dumont d'Urville) show a lower loss than the stations inside the vortex core (e.g. South Pole). In general, the ozone loss in the Antarctic starts by mid-June and intensifies in August–September, peaks by the end of September/early October (coincides with the minimum ozone period), and ozone recovers thereafter.

The estimated ozone loss time series is consistent with the EEASC and temperature distribution in each winter. Probably because of saturation of the vortex core with PSCs and small inter-annual variability of ozone loss, the V_{PSC}×EEASC—ozone loss correlation yields about 0.61–0.69, which stands in stark contrast with the Arctic scenario where the correlation between V_{PSC} and ozone loss (DU) is about 0.9, as the large inter-annual variability in the Arctic meteorology suppresses the gross effect of stratospheric halogens on the ozone loss. The ozone loss estimated from TOMS/OMI, Aura MLS and MSR data also exhibits a proportional progress of ozone and ozone loss as for the ground-based measurements throughout the period (1989–2010). The differences among these data are within ±5%, and are within the error limits of the respective observations.

Chapter 8

Vertical structure of Antarctic ozone loss

Contents

Large variability in the Antarctic ozone loss has been witnessed in the last few years (2004–2010) relative to other winters since 1992 (e.g. WMO, 2011; de Laat and van Weele, 2011; Santee et al., 2004). For instance, the winters 2004 and 2010 were warm with minor warmings and hence, showed limited ozone loss (Sonkaew et al., 2013; Huck et al., 2007; Tilmes et al., 2006; Yang et al., 2006). The first fortnight of August 2005 witnessed a high rate of ozone loss and an unprecedented ozone hole (WMO, 2011). The winter 2006 was one of the coldest and hence, experienced the largest ozone hole of Antarctica to date (Santee et al., 2011; WMO, 2011). The winters 2007 and 2009 were characterised by average temperatures and hence, ozone holes of a moderate size (Kuttippurath et al., 2013; Tully et al., 2008). However, the winter 2008 was again very cold and characterised by a large ozone hole (WMO, 2011). Therefore, these seven winters merit a detailed discussion in terms of polar processing and ozone loss during the period.

Figure 8.1 shows the position of the polar vortex on 1 October of each year at two representative altitudes in the lower and middle stratosphere, at 500 and 675 K. The maps also demonstrate the inter-annual variability of the winters, with the largest and strongest vortex in 2005 and 2006, and the warmest and weakest in 2004 and 2010. Therefore, in this study, we discuss (i) the inter-annual variability of ozone loss and chlorine activation during these winters, (ii) spatial, temporal and vertical variability of Antarctic ozone loss and (iii) contribution of various chemical cycles to the ozone loss in the stratosphere. Additionally, (iv) we also analyse the ozone loss driven by the NO_x cycle in the middle stratosphere and its contribution to the total column ozone loss in the stratosphere. Apart from that, the past seven Antarctic winters offer a good opportunity to test the chemical process in numerical models. Furthermore, the Aura MLS observations (e.g. Nair et al., 2011; Santee et al., 2008; Froidevaux et al., 2006), the best vortex sampled satellite measurements currently available, are compared to the model results. Therefore, for the first time the ozone loss can be studied with such high resolution measurements with high spatial and temporal coverage inside the Antarctic vortex. Previous satellite measurements were relatively limited to a small temporal and spatial area as far as the high latitude observations are concerned (e.g. Kuttippurath et al., 2013; Tilmes et al., 2006; Hoppel et al., 2005). While the UARS MLS had a similar latitudinal coverage (e.g. Nair et al., 2012; Waters et al., 1993), the frequency of its polar measurements was lower than that of Aura MLS (Kuttippurath et al., 2012a). Therefore, this study offers some new insights on the polar processing and ozone loss features of the Antarctic stratosphere.

Here we use the same model that used for the Arctic ozone loss studies described in Sect. I and Kuttippurath et al. (2010a). For each Antarctic winter considered the model was run from 1 May to 30 November. The chemical species were initialised from a long-term simulation of the REPROBUS CTM. We use the Aura MLS measurements v2.2 for comparison with our simulations. Note that there is a new v3.3, but the difference between the two versions in the daily vortex averaged data is negligible.

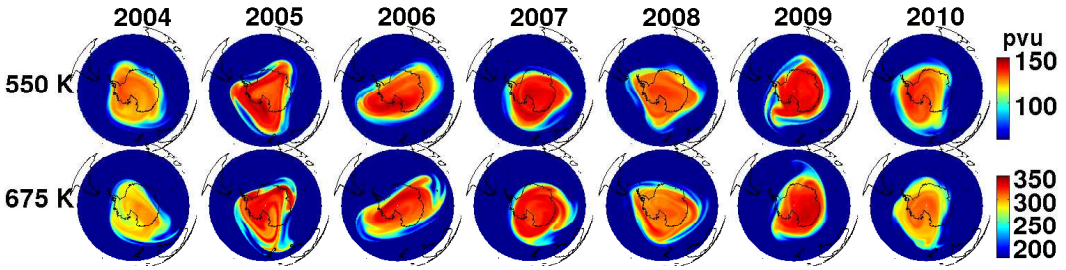

Figure 8.1: The potential vorticity maps from ECMWF operational analyses at 500 and 675 K on 1 October of the Antarctic winters 2004–2010.

8.1 Results and discussions

8.1.1 Ozone loss: the 2004–2010 average

To elucidate various chemical ozone loss features, we analyse the vertical distribution of the average ozone loss in 2004–2010 for different EqL bins estimated from the model and MLS data from May to November, and is shown in Fig. 8.2. The EqL based analyses extend from 63° to 83° S in 2° increments and the final EqL coincides with the highest EqL calculated for the measurement points. Our analysis shows that the chemical loss starts at lower EqLs of 63°–67° S at the edge of the Antarctic vortex in June, above 600 K, as also shown by Lee et al. (2000) and Roscoe et al. (2012). It propagates down to the lower altitudes by July and the loss is largest at the 63°–69° S EqL. The loss increased again in August, with the EqLs of 63° and 83° S showing the largest and smallest loss, respectively, and is in accordance with the increase in incidence of sunlight over the region. A clear difference in the amount of ozone loss estimated at different EqLs is well simulated. At the edge of the vortex, maximum ozone loss of 2.2 ppmv is found around 500 K, while in the 70°–80° S EqL range the peak loss is estimated above 600 K.

The ozone loss is continued through to September, where all EqLs show very large loss. The largest loss is still found in the lower EqLs of 63°–69° S, reaching about 3 ppmv at 500 K. The higher EqLs (83°–75° S) show the smallest ozone loss and it peaks in the middle stratosphere (around 600 K) and other EqLs show their peak loss in the lower stratosphere, below 575 K. Above 600 K, all EqLs show similar ozone loss of about 1.5 ppmv. The maximum loss is about 3.4 ppmv in 65°–70° S at 500 K, 2.7 ppmv in 70°–75° S at 550 K, 1.9 ppmv in 75°–80° S at 575 K and 1.5 ppmv over 80°–

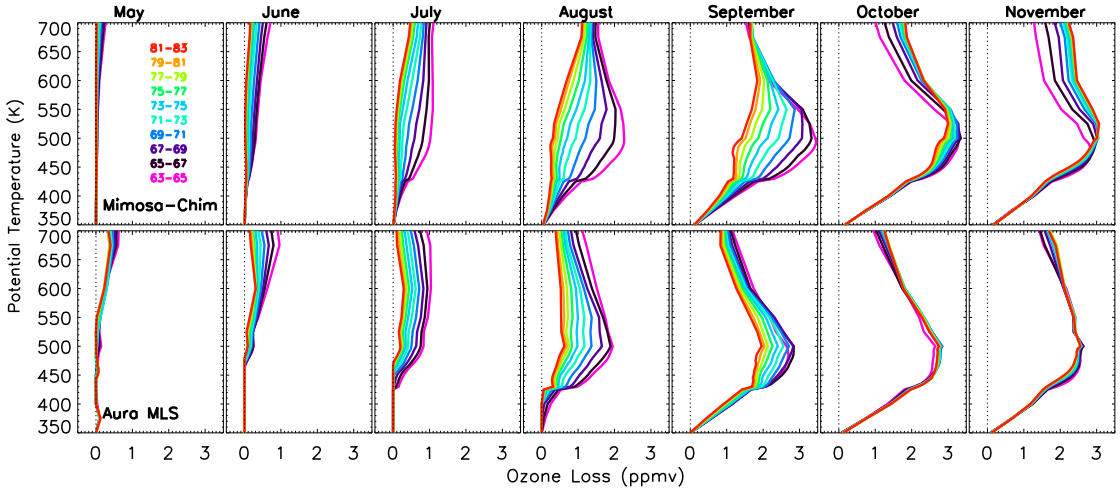

Figure 8.2: The seven year average (2004–2010) monthly mean ozone loss estimated at different EqL bins from 63° to 83°S EqL (in 2°S) from the MIMOSA-CHIM simulations and MLS measurements. The black dotted lines represent 0 ppmv.

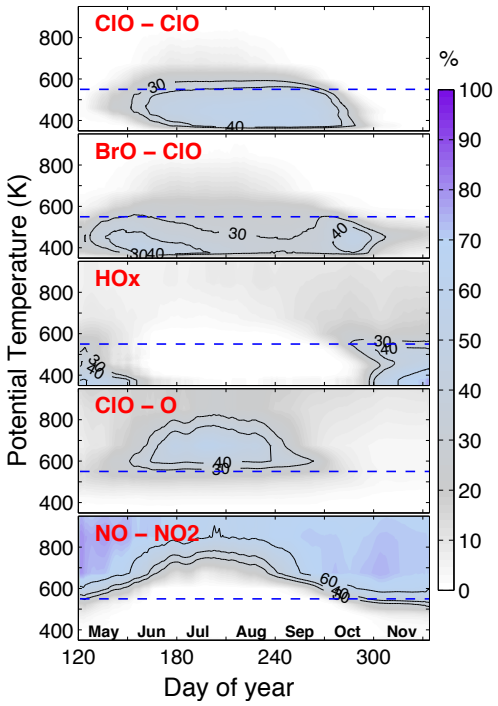

Figure 8.3: Vortex averaged (≥65° EqL) relative contribution of selected ozone depleting chemical cycles (as noted in the plots) to the total chemical ozone loss averaged for the seven Antarctic winters in 2004–2010. The blue dashed-lines represent 550 K.

83° S at 600 K, and thus the altitude of maximum loss increases with EqL until September. The maximum loss is recorded in October, as expected, but the difference between the loss in October and November is very small as there is no (significant) sustained ozone loss in November in the lower stratosphere. The maximum loss still remains around 3 ppmv in October, and all EqLs show more or less the same loss at the peak loss altitude of around 500 K. In addition, all EqLs show similar or the same ozone loss below this altitude. Above 500 K, the ozone loss shows slight differences, with the largest loss occurring at the highest EqLs. As the ozone recovers in November through dynamical process, the maximum ozone loss reduced to 2.7 ppmv, although the pattern of ozone loss with EqL is the same as that of October.

The analyses with model results are in good agreement with those of the MLS observations. Nevertheless, the loss estimated from the observations is comparatively more compact with altitude in October–November, and the model–measurement differences are a little larger in September. The comparison of ozone loss above 550 K shows that the model slightly overestimates the ozone loss there. These differences will be discussed in Sect. 8.1.3.1.

8.1.2 Chemical cycles: the 2004–2010 average

Since there has been no comprehensive evaluation of the contributions of various chemical cycles to the ozone loss in the stratosphere throughout various Antarctic winters, we calculate the mean contributions of various cycles to the ozone loss in 2004–2010, and the results are presented in Fig. 8.3. Contribution of each cycle is given in percent of the total contribution, as discussed in Chapter 4. In the lower stratosphere, about 90% of ozone loss is controlled by the ClO–ClO and BrO–ClO cycles from June to October, with the former dominating in the July–September period and the latter in June and October. Therefore, contributions of these cycles are complementary with time, and their contributions are maximum and nearly equal during the peak loss period of mid-September/mid-October, about 35–45%. A constant contribution of about 5–10% from the ClO–O cycle is also evident from May to November in the lower stratosphere (below 500 K). Conversely, the ozone loss in late October and November is controlled by the HO_x cycle with about 40%, as there are no PSCs and activated ClO in this period. However, it should be noted that, contribution of this cycle has little significance in the ozone hole period (June–October). Above 550 K, contribution from NO_x dominates in spring while ClO–O dominates in winter, depending on day of the year and altitude. Contributions of these cycles principally depend on the available O-atoms, as the rate limiting step of these cycles is the combination of a specific molecule with an O-atom (as NO_2+O

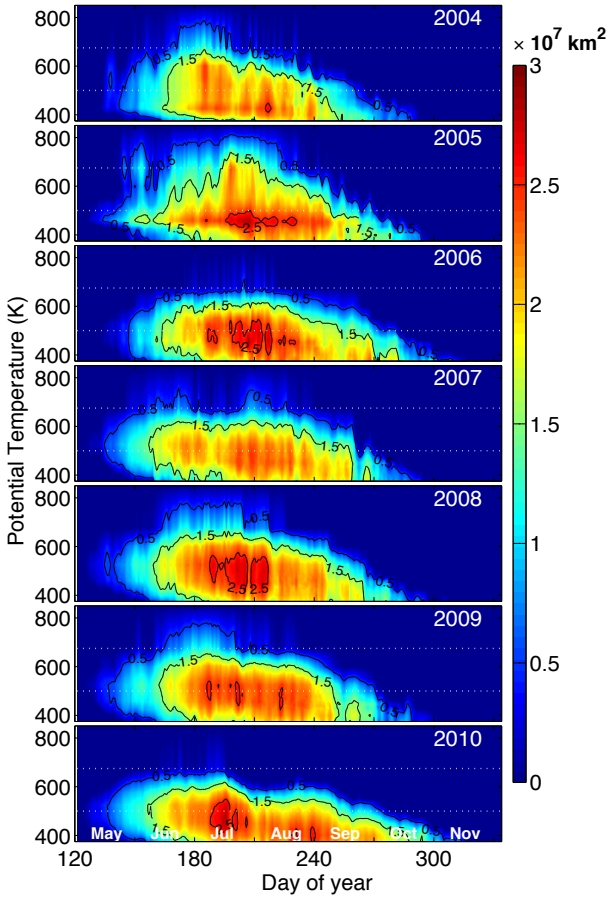

Figure 8.4: The area of PSCs estimated from the ECMWF operational meteorological data using the Hanson and Mauersberger (1998) criterion. The daily simulations of H_2O and HNO_3 from the MIMOSA-CHIM model are used for these calculations. The white dotted lines represent 500 and 675 K.

for NO_x for the middle stratosphere). The analysis shows that the Antarctic ozone hole is primarily controlled by the halogen cycles in tune with previous findings (e.g. WMO, 2011 and references therein), but the ozone loss above 550 K depends on the dynamics, availability of NO_x and presence of O-atmos in each winter.

8.1.3 Inter-annual variability

We have already seen the general features of ozone loss evolution and related chemical cycles in the stratosphere. We now discuss the inter-annual variations in the area of PSCs (A_{PSC}), chlorine activation, ozone loss, and ozone production and loss rates during 2004–2010.

8.1.3.1 PSC and chlorine activation

Figure 8.4 shows A_{PSC} calculated by applying the T_{NAT} threshold given by Hanson and Mauersberger (1998) using the ECMWF pressure and temperature data, as discussed in previous chapters. The A_{PSC} data are averaged meridionally over 50°–90°S. In general, the areas of PSCs show similar timing of onset, around mid-May, and they mostly disappear by early October. However, the areas of PSCs and their vertical extension are comparatively smaller in May, September and October, consistent with the results of previous studies of various Antarctic winters (e.g. Solomon et al., 1986; Shibata et al., 2003; Pitts et al., 2009). The maximum areas of PSCs are generally found in the July–August period and are estimated to be about 2.5×10^7 km^2. While the frequency of these high values is of the order of a few days in 2004, 2009 and 2010, those high values were never reached in 2007. The areas of PSCs in 2006 and 2008 show the largest values of $>2\times10^7$ km^2 for a longer period from mid-June to mid-September over a broader vertical range. In 2005, the A_{PSC} ($>2\times10^7$ km^2) spreads to a vertical extent over 400–750 K, wider than any other winter in June–July, indicating the coldest June–July amongst the winters. Yet, the maximum areas of PSCs (2.5×10^7 km^2) are still confined to comparatively a small vertical region of 425–500 K in July–August. These analyses

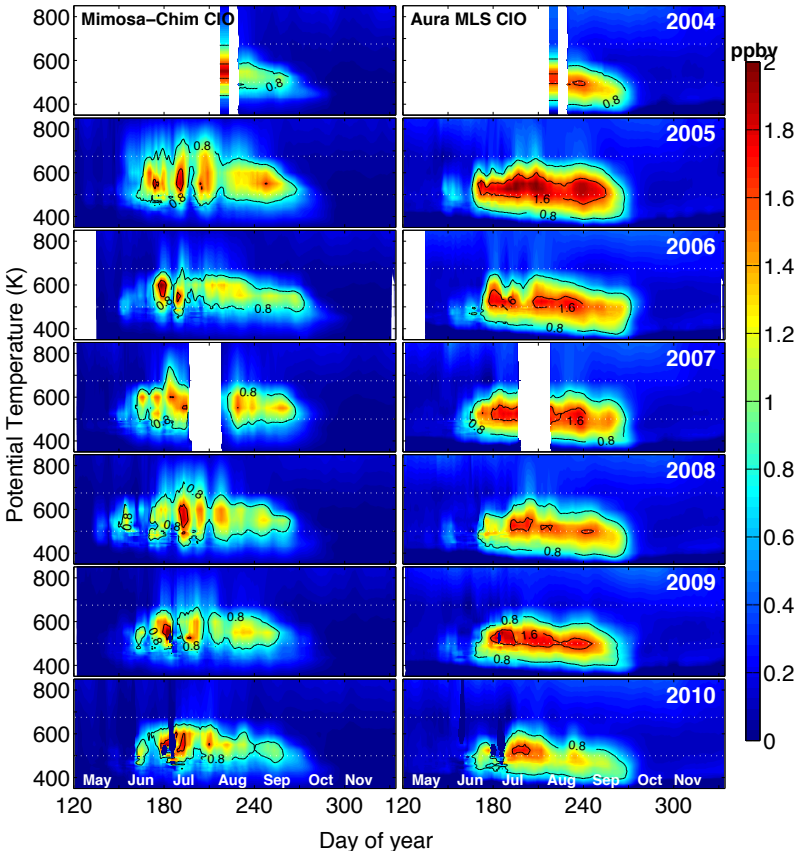

Figure 8.5: Vertical distribution of the vortex averaged (≥65° EqL) ClO estimated from the MIMOSA-CHIM model and MLS observations for the Antarctic winters 2004–2010. The model fields are sampled at the location of the MLS observations for each measurement inside the vortex and then averaged for the corresponding day. The measurements are selected between 10 and 16 h (local solar time) and solar zenith angles below 89° as they available. Both model results and data are smoothed for seven days. The white dotted lines represent 500 and 675 K.

suggest that winters 2005, 2006 and 2008 were the coldest and 2004 and 2010 were the warmest amongst the winters.

Compared to the PSC observations by the CALIPSO (Cloud Aerosol Lidar and Infrared Pathfinder Satellite Observations), the simulated PSC areas are in reasonable agreement as far as the spatio-temporal extension of the observed PSCs are concerned (Pitts et al., 2009). The altitude and time of the maximum area of PSCs are also in accordance with those of the satellite observations. However, the calculated PSC areas consistently and systematically overestimate (around 0.5×10^7 km^2) the observed ones at 425–550 K in July and August in all winters. This is due to the fact that, the calculations assume to form the PSCs whenever the temperatures are below the T_{NAT} threshold, which is not necessarily the case for the PSC formation in the real atmospheric conditions.

Figure 8.5 compares the simulated and measured ClO at the MLS sampling points inside the vortex, with solar zenith angle (SZA) less than 89° and local solar time between 10 and 16 h as they were available, for the Antarctic winters 2004–2010. In MIMOSA-CHIM, strong chlorine activation is found in 2005, where a maximum of 1.6 ppbv is simulated in July, consistent with the areas of PSCs in that winter. The other winters show a similar distribution of ClO and thus the chlorine activation. The simulated ClO stands in contrast to the PSC areas estimated in each winter, which showed the largest A_{PSC} in the coldest winters of 2005, 2006 and 2008. However, when we examine the MLS measurements, they mostly follow the temperature history of each winter and hence, PSC area calculations, as the ClO observations show the strongest chlorine activation in 2005 and the weakest in 2010. The high ClO values of >1.5 ppbv are found from July to the end of September over 450–600 K in the colder winters, but around 550 K episodically in July–August in the warmer winters in the observations. Therefore, contrary to the model results, the vortex averaged MLS observations display a clear inter-annual variation in the chlorine activation. These comparisons show that the model underestimates the observed ClO over 450–600 K.

In order to find out the reasons for the differences between simulated and measured ClO, we compared the simulated HCl, N_2O and HNO_3 with the MLS observations and are presented in Fig. 8.6. On average, the N_2O comparisons show that the simulations are higher than the measure-

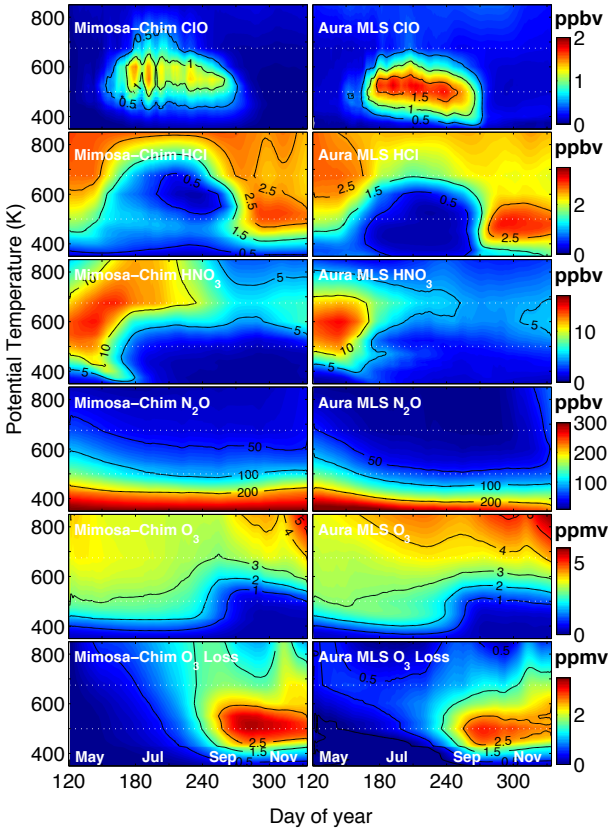

Figure 8.6: The vortex averaged (≥65° EqL) vertical and temporal evolution of ClO, HCl, HNO_3, N_2O, O_3 and ozone loss from the MIMOSA-CHIM model and MLS measurements. The data are the average of seven Antarctic winters 2004–2010 and are smoothed for 7 days.

ments, as illustrated by the 50 ppbv and 100 ppbv isopleths. This bias in simulations implies that the vertical descent in the model is slower during the polar winters. Consequently, the Cl_y (and thus ClO) and ozone in the model are relatively lower. Both HCl and ozone comparisons corroborate this feature of simulations, as the HCl values are higher (about 0.5 ppbv), and ozone and ClO are lower (about 0.5 ppmv of O_3 and 0.3–0.5 ppbv of ClO) in the calculations. The HNO_3 comparisons also point out that the denitrification in the model is slightly overestimated. Therefore, we applied the Cl_2O_2 recombination rate constant of Nickolaisen et al. (2006) instead of the JPL recommendation, as suggested by von Hobe et al. (2007). However, the ClO results did not improve significantly and hence, the original simulations are presented.

Note that the lower model top (850 K) could also influence the slower descent in the model. Furthermore, the interpolated data can sometimes be at the edge of the vortex in contrast to real atmospheric situations, which could make lower simulated values, such as the gaps or near-zero values shown in the ClO plots. Also, the simulations use different meteorological data for each year and there can be small interannual differences in the diabatic descent, depending on the accuracy of the wind fields. These have to be kept in mind while interpreting the simulations. However, in a similar study, Santee et al. (2008) compared the MLS measurements to SLIMCAT model results and found that their simulations slightly overestimate the measurements for the Antarctic winters 2004 and 2005. They attributed these differences to the equilibrium PSC scheme of the model. In contrast, our model ClO results underestimate the observations, although using a very similar PSC scheme in the model. It suggests that even if the models use similar PSC schemes, the difference in model dynamics can induce changes in the simulated results. Nevertheless, it has to be noted that the model has performed better in the northern hemispheric simulations, where the ClO simulations slightly overestimate the MLS measurements in the 2011 winter (Kuttippurath et al., 2012a), but slightly underestimate them in 2005–2010 (Kuttippurath et al., 2010a), indicating the problems in modelling the vertical transport in CTMs.

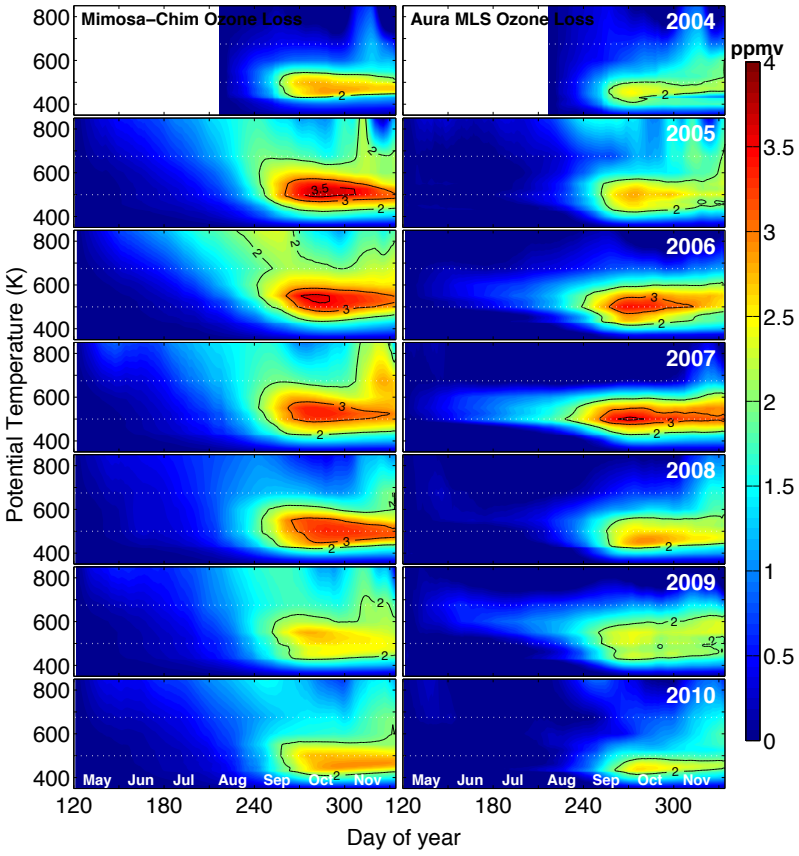

Figure 8.7: Vertical distribution of the vortex averaged (≥65° EqL) ozone loss estimated for the Antarctic winters 2004–2010. The model fields are sampled at location of the MLS observations for each measurement inside the vortex and then averaged for the corresponding day. Left: the ozone loss derived from the difference between the passive tracer and the chemically integrated ozone by MIMOSA-CHIM. Right: the ozone loss derived from the difference between the MIMOSA-CHIM passive tracer and the ozone measured by MLS. Both model results and observations are smoothed for seven days. The white dotted lines represent 500 and 675 K.

8.1.3.2 Ozone loss: vertical and temporal features

Figure 8.7 shows the vortex averaged ozone loss estimated from the model and MLS at the MLS sampling locations inside the vortex in 2004–2010. As discussed in Sect. 8.1.1, the ozone loss onset in the model occurs in mid-June at altitudes above 550 K and gradually propagates down to the lower stratosphere by mid-August. The loss intensifies by mid-August, peaks by late September/early October and slows down thereafter. As expected, the colder winters of 2005 and 2006 show early onset, in mid-June at the sunlit latitudes.

The estimated ozone loss is less than 0.5 ppmv above 675 K until mid-August, increases to 1–1.5 ppmv by mid-September in the lower stratosphere and peaks to 2.5–3.7 ppmv over 450–600 K by early October, consistent with the temporal and vertical extent of the area of PSCs in these winters. The maximum ozone loss of about 3.5–3.7 ppmv is derived around 550 K in 2005–2006 and about 3 ppmv around 500 K in 2007–2008. Relatively smaller ozone loss is found in the warmer winters of 2004 and 2010, where the peak loss is about 2.6 ppmv around 475 K. A similar range of ozone loss of around 2 ppmv, but in a slightly broader vertical extent of 450–600 K, is simulated in 2009. Therefore, the center of the peak ozone loss altitude (loss >2 ppmv) shows interesting variations with the meteorology of the winters, as it is located around 550 K in the very cold winters (e.g. 2005 and 2006), around 500 K in the moderately warm winters (e.g. 2007) and around 475 K in the warm winters (e.g. 2004 and 2010).

The timing and vertical range of ozone loss in the simulations are similar to those of the observations in the lower stratosphere. The ozone loss onset is in mid-June, except for the colder winters as discussed previously. The lower stratospheric ozone loss starts by early August, strengthens by mid-September and maximises in late September to early October period, consistent with those of the observations. The large ozone loss observed above 550 K in September–October in the colder winters and in November of all winters are also reproduced by the model. However, the model consistently overestimates the measured ozone loss in the middle stratosphere in all years by about 0.2–0.5 ppmv in spring, as the model underestimates the measured ozone by the same amount at these altitudes, primarily due to the slower descent in the model. Note that both the simulations

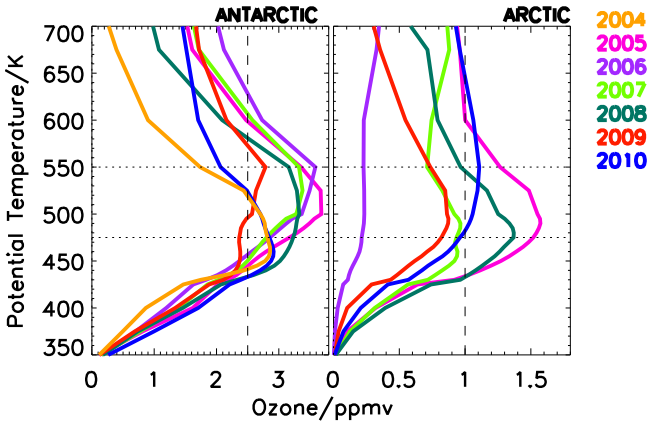

Figure 8.8: The maximum ozone loss estimated in the Arctic (depending on final warming and major warmings in each winter) and Antarctic (averaged between 26 September and 5 October) winters 2004–2010 inside the vortex. The ozone loss is derived from the difference between the passive tracer and the chemically integrated ozone by MIMOSA-CHIM. The vertical dashed lines represent 2.5 ppmv (left) and 1 ppmv (right) ozone loss, and the horizontal dotted lines represent 475 and 550 K.

and measurements provide consistent results for the peak ozone loss altitudes in each winter.

The ozone loss derived from the SCanning Imaging Absorption spectroMeter for Atmospheric CHartographY (SCIAMACHY) ozone profiles using the vortex descent method shows comparable values for the Antarctic winters 2004–2008 (Sonkaew et al., 2013). There is also a good agreement in deriving peak ozone loss values (around 3–3.5 ppmv) and the differences in the altitudes of maximum loss for various winters, as discussed previously for the modeled/MLS ozone loss. In addition, the large loss above 500 K found in the model/MLS data is also inferred from the SCIAMACHY measurements, confirming the findings of this study.

8.1.3.3 Column ozone loss

We have calculated the partial column ozone loss from the simulations and observations at the MLS footprints inside the vortex for each winter. Since significant ozone loss is found over 400–600 K, we have calculated the loss in this altitude range together with the complete altitude bound of the model. The partial ozone column loss computed over various altitude ranges is given in Table 8.1. The lowest loss among the winters is in 2004 and the highest in 2005, consistent with the meteorological situation of the winters. All other winters show ozone loss of around 170±10 DU. The average partial column ozone loss above the 550 K level computed from the modelled and measured data for the seven winters is about 50±5 DU. Since the ozone loss above 550 K is largely controlled by the NO_x cycle, as discussed in Sect. 8.1.2, it indicates that this cycle contributes about one-third of the average total column ozone loss (i.e. 50–60 DU on 160–180 DU) in the Antarctic. The situation is slightly different from the Arctic, where significant ozone loss occurs mostly in the lower stratosphere over 350–550 K in colder winters and therefore, the contribution from NO_x cycles above 550 K is limited to about 19±7 DU (Kuttippurath et al., 2010a) and this is roughly three times lower than that of the Antarctic. The higher contribution is consistent with the larger ozone loss (both spatially and temporally) in the Antarctic stratosphere compared to that of the Arctic, as shown by the model results in both polar regions in Fig. 8.8. This is also evident from the maximum ozone loss altitudes shown in the figure, as most Antarctic winters have their peak loss altitudes around 550 K against 475 K in the Arctic (e.g. Kuttippurath et al., 2012a; Tripathi et al., 2007; Grooß et al., 2005b; Rex et al., 2004).

The partial column loss estimated from the Halogen Occultation Experiment ozone measurements (∼172 DU) over 350–600 K (Tilmes et al., 2006) is larger than our results for 2004. Our loss estimates over 350–850 K for 2004–2010 are in agreement with those derived from the ground-based and satellite total ozone observations in the Antarctic (Kuttippurath et al., 2013). The ozone loss computed from a bias-corrected satellite data set using a parameterised tracer by Huck et al. (2007) for the Antarctic winter 2004 also shows a similar estimate. The slight differences amongst various ozone loss estimates can be due to the differences in the column ranges, vortex definition, vortex sampling and the method used to quantify the loss by the respective studies.

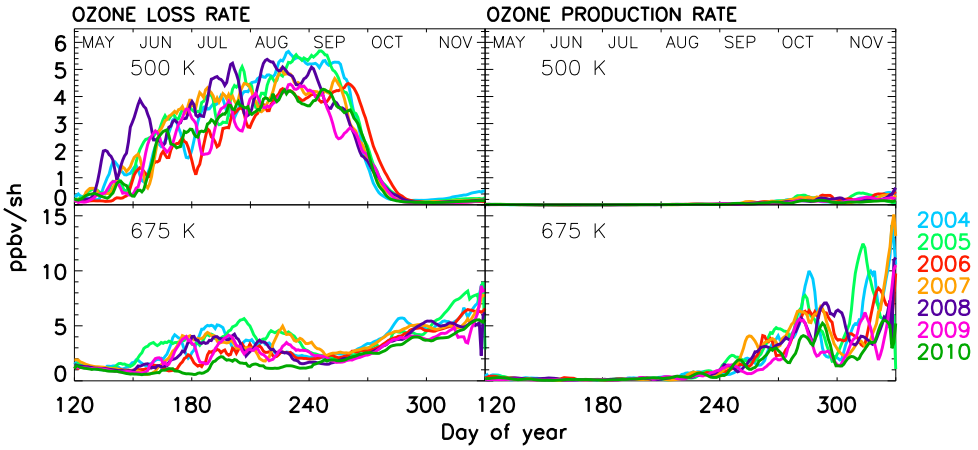

Figure 8.9: Vortex averaged (≥65° EqL) ozone loss and production rates at 500 and 675 K in ppbv per sunlit hour (ppbv sh^{-1}) for the Antarctic winters 2004–2010. The data are exempted from temporal smoothing to show the effect of daily movement of vortex and its impact on ozone production and loss rates

8.1.3.4 Ozone loss and production rates

The inter-annual variability of ozone loss is further analysed with the ozone loss and production rates. Fig. 8.9 shows the instantaneous loss and production rates at two representative altitudes in the lower and middle stratosphere, at 500 and 675 K. In general, at 500 K, the loss rates are about 1 ppbv sh^{-1} in mid-June during the onset of ozone loss, about 4–5 ppbv sh^{-1} by late August as the loss advances to the vortex core and about 5–6 ppbv sh^{-1} by late September during the peak loss period. The loss rates decrease from late September onwards and reach zero by mid-October, and stay at near-zero values thereafter.

The colder winter of 2006 shows an extended period of loss rates of about 4 ppbv sh^{-1} until early October, while the winter 2009 shows the shortest span of the large loss rates, only until mid-August. The colder winter 2008 also exhibits large loss rates in most months, May–August in particular. The model studies of Tripathi et al. (2007) and Frieler et al. (2006) also show comparable loss rates in the Antarctic winter 2003 at 475 K. Our analyses are consistent with the loss rates found in the very cold Arctic winters (e.g. 1994/95, 1999/00, 2004/05 and 2010/11) during the peak loss rate period in January–February, for which loss rates of about 5–8 ppbv sh^{-1} around 450–500 K are estimated (Kuttippurath et al., 2012a, 2010a; Frieler et al., 2006).

At 675 K, generally, the loss rates are about 1–3 ppbv sh^{-1} until early September and then increase rapidly to 6–8 ppbv sh^{-1} from mid-September onwards. The loss rates increase again from late October through to mid-November, from 2 to 7 ppbv sh^{-1}, depending on day of year. The inter-annual variability of loss rates from mid-September to late November is small and most winters show loss rates of about 2–7 ppbv sh^{-1} episodically. However, significant year-to-year variations are noted

Table 8.1: The vortex averaged (≥65° EqL) accumulated ozone partial column loss for the maximum ozone loss period in the Antarctic (26 September to 5 October) in DU estimated over 350–850 and 400–600 K from the MLS sampling inside the vortex and corresponding MIMOSA-CHIM simulations interpolated to the observed points for each winter. The estimated error of the ozone loss is about 10%.

350/850 K							
Year	2004	2005	2006	2007	2008	2009	2010
Model	121	183	163	174	167	159	163
MLS	145	171	170	155	160	141	150
400/600 K							
Model	95	127	109	119	120	105	100
MLS	95	120	125	122	112	103	93

from mid-June to mid-August. For instance, in 2005, the largest ozone loss rates of 3–5 ppbv sh^{-1} are simulated in early winter, whereas about 3 ppbv sh^{-1} is calculated in 2008 for the same period. The smallest loss rates among the seven winters are found in 2010, about 1–2 ppbv sh^{-1}, which are quite in line with our previous discussions on meteorology of the winters. Note that a similar range of loss rates of 2–7 ppbv sh^{-1} were also calculated for the colder Arctic winters in late March and mid- to late April in 2010/11, February–March in 2008/09 and March in 2004/05, depending on day of year (Kuttippurath et al., 2010a, 2012a).

The production rates at 675 K show significant variations from one year to the other, from zero in mid-August to 15 ppbv sh^{-1} in late November, with intermittent high values of ∼8 ppbv sh^{-1} in late October and mid-November. These substantial production rates, however, mask the large loss rates during the same period. The high production rates at the end of winter are expected due to the exposure of vortex to the sunlight. Also, the small disturbances at the end of the winter shift the polar vortices to the sunlit parts of the mid-latitudes or tilt their axis off the pole, as illustrated in the PV maps at 675 K as shown in Fig. 8.1. This implies that the ozone loss in the middle stratosphere also depends on the position of the polar vortex in the sunlight and the dynamics of the winter.

8.2 Conclusions

A detailed analysis of the polar ozone loss processes during seven recent Antarctic winters (2004–2010) is presented with high resolution model simulations and high frequency polar vortex observations from the Aura MLS instrument. The inter-annual variability in the Antarctic meteorology was relatively large during the studied winters, as it consisted of one of the coldest winters (2006), two warmer winters (2004 and 2010), two very cold winters (2007 and 2008). On average, as analysed from the average of the seven Antarctic winters, ozone loss in the Antarctic starts at the edge of the vortex at low EqLs (63–67° EqL) by mid-June, consistent with the findings of Lee et al. (2000). It progresses with time and advances to higher EqLs (69–83° EqL) with the largest loss at lower EqLs (63–69° EqL) in June–August in agreement with the incidence of sunlight over the region. The maximum ozone loss is attained by mid-September to mid-October period. The peak (>2 ppmv) ozone loss in the Antarctic winters is found over a broad altitude range of 475–550 K. The average cumulative maximum ozone loss is about 3.5 ppmv around 550 K or 180 DU over 350–675 K in 2005 and 2006, the coldest winters with the largest loss. In contrast, the maximum loss in the warmer winters of 2004 and 2010 was restricted to 2.6 ppmv around 475–500 K or 141–160 DU over 350–675 K. Analyses with various trace gas data suggest that the polar descent during spring is slower in the model.

In the lower stratosphere at 500 K, the ozone loss rates have a comparable distribution in all winters, about 2–3 ppbv sh^{-1} in July and 4–5 ppbv sh^{-1} from August to late September. However, as expected, the colder winters are characterised by slightly larger and extended periods of high loss rates. Therefore, the inter-annual variations are slightly larger in August–October period. In the middle stratosphere at 675 K, a loss rate of about 3–5 ppbv sh^{-1} in July, August and October–November, and a production rate of about 5–10 ppbv sh^{-1} in October–November, are simulated. Therefore, these higher production rates largely outweigh the loss rates in October–November.

Our study using vortex averages over the seven Antarctic winters shows that the halogen cycles contribute about 85–90% of ozone loss in the lower stratosphere (below 550 K) and the NO_x and ClO–O cycles contribute about 75–80% of ozone loss in the middle stratosphere with little inter-annual variability. Since much of the Antarctic ozone hole resides in the lower stratosphere, the ozone hole is still controlled by the abundances of halogen cycles. However, as there is an average ozone column loss of about 50±5 DU above 550 K, this further points out that about one-third of the ozone column loss in the Antarctic is contributed by the NO_x cycle.

The number of studied winters is very small to quantify any meaningful trends in the Antarctic ozone. In addition, although the decrease in stratospheric halogens has already been spotted (Montzka et al., 1999; Jones et al., 2011), the rate of this decrease is very slow and is about 10% $decade^{-1}$ (WMO, 2011). Furthermore, as also discussed in Chapter 6, our study points out that these lower ozone loss episodes in the recent winters (e.g. 2004, 2009 and 2010) are due to

relatively warm stratosphere, as analysed from temperature and PSCs during the winters (WMO, 2011). Therefore, these results are consistent with those of de Laat and van Weele (2011), who also report that the recent reduction in ozone loss is due to the minor warmings in the Antarctic winters of 2004 and 2010. Nevertheless, a detailed ozone trend analysis using a multi-variate regression model with various proxies to diagnose the impact of halogen decrease on the Antarctic ozone hole is presented in Chapter 9.

SECTION III

POLAR OZONE TRENDS

Chapter 9

Trends in polar ozone

Contents

Many studies have already discussed the trends of ozone in the Antarctic stratosphere. For instance, a study by Yang et al. (2008) discussed the trends in Antarctic ozone using ground-based and satellite measurements and showed a trend of around $-4.5\,\mathrm{DU\,yr^{-1}}$ during 1978–1996 and an insignificant positive trend thereafter. Similar trends were also estimated by Wohltmann et al. (2007), who applied a multi-variate regression model to the total ozone measurements. A study by Hassler et al. (2011) showed the stabilisation of ozone loss rates at South Pole over 1991–2009. A recent work by Salby et al. (2011) reported a significant positive trend in the September–November TOMS/OMI ozone during 1997–2009. Therefore, we also check weather the significant positive signal can be found in vortex averaged ozone. However, we use different data sets and estimation method to find the trends in ozone during the period 1979–2010. These data and approach have hitherto not been used for trend studies for this region, which is the importance of this diagnosis.

9.1 Multi-variate regression of vortex averaged ozone

9.1.1 Data and methods

A process oriented multi-variate regression model is constructed and applied to determine the ozone trends. We use the September–November ground-based and TOMS/OMI vortex averaged ozone (as discussed in Chapters 6 and 7) for this study. The 1994–1995 data gap in TOMS/OMI is filled with corresponding overpass analyses using the MSR data, which primarily consists of the Solar Backscatter Ultraviolet (SBUV) ozone observations during the period. Previous studies have successfully used this data in various scientific and trend studies (e.g. de Laat and van Weele, 2011). Therefore, the MSR data from 1979 to 2008 is also considered for this trend analysis, as they are compiled from bias corrected multi satellite observations. The 2009–2010 data for the MSR based regression analyses are taken from the combined average of the bias corrected OMI, GOME-2 (Van Roozendael et al., 2012), SCIAMACHY (Bovensman et al., 1999) and Aura MLS (Livesey et al., 2011; Nair et al., 2013) observations.

We consider the September–November ozone average over 1979–2010 for the trend analyses. More importantly, we use the vortex averaged ground-based, TOMS/OMI and MSR data sets to further elucidate the significance of the trends and we have used the deseasonalised ozone data in the regression model. The model is similar to that of Wohltmann et al. (2007) and Steinbrecht et al. (2004), where ozone (Y) variability is expressed as:

$$Y(t) = K + C_1 t1 + C_2 t2 + C_3(SF \times QBO)(t) + C_4 Aer(t) + C_5 HF(t) + C_6 AAO(t) + \varepsilon$$

where t is time period from 1979 to 2010, $t1$ is the number of years from 1979 to 2010, $t2$ is the number of years from 2000 to 2010, K is a constant, C_1 is the linear trend, C_2 is the change in trend, C_3 to C_6 are the regression coefficients of solar flux (SF)×QBO, aerosols (Aer), heat flux (HF) and Antarctic oscillation (AAO), respectively, and ε is the residual.

To describe the total ozone variability, we use the planetary wave drive proxy, i.e. heat flux calculated from the ERA interrim analysis at 70 hPa/40–90° S, averaged over August and September as described by Kuttippurath and Nikulin (2012), the Antarctic Oscillation (AAO) (ftp://ftp.cpc.

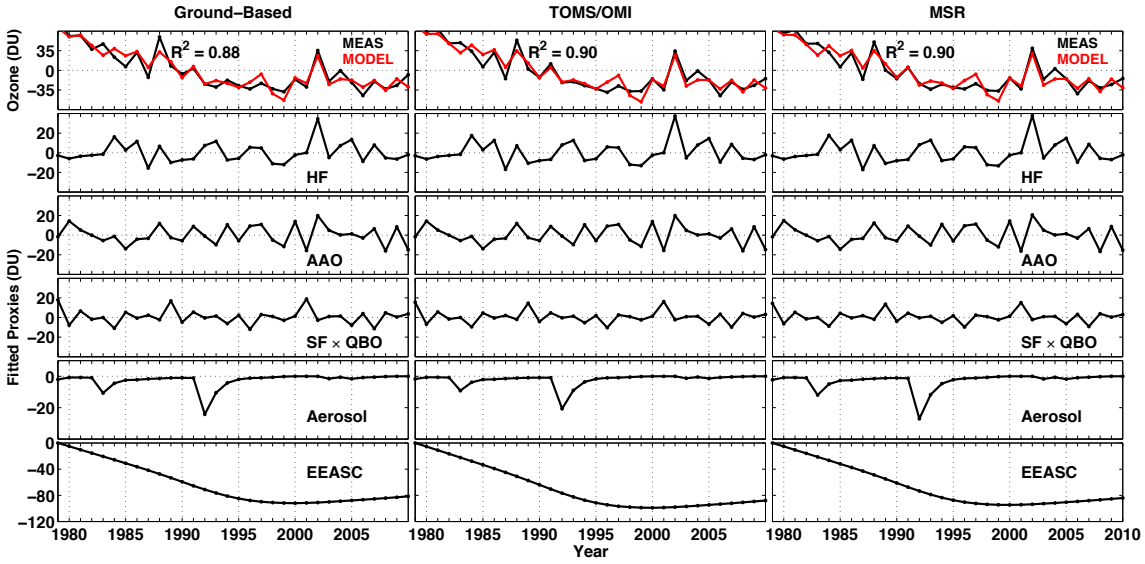

Figure 9.1: The vortex averaged (Nash et al., 1996) September–November O_3 trends estimated using a multi-variate regression model based on the EEASC (equivalent effective Antarctic stratospheric chlorine) for the ground-based, TOMS/OMI and MSR data in 1979–2010. Top to bottom: deseasonalised O_3 (MEAS) and the regression model (MODEL) (top panel), the contribution of heat flux – HF (second panel), Antarctic Oscillation – AAO (third panel), solar flux (SF) multiplied by quasi-biennial oscillation (QBO) at 40 hPa (fourth panel), aerosol (fifth panel) and EEASC (bottom panel).

ncep.noaa.gov/cwlinks/), solar flux (SF) (ftp://ftp.ngdc.noaa.gov/STP/SOLAR_DATA/SOLAR_RADIO/FLUX/Penticton_Adjusted/monthly/) at 10.7 cm wavelength, the quasi-biennial oscillation (QBO) at 40 hPa (http://www.geo.fu-berlin.de/met/ag/strat/produkte/qbo/), and the aerosol optical thickness (http://data.giss.nasa.gov/modelforce/strataer/) to account for the El Chichon (1982) and Mount Pinatubo (1991) volcanic aerosol injections. In order to better explain the variability of ozone, we use SF × QBO instead of individual solar flux and QBO terms, as explained by Roscoe and Haigh (2007). All proxies, except heat flux, are averaged over the September–November period to match the mean ozone taken during the same period. The southern hemispheric aerosol average data, which are shifted by +6 months to account for the transport of aerosols to the Antarctic, are considered. The selection of a 6 month shift of the aerosol data was based on a sensitivity test using various options (0, 3, 6 and 9 months of shift), for which a 6 month shift gave the best correlation between the regression model and ozone.

We have repeated the regression analysis after replacing the Piece-wise Linear Trend (PWLT) term ($C_1 t1 + C_2 t2$) by C_1 EEASC(t), EEASC being the equivalent effective Antarctic stratospheric chlorine (e.g. Brunner et al., 2006; Vyushin et al., 2010). Our EEASC uses the WMO A1-2010 scenario with a mean age of air of 5.5 yr for the polar stratosphere, age of air spectrum width of 2.75 yr (i.e. the half width of the age of air) and the bromine scaling factor of 60 to account for the greater ozone depletion potential of bromine compared to that of chlorine on a per atom basis. Further details about the EEASC formulation can be found in Newman et al. (2007). It should be noted that the trend in EEASC is in pptv yr^{-1} and the regression coefficient of EEASC from the model is in DU pptv^{-1} and hence the trend in ozone is expressed in DU yr^{-1} (i.e. DU pptv^{-1} × pptv yr^{-1}) (e.g. Stolarski et al., 2006). Since the trends derived from the PWLT model is in DU yr^{-1} itself, the estimated trends from both models can be compared directly. Apart from using various data sets (ground-based, TOMS/OMI and MSR) for the trend analysis, we have also tested various vortex definitions to group each data set, i.e. the data averaged inside the vortex, vortex core and over 65–90° S EqL to diagnose the robustness of the derived trend values and their significance.

9.1.2 Results: drivers of ozone change

Figure 9.1 shows the contribution of explanatory variables and resulting diagnosis using the EEASC regression for ground-based, TOMS/OMI and MSR data. We have taken the turning point (TP) or

break point for the PWLT regression as 2000, to coincide with the peak in EEASC. The regression analyses on all three data sets show similar evolution of ozone, regressed data and the explanatory parameters. The PWLT and EEASC regression models explain about 88–90% of the ozone variability as deduced from the R^2 estimate (e.g. Roscoe and Haigh, 2007). The SF × QBO contributes about +20 DU in 1979, 1989 and 2001, and −10 DU in 1984, 1996 and 2007. The variability in ozone column resulting from the changes in solar activity is about 2–3%, (Soukharev and Hood, 2006) and our results are within the expected range. The aerosol loading due to the eruption of El Chichon and Pinatubo significantly contribute to the ozone reduction of about −10 DU in 1983 and −26 DU in 1992, respectively, which reiterates the key role of aerosols on the heterogeneous ozone loss processes (e.g. Hofmann et al., 1992). The heat flux and AAO contributions mostly follow the dynamics of each winter, as both explain wave forcing and meteorology of the winters (Sexton, 2001; Randel et al., 2002). The contribution of AAO is between −18 DU (e.g. 1985, 2001, 2008 and 2010) and +20 DU (e.g. 1980, 2000 and 2002). The enhanced wave activity (heat flux) contributes about +18 DU in 1984, 1993 and 2005, with the largest contribution of about +38 DU in 2002. Similarly, suppressed planetary wave activity makes strong vortices, and hence, higher ozone reduction in the very cold winters of 1987 (−18 DU), 1998 (−12 DU) and 2006 (−10 DU). The analyses with PWLT regression also yield a very similar contribution of the proxies, which are exempted from this discussion to avoid repetitions. The regression analysis shows that the halogen loading (EEASC) dominates the ozone reduction. The resulting ozone trends computed from the deseasonalised ozone anomalies after removing the contribution of the explanatory variables are given in Table 9.1.

9.1.3 Results: ozone trends

The regression functions applied to the ground-based measurements show a trend of about −4.1 to −5.2 DU yr^{-1} from both regressions over 1979–1999 and are significant at 95% confidence intervals. As presented in Table 9.1 (top panel), these results did not change significantly when the data were analysed with respect to different vortex criteria (i.e. inside vortex, vortex core and over the EqLs 65–90° S). The trends derived from ground-based observations are in very good agreement with those found from TOMS/OMI and MSR data. The similar trends deduced from both EEASC and PWLT regressions imply that the ozone decrease over 1979–1999 is dominated by the increase in halogens during the period, consistent with the results of previous studies (e.g. WMO, 2011, and references therein). These trends are in good agreement with those found by Yang et al. (2008), who estimated a corresponding value (−4.5 to −5 DU yr^{-1} in 1978–1996) from the ground-based and satellite data using the cumulative sum method. A very similar trend of around −4 DU yr^{-1} was also deduced from an assimilated ozone data set by Brunner et al. (2006). The slight differences in the trend values of these studies are within error bars.

The results for the 2000–2010 period show a trend of about +1 DU yr^{-1} from the EEASC and +2.3 to +2.9 DU yr^{-1} from PWLT functions and are significant at 95% confidence intervals for the ground-based data averaged with respect to various vortex criteria. These trends are also in very good agreement with those estimated from TOMS/OMI and MSR data. The EEASC-based results are consistent with those derived from the CCM/CTM simulations for the 1997–2009 period, which exhibit an EEASC-based ozone trend of around +1 DU yr^{-1} (Austin et al., 2010a,b; Kiesewetter et al., 2010). The results derived from EEASC regression are smaller than those obtained from PWLT. This implies that the ozone increase during 2000–2010 cannot be explained by the reduction in ozone depleting substances alone, but there are strong influences from the dynamics and other parameters. Note also that similar differences between the PWLT and EEASC-based trend values are also reported in previous studies for mid-latitude (up to 60° N/S) ozone (Nair et al., 2013; WMO, 2011; Vyushin et al., 2010). The significant positive trend during the period reinforces the notion that the Antarctic ozone is recovering, as reported by Salby (2011).

It is well known that the temperature controls the PSC formation, chlorine and bromine activation, and hence, the springtime ozone depletion. Therefore, to test the strength of the positive trends and to understand the impact of inter-annual variability of Antarctic meteorology on the derived results during 2000–2010, we computed the trends without heat flux in the regression models, which are shown in Table 9.1 (lower panel). The resulting estimates show similar values for EEASC-based regression, around +1 DU yr^{-1} using all data sets, and are significant at 95% (and 99%)confidence

Table 9.1: Antarctic ozone trends in DU yr^{-1} estimated from the deseasonalised September–November vortex averaged ground-based, TOMS/OMI and MSR data using the PWLT (piecewise linear trend) and EEASC (equivalent effective Antarctic stratospheric chlorine) regressions. The regression results without considering heat flux are also shown in the bottom panel. The error values represent 95% confidence intervals. The results are shown for various vortex averaged calculations: inside vortex (Nash et al., 1996), over the equivalent latitudes (EqLs) 65–90° S and inside vortex core.

Data	Period	Inside vortex		EqL: 65–90° S		Vortex core	
		PWLT	EEASC	PWLT	EEASC	PWLT	EEASC
with heat flux							
Ground-based	1979–1999	-4.68 ± 0.88	-4.18 ± 0.65	-4.62 ± 0.87	-4.14 ± 0.66	-5.02 ± 0.89	-4.51 ± 0.65
	2000–2010	$+2.58 \pm 2.16$	$+1.03 \pm 0.16$	$+2.33 \pm 2.13$	$+1.02 \pm 0.16$	$+2.59 \pm 2.19$	$+1.11 \pm 0.16$
TOMS/OMI	1979–1999	-5.03 ± 1.12	-4.50 ± 0.63	-4.89 ± 1.00	-4.38 ± 0.62	-5.24 ± 1.12	-4.70 ± 0.66
	2000–2010	$+2.87 \pm 2.74$	$+1.11 \pm 0.16$	$+2.67 \pm 2.47$	$+1.08 \pm 0.15$	$+2.84 \pm 2.74$	$+1.16 \pm 0.16$
MSR	1979–1999	-4.81 ± 1.11	-4.31 ± 0.62	-4.68 ± 0.99	-4.19 ± 0.62	-5.02 ± 1.11	-4.50 ± 0.65
	2000–2010	$+2.91 \pm 2.73$	$+1.06 \pm 0.15$	$+2.68 \pm 2.43$	$+1.03 \pm 0.15$	$+2.91 \pm 2.73$	$+1.11 \pm 0.16$
without heat flux							
Ground-based	1979–1999	-4.53 ± 1.08	-4.07 ± 0.80	-4.45 ± 1.13	-4.01 ± 0.85	-4.87 ± 1.10	-4.40 ± 0.80
	2000–2010	$+2.77 \pm 2.66$	$+1.00 \pm 0.20$	$+2.55 \pm 2.78$	$+0.99 \pm 0.21$	$+2.79 \pm 2.70$	$+1.08 \pm 0.20$
TOMS/OMI	1979–1999	-4.87 ± 1.15	-4.38 ± 0.80	-4.72 ± 1.14	-4.25 ± 0.84	-5.09 ± 1.12	-4.58 ± 0.81
	2000–2010	$+3.08 \pm 2.82$	$+1.08 \pm 0.20$	$+2.90 \pm 2.81$	$+1.05 \pm 0.21$	$+3.04 \pm 2.75$	$+1.13 \pm 0.20$
MSR	1979–1999	-4.66 ± 1.22	-4.18 ± 0.80	-4.51 ± 1.15	-4.06 ± 0.84	-4.87 ± 1.21	-4.38 ± 0.81
	2000–2010	$+3.12 \pm 3.00$	$+1.03 \pm 0.20$	$+2.91 \pm 2.83$	$+1.00 \pm 0.21$	$+3.11 \pm 2.98$	$+1.08 \pm 0.20$

intervals. The PWLT regressions show slightly higher values, +2.5 to +3.1 DU yr^{-1}, and are also significant at 95% confidence intervals, except for the ground-based measurements averaged over 65–90° S EqLs. These results, however, show a clear ozone recovery signal even without subtracting the added variability induced by dynamics.

9.2 Conclusions

The trends in Antarctic ozone is estimated using the ground-based, TOMS/OMI and MSR data from 1979 to 2010 by analysing them using three different vortex edge criterion (inside vortex, vortex core and over EqLs 65–90° S). The piecewise and EEASC-based trends estimated from the September–November vortex averaged ground-based ozone column show a trend of about −4.1 to −5.2 DU yr^{-1} for the period 1979–1999 and around +1 DU yr^{-1} with EEASC and +2.3 to +2.9 DU yr^{-1} with PWLT functions during 2000–2010. These trend analyses are significant at the 95% confidence levels (the EESC based results are significant at the 99% confidence levels as well) in both periods for all vortex averaged data clusters. The ground-based analyses are well supported by those of the TOMS/OMI and MSR data. In 1979–1999, both piecewise and EEASC-based ozone trends show very similar values, corroborating the dominance of stratospheric halogens on the ozone decrease in that period. However, the larger values derived from the PWLT regression for the 2000–2010 period suggest the greater influence of dynamics plus other regression indices not considered here on the increase of ozone during the period. These results thus show the first sign of ozone recovery. However, the Antarctic ozone loss/hole will prevail in much of this century with the given rate of the estimated positive trend and due to the still high levels of stratospheric chlorine. It will take another fifty years to regain the 1980 level of ozone.

SUMMARY

CONCLUSIONS AND PERSPECTIVES

Chapter 10
Conclusions and Perspectives

10.1 Conclusions

10.1.1 Arctic stratosphere

Analysis of the major warmings (MWs) in the Arctic winters 2003/04–2009/10 shows that there were 6 MWs in 6 out of the 7 winters, in which the MWs of 2003/04, 2005/06 and 2008/09 were in January and those of 2006/07, 2007/08 and 2009/10 were in February. Although the winter 2009/10 was relatively cold from mid-December to mid-January, strong wave 1 activity led to a MW in early February, for which the largest momentum flux among the winters was estimated at 60° N/10 hPa, about 450 $m^2 s^{-2}$. The strongest MW, however, was observed in 2008/09 and the weakest in 2006/07. The MW in 2008/09 was triggered by intense wave 2 activity and was a vortex split event. In contrast, strong wave 1 activity led to the MWs of other winters and were vortex displacement events. Large amounts of EP (Eliassen-Palm) and wave 1/2 EP fluxes (about 2–4 $\times 10^5$ kg s^{-2}) are estimated shortly before the MWs at 100 hPa averaged over 45–75° N in all winters, suggesting profound tropospheric forcing for the MWs. We observe an increase in the occurrence of MWs ($\sim$ 1.1 events/winter) in recent years (1998/99–2009/10), as there were 13 MWs in the 12 Arctic winters, although the long-term average (1957/58–2009/10) of the frequency stays around its historical value ($\sim$ 0.7 events/winter), consistent with the findings of previous studies. An analysis of the chemical ozone loss in the past 17 Arctic winters (1993/94–2009/10) suggests that the loss is inversely proportional to the intensity and timing of MWs in each winter, where early (December–January) MWs lead to minimal ozone loss. Therefore, this high frequency of MWs in recent Arctic winters has significant implications for stratospheric ozone trends in the northern hemisphere, and hence, the regional and global climate.

The Arctic winter 2002/03 was characterised by unusually cold temperatures in early winter and a MW around 15–18 January 2003. The potential vorticity maps show a vortex split in the lower stratosphere during the MW in late January and during the minor warming in mid-February due to wave 1 amplification. However, the warming can be termed as a vortex displacement event as there was no vortex split during the MW period at 10 hPa. Very low temperatures, large areas of PSCs (polar stratospheric clouds), and high chlorine activation triggered significant ozone loss in the early winter, as the vortex moved to the mid-latitude regions. The ozone loss derived from ASUR (Airborne Sub-millimeter Radiometer) measurements sampled inside the vortex, in conjunction with the MIMOSA-CHIM model tracer, shows a maximum of 1.3±0.2 ppmv at 450–500 K by late March. The partial column ozone loss derived from ASUR ozone profiles reaches up to 61±4 DU (Dobson Unit) over 400–550 K in the same period. The evolution of ozone and ozone loss assessed from ASUR measurements is in very good agreement with POAM (Polar Ozone and Aerosol Measurement) observations. The loss estimated from POAM measurements shows a similar maximum of 1.3±0.2 ppmv at 400–500 K or 63±4 DU over 400–550 K in late March. Our study reveals that the Arctic winter 2002/03 was unique as it had three minor warmings and a MW, yet showed large loss in ozone. No such feature was observed in any other Arctic winter in the 1989–2010 period. In addition, an unusually large ozone loss in December, around 0.5±0.2 ppmv at 450–500 K or 12±1 DU over 400–550 K, was estimated for the first time in the Arctic (winters 1989–2011). A detailed diagnosis with all available published results for this winter exhibits an average ozone loss of 1.5±0.2 ppmv at 450–500 K or 65±5 DU over 400–550 K by the end of March, which exactly matches the ozone depletion derived from the ASUR, POAM and model data. The early ozone loss together with considerable loss afterwards classify the warm Arctic winter 2002/03 amongst the "moderately cold winters" in terms of the significance of the ozone loss.

The stratospheric ozone loss in the Arctic winters 2004/05–2009/10 is investigated by using MIMOSA-CHIM model and observations from Aura MLS (Microwave Limb Sounder), by applying the passive tracer technique. The ozone loss diagnosed from both simulations and measurements inside the polar vortex at 475 K ranges from 0.7 ppmv in the warm winter 2005/06 to 1.5–1.7 ppmv in the cold winter 2004/05. Halogenated (chlorine and bromine) catalytic cycles contribute to 75–

90% of the ozone loss at this level. At 675 K the lowest loss of 0.3–0.5 ppmv is computed in 2008/09, and the highest loss of 1.3 ppmv is estimated in 2006/07 by the model and in 2004/05 by MLS. Most of the ozone loss (60–75%) at this level results from nitrogen catalytic cycles rather than halogen cycles. At both 475 and 675 K levels the simulated ozone evolution inside the vortex is in reasonably good agreement with the observations. The partial column ozone loss over 350–850 K deduced from the model calculations at the MLS sampling locations inside the vortex ranges between 43 DU in 2005/06 and 109 DU in 2004/05, while that derived from observations ranges between 26 DU and 115 DU for the same winters. The partial column ozone loss derived in that vertical range is larger than that estimated over 350–550 K by 19±7 DU on average, mainly due to NO_x chemistry. The column ozone loss estimates from both MIMOSA-CHIM and MLS at 350–850 K are in general good agreement with those derived from ground-based UV-VIS spectrometer total ozone observations for the respective winters, except in 2010.

In the Arctic winter 2010/11, the lower stratospheric minimum temperatures were below 195 K for a record period, from December to mid-April, and a strong and stable vortex was present during that period. Analyses with the MIMOSA-CHIM CTM simulations show that the chemical ozone loss started by early January and progressed slowly to 1 ppmv by late February. The loss intensified by early March and reached a record maximum of ∼2.4 ppmv in the late March–early April period over a broad altitude range of 450–550 K. This coincides with elevated ozone loss rates of 2–4 ppbv sh^{-1} and a contribution of about 40% from the ClO–ClO cycle and about 35–40% from the ClO–BrO cycle in late February and March, and about 30–50% from the HO_x cycle in April. We also estimate a loss of around 0.7–1.2 ppmv contributed (75%) by the NO_x cycle at 550–700 K. The ozone loss estimated in the partial column range of 350–550 K also exhibits a record value of ∼148 DU. This is the largest ozone loss ever estimated in the Arctic and is consistent with the remarkable chlorine activation and strong denitrification during the winter, as the modeled ClO shows ∼1.8 ppbv in early January and ∼1 ppbv in March at 450–550 K. These model results are in excellent agreement with those found from the Aura MLS observations. Our analyses show that the ozone loss in 2010/11 is close to that found in some Antarctic winters, for the first time in the observed history. Though the winter 1996/97 was also very cold in March–April, the temperatures were higher in December–February, and, therefore, chlorine activation was moderate and ozone loss was average with about 1.2 ppmv at 475–550 K or 42 DU at 350–550 K, as diagnosed from the model simulations and measurements.

10.1.2 Antarctic stratosphere

A method is introduced to estimate ozone loss from ground-based measurements in the Antarctic. A sensitivity study shows that the ozone depletion can be estimated within an accuracy of ∼4%. The method is then applied to the ground-based observations from Arrival Heights, Belgrano, Concordia, Dumont d'Urville, Faraday, Halley, Marambio, Neumayer, Rothera, South Pole, Syowa and Zhongshan for the diagnosis of ozone loss in the Antarctic. The ozone loss computed from ground-based measurements is also in very good agreement with those derived from satellite measurements (Ozone Monitoring Instrument and SCIAMACHY) and model simulations (REPROBUS and SLIMCAT), where the differences are within ±3–5%.

Our analyses show that all ground-based observations exhibit their ozone annual minima in the late September–early October period. Among the stations, the lowest ozone annual minima are observed at South Pole and the highest at Dumont d'Urville. The ozone loss starts by mid-June at the vortex edge and then progresses towards the vortex core with time. The loss intensifies in August–September, peaks by the end of September–early October, and ozone recovers thereafter. The edge region stations (e.g. Dumont d'Urville and Marambio) show lower ozone loss (−38 to −45%) as compared to that in vortex core stations (e.g. −55 to −60% at South Pole and Belgrano). The average ozone loss in the Antarctic is about −33 to −50% in 1989–1992 in agreement with the increase in halogens during this period, and then stayed at around −48%. The ozone loss in the warmer winters (e.g. 2002 and 2004) is lower (−37 to −46%) and in the colder winters (e.g. 2003 and 2006) is higher (−52 to −55%). Due to the small inter-annual variability of both ozone loss and V_{PSC} during 1995–2010, the correlation (r) between ozone loss and the product of EEASC (Equivalent Effective Antarctic Stratospheric Chlorine) and V_{PSC} yields 0.61–0.69. The

ozone loss estimated from ground-based measurements is in good agreement with that of the space-based observations from TOMS/OMI, and Aura MLS as well as MSR data, where the difference between the ground-based and satellite observations is within ±5% and is within the error bars of the measurements.

The historical ground-based total ozone observations in October show that the depletion started in the late 1970s, reached a maximum in the early 1990s and stabilised afterwards due to saturation. At southern mid-latitudes, a reduction of 20–50% is observed for a few days in October–November at the newly installed Rio Gallegos station in 2005–2009. Similar depletion of ozone is also observed episodically during the vortex overpasses at Kerguelen in October–November and at Macquarie Island in July–August of the recent winters. This illustrates the significance of measurements at the edges of Antarctica.

In order to closely assess the vertical features of Antarctic ozone loss, a study was performed with high resolution satellite measurements and MIMOSA-CHIM simulations for the seven winters 2004–2010. The Antarctic winters 2004–2010 were characterised by comparatively large inter-annual variability and various ozone loss features. Generally, chemical ozone loss starts at the edge of the vortex at low EqLs (Equivalent Latitudes) of 63°–69° in mid-June/July. The loss progresses with time at higher EqLs and intensifies in August–September over 400–600 K. The loss peaks in late September/early October, where all EqLs (63°–83°) show similar loss and the maximum is found over a broad altitude range of 475–550 K. In the lower stratosphere, most winters show similar loss and production rates, in which the loss rates show about 2–3 ppbv sh^{-1} in July and 4–5 ppbv sh^{-1} in August/mid-September, while they rapidly drop to zero by late September. In the middle stratosphere, the loss rates show about 3–5 ppbv sh^{-1} in July, August and October–November. The loss in the lower stratosphere (<550 K) is dominated by the ClO–ClO and ClO–BrO cycles, whereas the loss in the middle stratosphere (>550 K) is controlled by the NO_x and ClO–O cycles, with 80–90% in each region. Our study finds that about one-third of the Antarctic column ozone loss (50±5 DU) is contributed by the NO_x cycle in the middle stratosphere, above 550 K. On average, the colder winters 2005 and 2006 show a maximum loss of about 3.5 ppmv around 550 K and the warmer winters 2004 and 2010 show a loss of about 2.6 ppmv around 475–500 K. The winters 2007 and 2009 were moderately cold and thus both ozone loss and peak loss altitudes are between these two extremes. The partial column loss at 350–850 K shows the largest value of ∼207 DU in 2005 and the smallest of ∼145 DU in 2004, consistent with meteorology of the winters. The simulated ozone loss values are in reasonably good agreement with those estimated from the Aura MLS measurements, but the model underestimates the observed ClO over 450–550 K primarily due to the slower vertical descent in the model in spring. This implies that vertical transport is still a critical issue in chemical transport models.

10.1.3 Ozone trends

The ozone trends based on the EEASC and piecewise linear trend (PWLT) functions for the vortex averaged ground-based, Total Ozone Mapping Spectrometer/Ozone Monitoring Instrument (TOMS/OMI), and MSR data averaged over September–November exhibit about -4.6 DU yr^{-1} over 1979–1999, corroborating the role of halogens in the ozone decrease during the period. The ozone trends computed for the 2000–2010 period are about $+1$ DU yr^{-1} for EEASC and $+2.6$ DU yr^{-1} for the PWLT functions. The larger positive PWLT trends for the 2000–2010 period indicate the influence of dynamics and other basis functions on the increase of ozone. The trends in both periods are significant at 95% confidence intervals for all analyses. Therefore, our study suggests that Antarctic ozone shows a significant positive trend toward its recovery, and hence, leaves a clear signature of the successful implementation of the Montreal Protocol.

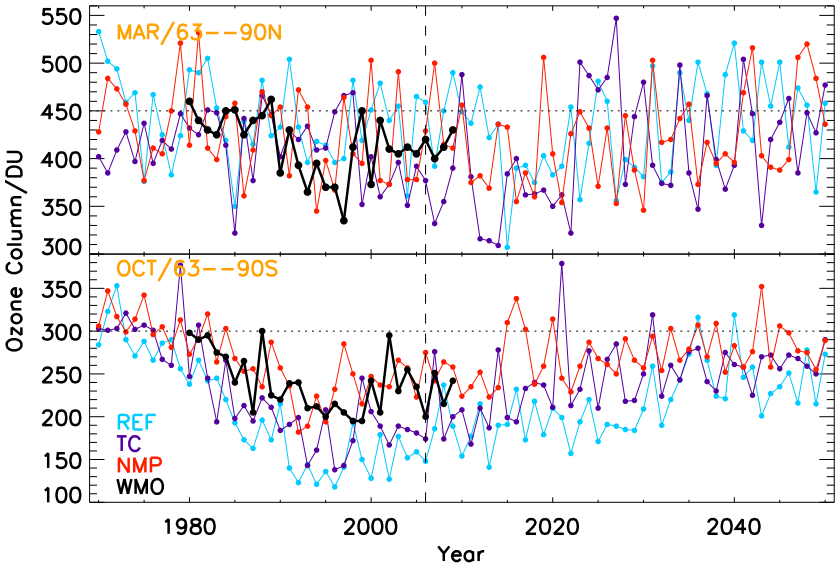

Figure 10.1: The spring-time evolution of ozone (both past and future) in the polar regions (63–90° N/S) in the chemistry climate model LMDz-reprobus. The reference run simulations are represented by REF, the temperature corrected run is represented by TC and the bias-corrected run with a new microphysics scheme for the polar stratospheric clouds is represented by NMP. The model simulations are compared to the satellite measurements TOMS, OMI and SBUV (black: merged data), as shown in WMO (2011).

10.2 Perspectives

There are a number of interesting and challenging topics that can be explored as a continuation of these studies. Since our study has already revealed positive trends in ozone in the Antarctic from total column ozone observations from a variety of measurements, it is also necessary to look at the ozone trends at different vertical layers in the stratosphere to test the strength of the recovery signal. Therefore, this is one of the future studies. In addition, we have seen that the ozone trends are positive and are significant at 95% confidence intervals inside the vortex core too. This points out the necessity of ozone trend analysis in the ozone saturation altitudes. In order to analyse these saturation layers closely, the ozonesonde observations in Antarctic will be utilised. There are 11 ozonesonde stations, in which many have soundings from the early 1980s and hence, this data set is ideal for these kinds of trend analyses. Furthermore, this data set will be complemented with available satellite observations since 1978. A similar trend analysis in the Arctic stratosphere using ground-based and space-based total column ozone observations and, ozonesonde and satellite profile measurements will also be performed. Apart from these, the polar ozone trends and its projections will be analysed from chemistry climate model output, LMDz-reprobus in particular. Fig. 10.1 shows an example of the ozone trends (i.e. deviation from the average ozone during the pre-ozone hole period) and its future projection as simulated by the LMDz-reprobus climate model.

As mentioned in **Motivation**, the stratospheric climate is influenced by many factors and the climate of the Earth is controlled by a number of physical, chemical and radiative processes. However, how the stratosphere evolve with climate change is still uncertain (Baldwin et al., 2007). Studies have mentioned that the stratosphere has changed considerably in the past 30 years. For instance, increase in the abundances of anthropogenic green-house gases and ozone depleting substances, and subsequent changes in the stratospheric ozone and temperature (e.g. stratosphere has cooled since 1979). Therefore, a study will be conducted to analyse the changes in composition of the stratosphere over the years and its influence on the surface climate. To perform this study, a suite of long-term chemistry climate model simulations that were carried out for the Intergovernmental Panel on Climate Change (IPCC) Report and chemistry climate model validation (CCM VAL) activities will be exploited.

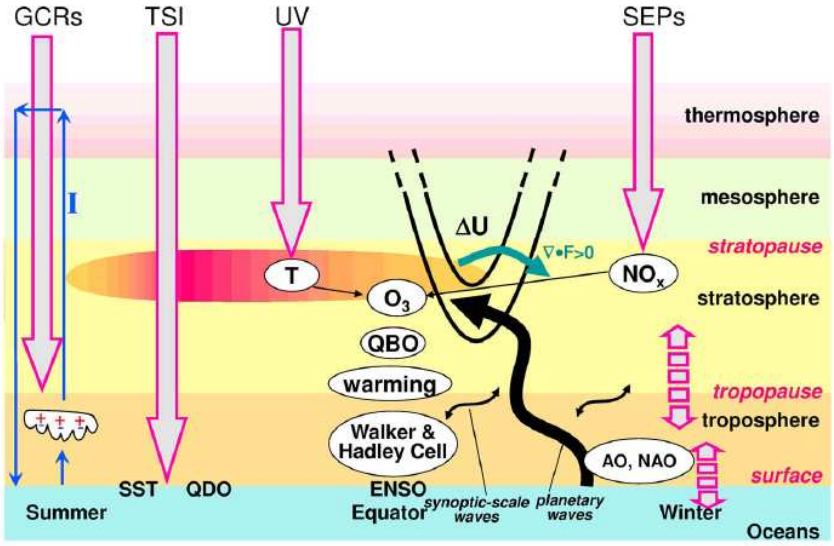

Figure 10.2: A schematic representation of solar activity and climate interactions (Gray et al., 2010).

Our understanding on the physical nature and scale of solar variability and its effect on the climate is limited (Gray et al., 2010). Climate change can occur on different time scales due to the results of natural variability, including solar variability (in the form of sunspots and related magnetic activity). Fig. 10.2 schematically illustrates the solar variability impact on various altitude layers of the atmosphere. Therefore, a study regarding the solar variability and its effect on the climate (including changes in temperature, winds and ozone) will be conducted with the assistance of long-term chemistry climate model simulations. To perform this study, the chemistry climate model LMDz-reprobus will be utilised. Therefore, as emphasised earlier, this challenging science always motivates!

Thesis.brfRerun to get bibliographical references right

Bibliography

Andersen, S. B. and B. M. Knudsen, 2002: The influence of vortex ozone depletion on Arctic ozone trends. *Geophys. Res. Lett.*, **29, doi:10.1029/2001GL014595**.

Andrews, D. G., J. R. Holton, and C. B. Leovy, 1987: *Middle atmosphere dynamics*. Academic Press Inc., California, USA, ISBN-10:0120585766.

Austin, J., et al., 2003: Uncertainties and assessments of chemistry-climate models of the stratosphere. *Atmos. Chem. Phys.*, **3, doi:10.5194/acp-3-1-2003**, 1–27.

Austin, J., et al., 2010a: Chemistry-climate model simulations of spring Antarctic ozone. *J. Geophys. Res.*, **115, doi:10.1029/2009JD013577**.

Austin, J., et al., 2010b: Decline and recovery of total column ozone using a multimodel time series analysis. *J. Geophys. Res.*, **115, doi:10.1029/2010JD013857**.

Ayarzagüena, B., U. Langematz, and E. Serrano, 2011: A comparative study of the two different major stratospheric warmings in 2009 and 2010. *J. Geophys. Res.*, **116, doi:10.1029/2010JD015023**.

Baldwin, M. P., M. Dameris, and T. G. Shepherd, 2007: How will the stratosphere affect climate change? *Science*, **316, doi:10.1126/science.1144303**, 1576–1577.

Baldwin, M. P. and T. J. Dunkerton, 2001b: Stratospheric harbingers of anomalous weather regimes. *Science*, **294, doi:10.1126/science.1063315**, 581–584.

Baldwin, M. P., L. Gray, T. Dunkerton, K. Hamilton, and et al., 2001a: The Quasi-Biennial Oscillation. *Rev. Geophys.*, **39, doi:10.1029/1999RG000073**, 179–229.

Balis, D., et al., 2011: Observed and modelled record ozone decline over the Arctic during winter/spring 2011. *Geophys. Res. Lett.*, **38, doi:10.1029/2011GL049259**.

Bancalá, S., K. Krüger, and M. Giorgetta, 2012: The preconditioning of major sudden stratospheric warmings. *J. Geophys. Res.*, **117, doi:10.1029/2011JD016769**.

Basher, R. E., 1982: Review of the Dobson spectrophotometer and its accuracy, WMO Global Ozone Research and Monitoring Project, Report No. 13, WMO, Geneva.

Bates, D. R. and M. Nicolet, 1950: The photochemistry of atmospheric water vapour. *J. Geophys. Res.*, **55, doi:10.1029/JZ055i003p00301**, 301–327.

Bekki, S. and J. A. Pyle, 1994: A 2-Dimensional modeling study of the volcanic-eruption of Mount-Pinatubo. *J. Geophys. Res.*, **99, doi:10.1029/94JD00667**, 18 861–18 869.

Bekki, S., R. Toumi, and J. A. Pyle, 1993: Role of sulfur photochemistry in tropical ozone changes after the eruption of Mount Pinatubo. *Nature*, **362, doi:10.1038/362331a0**, 331–333.

Bevilacqua, R. M., et al., 1997: POAM II ozone observations in the Antarctic ozone hole in 1994, 1995, and 1996. *J. Geophys. Res.*, **102, doi:10.1029/97JD01623**, 23 643–23 657.

Bhartia, P. K. and C. W. Wellemeyer, 2002: TOMS-V8 total O_3 algorithm, NASA Goddard Space Flight Centre, Greenbelt, MD, OMI Algorithm, Theoretical basis document, Vol II. 2387.

Blume, C., K. Matthes, and I. Horenko, 2012: Supervised learning approaches to classify sudden stratospheric warming events. *J. Atmos. Sci.*, **69, doi:10.1175/JAS-D-11-0194.1**, 1824–1840.

Blumenstock, T., F. Hase, I. Kramer, S. Mikuteit, H. Fischer, F. Goutail, and U. Raffalski, 2009: Winter to winter variability of chlorine activation and ozone loss as observed by ground-based FTIR measurements at Kiruna since winter 1993/94. *Int. J. Remote Sens.*, **30, doi:10.1080/01431160902821916**, 4055–4064.

Boccara, G., A. Hertzog, C. Basdevant, and F. Vial, 2008: Accuracy of NCEP/NCAR reanalyses and ECMWF analyses in the lower stratosphere over Antarctica in 2005. *J. Geophys. Res.*, **113, doi:10.1029/2008JD010116**.

Bodeker, G. E., J. C. Scott, K. Kreher, and R. L. McKenzie, 2001: Global ozone trends in potential vorticity coordinates using TOMS and GOME inter-compared against the Dobson network: 1978–1998. *J. Geophys. Res.*, **106, doi:10.1029/2001JD900220**, 23 029–23 042.

Bojkov, R. D., L. Bishop, and V. E. Fioletov, 1995: Total ozone trends from quality-controlled ground-based data (1964–1994). *J. Geophys. Res.*, **100, doi:10.1029/95JD02907**, 25 867–25 876.

Bojkov, R. D. and V. E. Fioletov, 1995: Estimating the global ozone characteristics during the last 30 years. *J. Geophys. Res.*, **100, doi:10.1029/95JD00692**, 16 537–16 551.

Bovensman, H., J. P. Burrows, M. Buchwitz, J. Frerick, S. Noël, V. V. Rozanov, K. V. Chance, and A. P. H. Goede, 1999: SCIAMACHY–mission objectives and measurement modes. *J. Atmos. Sci.*, **56, doi:10.1175/1520-0469(1999)056<0127:SMOAMM>2.0.CO;2**, 127–150.

Brasseur, G. P., 2008: *Climate Variability and Extremes during the Past 100 years: Creating Knowledge from the Controntation of Observations and Models: The Case of Stratospheric Ozone*, Advances in Global Change Research, Vol. 33, doi:10.1007/978-1-4020-6766-2_21. Springer, 303–316 pp.

Brasseur, G. P. and S. Solomon, 2005: *Aeronomy of the middle atmosphere*. Springer, Dordrecht, ISBN 978-1-4020-3824-2, 646 pp.

Bremer, H., et al., 2002: Ozone depletion observed by ASUR during the Arctic winter 1999/2000. *J. Geophys. Res.*, **107, doi:10.1029/2001JD000546**.

Brewer, A. W., 1949: Evidence for a world circulation provided by the measurements of helium and water vapour distribution in the stratosphere. *Quart. J. Roy. Meteor. Soc.*, **75, doi:10.1002/qj.49707532603**, 351–363.

Brewer, A. W., 1973: A replacement for the Dobson spectrophotometer? *Pure Appl. Geophys.*, **919, doi:10.1007/BF00881042**, 106–108.

Brunner, D., J. Staehelin, J. A. Maeder, I. Wohltmann, and G. E. Bodeker, 2006: Variability and trends in total and vertically resolved stratospheric ozone based on the CATO ozone data set. *Atmos. Chem. Phys.*, **6, doi:10.5194/acp-6-4985-2006**, 4985–5008.

Burkholder, J. B., J. J. Orlando, and C. J. Howard, 1990: Ultraviolet absorption cross-sections of Cl_2O_2 between 210 and 410 nm. *J. Phys. Chem.*, **94, doi:10.1021/j100365a033**, 687–695.

Butchart, N. and E. E. Remsberg, 1986: The area of the stratospheric polar vortex as a diagnostic for tracer transport on an isentropic surface. *J. Atmos. Sci.*, **43, doi:10.1175/1520-0469(1986)043<1319:TAOTSP>2.0.CO;2**, 1319–1339.

Butchart, N., et al., 2010: Chemistry-climate model simulations of 21st century stratospheric climate and circulation changes. *J. Climate*, **23, doi:10.1175/2010JCLI3404.1**, 5349–5374.

Butler, A. H. and L. M. Polvani, 2011: El Niño, La Niña, and stratospheric sudden warmings: A reevaluation in light of the observational record. *Geophys. Res. Lett.*, **38, doi:10.1029/2011GL048084**.

Butz, A., H. Bösch, C. Camy-Peyret, M. Dorf, A. Engel, S. Payan, and K. Pfeilsticker, 2007: Observational constraints on the kinetics of the ClO-BrO and ClO-ClO ozone loss cycles in the Arctic winter stratosphere. *Geophys. Res. Lett.*, **34, doi:10.1029/2006GL028718**.

Cacciani, M., G. Fiocco, P. Colagrande, P. D. Girolamo, A. di Sarra, and D. Fuà, 1997: Lidar observations of polar stratospheric clouds at the South Pole 1. stratospheric unperturbed conditions. *J. Geophys. Res.*, **102, doi:10.1029/97JD00360**, 12 937–12 943.

Cagnazzo, C., C. Claud, and S. Hare, 2006: Aspects of stratospheric long-term changes induced by ozone depletion. *Clim. Dyn.*, **27, doi:10.1007/s00382-006-0120-1**, 101–111.

Cariolle, D., M. Déqué, and J. Morcrette, 1986: A GCM simulation of the ozone seasonal variations at high latitudes in the Southern Hemisphere. *Geophys. Res. Lett.*, **95, doi:10.1029/GL013i012p01304**, 1304–1307.

Cariolle, D., A. Lasserre-Bigorry, J.-F. Royer, and J.-F. Geleyn, 1990: A general circulation model simulation of the springtime Antarctic ozone decrease and its impact on mid-latitudes. *J. Geophys. Res.*, **95, doi:10.1029/JD095iD02p01883**, 1883–1898.

Castanheira, J. M. and D. Barriopedro, 2010: Dynamical connection between tropospheric blockings and stratospheric polar vortex. *Geophys. Res. Lett.*, **37, doi:10.1029/2010GL043819**.

Chapman, S., 1930: A theory of upper-atmospheric ozone. *Memoirs of the Royal Meteorological Society*, **3**, 103–125.

Charlton, A. J. and L. M. Polvani, 2007: A new look at stratospheric sudden warmings. Part I: Climatology and modeling benchmarks. *J. Climate*, **20, doi:10.1175/JCLI3996.1**, 449–469.

Charlton-Perez, A. J., L. M. Polvani, J. Austin, and F. Li, 2008: The frequency and dynamics of stratospheric sudden warmings in the 21st century. *J. Geophys. Res.*, **113, doi:10.1029/2007JD009571**.

Charney, J. G. and P. G. Drazin, 1961: Propagation of planetary-scale disturbances from the lower into the upper atmosphere. *J. Geophys. Res.*, **66, doi:10.1029/JZ066i001p00083**, 83–109.

Chipperfield, M. P., 1999: Multiannual simulations with a three-dimensional chemical transport model. *J. Geophys. Res.*, **104, doi:10.1029/98JD02597**, 1781–1805.

Chipperfield, M. P., 2006: Inter-comparison of stratospheric tracer experiments. *Q. J. Roy. Meteorol. Soc.*, **132, doi:10.1256/qj.05.51**, 1179–1203.

Christensen, T., et al., 2005: Vortex-averaged Arctic ozone depletion in the winter 2002/2003. *Atmos. Chem. Phys.*, **5, doi:10.5194/acp-5-131-2005**, 131–138.

Chubachi, S., 1984: Preliminary result of ozone observations at Syowa station from February 1982 to January 1983. *Memoirs of National Institute of Polar Research*, **34, doi:10.1007/978-94-009-5313-0**$_5$8.

Chubachi, S., 2009: Seasonal start of the Antarctic ozone hole derived from observations with Dobson spectrophotometers. *Int. J. Remote Sens.*, **30, doi:10.1080/01431160902821957**, 3907–3916.

Claud, C., J. Ovarlez, and N. A. Scott, 1996: Assessment of TOVS-derived stratospheric temperatures up to 10 hpa for episodes of the European Arctic Stratospheric Ozone Experiment campaign. *J. Geophys. Res.*, **101, doi:10.1029/95JD01921**, 3941–3956.

Cohen, J. and J. Jones, 2011: Tropospheric precursors and stratospheric warmings. *J. Climate*, **24, doi:10.1175/2011JCLI4160.1**, 6562–6572.

Coy, L., S. Eckermann, and K. Hoppel, 2009: Planetary wave breaking and tropospheric forcing as seen in the stratospheric sudden warming of 2006. *J. Atmos. Sci.*, **66, doi:10.1175/2008JAS2784.1**, 495–507.

Coy, L., E. R. Nash, and P. A. Newman, 1997: Meteorology of the polar vortex: Spring 1997. *Geophys. Res. Lett.*, **24, doi:10.1029/97GL52832**, 2693–2696.

Crutzen, P. J., 1970: The influence of nitrogen oxides on the atmospheric ozone content. *Q. J. R. Meteorol. Soc.*, **96, doi: 10.1002/qj.49709640815**, 320–325.

Crutzen, P. J., 1971: Ozone production rates in an Oxygen-Hydrogen-Nitrogen Oxide atmosphere. *J. Geophys. Res.*, **76, doi:10.1029/JC076i030p07311**, 7311–7327.

Dameris, M., T. Peter, U. Schmidt, and R. Zellner, 2007: The ozone hole and its causes. *Chemie in unserer zeit*, **41, doi:10.1002/ciuz.200700418**, 152–168.

Davies, S., et al., 2002: Modelling the effect of denitrification on Arctic ozone depletion during winter 1999/2000. *J. Geophys. Res.*, **107, doi:10.1029/2001JD000445**.

de Laat, A. T. J. and M. van Weele, 2011: The 2010 Antarctic ozone hole: Observed reduction in ozone destruction by minor sudden stratospheric warmings. *Sci. Rep.*, **1, doi:10.1038/srep00038**.

Dee, D. P., et al., 2011: The ERA-Interim reanalysis: Configuration and performance of the data assimilation system. *Q. J. R. Meteorol. Soc.*, **137, doi:10.1002/qj.828**, 553–597.

Dobson, G. M. B., 1956: Origin and distribution of polyatomic molecules in the atmosphere. *Proc. Roy. Soc. London.*, The Royal Society, A, Mathematical and Physical Sciences, Vol. 236, 187–193.

Dobson, G. M. B., 1957: Observer's handbook for the ozone spectrophotometer. *Ann. Int. Geophys.*, **5**, 46–89.

Donner, L. J. and W. G. Large, 2008: Climate modeling. *Annu. Rev. Environ. Resour.*, **33, doi:10.1146/annurev.environ.33.020707.160752**, 1–17.

Dörnbrack, A., M. C. Pitts, L. R. Poole, Y. J. Orsolini, K. Nishii, and H. Nakamura, 2012: The 2009–2010 Arctic stratospheric winter – general evolution, mountain waves and predictability of an operational weather forecast model. *Atmos. Chem. Phys.*, **12, doi:10.5194/acp-12-3659-2012**, 3659–3675.

El Amraoui, L., V.-H. Peuch, P. Ricaud, S. Massart, N. Semane, H. Teyssèdre, D. Cariolle, and F. Karcher, 2008a: Ozone loss in the 2002–2003 Arctic vortex deduced from the assimilation of Odin/SMR O_3 and N_2O measurements: N_2O as a dynamical tracer. *Q J R Met. Soc.*, **134, doi:10.1002/qj.191**, 217–228.

El Amraoui, L., N. Semane, V.-H. Peuch, and M. L. Santee, 2008b: Investigation of dynamical processes in the polar stratospheric vortex during the unusually cold winter 2004/2005. *Geophys. Res. Lett.*, **35, doi:10.1029/2007GL031251**.

Enfield, D. B., 1989: El niño, past and present. *Rev. Geophys.*, **27, doi:10.1029/RG027i001p00159**, 159–187.

Eskes, H. J., A. R. J. van der, E. J. Brinksma, J. P. Veefkind, J. F. de Haan, and P. J. M. Valks, 2005: Retrieval and validation of ozone columns derived from measurements of SCIAMACHY on Envisat. *Atmos. Chem. Phys. Discuss.*, **5, doi:10.5194/acpd-5-4429-2005**, 4429–4475.

Eyring, V., et al., 2010: Multi-model assessment of stratospheric ozone return dates and ozone recovery in CCMVal–2 models. *Atmos. Chem. Phys.*, **10, doi:10.5194/acp-10-9451-2010**, 9451–9472.

Fahey, D. W., K. K. Kelly, S. R. Kawa, A. F. Tuck, M. Loewenstein, K. R. Chan, and L. E. Heidt, 1990: Observations of denitrification and dehydration in the winter polar stratospheres. *Nature*, **344, doi:10.1038/344321a0**, 321–324.

Farman, J. C., B. G. Gardiner, and J. D. Shanklin, 1985: Large losses of total ozone in Antarctica reveal seasonal ClO_x/NO_x interaction. *Nature*, **315, doi:10.1038/315207a0**.

Feng, W., M. P. Chipperfield, S. Davies, P. von der Gathen, E. Kyrö, C. M. Volk, A. Ulanovsky, and G. Belyaev, 2007a: Large chemical ozone loss in 2004/2005 Arctic winter/spring. *Geophys. Res. Lett.*, **34, doi:10.1029/2006GL029098**.

Feng, W., M. P. Chipperfield, M. Dorf, K. Pfeilsticker, and P. Ricaud, 2007b: Mid-latitude ozone changes: Studies with a 3-D CTM forced by ERA-40 analyses. *Atmos. Chem. Phys.*, **7, doi:10.5194/acp-7-2357-2007**, 2357–2369.

Feng, W., et al., 2005a: Three-dimensional model study of the Antarctic ozone hole in 2002 and comparison with 2000. *J. Atmos. Sci.*, **62, doi:10.1175/JAS-3335.1**, 822–837.

Feng, W., et al., 2005b: Three-dimensional model study of the Arctic ozone loss in 2002/2003 and comparison with 1999/2000 and 2003/2004. *Atmos. Chem. Phys.*, **5, doi:10.5194/acp-5-139-2005**, 139–152.

Fioletov, V. E., G. E. Bodeker, A. J. Miller, R. D. McPeters, and R. Stolarski, 2002: Global and zonal total ozone variations estimated from ground-based and satellite measurements: 1964–2000. *J. Geophys. Res.*, **17, doi:10.1029/2001JD001350**.

Fix, A., et al., 2005: (including J. Kuttippurath): SCIAMACHY validation by aircraft remote sensing: design, execution, and first measurement results of the SCIA–VALUE mission. *Atmos. Chem. Phys.*, **5, doi:10.5194/acp-5-1273-2005**, 1273–1290.

Flury, T., K. Hocke, A. Haefele, N. Kämpfer, and R. Lehmann, 2009: Ozone depletion, water vapor increase, and PSC generation at mid-latitudes by the 2008 major stratospheric warming. *J. Geophys. Res.*, **114, doi:10.1029/2009JD011940**.

Fortuin, J. P. F. and H. Kelder, 1998: An ozone climatology based on ozonesonde and satellite measurements. *J. Geophys. Res.*, **103, doi:10.1029/1998JD200008**, 31 709–31 734.

Frieler, K., et al., 2006: Toward a better quantitative understanding of polar stratospheric ozone loss. *Geophys. Res. Lett.*, **33, doi:10.1029/2005GL025466**.

Frieß, U., K. Kreher, P. V. Johnston, and U. Platt, 2005: Ground-based DOAS measurements of stratospheric trace gases at two Antarctic stations during the 2002 ozone hole period. *J. Atmos. Sci.*, **62, doi:10.1175/JAS-3319.1**, 765–777.

Froidevaux, L., et al., 2006: Early validation analyses of atmospheric profiles from EOS MLS on the Aura satellite. *IEEE Trans. Geosci. Remote Sens.*, **44, doi:10.1109/TGRS.2006.864366**, 1106–1121.

Froidevaux, L., et al., 2008: Validation of Aura Microwave Limb Sounder stratospheric ozone measurements. *J. Geophys. Res.*, **113, doi:10.1029/2007JD008771**.

Gillett, N. P., et al., 2011: Attribution of observed changes in stratospheric ozone and temperature. *Atmos. Chem. Phys.*, **11, doi:10.5194/acp-11-599-2011**, 599–609.

Goutail, F., et al., 1999: Depletion of column ozone in the Arctic during the winters 1993–94 and 1994–95. *J. Atmos. Chem.*, **32, doi:10.1023/A:1006132611358**, 1–34.

Goutail, F., et al., 2005: Early unusual ozone loss during the Arctic winter 2002/2003 compared to other winters. *Atmos. Chem. Phys.*, **5, doi:10.5194/acp-5-665-2005**, 665–677.

Goutail, F., et al., 2010: Total ozone loss during the 2009/2010 Arctic winter and comparison to previous years. *Geophys. Res. Abs.*, **12, EGU2010-3725-2**.

Gray, L. J., et al., 2010: Solar influences on climate. *Rev. Geophys.*, **48, doi:10.1029/2009RG000282**.

Grooß, J.-U., K. R. Brautzsch, Pommrich, S. Solomon, and R. Müller, 2011: Stratospheric ozone chemistry in the Antarctic: what determines the lowest ozone values reached and their recovery? *Atmos. Chem. Phys.*, **11, doi:10.5194/acp-11-12217-2011**, 12 217–12 226.

Grooß, J.-U., P. Konopka, and R. Müller, 2005a: Ozone chemistry during the 2002 Antarctic vortex split. *J. Atmos. Sci.*, **62, doi:10.1175/JAS-3330.1**, 860–870.

Grooß, J.-U. and R. Müller, 2007: Simulation of ozone loss in Arctic winter 2004/2005. *Geophys. Res. Lett.*, **34, doi:10.1029/2006GL028901**.

Grooß, J.-U., et al., 2005b: Simulation of denitrification and ozone loss for the Arctic winter 2002/2003. *Atmos. Chem. Phys.*, **5, doi:10.5194/acp-5-1437-2005**, 1437–1448.

Günther, G., R. Müller, M. von Hobe, F. Stroh, P. Konopka, and C. M. Volk, 2008: Quantification of transport across the boundary of the lower stratospheric vortex during Arctic winter 2002/2003. *Atmos. Chem. Phys.*, **8, doi:10.5194/acp-8-3655-2008**, 3655–3670.

Hanson, D. and K. Mauersberger, 1998: Laboratory studies of the nitric acid trihydrate: implications for the south polar stratosphere. *Geophys. Res. Lett.*, **15, doi:10.1029/GL015i008p00855**, 855–858.

Hanson, G. and M. Chipperfield, 1999: Ozone loss at the edge of the polar vortex. *J. Geophys. Res.*, **104, doi:10.1029/1998JD100021**, 1837–1845.

Harada, Y., A. Goto, H. Hasegawa, N. Fujikawa, H. Naoe, and T. Hirooka, 2010: A major stratospheric sudden warming event in January 2009. *J. Atmos. Sci.*, **67, doi:10.1175/2009JAS3320.1**.

Harris, J. M., S. J. Oltmans, G. E. Bodeker, R. Stolarski, R. D. Evans, and D. M. Quincy, 2003: Long-term variations in total ozone derived from Dobson and satellite data. *Atmos. Environ.*, **37, doi:10.1016/S1352-2310(03)00347-9**, 3167–3175.

Harris, N. R. P., R. Lehmann, M. Rex, and P. von der Gathen, 2010: A closer look at Arctic ozone loss and polar stratospheric clouds. *Atmos. Chem. Phys.*, **10, doi:10.5194/acp-10-8499-2010**, 8499–8510.

Harris, N. R. P., M. Rex, F. Goutail, B. M. Knudsen, G. L. Manney, R. Müller, and P. von der Gathen, 2002: Comparison of empirically derived ozone losses in the Arctic vortex. *J. Geophys. Res.*, **107, doi:10.1029/2001JD000482**.

Harvey, V. L., R. B. Pierce, and M. H. Hitchman, 2002: A climatology of stratospheric polar vortices and anticyclones. *J. Geophys. Res.*, **107, doi:10.1029/2001JD001471**.

Hassler, B., G. E. Bodeker, S. Solomon, and P. J. Young, 2011: Changes in the polar vortex: Effects on Antarctic total ozone observations at various stations. *Geophys. Res. Lett.*, **38, doi:10.1029/2010GL045542**.

Hauchecorne, A., S. Godin, M. Marchand, B. Heese, and C. Souprayen, 2002: Quantification of the transport of chemical constituents from the polar vortex to mid-latitudes in the lower stratosphere using the high-resolution advection model MIMOSA and effective diffusivity. *J. Geophys. Res.*, **107, doi:10.1029/2001JD000491**.

Haynes, P., 2005: Stratospheric dynamics. *Annu. Rev. Fluid Mech.*, **37, doi:10.1146/annurev.fluid.37.061903.175710**, 263–293.

Haynes, P. H., C. J. Marks, M. E. McIntyre, T. G. Shepherd, and K. P. Shine, 1991: On the downward control of extratropical diabatic circulations by eddy-induced mean zonal forces. *J. Atmos. Sci.*, **48, doi:10.1175/1520-0469(1991)048<0651:OTCOED>2.0.CO;2**, 651–678.

Hendrick, F., et al., 2011: NDACC/SAOZ UV-visible total ozone measurements: improved retrieval and comparison with correlative ground-based and satellite observations. *Atmos. Chem. Phys.*, **11, doi:10.5194/acp-11-5975-2011**, 5975–5995.

Hirooka, T., T. Ichimaru, and H. Mukougawa, 2007: Predictability of stratospheric sudden warmings as inferred from ensemble forecast data: Intercomparison of 2001/02 and 2003/04 winters. *J. Met. Soc. Japan*, **85, doi:10.2151/jmsj.85.919**.

Hofmann, D. J., S. J. Oltmans, J. M. Harris, B. J. Johnson, and J. A. Lathrop, 1997: Ten years of ozonesonde measurements at the south pole: Implications for recovery of springtime Antarctic ozone. *J. Geophys. Res.*, **102, doi:10.1029/96JD03749**, 8931–8943.

Hofmann, D. J., S. J. Oltmans, J. M. Harris, S. Solomon, T. Deshler, and B. J. Johnson, 1992: Observation and possible causes of new ozone depletion in Antarctica in 1991. *Nature*, **359, doi:10.1038/359283a0**, 283–287.

Hofmann, D. J., et al., 1989: Stratospheric clouds and ozone depletion in the Arctic during January 1989. *Nature*, **340, doi:10.1038/340117a0**, 117–121.

Holton, J. R., 1980: The dynamics of sudden stratospheric warmings. *Ann. Rev. Earth Planet. Sci.*, **8, doi:10.1146/annurev.ea.08.050180.001125**, 169–190.

Holton, J. R., P. H. Haynes, M. E. McIntyre, A. R. Douglass, R. B. Rood, and L. Pfister, 1995: Stratosphere-troposphere exchange. *Rev. Geophys.*, **33, doi:10.1029/95RG02097**, 403–439.

Hood, L. L. and B. E. Soukharev, 2005: Interannual variations of total ozone at northern midlatitudes correlated with stratospheric EP Flux and potential vorticity. *J. Atmos. Sci.*, **62, doi:10.1175/JAS3559.1**, 3724–3740.

Hoppel, K., R. Bevilacqua, D. Allen, G. Nedoluha, and C. Randall, 2003: POAM III observations of the anomalous 2002 Antarctic ozone hole. *Geophys. Res. Lett.*, **30, doi:10.1029/2003GL016899**.

Hoppel, K., G. Nedoluha, M. Fromm, D. Allen, R. Bevilacqua, J. Alfred, B. Johnson, and G. König-Langlo, 2005: Reduced ozone loss at the upper edge of the Antarctic ozone hole during 2001–2004. *Geophys. Res. Lett.*, **32, doi:10.1029/2005GL023968**.

Hoskins, B. J., M. E. McIntyre, and A. W. Robertson, 1985: On the use and significance of isentropic potential vorticity maps. *Quart. J. Roy. Meteor. Soc.*, **111, doi:10.1256/smsqj.47001**.

Huck, P. E., S. Tilmes, G. E. Bodeker, W. J. Randel, A. J. McDonald, and H. Nakajima, 2007: An improved measure of ozone depletion in the Antarctic stratosphere. *J. Geophys. Res.*, **112, doi:10.1029/2006JD007860**.

Huret, N., M. Pirre, A. Hauchecorne, C. Robert, and V. Catoire, 2006: On the vertical structure of the stratosphere at mid-latitude during the first stage of the polar vortex formation and in polar region in presence of a large mesospheric descent. *J. Geophys. Res.*, **111, doi:10.1029/2005JD006102**.

Hurwitz, M. M., P. A. Newman, and C. I. Garfinkel, 2011: The Arctic vortex in March 2011: a dynamical perspective. *Atmos. Chem. Phys.*, **11, doi:10.5194/acp-11-11447-2011**, 11 447–11 453.

IPCC, 2007: *Climate Change 2007: The Physical Science Basis. Contribution of working group I to the fourth assessment report of the Intergovernmental Panel on Climate Change*. Edited by S. Solomon, D. Qin, M. Manning, Z. Chen, M. Marquis, K. B. Averyt, M. Tignor and H. L. Miller, Cambridge University Press, Cambridge, United Kingdom and New York, NY, USA, 996 pp.

Jackson, D. R. and Y. J. Orsolini, 2008: Estimation of Arctic ozone loss in winter 2004/2005 based on assimilation of EOS MLS and SBUV/2 observations. *Q. J. Roy. Meteorol. Soc.*, **134, doi:10.1002/qj.316**, 1833–1841.

Jacobson, M. Z., 2005: *Fundamentals of Atmospheric Modeling*. Cambridge University Press, ISBN:978-0-521-83970-9, 813 pp.

Jiang, Y., Y. L. Yung, and R. W. Zurek, 1996: Decadal evolution of the Antarctic ozone hole. *J. Geophys. Res.*, **101, doi:10.1029/96JD00063**, 8985–8999.

Jin, J. J., et al., 2006: Severe Arctic ozone loss in the winter 2004/2005: Observations from ACE-FTS. *Geophys. Res. Lett.*, **33, doi:10.1029/2006GL026752**.

Jones, A., J. Urban, D. P. Murtagh, C. Sanchez, K. A. Walker, N. J. Livesey, L. Froidevaux, and M. L. Santee, 2011: Analysis of HCl and ClO time series in the upper stratosphere using satellite data sets. *Atmos. Chem. Phys.*, **11, doi:10.5194/acp-11-5321-2011**, 5321–5333.

Jonsson, A. I., V. I. Fomichev, and T. G. Shepherd, 2009: The effect of nonlinearity in CO_2 heating rates on the attribution of stratospheric ozone and temperature changes. *Atmos. Chem. Phys.*, **9, doi:10.5194/acp-9-8447-2009**, 8447–8452.

Kane, R. P., 1991: Extension of Antarctic ozone hole to lower latitudes in the South American region. *Pure Appl. Geophys.*, **135, doi:10.1007/BF01772410**, 611–624.

Kane, R. P., 2008: Is ozone depletion really recovering? *J. Atmos. Solar Terr. Phys.*, **70**, 1455–1459.

Kasahara, A., 1974: Various vertical coordinate systems used for numerical weather prediction. *Mon. Weather Rev.*, **102, doi:10.1175/1520-0493(1974)102<0509:VVCSUF>2.0.CO;2**, 509–522.

Khosrawi, F., et al., 2011: Denitrification and polar stratospheric cloud formation during the Arctic winter 2009/2010. *Atmos. Chem. Phys.*, **11, doi:10.5194/acp-11-8471-2011**, 8471–8487.

Kiesewetter, G., B.-M. Sinnhuber, M. Weber, and J. P. Burrows, 2010: Attribution of stratospheric ozone trends to chemistry and transport: a modelling study. *Atmos. Chem. Phys.*, **10, doi:10.5194/acp-10-12073-2010**, 12 073–12 089.

Kleinböhl, A., J. Kuttippurath, M. Sinnhuber, B.-M. Sinnhuber, H. Küllmann, K. Künzi, and J. Notholt, 2005a: Rapid meridional transport of tropical air masses to the Arctic during the major stratospheric warming in January 2003. *Atmos. Chem. Phys.*, **5, doi:10.5194/acp-5-1291-2005**, 1291–1299.

Kleinböhl, A., et al., 2002: Vortexwide denitrification of the Arctic polar stratosphere in winter 1999/2000 determined by remote observations. *J. Geophys. Res.*, **107, doi:10.1029/2001JD001042**.

Kleinböhl, A., et al., 2005b: (including J. Kuttippurath): Denitrification in the Arctic mid-winter 2004/2005 observed by airborne submillimeter radiometry. *Geophys. Res. Lett.*, **32, doi:10.1029/2005GL023408**.

Knudsen, B. M., et al., 1998: Ozone depletion in and below the Arctic vortex for 1997. *Geophys. Res. Lett.*, **25, doi:10.1029/98GL00300**, 627–630.

Kolstad, E. W. and A. J. Charlton-Perez, 2011: Observed and simulated precursors of stratospheric polar vortex anomalies in the Northern Hemisphere. *Clim. Dyn.*, **37, doi:10.1007/s00382-010-0919-7**, 1443–1456.

Kondo, Y., H. Irie, M. Koike, and G. E. Bodeker, 2000: Denitrification and nitrification in the Arctic stratosphere during the winter of 1996–1997. *Geophys. Res. Lett.*, **27, doi:10.1029/1999GL011081**, 337–340.

Konopka, P., et al., 2007: Ozone loss driven by nitrogen oxides and triggered by stratospheric warmings can outweigh the effect of halogens. *J. Geophys. Res.*, **112, doi:10.1029/2006JD007064**.

Kroon, M., J. P. Veefkind, M. Sneep, R. D. McPeters, P. K. Bhartia, and P. F. Levelt, 2008: Comparing OMI–TOMS and OMI–DOAS total ozone column data. *J. Geophys. Res.*, **113, doi:10.1029/2007JD008798**.

Krüger, K., B. Naujokat, and K. Labitzke, 2005: The unusual midwinter warming in the southern hemisphere stratosphere 2002: a comparison to northern hemisphere phenomena. *J. Atmos. Sci.*, **62, doi:10.1175/JAS-3316.1**, 603–613.

Kuttippurath, J., 2005: *Study of Stratospheric Composition using Airborne Submillimeter Radiometry and a Chemical Transport Model*. Logos Verlag Berlin, ISBN:3832510699, 164 pp.

Kuttippurath, J., S. Godin-Beekmann, F. Lefèvre, and F. Goutail, 2010a: Spatial, temporal, and vertical variability of polar stratospheric ozone loss in the Arctic winters 2004/2005–2009/2010. *Atmos. Chem. Phys.*, **10, doi:10.5194/acp-10-9915-2010**, 9915–9930.

Kuttippurath, J., S. Godin-Beekmann, F. Lefèvre, G. Nikulin, M. L. Santee, and L. Froidevaux, 2012a: Record-breaking ozone loss in the Arctic winter 2010/2011: comparison with 1996/1997. *Atmos. Chem. Phys.*, **12, doi:10.5194/acp-12-7073-2012**, 7073–7085.

Kuttippurath, J., S. Godin-Beekmann, F. Lefèvre, and A. Pazmino, 2009: Ozone depletion in the Arctic winter 2007/08. *Int. J. Remote sens.*, **30, doi:10.1080/01431160902821965**, 4071–4082.

Kuttippurath, J., A. Kleinböhl, H. Bremer, H. Küllmann, J. Notholt, B.-M. Sinnhuber, W. Feng, and M. Chipperfield, 2010: Aircraft measurements and model simulations of stratospheric ozone and N_2O: Implications for chemistry and transport processes in the models. *J. Atmos. Chem.*, **66, doi:10.1007/s10874-011-9191-4**.

Kuttippurath, J., F. Lefèvre, J.-P. Pommereau, H. K. Roscoe, F. Goutail, A. Pazmino, and J. D. Shanklin, 2013: Antarctic ozone loss in 1979–2010: First sign of ozone recovery. *Atmos. Chem. Phys.*, **13, doi:10.5194/acp-13-1625-2013**, 1625–1635.

Kuttippurath, J. and G. Nikulin, 2012: A comparative study of the major sudden stratospheric warmings in the Arctic winters 2003/2004–2009/2010. *Atmos. Chem. Phys.*, **12, doi:10.5194/acp-12-8115-2012**, 8115–8129.

Kuttippurath, J., et al., 2007: Intercomparison of ozone profile measurements from ASUR, SCIAMACHY, MIPAS, OSIRIS and SMR. *J. Geophys. Res.*, **112, doi:10.1029/2006JD007830**.

Kuttippurath, J., et al., 2010b: Estimation of Antarctic ozone loss from ground-based total column measurements. *Atmos. Chem. Phys.*, **10, doi:10.5194/acp-10-6569-2010**, 6569–6581.

Kuttippurath, J., et al., 2011: Arctic ozone depletion in 2002–2003 measured by ASUR and comparison with POAM observations. *J. Geophys. Res.*, **116, doi:10.1029/2011JD016020**.

Labitzke, K., 1981: Stratospheric-mesospheric midwinter disturbances: A summary of observed characteristics. *J. Geophys. Res.*, **86, doi:10.1029/JC086iC10p09665**.

Labitzke, K. and M. Kunze, 2009: On the remarkable Arctic winter in 2008/2009. *J. Geophys. Res.*, **114, doi:10.1029/2009JD012273**.

Labitzke, K. and B. Naujokat, 2000: The lower Arctic stratosphere in winter since 1952. *SPARC Newsletter*, **15**, 11–14.

Lee, A. M., H. K. Roscoe, and S. Oltmans, 2000: Model and measurements show Antarctic ozone loss follows edge of polar night. *Geophys. Res. Lett.*, **112, doi:10.1029/2000GL01144**, 3845–3848.

Lefèvre, F., G. P. Brasseur, I. Folkins, A. K. Smith, and P. Simon, 1994: Chemistry of the 1991/1992 stratospheric winter: three dimensional model simulation. *J. Geophys. Res.*, **99, doi:10.1029/93JD03476**, 8183–8195.

Lefèvre, F., F. Figarol, K. S. Carslaw, and T. Peter, 1998: The 1997 Arctic ozone depletion quantified from three-dimensional model simulations. *Geophys. Res. Lett.*, **25, doi:10.1029/98GL51812**, 2425–2428.

Lemmen, C., M. Dameris, R. Müller, and M. Riese, 2006: Chemical ozone loss in a chemistry-climate model from 1960 to 1999. *Geophys. Res. Lett.*, **33, doi:10.1029/2006GL026939**.

Levelt, P. F., et al., 2006: The Ozone Monitoring Instrument. *IEEE Trans. Geosci. Remote Sens.*, **44, doi:10.1109/TGRS.2006.872333**, 1093–1101.

Limpasuvan, V., D. W. J. Thompson, and D. L. Hartmann, 2004: The life cycle of the northern hemisphere sudden stratospheric warmings. *J. Climate*, **17, doi:10.1175/1520-0442(2004)017<2584:TLCOTN>2.0.CO;2**.

Liu, Y., C. X. Liu, H. P. Wang, X. X. Tie, S. T. Gao, D. Kinnison, and G. Brasseur, 2009: Atmospheric tracers during the 2003–2004 stratospheric warming event and impact of ozone intrusions in the troposphere. *Atmos. Chem. Phys.*, **9, doi:10.5194/acp-9-2157-2009**, 2157–2170.

Livesey, N. J., et al., 2003: The UARS Microwave Limb Sounder version 5 data set: theory, characterization, and validation. *J. Geophys. Res.*, **108, doi:10.1029/2002JD002273**.

Livesey, N. J., et al., 2011: Earth Observing System (EOS) Aura Microwave Limb Sounder (MLS) version 3.3 level 2 data quality and description document. *PL D-33509, Jet Propulsion Laboratory California Institute of Technology, Pasadena, California*, 91 109–8099.

Lott, F., J. Kuttippurath, and F. Vial, 2009: A climatology of the gravest waves in the equatorial lower and middle stratosphere: Method and results for the ERA-40 re-analysis and the LMDz GCM. *J. Atmos. Sci.*, **66, doi:10.1175/2008JAS2880.1**, 1327–1346.

Luo, B., K. S. Carslaw, T. Peter, and S. L. Clegg, 1995: Vapour pressures of $H_2SO_4/HNO_3/HCl/HBr/H_2O$ solutions to low stratospheric temperatures. *Geophys. Res. Lett.*, **22, doi:10.1029/94GL02988**, 247–250.

MacKenzie, I., R. Harwood, L. Froidevaux, W. Read, and J. Waters, 1996: Chemical loss of polar vortex ozone inferred from UARS MLS measurements of ClO during the Arctic and Antarctic late winters of 1993. *J. Geophys. Res.*, **101, doi:10.1029/JD101iD09p14505**, 14 505–14 518.

Mahfouf, J. F., D. Cariolle, J. F. Royer, J. F. Geleyn, and B. Timbal, 1994: Response of the Météo-France climate model to changes in CO_2 and sea surface temperature. *Clim. Dyn.*, **9, doi:10.1007/BF00223447**, 345–362.

Manney, G., L. Froidevaux, M. L. Santee, N. Livesey, J. Sabutis, and J. Waters, 2003: Variability of ozone loss during Arctic winter (1991–2000) estimated from UARS Microwave Limb Sounder measurements. *J. Geophys. Res.*, **108, doi:10.1029/2002JD002634**.

Manney, G. L., L. Froidevaux, M. L. Santee, R. Zurek, and J. W. Waters, 1997: MLS observations of Arctic ozone loss in 1996–97. *Geophys. Res. Lett.*, **24, doi:10.1029/97GL52827**, 2697–2700.

Manney, G. L., K. Krüger, J. L. Sabutis, S. A. Sena, and S. Pawson, 2005: The remarkable 2003–2004 winter and other recent warm winters in the Arctic stratosphere since the late 1990s. *J. Geophys. Res.*, **34, doi:10.1029/2004JD005367**.

Manney, G. L., N. J. Livesey, C. J. Jimenez, H. C. Pumphrey, M. L. Santee, I. A. MacKenzie, and J. W. Waters, 2006: EOS MLS observations of ozone loss in the 2004–2005 Arctic winter. *Geophys. Res. Lett.*, **33, doi:10.1029/2005GL024494**.

Manney, G. L., R. W. Zurek, L. Froidevaux, and J. W. Waters, 1995: Evidence for Arctic ozone depletion in late February and early March 1994. *Geophys. Res. Lett.*, **22, doi:10.1029/95GL02229**, 2941–2944.

Manney, G. L., et al., 2007: Solar occultation satellite data and derived meteorological products: sampling issues and comparisons with Aura MLS. *J. Geophys. Res.*, **112, doi:10.1029/2007JD008709**.

Manney, G. L., et al., 2008: The evolution of the stratopause during the 2006 major warming: Satellite data and assimilated meteorological analyses. *J. Geophys. Res.*, **113, doi:10.1029/2007JD009097**.

Manney, G. L., et al., 2009: Aura Microwave Limb Sounder observations of dynamics and transport during the record-breaking 2009 Arctic stratospheric major warming. *Geophys. Res. Lett.*, **36, doi:10.1029/2009GL038586**.

Manney, G. L., et al., 2011: Unprecedented Arctic ozone loss in 2011. *Nature*, **478, doi:10.1038/nature10556**, 469–475.

Martius, O., L. M. Polvani, and H. C. Davies, 2009: Blocking precursors to stratospheric sudden warming events. *Geophys. Res. Lett.*, **36, doi:10.1029/2009GL038776**.

Matsuno, T., 1971: Circulation and waves in the middle atmosphere in winter. *Space Sci. Rev.*, **34, doi:10.1007/978-94-009-7096-0**$_3$0.

McConnell, J. C. and J. J. Jin, 2008: Stratospheric ozone chemistry. *Atmos. Ocean*, **46, doi:10.3137/ao.460104**, 69–92.

McCormick, M. P., H. M. Steele, P. Hamill, W. P. Chu, and T. J. Swissler, 1982: Polar Stratospheric Clouds sightings by SAM II. *J. Atmos. Sci.*, **39, doi:10.1175/1520-0469(1982)039<1387:PSCSBS>2.0.CO;2**, 1387–1397.

McElroy, M. B. and R. J. Salawitch, 1989: Changing composition of the global stratosphere. *Science*, **243, doi:10.1126/science.243.4892.763**, 763–770.

McElroy, M. B., R. J. Salawitch, S. C. Wofsy, and J. A. Logan, 1986: Reductions of Antarctic ozone due to synergistic interactions of chlorine and bromine. *Nature*, **321, doi:10.1038/321759a0**, 759–762.

McInturff, R. M., 1978: Stratospheric warmings: Synoptic, dynamic and general-circulation aspects. *NASA*, **Ref. Publ.**, 50.

Mitchell, D. M., S. M. Osprey, L. J. Gray, N. Butchart, S. C. Hardiman, A. J. Charlton-Perez, and P. Watson, 2012: The effect of climate change on the variability of the northern hemisphere stratospheric polar vortex. *J. Atmos. Sci.*, **69, doi:10.1175/JAS-D-12-021.1**, 2608–2618.

Mohankumar, K., 2008: *Stratosphere-Troposphere Interactions: An Introduction*. Springer Science Netherlands, ISBN:978-1-4020-8216-0, 416 pp., doi:10.1007/978-1-4020-8217-7.

Molina, L. T. and M. J. Molina, 1987: Production of chlorine oxide (Cl_2O_2) from the self-reaction of the chlorine oxide (ClO) radical. *J. Phys. Chem.*, **91, doi:10.1021/j100286a035**, 433–436.

Molina, M. J. and F. S. Rowland, 1974: Stratospheric sink for chlorofluoromethanes, chlorine atom catalysed destruction of ozone. *Nature*, **249, doi:10.1038/249810a0**, 810–812.

Montzka, S. A., J. H. Butler, J. Elkins, T. M. Thompson, A. D. Clarke, and L. T. Lock, 1999: Present and future trends in the atmospheric burden of ozone-depleting halogens. *Nature*, **398, doi:10.1038/19499**, 690–694.

Müller, R., 2009: A brief history of stratospheric ozone research. *Meteorol. Z.*, **18, doi:10.1127/0941-2948/2009/353**, 3–24.

Müller, R., 2011: *Stratospheric Ozone Depletion and Climate Change*. Royal Society of Chemistry, ISBN:978-1-84973-318-2, 346 pp., doi:10.1039/9781849733182.

Müller, R., P. J. Crutzen, J.-U. Grooß, C. Bürhl, J. M. Russell-III, H. Gernandt, D. S. McKenna, and A. F. Tuck, 1997: Severe chemical ozone loss in the Arctic during the winter of 1995–96. *Nature*, **389, doi:10.1038/39564**, 709–712.

Müller, R., J.-U. Grooß, C. Lemmen, D. Heinze, M. Dameris, and G. Bodeker, 2008: Simple measures of ozone depletion in the polar stratosphere. *Atmos. Chem. Phys.*, **8, doi:10.5194/acp-8-251-2008**, 251–264.

Müller, R., et al., 2007: Impact of mesospheric intrusions on ozone–tracer relations in the stratospheric polar vortex. *J. Geophys. Res.*, **112, doi:10.1029/2006JD008315**.

Murray, F. W., 1967: On the computation of saturation vapour pressure,. *J. Appl. Meterol.*, **6, doi:10.1175/1520-0450(1967)006<0203:OTCOSV>2.0.CO;2**, 203–204.

Nair, P. J., S. Godin-Beekmann, A. Pazmino, A. Hauchecorne, G. Ancellet, I. Petropavlovskikh, L. E. Flynn, and L. Froidevaux, 2011: Coherence of long-term stratospheric ozone vertical distribution time series used for the study of ozone recovery at a northern mid-latitude station. *Atmos. Chem. Phys.*, **11, doi:10.5194/acp-11-4957-2011**, 4957–4975.

Nair, P. J., et al., 2012: Relative drifts and stability of satellite and ground-based stratospheric ozone profiles at NDACC lidar stations. *Atmos. Meas. Tech.*, **5, doi:10.5194/amt-5-1301-2012**, 1301–1318.

Nair, P. J., et al., 2013: Ozone trends derived from the total column and vertical profiles at a northern mid-latitude station. *Atmos. Chem. Phys.*, **13, doi:10.5194/acp-13-1-2013**, 10 373–10 384.

Nash, E. R., P. A. Newman, J. E. Rosenfield, and M. R. Schoeberl, 1996: An objective determination of the polar vortex using Ertel's potential vorticity. *J. Geophys. Res.*, **101, doi:10.1029/96JD00066**, 9471–9478.

Naujokat, B., K. Krüger, K. Matthes, J. Hoffmann, M. Kunze, and K. Labitzke, 2002: The early major warming in December 2001–exceptional? *Geophys. Res. Lett.*, **294, doi:10.1029/2002GL015316**.

Negro, L. A. D., et al., 1997: Evaluating the role of NAT, NAD, and liquid $H_2SO_4/H_2O/HNO_3$ solutions in Antarctic polar stratospheric cloud aerosol: Observations and implications. *J. Geophys. Res.*, **102, doi:10.1029/97JD00764**, 13 255–13 282.

Newman, P., J. S. Daniel, D. Waugh, and E. R. Nash, 2007: A new formulation of equivalent effective stratospheric chlorine (EESC). *Atmos. Chem. Phys.*, **7, doi:10.5194/acp-7-4537-2007**.

Newman, P., E. Nash, and J. Rosenfield, 2001: The cold winters of the middle 1990s in the northern lower stratosphere. *Geophys. Res. Lett.*, **104, doi:10.1029/1999JD900211**, 19 999–20 010.

Newman, P. A., et al., 2002: An overview of the SOLVE/THESEO 2000 campaign. *J. Geophys. Res.*, **107, doi:10.1029/2001JD001303**.

Nickolaisen, S. L., R. R. Friedl, and S. P. Sander, 2006: Kinetics and mechanism of the ClO+ClO reaction - pressure and temperature dependences of the bimolecular and termolecular channels and thermal-decomposition of chlorine peroxide. *J. Phys. Chem.*, **98, doi:10.1021/j100052a027**, 155–169.

Orsolini, Y. J., J. Urban, D. P. Murtagh, S. Lossow, and V. Limpasuvan, 2010: Descent from the polar mesosphere and anomalously high stratopause observed in 8 years of water vapor and temperature satellite observations by the Odin Sub-Millimeter Radiometer. *J. Geophys. Res.*, **115, doi:10.1029/2009JD013501**.

Papanastasiou, D. K., V. C. Papadimitriou, D. W. Fahey, and J. B. Burkholder, 2009: UV Absorption spectrum of the ClO dimer (Cl_2O_2) between 200 and 420 nm. *J. Phys. Chem. A*, **113, doi:10.1021/jp9065345**, 13 711–13 726.

Pawson, S. and B. Naujokat, 1999: The cold winters of the middle 1990s in the northern lower stratosphere. *J. Geophys. Res.*, **104, doi:10.1029/1999JD900211**.

Peter, T., 1997: Microphysics and heterogeneous chemistry of Polar Stratospheric Clouds. *Ann. Rev. Phys. Chem.*, **39, doi:10.1146/annurev.physchem.48.1.785**, 785–822.

Pitts, M. C., L. R. Poole, and L. W. Thomason, 2009: CALIPSO polar stratospheric cloud observations: second-generation detection algorithm and composition discrimination. *Atmos. Chem. Phys.*, **9, doi:10.5194/acp-9-7577-2009**, 7577–7589.

Pitts, M. C., L. W. Thomason, L. R. Poole, and D. M. Winker, 2007: Characterization of polar stratospheric clouds with spaceborne lidar: CALIPSO and the 2006 Antarctic season. *Atmos. Chem. Phys.*, **7, doi:10.5194/acp-7-5207-2007**, 5207–5228.

Plumb, R. A., 1996: A tropical pipe model of stratospheric transport. *J. Geophys. Res.*, **101, doi:10.1029/95JD03002**, 3957–3972.

Plumb, R. A., 2002: Stratospheric transport. *J. Meteor. Soc. Japan*, **80**, 793–809.

Plummer, D. A., J. F. Scinocca, T. G. Shepherd, M. C. Reader, and A. I. Jonsson, 2010: Quantifying the contributions to stratospheric ozone changes from ozone depleting substances and greenhouse gases. *Atmos. Chem. Phys.*, **10, doi:10.5194/acp-10-8803-2010**, 8803–8820.

Polvani, L. M. and D. W. Waugh, 2004: Upward wave activity flux as precursor to extreme stratospheric events and subsequent anomalous surface weather regimes. *J. Climate*, **17, doi:10.1175/1520-0442(2004)017<3548:UWAFAA>2.0.CO;2**, 3548–3554.

Pommereau, J.-P. and F. Goutail, 1988: Stratospheric O_3 and NO_2 Observations at the Southern polar circle in summer and fall 1988. *Geophys. Res. Lett.*, **15, doi:10.1029/GL015i008p00895**, 891–894.

Portmann, R., S. Solomon, R. Garcia, L. Thomason, L. Poole, and M. McCormick, 1996: Role of aerosol variations in anthropogenic ozone depletion in the polar regions. *J. Geophys. Res.*, **101, doi:10.1029/96JD02608**, 22 991–23 006.

Prather, M. J., 1986: Numerical advection by conservation of second-order moments. *J. Geophys. Res.*, **91, doi:10.1029/JD091iD06p06671**, 6671–6681.

Pruppacher, H. R. and J. D. Klett, 1997: *Microstructure of atmospheric clouds and precipitations.* 2^{nd} ed. Kluwer Academic Publishers, Mainz, ISBN:978-0-7923-4211-3, 10–73 pp., doi:10.1007/978-0-306-48100-0_2.

Raffalski, U., G. Hochschild, G. Kopp, and J. Urban, 2005: Evolution of stratospheric ozone during winter 2002/2003 as observed by a ground-based millimetre wave radiometer at Kiruna, Sweden. *Atmos. Chem. Phys.*, **5, doi:10.5194/acp-5-1399-2005**, 1399–1407.

Randall, C. E., V. L. Harvey, D. E. S. J. France, P. F. Bernath, C. D. Boone, and K. A. Walker, 2009: NO_x descent in the Arctic middle atmosphere in early 2009. *Geophys. Res. Lett.*, **36, doi:10.1029/2009GL039706**.

Randall, C. E., D. Rusch, R. Bevilacqua, K. W. Hoppel, and J. D. Lumpe, 2003: Validation of POAM-3 O_3: Comparison to ozonesonde and satellite data. *J. Geophys. Res.*, **108, doi:10.1029/2002JD002**.

Randel, W. J., J. C. Gille, A. E. Roche, J. B. Kumer, J. L. Mergenthaler, J. W. Waters, E. F. Fishbein, and W. A. Lahoz, 1993: Stratospheric transport from tropics to middle latitudes by planetary wave mixing. *Nature*, **365, doi:10.1038/365533a0**, 533–535.

Randel, W. J., F. Wu, and R. Stolarski, 2002: Changes in column ozone correlated with the stratospheric EP Flux. *J. Meteorol. Soc. Japan*, **80, doi:10.2151/jmsj.80.849**, 849–862.

Reed, R. G., W. J. Campbell, L. A. Rasmussen, and D. G.Rogers, 1961: Evidence of downward-propagating annual wind reversal in the equatorial stratosphere. *J. Geophys. Res.*, **66, doi:10.1029/JZ066i003p00813**, 813–818.

Rex, M., R. J. Salawitch, P. von der Gathen, N. R. P. Harris, M. P. Chipperfield, and B. Naujoka, 2004: Arctic ozone loss and climate change. *Geophys. Res. Lett.*, **31, doi:10.1029/2003GL018844**.

Rex, M., et al., 2002: Chemical depletion of Arctic ozone in winter 1999/2000. *J. Geophys. Res.*, **107, doi:10.1029/2001JD000533**.

Rex, M., et al., 2006: Arctic winter 2005: Implications for stratospheric ozone loss and climate change. *Geophys. Res. Lett.*, **33, doi:10.1029/2006GL026731**.

Rodgers, C. D., 1976: Retrieval of atmospheric temperature and composition from remote measurements of thermal radiation. *Rev. Geophys.*, **14, doi:10.1029/RG014i004p00609**, 609–624.

Roscoe, H. K., W. Feng, M. P. Chipperfield, M. Trainic, and E. F. Shuckburgh, 2012: The existence of the edge region of the Antarctic stratospheric vortex. *J. Geophys. Res.*, **117, doi:10.1029/2011JD015940**.

Roscoe, H. K. and J. D. Haigh, 2007: Influences of ozone depletion, the solar cycle and the QBO on the Southern Annular Mode. *Quart. J. Roy. Met. Soc.*, **133, doi:10.1002/qj.153**, 1855–1864.

Roscoe, H. K., P. V. Johnston, M. V. Roozendael, A. Richter, A. Sarkissian, F. Goutail, J.-P. Pommereau, and et al., 1999: Slant column measurements of O_3 and NO_2 during the NDSC Intercomparison of zenith-sky UV-visible spectrometers in June 1996. *J. Atmos. Chem.*, **32, doi:10.1023/A:1006111216966**, 281–314.

Roscoe, H. K., J. D. Shanklin, and S. R. Colwell, 2006: Has the Antarctic vortex ever split before 2002? *J. Atmos. Sci.*, **62, doi:10.1175/JAS-3331.1**, 581–588.

Rösevall, J., D. P. Murtagh, and J. Urban, 2007: Ozone depletion in the 2006/2007 Arctic winter. *Geophys. Res. Lett.*, **34, doi:10.1029/2007GL030620**.

Rösevall, J., D. P. Murtagh, J. Urban, W. Feng, P. Eriksson, and S. Brohede, 2008: A study of ozone depletion in the 2004/2005 Arctic winter based on data from Odin/SMR and Aura/MLS. *J. Geophys. Res.*, **113, doi:10.1029/2007JD009560**.

Ryskin, V. G. and Y. Y. Kulikov, 2008: Evaluation of chemical ozone loss in the stratosphere over the Kola Peninsula in the 2002/2003 winter from microwave sounding data. *Izvestiya, Atmospheric and Oceanic Physics*, **44, doi:10.1134/S0001433808020060**, 199–205.

Salby, M. L., 2011: Interannual changes of stratospheric temperature and ozone: Forcing by anomalous wave driving and the QBO. *J. Atmos. Sci.*, **68, doi:10.1175/2011JAS3671.1**.

Salby, M. L. and P. F. Callaghan, 2002: Interannual changes of the stratospheric circulation: relationship to ozone and tropospheric structure. *J. Climate*, **15, doi:10.1175/1520-0442(2003)015<3673:ICOTSC>2.0.CO;2**, 3673–3685.

Salby, M. L., E. Titova, and L. Deschamps, 2011: Rebound of Antarctic ozone. *Geophys. Res. Lett.*, **38, doi:10.1029/2011GL047266**.

Sander, S., et al., 2006: Chemical kinetics and photochemical data for use in atmospheric studies. *Jet Propul. Lab, California, Eval. 15, JPL Publ.*

Sander, S. P., et al., 2003: Chemical kinetics and photochemical data for use in stratospheric modeling. *Jet Propul. Lab, California, Eval. 13, JPL Publ.*

Santee, M. L., G. L. Manney, L. Froidevaux, W. G. Read, and J. W. Waters, 1999: Six years of UARS Microwave Limb Sounder HNO_3 observations: Seasonal, interhemispheric, and interannual variations in the lower stratosphere. *Geophys. Res.*, **104, doi:10.1029/1998JD100089**, 8225–8246.

Santee, M. L., G. L. Manney, L. Froidevaux, R. W. Zurek, and J. W. Waters, 1997: MLS observations of ClO and HNO_3 in the 1996–97 Arctic polar vortex. *Geophys. Res. Lett.*, **24, doi:10.1029/97GL52830**, 2713–2716.

Santee, M. L., G. L. Manney, N. J. Livesey, L. Froidevaux, M. J. Schwartz, and W. G. Read, 2011: Trace gas evolution in the lowermost stratosphere from Aura Microwave Limb Sounder measurements. *J. Geophys. Res.*, **116, doi:10.1029/2011JD015590**.

Santee, M. L., G. L. Manney, N. J. Livesey, and J. W. Waters, 2000: UARS Microwave Limb Sounder observations of denitrification and ozone loss in the 2000 Arctic late winter. *Geophys. Res. Lett.*, **27, doi:10.1029/2000GL011738**, 3213–3216.

Santee, M. L., et al., 1995: Inter-hemispheric differences in polar stratospheric HNO_3, H_2O, ClO, and O_3. *Science*, **267, doi:10.1126/science.267.5199.849**, 849–852.

Santee, M. L., et al., 2004: Polar processing and development of the 2004 Antarctic ozone hole: First results from MLS on Aura. *Geophys. Res. Lett.*, **32, doi:10.1029/2005GL022582**.

Santee, M. L., et al., 2008: (including J. Kuttippurath): Validation of the Aura Microwave Limb Sounder ClO measurements. *J. Geophys. Res.*, **113, doi:10.1029/2007JD008762**.

Scarnato, B., J. Staehelin, R. Stüi, and H. Schill, 2010: Long-term total ozone observations at Arosa (Switzerland) with Dobson and Brewer instruments (1988–2007). *J. Geophys. Res.*, **115, doi:10.1029/2009JD011908**.

Scherhag, R., 1952: Die explosionsartige Stratosphärenerwarmug des Spätwinters 1951/52. *Ber. Deut. Wetterdieustes*, **6**, 51–63.

Schneider, T., 2006: The general circulation of the atmosphere. *Ann. Rev. Earth Planet. Sci.*, **34, doi:10.1146/annurev.earth.34.031405.125144**, 655–688.

Schoeberl, M. R., 1978: Stratospheric warmings: observations and theory. *Rev. Geophys.*, **16, doi:10.1029/RG016i004p00521**.

Sexton, D. M. H., 2001: The effect of stratospheric ozone depletion on the phase of the Antarctic Oscillation. *Geophys. Res. Lett.*, **28, doi:10.1029/2001GL013376**, 3697–3700.

Shepherd, T. G., 2008: Dynamics, stratospheric ozone, and climate change. *Atmos.-Ocean*, **46, doi:10.3137/ao.460106**, 117–138.

Shibata, T., K. Sato, H. Kobayashi, M. Yabuki, and M. Shiobara, 2003: Antarctic polar stratospheric clouds under temperature perturbation by nonorographic inertia gravity waves observed by micropulse lidar at Syowa station. *J. Geophys. Res.*, **108, doi:10.1029/2002JD002713**.

Shine, K. P., 1987: The middle atmosphere in the absence of dynamical heat fluxes. *Q. J. Roy. Meteorol. Soc.*, **113, doi:10.1002/qj.49711347610**, 603–633.

Singleton, C. S., et al., 2005: 2002–2003 Arctic ozone loss deduced from POAM III satellite observations and SLIMCAT chemical transport model. *Atmos. Chem. Phys.*, **5, doi:10.5194/acp-5-597-2005**, 597–609.

Singleton, C. S., et al., 2007: Quantifying Arctic ozone loss during the 2004–2005 winter using satellite observations and a chemical transport model. *J. Geophys. Res.*, **112, doi:10.1029/2006JD007463**.

Sinnhuber, B.-M., G. P. Stiller, R. Ruhnke, T. von Clarmann, S. Küllmann, and J. Aschmann, 2011: Arctic winter 2010/2011 at the brink of an ozone hole. *Geophys. Res. Lett.*, **38, doi:10.1029/2011GL049784**.

Siskind, D. E., S. D. Eckermann, J. P. McCormack, L. Coy, K. W. Hoppel, and N. L. Baker, 2010: Case studies of the mesospheric response to recent minor, major and extended stratospheric warmings. *J. Geophys. Res.*, **115, doi:10.1029/2010JD014114**.

Solomon, S., 1999: Stratospheric ozone depletion: A review of concepts and history. *Rev. Geophys.*, **37, doi:10.1029/1999RG900008**, 275–316.

Solomon, S., P. J. Crutzen, and R. G. Roble, 1982: Photochemical coupling between the thermosphere and the lower atmosphere. *J. Geophys. Res.*, **87, doi:10.1029/JC087iC09p07206**, 7206–7220.

Solomon, S., R. R. Garcia, F. S. Rowland, and D. J. Wuebbles, 1986: On the depletion of Antarctic ozone. *Nature*, **321, doi:10.1038/321755a0**.

Solomon, S., R. W. Portmann, T. Sasaki, D. J. Hofmann, and D. W. J. Thompson, 2005: Four decades of ozonesonde measurements over Antarctica. *J. Geophys. Res.*, **110, doi:10.1029/2005JD005917**.

Solomon, S., R. W. Portmann, and D. W. J. Thompson, 2007: Contrasts between Antarctic and Arctic ozone depletion. *PNAS*, **104, doi:10.1073/pnas.0604895104**, 445–449.

Sonkaew, T., C. von Savigny, K.-U. Eichmann, M. Weber, A. Rozanov, H. Bovensmann, J. P. Burrows, and J.-U. Grooß, 2013: Chemical ozone loss in Arctic and Antarctic polar winter/spring season derived from SCIAMACHY limb measurements 2002–2009. *Atmos. Chem. Phys.*, **13, doi:10.5194/acp-13-1809-2013**, 1809–1835.

Soukharev, B. E. and L. L. Hood, 2006: Solar cycle variation of stratospheric ozone: Multiple regression analysis of long-term satellite data sets and comparisons with models. *J. Geophys. Res.*, **111, doi:10.1029/2006JD007107**.

SPARC, 2002: Stratospheric processes and their role in climate: SPARC Intercomparison of middle atmosphere climatologies, SPARC Report 3, Randel, W., Chanin, M.-L., and Michaut, C. (eds.), WMO/TD–No.1142.

SPARC, 2010: SPARC CCMVal – SPARC Report on the Evaluation of Chemistry-Climate Models, V. Eyring, T. G. Shepherd, D. W. Waugh (eds.), SPARC Report No. 5, WCRP-132, WMO/TD-No. 1526.

Steinbrecht, W., H. Claude, and P. Winkler, 2004: Enhanced upper stratospheric ozone: Sign of recovery or solar cycle effect? *J. Geophys. Res.*, **109, doi:10.1029/2003JD004284**.

Stimpfle, R. M., D. M. Wilmouth, R. J. Salawitch, and J. G. Anderson, 2004: First measurements of ClOOCl in the stratosphere: the coupling of ClOOCl and ClO in the Arctic polar vortex. *J. Geophys. Res.*, **109, doi:10.1029/2003JD003811**.

Stolarski, R., 1988: The Antarctic ozone hole. *Scientific American*, **258**, 30–36.

Stolarski, R., A. R. Douglass, S. Steenrod, and S. Pawson, 2006: Trends in stratospheric ozone: Lessons learned from a 3–D chemical transport model. *J. Atmos. Sci.*, **63, doi:10.1175/JAS3650.1**, 1028–1041.

Streibel, M., et al., 2006: Chemical ozone loss in the Arctic winter 2002/2003 determined with Match. *Atmos. Chem. Phys.*, **6, doi:10.5194/acp-6-2783-2006**, 2783–2792.

Taguchi, M., 2008: Is there a statistical connection between stratospheric sudden warming and tropospheric blocking events? *J. Atmos. Sci.*, **65, doi:10.1175/2007JAS2363.1**, 1442–1454.

Terao, Y., Y. Sasano, H. Nakajima, H. Tanaka, and T. Yasunari, 2002: Stratospheric ozone loss in the 1996/1997 Arctic winter: Evaluation based on multiple trajectory analysis for doublesounded air parcels by ILAS. *J. Geophys. Res.*, **107, doi:10.1029/2001JD000615**.

Thiéblemont, R., N. Huret, Y. J. Orsolini, A. Hauchecorne, and M.-A. Drouin, 2011: Frozen-in anticyclones occurring in polar Northern Hemisphere during springtime: characterization, occurrence and link with quasi-biennial oscillation. *J. Geophys. Res.*, **116, doi:10.1029/2011JD016042**.

Thurairajah, B., R. L. Collins, V. L. Harvey, R. S. Lieberman, M. Gerding, K. Mizutani, and J. M. Livingston, 2010: Gravity wave activity in the Arctic stratosphere and mesosphere during the 2007–2008 and 2008–2009 stratospheric sudden warming events. *J. Geophys. Res.*, **115, doi:10.1029/2010JD014125**.

Tilmes, S., M. Müller, J.-U. Grooß, M. Höpfner, G. C. Toon, and J. M. Russel-III, 2003: Very early chlorine activation and ozone loss in the Arctic winter 2002–2003. *Geophys. Res. Lett.*, **30, doi:10.1029/2003GL018079**.

Tilmes, S., R. Müller, A. Engel, M. Rex, and J. M. Russell-III, 2006: Chemical ozone loss in the Arctic and Antarctic stratosphere between 1992 and 2005. *Geophys. Res. Lett.*, **33, doi:10.1029/2006GL026925**.

Tilmes, S., R. Müller, J.-U. Grooß, and J. M. Russell-III, 2004: Ozone loss and chlorine activation in the Arctic winters 1991–2003 derived with the tracer-tracer correlations. *Atmos. Chem. Phys.*, **4, doi:10.5194/acp-4-2181-2004**, 2181–2213.

Tilmes, S., R. Müller, and R. Salawitch, 2008: The sensitivity of polar ozone depletion to proposed geoengineering schemes. *Science*, **320, doi:10.1126/science.1153966**, 1201–1204.

Tripathi, O. P., et al., 2006: High resolution simulation of recent Arctic and Antarctic stratospheric chemical ozone loss compared to observations. *J. Atmos. Chem.*, **55, doi:10.1007/s10874-006-9028-8**, 205–226.

Tripathi, O. P., et al., 2007: Comparison of polar ozone loss rates simulated by one-dimensional and three-dimensional models with Match observations in recent Antarctic and Arctic winters. *J. Geophys. Res.*, **112, doi:10.1029/2006JD008370**.

Tsvetkova, N. D., V. A. Yushkov, A. N. Luk'yanov, V. M. Dorokhov, and H. Nakane, 2007: Record-breaking chemical destruction of ozone in the Arctic during the winter of 2004/2005. *Izvestiya Atmos. Ocean. Phys.*, **43, doi:10.1134/S0001433807050076**, 592–598.

Tully, M. B., et al., 2008: The 2007 Antarctic ozone hole. *Australian Meteorological Magazine*, **57**, 279–298.

Tully, M. B., et al., 2011: The Antarctic ozone hole during 2008 and 2009. *Australian Meteorological and Oceanographic Journal*, **61**, 77–90.

Turner, J., 2004: The El Nino–Southern Oscillation and Antarctica. *Int. J. Climatol.*, **24, doi:10.1002/joc.965**, 1–31.

Urban, J., et al., 2004: The northern hemisphere stratospheric vortex during the 2002–03 winter: Subsidence, chlorine activation and ozone loss observed by the odin Sub–Millimetre Radiometer. *Geophys. Res. Lett.*, **31, doi:10.1029/2003GL019089**.

Van Roozendael, M., et al., 1998: Validation of ground-based visible measurements of total ozone by comparison with Dobson and Brewer spectrophotometers. *J. Atmos. Chem.*, **29, doi:10.1023/A:1005815902581**, 55–83.

Van Roozendael, M., et al., 2012: Sixteen years of GOME/ERS-2 total ozone data: The new direct-fitting GOME data processor (GDP) version 5 - algorithm description. *J. Geophys. Res.*, **117, doi:10.1029/2011JD016471**.

Velders, G. J., S. O. Andersen, J. S. Daniel, D. W. Fahey, and M. McFarland, 2007: The importance of the montreal protocol in protecting climate. *PNAS*, **104, doi:10.1073/pnas.0610328104**, 4814–4819.

Vogel, B., et al., 2008: Model simulations of stratospheric ozone loss caused by enhanced mesospheric NO_x during Arctic winter 2003/2004. *Atmos. Chem. Phys.*, **8, doi:10.5194/acp-8-5279-2008**, 5279–5293.

von Hobe, M., J.-U. Grooß, R. Müller, S. Hrechanyy, U. Winkler, and F. Stroh, 2005: A re-evaluation of the ClO/Cl_2O_2 equilibrium constant based on stratospheric in-situ observations. *Atmos. Chem. Phys.*, **5, doi:10.5194/acp-5-693-2005**, 693–702.

von Hobe, M., R. J. Salawitch, T. Canty, H. Keller-Rudek, G. K. Moortgat, J. U. Grooß, R. Müller, and F. Stroh, 2007: Understanding the kinetics of the clo dimer cycle. *Atmos. Chem. Phys.*, **7, doi:10.5194/acp-7-3055-2007**, 3055–3069.

von Hobe, M., et al., 2006: Severe ozone depletion in the cold Arctic winter 2004–05. *Geophys. Res. Lett.*, **33, doi:10.1029/2006GL026945**.

Vyushin, D. I., V. E. Fioletov, and T. G. Shepherd, 2007: Impact of long-range correlations on trend detection in total ozone. *J. Geophys. Res.*, **112, doi:10.1029/2006JD008168**.

Vyushin, D. I., T. G. Shepherd, and V. E. Fioletov, 2010: On the statistical modeling of persistence in total ozone anomalies. *J. Geophys. Res.*, **115, doi:10.1029/2009JD013105**.

Waibel, A. E., et al., 1999: Arctic ozone loss due to denitrification. *Science*, **283, doi:10.1126/science.283.5410.2064**, 2064–2069.

Wamsley, P. R., et al., 1998: Distribution of halon-1211 in the upper troposphere and lower stratosphere and the 1994 total bromine budget. *J. Geophys. Res.*, **103, doi:10.1029/97JD02466**, 1513–1526.

Wanner, H., S. Brönnimann, C. Casty, D. Gyalistras, J. Luterbacher, C. Schmutz, D. Stephenson, and E. Xoplaki, 2001: North Atlantic Oscillation - concepts and studies. *Surv. Geophys.*, **22, doi:10.1023/A:1014217317898**, 321–382.

Waters, J. W., L. Froidevaux, W. G. Read, G. L. Manney, L. S. Elson, D. A. Flower, R. F. Jarnot, and R. S. Harwood, 1993: Stratospheric ClO and ozone from the Microwave Limb Sounder on the Upper Atmosphere Research Satellite. *Nature*, **362, doi:10.1038/362597a0**, 597–602.

Waugh, D. W. and T. M. Hall, 2002: Age of stratospheric air: Theory, observations, and models. *Rev. Geophys.*, **40, doi:10.1029/2000RG000101**.

Waugh, D. W., L. Oman, S. R. Kawa, R. S. Stolarski, S. Pawson, A. R. Douglass, P. A. Newman, and J. E. Nielsen, 2009: Impacts of climate change on stratospheric ozone recovery. *Geophys. Res. Lett.*, **36, doi:10.1029/2008GL036223**.

Waugh, D. W. and L. M. Polvani, 2010: *Stratospheric Polar Vortices – The Stratosphere: Dynamics, Transport and Chemistry*. Geophysical Monograph Series 190, American Geophysical Union, Washington, D.C., doi:10.1029/2009GM000887, 491 pp.

Waugh, D. W., W. J. Randel, S. Pawson, P. A. Newman, and E. R. Nash, 1999: Persistence of lower stratospheric polar vortices. *J. Geophys. Res.*, **104, doi:10.1029/1999JD900795**, 27 191–27 201.

Weber, M., S. Dikty, J. P. Burrows, H. Garny, M. Dameris, A. Kubin, J. Abalichin, and U. Langematz, 2011: The Brewer-Dobson circulation and total ozone from seasonal to decadal time scales. *Atmos. Chem. Phys.*, **11, doi:10.5194/acp-11-11221-2011**, 11 221–11 235.

Williamson, D. L. and P. J. Rasch, 1989: Two-dimensional semi-lagrangian transport with shape-preserving interpolation. *Mon. Weather Rev.*, **117, doi:10.1175/1520-0493(1989)117<0102:TDSLTW>2.0.CO;2**, 102–129.

WMO, 1978: Abridged final report of the seventh session (27 February – 10 March 1978; Manila, Philippines) of the Commission for Atmospheric Sciences, WMO Rep. 509, 113 pp.

WMO, 1993: The Global Atmosphere Watch guide, WMO TD No. 553.

WMO, 2007: World Meteorological Organization: Scientific assessment of ozone depletion: 2006, Global Ozone Research and Monitoring Project-Report No. 50, 572 pp, Geneva, Switzerland.

WMO, 2011: World Meteorological Organization: Scientific assessment of ozone depletion: 2010, Global Ozone Research and Monitoring Project-Report No. 52, 516 pp, Geneva, Switzerland.

Wohltmann, I., R. Lehmann, M. Rex, D. Brunner, and J. A. Mäder, 2007: A process-oriented regression model for column ozone. *J. Geophys. Res.*, **112, doi:10.1029/2006JD007573**.

Woods, A., 2006: *Medium-Range Weather Prediction - the European Approach*. Springer, ISBN:978-0387269283.

Woollings, T. A., Charlton-Perez, S. Ineson, A. G. Marshall, and G. Masato, 2010: Associations between stratospheric variability and tropospheric blocking. *J. Geophys. Res.*, **115, doi:10.1029/2009JD012742**.

Woyke, T., R. Müller, F. Stroh, D. S. McKenna, A. Engel, J. J. Margitan, M. Rex, and K. S. Carslaw, 1999: A test of our understanding of the ozone chemistry in the Arctic polar vortex based on in situ measurements of ClO, BrO, and O_3 in the 1994/1995 winter. *J. Geophys. Res.*, **104, doi:10.1029/1999JD900287**, 18 755–18 768.

Wu, J. and A. E. Dessler, 2001: Comparisons between measurements and models of Antarctic ozone loss. *J. Geophys. Res.*, **106, doi:10.1029/2000JD900606**, 3195–3201.

Yang, E. S., D. M. Cunnold, M. J. Newchurch, R. J. Salawitch, M. P. McCormick, J. M. Russell-III, J. M. Zawodny, and S. J. Oltmans, 2008: First stage of Antarctic ozone recovery. *J. Geophys. Res.*, **113, doi:10.1029/2007JD009675**.

Yang, E. S., D. M. Cunnold, R. J. Salawitch, M. P. McCormick, J. M. Russell-III, J. M. Zawodny, S. Oltmans, and M. J. Newchurch, 2006: Attribution of recovery in lower-stratospheric ozone. *J. Geophy. Res.*, **111, doi:10.1029/2005JD006371**.

Chapter 11

PUBLICATIONS

Publications relevant to this study:

Atmos. Chem. Phys., 13, 1625–1635, 2013
www.atmos-chem-phys.net/13/1625/2013/
doi:10.5194/acp-13-1625-2013

Atmospheric Chemistry and Physics Open Access

Antarctic ozone loss in 1979–2010: first sign of ozone recovery

J. Kuttippurath[1], F. Lefèvre[1], J.-P. Pommereau[1], H. K. Roscoe[2], F. Goutail[1], A. Pazmiño[1], and J. D. Shanklin[2]

[1]UPMC Université de Paris 06, Université Versailles-Saint-Quentin, LATMOS-IPSL, CNRS/INSU, UMR8190, Paris, France
[2]British Antarctic Survey, Cambridge, UK

Correspondence to: J. Kuttippurath (jayanarayanan.kuttippurath@latmos.ipsl.fr)

Received: 29 February 2012 – Published in Atmos. Chem. Phys. Discuss.: 25 April 2012
Revised: 28 November 2012 – Accepted: 17 January 2013 – Published: 8 February 2013

Abstract. A long-term ozone loss time series is necessary to understand the evolution of ozone in Antarctica. Therefore, we construct the time series using ground-based, satellite and bias-corrected multi-sensor reanalysis (MSR) data sets for the period 1989–2010. The trends in ozone over 1979–2010 are also estimated to further elucidate its evolution in the wake of decreasing halogen levels in the stratosphere. Our analysis with ground-based observations shows that the average ozone loss in the Antarctic is about −33 to −50 % (−90 to −155 DU (Dobson Unit)) in 1989–1992, and then stayed at around −48 % (−160 DU). The ozone loss in the warmer winters (e.g. 2002 and 2004) is lower (−37 to −46 %), and in the very cold winters (e.g. 2003 and 2006) it is higher (−52 to −55 %). These loss estimates are in good agreement with those estimated from satellite observations, where the differences are less than ±3 %. The ozone trends based on the equivalent effective Antarctic stratospheric chlorine (EEASC) and piecewise linear trend (PWLT) functions for the vortex averaged ground-based, Total Ozone Mapping Spectrometer/Ozone Monitoring Instrument (TOMS/OMI), and MSR data averaged over September–November exhibit about −4.6 DU yr^{-1} over 1979–1999, corroborating the role of halogens in the ozone decrease during the period. The ozone trends computed for the 2000–2010 period are about +1 DU yr^{-1} for EEASC and +2.6 DU yr^{-1} for the PWLT functions. The larger positive PWLT trends for the 2000–2010 period indicate the influence of dynamics and other basis functions on the increase of ozone. The trends in both periods are significant at 95 % confidence intervals for all analyses. Therefore, our study suggests that Antarctic ozone shows a significant positive trend toward its recovery, and hence, leaves a clear signature of the successful implementation of the Montreal Protocol.

1 Introduction

Ozone loss in the Antarctic stratosphere has been an issue of intense research since its discovery in the 1980s (Farman et al., 1985). Several estimates of ozone loss are available for Antarctica since then. However, most of them deal with the ozone loss analysis for individual winters, modelled or incomplete due to limitations of the analysed observations (e.g. Austin et al., 2010; Lemmen et al., 2006; Tilmes et al., 2006; Hoppel et al., 2005), and thus this makes the inter-annual comparison very difficult. For instance, the chemistry–climate model (CCM)-based studies are mostly exploited for the projection of ozone recovery (e.g. Austin et al., 2010). Although there are many studies using satellite data, a continuous long-term ozone loss analysis is still not available using these data (Bevilacqua et al., 1997; Hoppel et al., 2005; Tilmes et al., 2006). Therefore, we present a comprehensive ozone loss analysis in the Antarctic using ground-based and satellite measurements for the 1989–2010 period, similar to that in the Arctic (Goutail et al., 2005). In this we use the same model, measurements, and method to construct the whole time series, which makes a continuous, coherent and comparable long-term analysis. This analysis can also be regarded as an extension of the study of Huck et al. (2007), who presented an ozone loss analysis using the total column for the 1992–2004 period. The passive technique is used to derive the ozone loss from observations, in which the contribution from transport is separated from the photochemical ozone loss. A detailed description of this approach (e.g. Goutail et al., 1999) and its application to the Antarctic winters 2005–2009 can be found in Kuttippurath et al. (2010).

Atmos. Chem. Phys., 12, 7073–7085, 2012
www.atmos-chem-phys.net/12/7073/2012/
doi:10.5194/acp-12-7073-2012

Atmospheric Chemistry and Physics

Record-breaking ozone loss in the Arctic winter 2010/2011: comparison with 1996/1997

J. Kuttippurath[1], S. Godin-Beekmann[1], F. Lefèvre[1], G. Nikulin[2], M. L. Santee[3], and L. Froidevaux[3]

[1]UPMC Université Paris 06, LATMOS-IPSL, CNRS/INSU, UMR8190, 75005 Paris, France
[2]Swedish Meteorological Hydrological Institute, Kiruna, Sweden
[3]JPL/NASA, California Institute of Technology, Pasadena, California, USA

Correspondence to: J. Kuttippurath (jayanarayanan.kuttippurath@latmos.ipsl.fr)

Received: 5 February 2012 – Published in Atmos. Chem. Phys. Discuss.: 6 March 2012
Revised: 25 July 2012 – Accepted: 27 July 2012 – Published: 6 August 2012

Abstract. We present a detailed discussion of the chemical and dynamical processes in the Arctic winters 1996/1997 and 2010/2011 with high resolution chemical transport model (CTM) simulations and space-based observations. In the Arctic winter 2010/2011, the lower stratospheric minimum temperatures were below 195 K for a record period of time, from December to mid-April, and a strong and stable vortex was present during that period. Simulations with the Mimosa-Chim CTM show that the chemical ozone loss started in early January and progressed slowly to 1 ppmv (parts per million by volume) by late February. The loss intensified by early March and reached a record maximum of ∼2.4 ppmv in the late March–early April period over a broad altitude range of 450–550 K. This coincides with elevated ozone loss rates of 2–4 ppbv sh^{-1} (parts per billion by volume/sunlit hour) and a contribution of about 30–55 % and 30–35 % from the ClO-ClO and ClO-BrO cycles, respectively, in late February and March. In addition, a contribution of 30–50 % from the HO_x cycle is also estimated in April. We also estimate a loss of about 0.7–1.2 ppmv contributed (75 %) by the NO_x cycle at 550–700 K. The ozone loss estimated in the partial column range of 350–550 K exhibits a record value of ∼148 DU (Dobson Unit). This is the largest ozone loss ever estimated in the Arctic and is consistent with the remarkable chlorine activation and strong denitrification (40–50 %) during the winter, as the modeled ClO shows ∼1.8 ppbv in early January and ∼1 ppbv in March at 450–550 K. These model results are in excellent agreement with those found from the Aura Microwave Limb Sounder observations. Our analyses also show that the ozone loss in 2010/2011 is close to that found in some Antarctic winters, for the first time in the observed history. Though the winter 1996/1997 was also very cold in March–April, the temperatures were higher in December–February, and, therefore, chlorine activation was moderate and ozone loss was average with about 1.2 ppmv at 475–550 K or 42 DU at 350–550 K, as diagnosed from the model simulations and measurements.

1 Introduction

Chemical ozone loss in the Arctic stratosphere has been observed since 1989. Since then, cold winters are prone to large chemical ozone loss due to the still high amounts of ozone depleting substances in the atmosphere (Rex et al., 2004). However, because of large planetary wave activity, the polar vortex breaks up or dissipates early in most Arctic winters (WMO, 2011; Harris et al., 2010; Kuttippurath et al., 2010b; Manney et al., 2003). Therefore, the vortex persistence has been comparatively shorter and the associated ozone loss smaller in the Arctic as compared to the Antarctic (WMO, 2011; Solomon et al., 2007). The longest vortex persistence in the Arctic was found in 1996/1997, in which the wave activity was considerably suppressed, and therefore the vortex was sustained until early May (Lefèvre et al., 1998; Coy et al., 1997). Nevertheless, the ozone loss in 1996/1997 was lower than that of other cold winters such as 1994/1995, 1999/2000, and 2004/2005 due to relatively higher temperatures in December–February 1996/1997, when chlorine activation plays a key role in determining the magnitude of ozone loss (Manney et al., 2003; Santee et al., 1997). In contrast, very low temperatures were observed in March–April due

Atmos. Chem. Phys., 12, 8115–8129, 2012
www.atmos-chem-phys.net/12/8115/2012/
doi:10.5194/acp-12-8115-2012

Atmospheric Chemistry and Physics

A comparative study of the major sudden stratospheric warmings in the Arctic winters 2003/2004–2009/2010

J. Kuttippurath[1] **and G. Nikulin**[2]

[1]UPMC Université Paris 06, LATMOS-IPSL, CNRS/INSU, UMR8190, 75005 Paris, France
[2]Rossby Centre, Swedish Meteorological and Hydrological Institute, Norrköping, Sweden

Correspondence to: J. Kuttippurath (jayanarayanan.kuttippurath@latmos.ipsl.fr)

Received: 1 February 2012 – Published in Atmos. Chem. Phys. Discuss.: 12 March 2012
Revised: 23 August 2012 – Accepted: 23 August 2012 – Published: 10 September 2012

Abstract. We present an analysis of the major sudden stratospheric warmings (SSWs) in the Arctic winters 2003/04–2009/10. There were 6 major SSWs (major warmings [MWs]) in 6 out of the 7 winters, in which the MWs of 2003/04, 2005/06, and 2008/09 were in January and those of 2006/07, 2007/08, and 2009/10 were in February. Although the winter 2009/10 was relatively cold from mid-December to mid-January, strong wave 1 activity led to a MW in early February, for which the largest momentum flux among the winters was estimated at 60° N/10 hPa, about 450 $m^2 s^{-2}$. The strongest MW, however, was observed in 2008/09 and the weakest in 2006/07. The MW in 2008/09 was triggered by intense wave 2 activity and was a vortex split event. In contrast, strong wave 1 activity led to the MWs of other winters and were vortex displacement events. Large amounts of Eliassen-Palm (EP) and wave 1/2 EP fluxes (about 2–4×10^5 kg s^{-2}) are estimated shortly before the MWs at 100 hPa averaged over 45–75° N in all winters, suggesting profound tropospheric forcing for the MWs. We observe an increase in the occurrence of MWs (∼ 1.1 MWs/winter) in recent years (1998/99–2009/10), as there were 13 MWs in the 12 Arctic winters, although the long-term average (1957/58–2009/10) of the frequency stays around its historical value (∼ 0.7 MWs/winter), consistent with the findings of previous studies. An analysis of the chemical ozone loss in the past 17 Arctic winters (1993/94–2009/10) suggests that the loss is inversely proportional to the intensity and timing of MWs in each winter, where early (December–January) MWs lead to minimal ozone loss. Therefore, this high frequency of MWs in recent Arctic winters has significant implications for stratospheric ozone trends in the northern hemisphere.

1 Introduction

One of the intriguing phenomena in climate science is the large interannual variability of Arctic stratospheric winters, characterized by extremely warm and very cold winters. This year-to-year variability is dominated by sudden stratospheric warmings (SSWs) during which the polar temperature rises and the zonal flow weakens or reverses (Scherhag, 1952). There are different definitions for a SSW to be called major or minor. According to the World Meteorological Organisation (WMO) a SSW can be said to be *major* if at 10 hPa or lower altitudes the latitudinal mean temperature increases abruptly poleward from 60° latitude with an associated circulation reversal in a short period of time. If the reversal of temperature gradient does not follow the zonal-mean wind reversal, then it is a *minor* SSW (e.g. WMO, 1978, item 9.4, 35–36; Andrews et al., 1987; Labitzke and Naujokat, 2000). In some cases the increase in temperature near the pole can be up to 40–60 K in a week at 10 hPa (Limpasuvan et al., 2004; Andrews et al., 1987). The followed zonal wind reversal displaces or splits the polar vortex toward midlatitudes (e.g. Kuttippurath et al., 2010; Charlton and Polvani, 2007). Since the WMO definition considers the major SSWs (hereafter major warmings–MWs) from November to February, studies have slightly modified this criterion to account for the warmings from October through May (e.g. Charlton and Polvani, 2007; Bancalá et al., 2012). Also, there is an ambiguity regarding the temperature gradient criterion of the WMO definition (e.g. the difference between Limpasuvan et al., 2004 and Krüger et al., 2005). Apart from these, classifications of MWs based on the northern annular mode (Baldwin and Dunkerton, 2001) and external

JOURNAL OF GEOPHYSICAL RESEARCH, VOL. 116, D22305, doi:10.1029/2011JD016020, 2011

Arctic ozone depletion in 2002–2003 measured by ASUR and comparison with POAM observations

Jayanarayanan Kuttippurath,[1,2] Armin Kleinböhl,[3] Miriam Sinnhuber,[1,4] Holger Bremer,[1,5] Harry Küllmann,[1] Justus Notholt,[1] Sophie Godin-Beekmann,[2] Omprakash Tripathi,[6] and Grigory Nikulin[7]

Received 27 March 2011; revised 25 September 2011; accepted 28 September 2011; published 22 November 2011.

[1] We present ozone loss estimated from airborne measurements taken during January–February and March in the Arctic winter 2002/2003. The first half of the winter was characterized by unusually cold temperatures and the second half by a major stratospheric sudden warming around 15–18 January 2003. The potential vorticity maps show a vortex split in the lower stratosphere during the major warming (MW) in late January and during the minor warming in mid-February due to wave 1 amplification. However, the warming can be termed as a vortex displacement event as there was no vortex split during the MW period at 10 hPa. Very low temperatures, large areas of polar stratospheric clouds (PSCs), and high chlorine activation triggered significant ozone loss in the early winter, as the vortex moved to the midlatitude regions. The ozone depletion derived from the ASUR measurements sampled inside the vortex, in conjunction with the Mimosa-Chim model tracer, shows a maximum of 1.3 ± 0.2 ppmv at 450–500 K by late March. The partial column loss derived from the ASUR ozone profiles reaches up to 61 ± 4 DU in 400–550 K in the same period. The evolution of ozone and ozone loss assessed from the ASUR measurements is in very good agreement with POAM observations. The reduction in ozone estimated from the POAM measurements shows a similar maximum of 1.3 ± 0.2 ppmv at 400–500 K or 63 ± 4 DU in 400–550 K in late March. Our study reveals that the Arctic winter 2002/2003 was unique as it had three minor warmings and a MW, yet showed large loss in ozone. No such feature was observed in any other Arctic winter in the 1989–2010 period. In addition, an unusually large ozone loss in December, around 0.5 ± 0.2 ppmv at 450–500 K or 12 ± 1 DU in 400–550 K, was estimated for the first time in the Arctic. A careful and detailed diagnosis with all available published results for this winter exhibits an average ozone loss of 1.5 ± 0.3 ppmv at 450–500 K or 65 ± 5 DU in 400–550 K by the end of March, which exactly matches the ozone depletion derived from the ASUR, POAM and model data. The early ozone loss together with considerable loss afterwards put the warm Arctic winter 2002/2003 amongst the moderately cold winters in terms of the significance of the ozone loss.

Citation: Kuttippurath, J., A. Kleinböhl, M. Sinnhuber, H. Bremer, H. Küllmann, J. Notholt, S. Godin-Beekmann, O. Tripathi, and G. Nikulin (2011), Arctic ozone depletion in 2002–2003 measured by ASUR and comparison with POAM observations, *J. Geophys. Res.*, *116*, D22305, doi:10.1029/2011JD016020.

1. Introduction

[2] Polar stratospheric ozone depletion in the Arctic was first identified in 1989 [*Hofmann et al.*, 1989] and significant reduction in ozone has been measured since then in each cold winter [*World Meteorological Organization* (*WMO*), 2007]. The difference in ozone loss from one winter to the other is found to be extremely large and is highly controlled by temperature history of the winters. The meteorology of Arctic winters is characterized by intermittent stratospheric sudden warmings. Therefore, the extent of ozone loss in an Arctic winter is determined by the dynamics of the region. This is clearly manifested with the range of ozone depletion

[1]Institute of Environmental Physics, University of Bremen, Bremen, Germany.
[2]CNRS/LATMOS/UPMC, Paris, France.
[3]NASA Jet Propulsion Laboratory, California Institute of Technology, Pasadena, California, USA.
[4]IMK, Karlsruhe Institute of Technology, Karlsruhe, Germany.
[5]Physikalisch-Technische Bundesanstalt, Braunschweig, Germany.
[6]Department of Atmospheric Sciences, University of Arizona, Tucson, Arizona, USA.
[7]Rossby Centre, Swedish Meteorological and Hydrological Institute, Norrköping, Sweden.

0148-0227/11/2011JD016020

Atmos. Chem. Phys., 10, 9915–9930, 2010
www.atmos-chem-phys.net/10/9915/2010/
doi:10.5194/acp-10-9915-2010

Atmospheric Chemistry and Physics

Spatial, temporal, and vertical variability of polar stratospheric ozone loss in the Arctic winters 2004/2005–2009/2010

J. Kuttippurath, S. Godin-Beekmann, F. Lefèvre, and F. Goutail

UPMC Université Paris 06, Université Versailles-Saint-Quentin, UMR 8190 LATMOS-IPSL, CNRS/INSU, Paris, France

Received: 10 May 2010 – Published in Atmos. Chem. Phys. Discuss.: 15 June 2010
Revised: 5 October 2010 – Accepted: 8 October 2010 – Published: 20 October 2010

Abstract. The polar stratospheric ozone loss during the Arctic winters 2004/2005–2009/2010 is investigated by using high resolution simulations from the chemical transport model Mimosa-Chim and observations from Aura Microwave Limb Sounder (MLS), by applying the passive tracer technique. The winter 2004/2005 shows the coldest temperatures, highest area of polar stratospheric clouds and strongest chlorine activation in 2004/2005–2009/2010. The ozone loss diagnosed from both simulations and measurements inside the polar vortex at 475 K ranges from 0.7 ppmv in the warm winter 2005/2006 to 1.5–1.7 ppmv in the cold winter 2004/2005. Halogenated (chlorine and bromine) catalytic cycles contribute to 75–90% of the ozone loss at this level. At 675 K the lowest loss of 0.3–0.5 ppmv is computed in 2008/2009, and the highest loss of 1.3 ppmv is estimated in 2006/2007 by the model and in 2004/2005 by MLS. Most of the ozone loss (60–75%) at this level results from nitrogen catalytic cycles rather than halogen cycles. At both 475 and 675 K levels the simulated ozone and ozone loss evolution inside the vortex is in reasonably good agreement with the MLS observations. The ozone partial column loss in 350–850 K deduced from the model calculations at the MLS sampling locations inside the polar vortex ranges between 43 DU in 2005/2006 and 109 DU in 2004/2005, while those derived from the MLS observations range between 26 DU and 115 DU for the same winters. The partial column ozone depletion derived in that vertical range is larger than that estimated in 350–550 K by 19±7 DU on average, mainly due to NO_x chemistry. The column ozone loss estimates from both Mimosa-Chim and MLS in 350–850 K are generally in good agreement with those derived from ground-based ultraviolet-visible spectrometer total ozone observations for the respective winters, except in 2010.

Correspondence to: J. Kuttippurath
(jayan@aero.jussieu.fr)

1 Introduction

Unlike in the Antarctic winter stratosphere, the chemical ozone loss in the Arctic is highly variable. This variability is primarily caused by the variations in Arctic meteorology. That is, the Arctic stratosphere is often disturbed by planetary wave forcing triggered by mountain orography that disrupts the unstable polar vortex in most winters. Therefore, the Arctic experiences high extreme cold as well as sudden stratospheric warmings (SSWs) at times. As a result the degree of ozone loss is mostly controlled by the strength of the vortex and magnitude of air temperature within. For instance, the winters 1995, 1996, 2000, and 2005 were very cold and the cumulative total ozone loss was as high as ∼25–35% (Rex et al., 2006; WMO, 2007; Goutail et al., 2005). On the other-hand, the winters 1997, 1998, 1999, 2001, 2002, 2006, and 2009 were relatively warm and the loss was minimal, about 10–15%, while the winters 2003, 2007, and 2008 were moderately cold and hence, the loss was in an average scale of about 15–20% (WMO, 2007; Goutail et al., 2010).

Significant improvements have been made in understanding the chemistry of ozone loss in the polar lower stratosphere in the last decade. Studies suggest that very low temperatures (<195 K) initiate the formation of Polar Stratospheric Clouds (PSCs), and chlorine activation on these PSCs triggers the ozone depletion when the sun returns over the Arctic in spring. The halogen cycles ClO–ClO and BrO–ClO contribute about 80–90% of ozone loss in this region through the above-said processes (WMO, 2007). However, ozone loss at higher altitudes is driven by different chemical cycles than those discussed in the lower stratosphere. A detailed study on the ozone loss process at higher altitudes is still lacking. The available studies deal with specific issues of mid-winter warming and concomitant mid-latitude ozone loss (for e.g. Grooß et al., 2005a; Vogel et al., 2008). None of these studies perform a detailed analysis of the winter stratosphere in different conditions to diagnose the contribution

Published by Copernicus Publications on behalf of the European Geosciences Union.

Atmos. Chem. Phys., 10, 6569–6581, 2010
www.atmos-chem-phys.net/10/6569/2010/
doi:10.5194/acp-10-6569-2010

Atmospheric Chemistry and Physics

Estimation of Antarctic ozone loss from ground-based total column measurements

J. Kuttippurath[1], F. Goutail[1], J.-P. Pommereau[1], F. Lefèvre[1], H. K. Roscoe[2], A. Pazmiño[1], W. Feng[3], M. P. Chipperfield[3], and S. Godin-Beekmann[1]

[1]Université Versailles-Saint-Quentin, UPMC Université Paris 06, CNRS/INSU, UMR 8190 LATMOS-IPSL, Paris, France
[2]British Antarctic Survey, Cambridge, UK
[3]School of Earth and Environment, University of Leeds, Leeds, UK

Received: 5 February 2010 – Published in Atmos. Chem. Phys. Discuss.: 24 March 2010
Revised: 28 June 2010 – Accepted: 5 July 2010 – Published: 16 July 2010

Abstract. The passive tracer method is used to estimate ozone loss from ground-based measurements in the Antarctic. A sensitivity study shows that the ozone depletion can be estimated within an accuracy of ∼4%. The method is then applied to the ground-based observations from Arrival Heights, Belgrano, Concordia, Dumont d'Urville, Faraday, Halley, Marambio, Neumayer, Rothera, South Pole, Syowa, and Zhongshan for the diagnosis of ozone loss in the Antarctic. On average, the ten-day boxcar average of the vortex mean ozone column loss deduced from the ground-based stations was about 55±5% in 2005–2009. The ozone loss computed from the ground-based measurements is in very good agreement with those derived from satellite measurements (OMI and SCIAMACHY) and model simulations (REPROBUS and SLIMCAT), where the differences are within ±3–5%.

The historical ground-based total ozone observations in October show that the depletion started in the late 1970s, reached a maximum in the early 1990s and stabilised afterwards due to saturation. There is no indication of ozone recovery yet. At southern mid-latitudes, a reduction of 20–50% is observed for a few days in October–November at the newly installed Rio Gallegos station. Similar depletion of ozone is also observed episodically during the vortex overpasses at Kerguelen in October–November and at Macquarie Island in July–August of the recent winters. This illustrates the significance of measurements at the edges of Antarctica.

Correspondence to: J. Kuttippurath
(jayan@aero.jussieu.fr)

1 Introduction

Stratospheric ozone has been a trace gas of great interest ever since the discovery of its dramatic decline in the Antarctic spring in early 1980s (Farman et al., 1985). Since then a string of ground-based (GB) and satellite sensors has been dedicated to observe the polar stratospheres in the framework of the international World Meteorological Organisation–Global Atmospheric Watch (WMO-GAW) programme (WMO, 1993) and the Network for Detection of Atmospheric Composition Change (NDACC) for the constant monitoring of ozone loss. Although satellites have the advantage of global coverage, they cannot observe at Solar Zenith Angle (SZA) >84° and thus not during the deep winter months. In addition, i) they have limited lifetime and cannot always be immediately replaced, ii) their measurements usually show progressive degradation, and iii) the discontinuity in the observations produce undesirable jumps in the trend analyses when the concatenated data are used. In contrast, though of limited geographical coverage, ground-based sensors offer the advantage of continuous record and easy repair or replacement if necessary. Further, those measuring at visible wavelengths, such as SAOZ (Système d'Analyse par Observation Zénithale) spectrometers used in this study, are capable of making reliable measurements until 91° SZA, which is throughout the winter at latitudes around 65° S. Therefore, the maintenance of an independent ground-based capacity is absolutely essential.

The passive tracer method has been successfully applied to the estimation of ozone depletion from ground-based total ozone measurements in the Arctic (Goutail et al., 1999). This approach separates the contribution due to transport

International Journal of Remote Sensing
Vol. 30, Nos. 15–16, August 2009, 4071–4082

Ozone depletion in the Arctic winter 2007–2008

J. KUTTIPPURATH*, S. GODIN-BEEKMANN, F. LEFÈVRE and A. PAZMIÑO

Service d'Aéronomie du CNRS/IPSL, Université de Pierre et Marie Curie, 75252 Paris, France

The Arctic winter 2007–08 was characterized by cold temperatures and a strong vortex. Potentials for large areas of ice and Polar Stratospheric Clouds (PSCs) are observed during the winter. A vortex wide denitrification (removal of 60–80% of NO_y) and intense chlorine activation (0.6 to 1.05 ppb of ClO) are found inside the vortex at 475 K. This chemical morphology triggered a high rate of ozone loss during the winter. The simulated results from MIMOSA-CHIM show a large loss of ozone at 425–550 K from January to March, about 1.5–2.3 ppm. The vortex averaged loss at 475 K is about 2.5 ppm in mid-March, which is in very good agreement with the estimated loss (2.3 ppm) from the Microwave Limb Sounder (MLS) measurements. Similar analyses from MIMOSA-CHIM for recent winters show a cumulative loss of 2.1 ppm in 2006–07 and 2.0 ppm in 2004–05 in tune with the measurements. The measured and simulated results show the highest loss in 2007–08 in comparison with the analyses for the last four winters at 475 K.

1. Introduction

Curiosity over the developments of the ozone layer in the Arctic stratosphere was raised when the first stamp of human activities on our environment appeared in the form of an ozone hole in the Antarctic (Farman *et al.* 1985). Even though not severe as it is seen in the south, a large loss of ozone is generally observed in unusually cold Arctic winters, like 1995–96, 1999–00, and 2004–05 (WMO 2007). The moderately warm winter of 1991–92 also witnessed a catastrophic loss of ozone due to the heterogeneous chemistry on sulphate aerosols, which were emitted from the Mt. Pinatubo volcanic explosion (WMO 2007, von der Gathen *et al.* 1995). Unprecedented variability in Arctic ozone loss has been observed in the last decade and studies reveal its impact on mid-latitudes too. (Reid *et al.* 1998, Goutail *et al.* 1999, Schulz *et al.* 2000, 2001, Rex *et al.* 2006, Singleton *et al.* 2008). The high inter-annual variability in ozone depletion hints at the necessity of constant monitoring of the stratosphere to predict future climate scenarios. This is also important to assess the impact of international treaties like the Montreal Protocol that aimed to phase-out ozone depleting substances (ODS) (WMO (2007) and references therein). In addition, continued and consistent monitoring of the ozone layer is inevitable for implementing further amendments to the treaties with a vision for a better environment and a more comfortable climate.

*Corresponding author. Email: jayan@aero.jussieu.fr

International Journal of Remote Sensing
ISSN 0143-1161 print/ISSN 1366-5901 online © 2009 Taylor & Francis
http://www.tandf.co.uk/journals
DOI: 10.1080/01431160902821965

Atmos. Meas. Tech., 6, 613–620, 2013
www.atmos-meas-tech.net/6/613/2013/
doi:10.5194/amt-6-613-2013

Atmospheric Measurement Techniques
Open Access

Intercomparison of polar ozone profiles by IASI/MetOp sounder with 2010 Concordiasi ozonesonde observations

J. Gazeaux[1,2], C. Clerbaux[1,3], M. George[1], J. Hadji-Lazaro[1], J. Kuttippurath[1], P.-F. Coheur[3], D. Hurtmans[3], T. Deshler[4], M. Kovilakam[4], P. Campbell[4], V. Guidard[5], F. Rabier[5], and J.-N. Thépaut[6]

[1]UPMC Univ. Paris 06; Université Versailles St-Quentin; CNRS/INSU, UMR8190, LATMOS-IPSL, Paris, France
[2]School of Civil Engineering and Geosciences, Newcastle University, Newcastle upon Tyne, UK
[3]Spectroscopie de l'Atmosphère, Université Libre de Bruxelles, Brussels, Belgium
[4]Department of Atmospheric Science, Wyoming University, Laramie, WY, USA
[5]CNRM/GAME (Météo-France and CNRS), Toulouse, France
[6]European Centre for Medium-Range Weather Forecasts, Reading, UK

Correspondence to: C. Clerbaux (cathy.clerbaux@latmos.ipsl.fr)

Received: 25 September 2012 – Published in Atmos. Meas. Tech. Discuss.: 29 October 2012
Revised: 12 February 2013 – Accepted: 22 February 2013 – Published: 8 March 2013

Abstract. Validation of ozone profiles measured from a nadir looking satellite instrument over Antarctica is a challenging task due to differences in their vertical sensitivity with ozonesonde measurements. In this paper, ozone observations provided by the Infrared Atmospheric Sounding Interferometer (IASI) instrument onboard the polar-orbiting satellite MetOp are compared with ozone profiles collected between August and October 2010 at McMurdo Station, Antarctica, during the Concordiasi measurement campaign. The main objective of the campaign was the satellite data validation. With this aim 20 zero-pressure sounding balloons carrying ozonesondes were launched during this period when the MetOp satellite was passing above McMurdo. This makes the dataset relevant for comparison, especially because the balloons covered the entire altitude range of IASI profiles. The validation methodology and the collocation criteria vary according to the availability of global positioning system auxiliary data with each electro-chemical cell ozonesonde observation. The relative mean difference is shown to depend on the vertical range investigated. The analysis shows a good agreement in the troposphere (below 10 km) and middle stratosphere (25–40 km), where the differences are lower than 10 %. However a significant positive bias of about 10–26 % is estimated in the lower stratosphere at 10–25 km, depending on altitude. The positive bias in the 10–25 km range is consistent with previously reported studies comparing in situ data with thermal infrared satellite measurements. This study allows for a better characterization of IASI-retrieved ozone over the polar region during ozone depletion/recovery processes.

1 Introduction

Surveying ozone distribution over Antarctica is an important task for quantifying ozone depletion over the poles (Newman et al., 2009), and to assess the efficiency of the international protocols controlling the emission of chlorine containing compounds. Stratospheric ozone is essential for ultraviolet radiation protection, which allows life to remain on earth and is closely linked to climate change and stratospheric circulation over the poles. For decades, satellites have provided valuable measurements of the composition of the atmosphere, in particular to follow the ozone chemistry in the polar stratosphere in spring (WMO, 2011).

In 2010 the Concordiasi campaign was organized at McMurdo Station (Long: 166.67°, Lat: −77.85°), Antarctica (Fig. 1), by teams from France and United States, to improve knowledge and understanding of the interactions between ozone depletion, stratospheric clouds and atmospheric dynamics (Rabier et al., 2012). This campaign also aimed to provide additional information to better exploit the temperature, water vapour and ozone observations provided by the Infrared Atmospheric Sounding Interferometer

Atmos. Chem. Phys., 13, 10373–10384, 2013
www.atmos-chem-phys.net/13/10373/2013/
doi:10.5194/acp-13-10373-2013

Atmospheric Chemistry and Physics Open Access

Ozone trends derived from the total column and vertical profiles at a northern mid-latitude station

P. J. Nair[1], S. Godin-Beekmann[1], J. Kuttippurath[1], G. Ancellet[1], F. Goutail[1], A. Pazmiño[1], L. Froidevaux[2], J. M. Zawodny[3], R. D. Evans[4], H. J. Wang[5], J. Anderson[6], and M. Pastel[1]

[1]UPMC Université Paris 06, Université Versailles-Saint-Quentin, UMR 8190, LATMOS-IPSL, CNRS/INSU, Paris, France
[2]Jet Propulsion Laboratory, California Institute of Technology, Pasadena, CA, USA
[3]Chemistry and Dynamics Branch, NASA Langley Research Center, Hampton, VA, USA
[4]NOAA, Earth System Research Laboratory, Global Monitoring Division, Boulder, Colorado, USA
[5]Georgia Institute of Technology, Atlanta, GA, USA
[6]Hampton University, Hampton, VA, USA

Correspondence to: P. J. Nair (gopalapi@aero.jussieu.fr)

Received: 17 February 2013 – Published in Atmos. Chem. Phys. Discuss.: 18 March 2013
Revised: 19 August 2013 – Accepted: 5 September 2013 – Published: 24 October 2013

Abstract. The trends and variability of ozone are assessed over a northern mid-latitude station, Haute-Provence Observatory (OHP: 43.93° N, 5.71° E), using total column ozone observations from the Dobson and Système d'Analyse par Observation Zénithale spectrometers, and stratospheric ozone profile measurements from light detection and ranging (lidar), ozonesondes, Stratospheric Aerosol and Gas Experiment (SAGE) II, Halogen Occultation Experiment (HALOE) and Aura Microwave Limb Sounder (MLS). A multivariate regression model with quasi-biennial oscillation (QBO), solar flux, aerosol optical thickness, heat flux, North Atlantic Oscillation (NAO) and a piecewise linear trend (PWLT) or equivalent effective stratospheric chlorine (EESC) functions is applied to the ozone anomalies. The maximum variability of ozone in winter/spring is explained by QBO and heat flux in the ranges 15–45 km and 15–24 km, respectively. The NAO shows maximum influence in the lower stratosphere during winter, while the solar flux influence is largest in the lower and middle stratosphere in summer. The total column ozone trends estimated from the PWLT and EESC functions are of -1.47 ± 0.27 and -1.40 ± 0.25 DU yr^{-1}, respectively, over the period 1984–1996 and about 0.55 ± 0.30 and 0.42 ± 0.08 DU yr^{-1}, respectively, over the period 1997–2010. The ozone profiles yield similar and significant EESC-based and PWLT trends for 1984–1996, and are about -0.5 and -0.8 % yr^{-1} in the lower and upper stratosphere, respectively. For 1997–2010, the EESC-based and PWLT estimates are of the order of 0.3 and 0.1 % yr^{-1}, respectively, in the 18–28 km range, and at 40–45 km, EESC provides significant ozone trends larger than the insignificant PWLT results. Furthermore, very similar vertical trends for the respective time periods are also deduced from another long-term satellite-based data set (GOZCARDS–Global OZone Chemistry And Related trace gas Data records for the Stratosphere) sampled at northern mid-latitudes. Therefore, this analysis unveils ozone recovery signals from total column ozone and profile measurements at OHP, and hence in the northern mid-latitudes.

1 Introduction

After two decades of regulated emissions, the level of stratospheric ozone depleting substances (ODSs) has been reduced, and some of its components have been phased out (WMO, 2007). The analyses show that total column ozone measurements in the mid-latitudes are stabilised from the mid-1990s onwards (Newchurch et al., 2003; Reinsel et al., 2005; Vyushin et al., 2007). Similarly, a significant change in trend is found in the upper stratosphere at mid-latitudes (Steinbrecht et al., 2006; Jones et al., 2009). Thus, stratospheric ozone showed a slowing of decline attributable to ODS decrease at mid-latitudes (WMO, 2011).

Ann. Geophys., 30, 1435–1449, 2012
www.ann-geophys.net/30/1435/2012/
doi:10.5194/angeo-30-1435-2012

Annales Geophysicae

The unusual persistence of an ozone hole over a southern mid-latitude station during the Antarctic spring 2009: a multi-instrument study

E. A. Wolfram[1], J. Salvador[1], F. Orte[1], R. D'Elia[1], S. Godin-Beekmann[2], J. Kuttippurath[2], A. Pazmiño[2], F. Goutail[2], C. Casiccia[3], F. Zamorano[3], N. Paes Leme[4], and E. J. Quel[1]

[1]Centro de Investigaciones en Láseres y Aplicaciones, CEILAP-UNIDEF (MINDEF-CONICET), UMI-IFAECI-CNRS-3351, UMI3351, Villa Martelli, Argentina
[2]Laboratoire Atmosphère, Milieux, Observations Spatiales (LATMOS), Institut Pierre Simon Laplace, Université Pierre et Marie Curie, Université Versailles St-Quentin-en-Yvelines, Centre National de la Recherche Scientifique, Paris, France
[3]Laboratorio de Ciencias Atmosféricas, Universidad de Magallanes, PuntaArenas, Chile
[4]Instituto Nacional de Pesquisas Espaciais, Brazil

Correspondence to: E. A. Wolfram (ewolfram@gmail.com)

Received: 6 February 2012 – Revised: 22 July 2012 – Accepted: 31 August 2012 – Published: 2 October 2012

Abstract. Record-low ozone column densities (with a minimum of 212 DU) persisted over three weeks at the Río Gallegos NDACC (Network for the Detection of Atmospheric Composition Change) station (51.5° S, 69.3° W) in November 2009. Total ozone remained two standard deviations below the climatological mean for five consecutive days during this period. The statistical analysis of 30 years of satellite data from the Multi Sensor Reanalysis (MSR) database for Río Gallegos revealed that such a long-lasting low-ozone episode is a rare occurrence. The event is examined using height-resolved ozone lidar measurements at Río Gallegos, and observations from satellite and ground-based instruments. The computed relative difference between the measured total ozone and the climatological monthly mean shows reductions varying between 10 and 30 % with an average decrease of 25 %. The mean absolute difference of total ozone column with respect to climatological monthly mean ozone column is around 75 DU. Extreme values of the UV index (UVI) were measured at the ground for this period, with the daily maximum UVI of around 13 on 15 and 28 November. The high-resolution MIMOSA-CHIM (Modélisation Isentrope du transport Méso-échelle de l'Ozone Stratosphérique par Advection) model was used to interpret the ozone depletion event. An ozone decrease of about 2 ppmv was observed in mid-November at the 550 K isentropic level (∼22 km). The position of Río Gallegos relative to the polar vortex was classified using equivalent latitude maps. During the second week of November, the vortex was over the station at all isentropic levels, but after 20 November and until the end of the month, only the 10 lower levels in the stratosphere were affected by vortex overpasses with ozone poor air masses. A rapid recovery of the ozone column density was observed later, due to an ozone rich filament moving over Río Gallegos between 18 and 24 km in the first two weeks of December 2009.

Keywords. Atmospheric composition and structure (Middle atmosphere – composition and chemistry)

1 Introduction

The Antarctic ozone hole is one of the most important perturbations that human activities have provoked in our atmosphere (WMO Report, 2007). The ozone hole started to develop each spring in the southern polar region in the early 1980s. Most recent studies point out that the detection of a statistically significant decrease in its area will not occur before about 2020 (Newman et al., 2006).

In the course of the past twenty years, this phenomenon has varied in size and minimum total ozone value. During spring, stratospheric dynamical processes cause changes in the size and shape of the polar vortex and sometimes it

Denitrification in the Arctic mid-winter 2004/2005 observed by airborne submillimeter radiometry

Armin Kleinböhl,[1] Holger Bremer,[2] Harry Küllmann,[2] Jayanarayanan Kuttippurath,[2] Edward V. Browell,[3] Timothy Canty,[1] Ross J. Salawitch,[1] Geoffrey C. Toon,[1] and Justus Notholt[2]

Received 3 May 2005; revised 9 August 2005; accepted 31 August 2005; published 11 October 2005.

[1] We present measurements of unusually low mixing ratios of HNO_3 in the exceptionally cold Arctic vortex of late-January and early-February 2005. The measurements were obtained by the airborne submillimeter radiometer ASUR during the polar aura validation experiment (PAVE). The distribution of HNO_3 inside the vortex reaches minima below 4 ppbv around 22 km altitude and maxima above 13 ppbv around 16 km altitude, with a considerable spatial variability. We estimate a vortex averaged denitrification of 3.1 ± 0.8 ppbv around 20 km altitude, and slight renitrification below ~15.5 km altitude. The observed HNO_3 deficit is largest (~6 ppbv) near the center of the vortex, where the air masses had experienced temperatures below the NAT formation threshold for 80–100% of the previous 20 days according to back trajectories. This suggests that the main denitrification mechanism is based on sedimenting nitric acid trihydrate particles. **Citation:** Kleinböhl, A., H. Bremer, H. Küllmann, J. Kuttippurath, E. V. Browell, T. Canty, R. J. Salawitch, G. C. Toon, and J. Notholt (2005), Denitrification in the Arctic mid-winter 2004/2005 observed by airborne submillimeter radiometry, *Geophys. Res. Lett.*, *32*, L19811, doi:10.1029/2005GL023408.

1. Introduction

[2] Denitrification is the irreversible removal of reactive nitrogen from an air mass by the sedimentation of HNO_3-containing particles. The resulting lack of reactive nitrogen causes a delay in chlorine deactivation and hence a more prolonged period of ozone loss [*Rex et al.*, 1997; *Waibel et al.*, 1999; *Tabazadeh et al.*, 2000]. Denitrification occurs frequently in the Antarctic winter [*Fahey et al.*, 1990; *Santee et al.*, 1999], and has also been observed several times in the Arctic [*Sugita et al.*, 1998; *Rex et al.*, 1999; *Kondo et al.*, 2000]. The most severe and extensive Arctic denitrification was observed in the unusually cold winter of 1999/2000 [*Popp et al.*, 2001; *Kleinböhl et al.*, 2002]. The Arctic winter of 2004/2005 was exceptionally cold and showed a larger area of potential PSC formation on the 475 K surface than any other winter in recent years (Figure 1). Also, the area for potential ice formation was larger than in the previous winters. Here we present measurements of HNO_3 and N_2O that were taken by the airborne submillimeter radiometer on board the NASA DC-8 research aircraft during the polar aura validation experiment (PAVE) between 24 Jan. and 9 Feb. 2005. We quantify the denitrification in the Arctic vortex and study how it correlates with equivalent latitude and airparcel temperature history, which provides information on the plausibility of denitrification mechanisms.

2. Measurements

[3] Remote measurements of gas-phase HNO_3 and N_2O were performed by the Airborne SUbmillimeter Radiometer ASUR [*von König et al.* [2000], and references therein]. The instrument operates in a frequency range between 604.3 and 662.3 GHz and uses a liquid helium cooled detector and an acousto-optical spectrometer for the acquisition of spectra. By analyzing the spectrally resolved pressure broadened emission lines using the optimal estimation method [*Rodgers*, 1976], vertical profiles of the volume mixing ratio (VMR) of HNO_3, N_2O, and other trace gases are retrieved in an altitude range of about 15–40 km with a typical vertical resolution of 6–10 km in the lower stratosphere. For a more detailed description of the measurement and retrieval the reader is referred to *Kleinböhl et al.* [2002].

[4] ASUR was operated on board the NASA DC-8 research aircraft during PAVE. Deployed from Portsmouth, NH, ASUR performed trace gas measurements inside the Arctic vortex on five research flights, which will

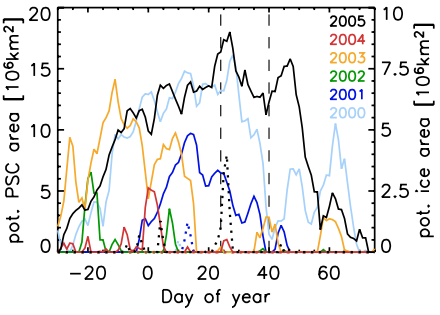

Figure 1. Potential PSC area (area below T_{NAT}, solid) and potential ice area (dotted) on a potential temperature level of 475 K for the Arctic winters since 1999/2000, based on meteorological analyses by ECMWF and assuming an HNO_3 VMR of 10 ppb and an H_2O VMR of 5 ppm. The dashed lines indicate the time period during which the DC-8 was deployed in 2005.

[1]Jet Propulsion Laboratory, California Institute of Technology, Pasadena, California, USA.
[2]Institute of Environmental Physics, University of Bremen, Bremen, Germany.
[3]NASA Langley Research Center, Hampton, Virginia, USA.

0094-8276/05/2005GL023408

Other publications during post-doctoral or research scientist tenure

J Atmos Chem (2010) 66:41–64
DOI 10.1007/s10874-011-9191-4

Aircraft measurements and model simulations of stratospheric ozone and N_2O: implications for chemistry and transport processes in the models

Jayanarayanan Kuttippurath · Armin Kleinböhl · Holger Bremer · Harry Küllmann · Justus Notholt · Björn-Martin Sinnhuber · Wuhu Feng · Martyn Chipperfield

Received: 25 December 2010 / Accepted: 1 June 2011 /
Published online: 1 July 2011

Abstract Airborne measurements of stratospheric ozone and N_2O from the SCIAMACHY (Scanning Imaging Absorption Spectrometer) Validation and Utilization Experiment (SCIA-VALUE) are presented. The campaign was conducted in September 2002 and February–March 2003. The Airborne Submillimeter Radiometer (ASUR) observed stratospheric constituents like O_3 and N_2O, among others, spanning a latitude from 5°S to 80°N during the survey. The tropical ozone source regions show high ozone volume mixing ratios (VMRs) of around 11 ppmv at 33 km altitude, and the altitude of the maximum VMR increases from the tropics to the Arctic. The N_2O VMRs show the largest value of 325 ppbv in the lower stratosphere, indicating their tropospheric origin, and they decrease with increasing altitude and latitude due to photolysis. The sub-tropical and polar mixing barriers are well represented in the N_2O measurements. The most striking seasonal difference found in the measurements is the large polar descent in February–March. The observed features are interpreted with the help of SLIMCAT and Bremen Chemical Transport

J. Kuttippurath · A. Kleinböhl · H. Bremer · H. Küllmann · J. Notholt · B.-M. Sinnhuber
Institute of Environmental Physics, University of Bremen, Bremen, Germany

J. Kuttippurath (✉)
LATMOS/CNRS/UPMC, 4 Place Jussieu, Paris, France
e-mail: jayan@aero.jussieu.fr

A. Kleinböhl
JPL/NASA, California Institute of Technology, Pasadena, CA, USA

H. Bremer
Physikalisch-Technische Bundesanstalt, Braunschweig, Germany

B.-M. Sinnhuber
Institute for Meteorology and Climate Research, Karlsruhe Institute of Technology, Karlsruhe, Germany

W. Feng · M. Chipperfield
School of the Environment, University of Leeds, Leeds, UK

A Climatology of the Gravest Waves in the Equatorial Lower and Middle Stratosphere: Method and Results for the ERA-40 Re-Analysis and the LMDz GCM

FRANÇOIS LOTT, JAYANARAYANAN KUTTIPPURATH, AND FRANÇOIS VIAL

Laboratoire de Météorologie Dynamique du CNRS, Paris, France

(Manuscript received 9 July 2008, in final form 22 October 2008)

ABSTRACT

A climatology of the three-dimensional life cycle of the gravest waves in the tropical lower and middle stratosphere is presented. It shows that at periods around 10 days the gravest waves correspond to Kelvin and Rossby–gravity wave packets that substantially affect specific regions in the lower stratosphere. It also shows that the planetary-scale Kelvin waves with zonal wavenumber $s = 1$ and periods between 10 and 20 days produce a substantial signal. Still at the planetary scales, the climatology also shows that the global planetary Rossby waves with $s = 1$ and periods around 5 and 16 days have a substantial equatorial signature. This climatology is for all the dynamical fields (horizontal wind, temperature, and geopotential height) and relates the equatorial waves to the equatorial zonal mean flow evolution associated with the quasi-biennial oscillation.

The method used to extract the climatology is a composite analysis of the dynamical fields keyed on simple indexes measuring when the waves enter in the stratosphere. For the Kelvin waves, the Rossby–gravity waves, and the 5- and 16-day Rossby planetary waves, these indexes are related to the latitudinal means over the equatorial band of the temperature, the meridional wind, the geopotential height, and the zonal wind respectively. The method is applied first to ERA-40 and then to a simulation done with the LMDz GCM. When compared to the results from ERA-40, this reveals that the LMDz GCM underestimates the Rossby–gravity wave packets and a fraction of the Kelvin wave packets. This deficit is attributed to the fact that the model has a too coarse vertical resolution and an insufficient tropospheric forcing for the horizontal wavenumbers $s > 3$.

1. Introduction

The equatorial waves play an important role in the equatorial stratosphere. Equatorial Kelvin waves and Rossby–gravity waves partly produce the quasi-biennial oscillation (QBO) through wave–mean flow interaction (Holton and Lindzen 1972; Baldwin et al. 2001), and the Kelvin waves are considered to be responsible for the westerly phase of the semi-annual oscillation. They can also contribute to the dehydration of the air at the tropical tropopause (Jensen et al. 2001; Fujiwara et al. 2001).

The theory of equatorial waves was developed by Matsuno (1966). The 15-day Kelvin waves and the 4–5-day Rossby–gravity waves were first observed in stratospheric soundings by Wallace and Kousky (1968) and Yanai and Maruyama (1966), respectively. Since then, many studies have documented the presence of equatorial waves in vertical soundings and ground-based observations using radar, lidar, rockets (Tsuda et al. 1994; Sasi et al. 2003; Fujiwara et al. 2003) or ultralong-duration balloons (Vial et al. 2001; Hertzog and Vial 2001). In addition to these equatorially trapped waves, there is a growing amount of evidence that the dynamics in the lower equatorial stratosphere is also modulated by the planetary Rossby waves that were described at higher altitudes and latitudes by Hirota and Hirooka (1984; see also Madden 1978, 2007).

Although the stratospheric equatorial waves are in good part forced by convection (Holton 1972; Manzini and Hamilton 1993), Hendon and Wheeler (2008) have given evidences that they are quite different from the convectively coupled equatorial waves described by Wheeler et al. (2000) that travel coherently with convective centers in the troposphere (Hendon and Wheeler 2008). This is because the coupled modes are rather slow: their periods correspond to small vertical wavelengths in the stratosphere, where they dissipate rapidly.

Corresponding author address: François Lott, Laboratoire de Météorologie Dynamique du CNRS, Ecole Normale Supérieure, 24, Rue Lhomond, 75231 Paris CEDEX 05, France.
E-mail: flott@lmd.ens.fr

DOI: 10.1175/2008JAS2880.1

Atmos. Chem. Phys., 9, 287–343, 2009
www.atmos-chem-phys.net/9/287/2009/

Atmospheric Chemistry and Physics

Validation of ozone measurements from the Atmospheric Chemistry Experiment (ACE)

E. Dupuy[1], K. A. Walker[1,2], J. Kar[2], C. D. Boone[1], C. T. McElroy[2,3], P. F. Bernath[1,4], J. R. Drummond[2,5], R. Skelton[1], S. D. McLeod[1], R. C. Hughes[1], C. R. Nowlan[2], D. G. Dufour[6], J. Zou[2], F. Nichitiu[2], K. Strong[2], P. Baron[7], R. M. Bevilacqua[8], T. Blumenstock[9], G. E. Bodeker[10], T. Borsdorff[11], A. E. Bourassa[12], H. Bovensmann[13], I. S. Boyd[14], A. Bracher[13], C. Brogniez[15], J. P. Burrows[13], V. Catoire[16], S. Ceccherini[17], S. Chabrillat[18], T. Christensen[19], M. T. Coffey[20], U. Cortesi[17], J. Davies[3], C. De Clercq[18], D. A. Degenstein[12], M. De Mazière[18], P. Demoulin[21], J. Dodion[18], B. Firanski[22], H. Fischer[9], G. Forbes[23], L. Froidevaux[24], D. Fussen[18], P. Gerard[18], S. Godin-Beekmann[25], F. Goutail[26], J. Granville[18], D. Griffith[27], C. S. Haley[28], J. W. Hannigan[20], M. Höpfner[9], J. J. Jin[29], A. Jones[30], N. B. Jones[27], K. Jucks[31], A. Kagawa[7,32], Y. Kasai[7], T. E. Kerzenmacher[2], A. Kleinböhl[13,24], A. R. Klekociuk[33], I. Kramer[9], H. Küllmann[13], J. Kuttippurath[13,25], E. Kyrölä[34], J.-C. Lambert[18], N. J. Livesey[24], E. J. Llewellyn[12], N. D. Lloyd[12], E. Mahieu[21], G. L. Manney[24,35], B. T. Marshall[36], J. C. McConnell[29], M. P. McCormick[37], I. S. McDermid[38], M. McHugh[36], C. A. McLinden[3], J. Mellqvist[30], K. Mizutani[7], Y. Murayama[7], D. P. Murtagh[30], H. Oelhaf[9], A. Parrish[39], S. V. Petelina[12,40], C. Piccolo[41], J.-P. Pommereau[26], C. E. Randall[42], C. Robert[16], C. Roth[12], M. Schneider[9], C. Senten[18], T. Steck[9], A. Strandberg[30], K. B. Strawbridge[22], R. Sussmann[11], D. P. J. Swart[43], D. W. Tarasick[3], J. R. Taylor[2], C. Tétard[15], L. W. Thomason[37], A. M. Thompson[44], M. B. Tully[45], J. Urban[30], F. Vanhellemont[18], C. Vigouroux[18], T. von Clarmann[9], P. von der Gathen[46], C. von Savigny[13], J. W. Waters[24], J. C. Witte[47,48], M. Wolff[2], and J. M. Zawodny[37]

[1]Department of Chemistry, University of Waterloo, Waterloo, ON, Canada
[2]Department of Physics, University of Toronto, Toronto, ON, Canada
[3]Environment Canada, Downsview, ON, Canada
[4]Department of Chemistry, University of York, Heslington, York, UK
[5]Department of Physics and Atmospheric Science, Dalhousie University, Halifax, Canada
[6]Picomole Instruments Inc., Edmonton, AB, Canada
[7]National Institute of Information and Communications Technology (NICT), Koganei, Tokyo, Japan
[8]Naval Research Laboratory, Washington, D.C., USA
[9]Institut für Meteorologie und Klimaforschung (IMK), Forschungszentrum Karlsruhe (FZK) and Universität Karlsruhe, Karlsruhe, Germany
[10]National Institute of Water and Atmospheric Research, Lauder, New Zealand
[11]Institut für Meteorologie und Klimaforschung Atmosphärische Umweltforschung (IMK-IFU), Forschungszentrum Karlsruhe, Garmisch-Partenkirchen, Germany
[12]Institute of Space and Atmospheric Studies, University of Saskatchewan, Saskatoon, SK, Canada
[13]Institut für Umweltphysik (IUP), Universität Bremen, Bremen, Germany
[14]NIWA - Environmental Research Institute, University of Massachusetts, Amherst, MA, USA
[15]Laboratoire d'Optique Atmosphérique, CNRS – Université des sciences et technologies de Lille, Villeneuve d'Ascq, France
[16]Laboratoire de Physique et Chimie de l'Environnement, CNRS – Université d'Orléans, Orléans, France
[17]Instituto di Fisica Applicata "N. Carrara" (IFAC) del Consiglio Nazionale delle Ricerche (CNR), Sesto Fiorentino, Italy
[18]Institut d'Aéronomie Spatiale de Belgique (BIRA-IASB), Bruxelles, Belgium

Correspondence to: K. A. Walker
(kwalker@atmosp.physics.utoronto.ca)

Published by Copernicus Publications on behalf of the European Geosciences Union.

Atmos. Chem. Phys., 9, 413–442, 2009
www.atmos-chem-phys.net/9/413/2009/

Atmospheric Chemistry and Physics

Validation of version-4.61 methane and nitrous oxide observed by MIPAS

S. Payan[1], C. Camy-Peyret[1], H. Oelhaf[2], G. Wetzel[2], G. Maucher[2], C. Keim[2], M. Pirre[3], N. Huret[3], A. Engel[4], M. C. Volk[4], H. Kuellmann[5], J. Kuttippurath[5,*], U. Cortesi[6], G. Bianchini[6], F. Mencaraglia[6], P. Raspollini[6], G. Redaelli[7], C. Vigouroux[8], M. De Mazière[8], S. Mikuteit[2], T. Blumenstock[2], V. Velazco[5], J. Notholt[5], E. Mahieu[9], P. Duchatelet[9], D. Smale[10], S. Wood[10], N. Jones[11], C. Piccolo[12], V. Payne[13], A. Bracher[5], N. Glatthor[2], G. Stiller[2], K. Grunow[14], P. Jeseck[1], Y. Te[1], and A. Butz[15]

[1]Laboratoire de Physique Moléculaire pour l'Atmosphère et l'Astrophysique, Université Pierre et Marie Curie-Paris 6, Paris, France
[2]Institut für Meteorologie und Klimaforschung, Forschungszentrum Karlsruhe, Karlsruhe, Germany
[3]Laboratoire de Physique et Chimie de l'Environnement/CNRS, Orléans, France
[4]Institut für Atmosphäre und Umwelt, J. W. Goethe Universität Frankfurt, Frankfurt, Germany
[5]Institute of Environmental Physics/Institute of Remote Sensing, University of Bremen, Bremen, Germany
[6]Istituto di Fisica Applicata "Nello Carrara", Sesto Fiorentino, Italy
[7]Università di L'Aquila, Dipartimento di Fisica, L'Aquila, Italy
[8]Belgian Institute for Space Aeronomy, Brussels, Belgium
[9]Institut d'Astrophysique et de Géophysique, University of Liège (ULg), Liège, Belgium
[10]National Institute for Water and Atmospheric Research (NIWA), Lauder, Otago, New Zeeland
[11]University of Wollongong, Wollongong, Australia
[12]Atmospheric, Oceanic and Planetary Physics, Department of Physics, Oxford University, Oxford, UK
[13]Atmospheric and Environmental Research, Inc, Lexington, Massachusetts, USA
[14]Meteorologisches Institut der FU Berlin, Berlin, Germany
[15]Institut für Umweltphysik, University of Heidelberg, Germany
[*]now at: Laboratoire de Météorologie Dynamique, Ecole Polytechnique, Palaiseau, France

Received: 18 June 2007 – Published in Atmos. Chem. Phys. Discuss.: 17 December 2007
Revised: 13 October 2008 – Accepted: 27 October 2008 – Published: 19 January 2009

Abstract. The ENVISAT validation programme for the atmospheric instruments MIPAS, SCIAMACHY and GOMOS is based on a number of balloon-borne, aircraft, satellite and ground-based correlative measurements. In particular the activities of validation scientists were coordinated by ESA within the ENVISAT Stratospheric Aircraft and Balloon Campaign or ESABC. As part of a series of similar papers on other species [this issue] and in parallel to the contribution of the individual validation teams, the present paper provides a synthesis of comparisons performed between MIPAS CH_4 and N_2O profiles produced by the current ESA operational software (Instrument Processing Facility version 4.61 or IPF v4.61, full resolution MIPAS data covering the period 9 July 2002 to 26 March 2004) and correlative measurements obtained from balloon and aircraft experiments as well as from satellite sensors or from ground-based instruments. In the middle stratosphere, no significant bias is observed between MIPAS and correlative measurements, and MIPAS is providing a very consistent and global picture of the distribution of CH_4 and N_2O in this region. In average, the MIPAS CH_4 values show a small positive bias in the lower stratosphere of about 5%. A similar situation is observed for N_2O with a positive bias of 4%. In the lower stratosphere/upper troposphere (UT/LS) the individual used MIPAS data version 4.61 still exhibits some unphysical oscillations in individual CH_4 and N_2O profiles caused by the processing algorithm (with almost no regularization). Taking

Correspondence to: S. Payan
(sebastien.payan@upmc.fr)

Published by Copernicus Publications on behalf of the European Geosciences Union.

Validation of the Aura Microwave Limb Sounder ClO measurements

M. L. Santee,[1] A. Lambert,[1] W. G. Read,[1] N. J. Livesey,[1] G. L. Manney,[1,2] R. E. Cofield,[1] D. T. Cuddy,[1] W. H. Daffer,[1] B. J. Drouin,[1] L. Froidevaux,[1] R. A. Fuller,[1] R. F. Jarnot,[1] B. W. Knosp,[1] V. S. Perun,[1] W. V. Snyder,[1] P. C. Stek,[1] R. P. Thurstans,[1] P. A. Wagner,[1] J. W. Waters,[1] B. Connor,[3] J. Urban,[4] D. Murtagh,[4] P. Ricaud,[5] B. Barret,[5] A. Kleinböhl,[1] J. Kuttippurath,[6,7] H. Küllmann,[6] M. von Hobe,[8] G. C. Toon,[1] and R. A. Stachnik[1]

Received 6 April 2007; revised 31 October 2007; accepted 16 December 2007; published 14 May 2008.

[1] We assess the quality of the version 2.2 (v2.2) ClO measurements from the Microwave Limb Sounder (MLS) on the Earth Observing System Aura satellite. The MLS v2.2 ClO data are scientifically useful over the range 100 to 1 hPa, with a single-profile precision of ~0.1 ppbv throughout most of the vertical domain. Vertical resolution is ~3–4 km. Comparisons with climatology and correlative measurements from a variety of different platforms indicate that both the amplitude and the altitude of the peak in the ClO profile in the upper stratosphere are well determined by MLS. The latitudinal and seasonal variations in the ClO distribution in the lower stratosphere are also well determined, but a substantial negative bias is present in both daytime and nighttime mixing ratios at retrieval levels below (i.e., pressures larger than) 22 hPa. Outside of the winter polar vortices, this negative bias can be eliminated by subtracting gridded or zonal mean nighttime values from the individual daytime measurements. In studies for which knowledge of lower stratospheric ClO mixing ratios inside the winter polar vortices to better than a few tenths of a ppbv is needed, however, day − night differences are not recommended and the negative bias must be corrected for by subtracting the estimated value of the bias from the individual measurements at each affected retrieval level.

Citation: Santee, M. L., et al. (2008), Validation of the Aura Microwave Limb Sounder ClO measurements, *J. Geophys. Res.*, *113*, D15S22, doi:10.1029/2007JD008762.

1. Introduction

[2] The partitioning between active and reservoir forms of chlorine modulates ozone destruction throughout the stratosphere [e.g., *Solomon*, 1999; *World Meteorological Organization*, 2007]. Chlorine monoxide, ClO, is the primary form of reactive chlorine in the stratosphere and thus a key catalyst for ozone loss. The Microwave Limb Sounder (MLS) on NASA's Earth Observing System (EOS) Aura satellite measures vertical profiles of ClO globally on a daily basis. Initial validation of the first publicly available Aura MLS ClO data set, version 1.5 (v1.5), was presented by *Barret et al.* [2006]. Here we report on the quality of the recently released version 2.2 (v2.2) Aura MLS ClO measurements. The measurement system is described in section 2. In addition to providing a review of instrumental and orbital characteristics, this section includes guidelines for quality control that should be applied to the v2.2 ClO measurements, documents their precision and spatial resolution, and quantifies sources of systematic uncertainty. Because the v1.5 Aura MLS ClO data have been featured in some previous studies [e.g., *Schoeberl et al.*, 2006a; *Santee et al.*, 2005], section 2 provides an overview of the differences between v2.2 and v1.5 ClO data. A systematic negative bias, present in v1.5 but, unfortunately, worse in v2.2, is also quantified in this section. In section 3, "zeroth-order" validation of the Aura MLS ClO data is accomplished by comparing against climatological averages in narrow equivalent latitude bands compiled from the multiyear Upper Atmosphere Research Satellite (UARS) MLS ClO data set. Accuracy is assessed through comparisons with correlative data sets from a variety of platforms in section 4. Finally, in section 5 we summarize the Aura MLS ClO validation results.

2. Aura MLS ClO Measurement Description

2.1. Overview of the MLS Measurement System

[3] Aura, the last in NASA's EOS series of satellites, was launched on 15 July 2004 into a near-polar, sun-synchronous,

[1]Jet Propulsion Laboratory, California Institute of Technology, Pasadena, California, USA.
[2]Also at Department of Physics, New Mexico Institute of Mining and Technology, Socorro, New Mexico, USA.
[3]National Institute of Water and Atmospheric Research, Omakau, New Zealand.
[4]Department of Radio and Space Science, Chalmers University of Technology, Göteborg, Sweden.
[5]Laboratoire d'Aérologie, Observatoire de Midi-Pyrénées, Toulouse, France.
[6]Institute of Environmental Physics, University of Bremen, Bremen, Germany.
[7]Now at LMD/CNRS Ecole Polytechnique, Palaiseau, France.
[8]Institut für Chemie und Dynamik der Geosphäre I: Stratosphäre, Forschungszentrum Jülich, Jülich, Germany.

0148-0227/08/2007JD008762

Original Paper

Indoor and Built Environment

Indoor Built Environ 2008;17;3:260–268

Accepted: August 7, 2007

VOC Concentrations in an Indoor Workplace Environment of a University Building

S.J. Solomon[a] G.W. Schade[a,b] J. Kuttippurath[a,c]
A. Ladstätter-Weissenmayer[a] J.P. Burrows[a]

[a]Institute of Environmental Physics, University of Bremen, Germany
[b]Department of Atmospheric Sciences, Texas A&M University, College Station, Texas, USA
[c]LMD/CNRS, Ecole Normale Supérieure, Paris Cedex 05, France

Key Words
BTEX · Environmental tobacco smoke · Indoor air quality · Methanalyser · PTR-MS · VOC

Abstract
An indoor air quality survey was conducted at selected indoor environments in the Department of Physics and Electrical Engineering of the University of Bremen, Germany, during August 2005. The mean indoor/outdoor (I/O) ratios of pollutants appeared to be higher than 1.0 for most volatile organic compounds (VOCs). Apart from direct emissions from indoor materials and infiltration of outdoor air, environmental tobacco smoke (ETS) was a dominant factor in indoor pollution. Pollutants which were commonly associated with cleaning products and materials, including monoterpenes, aldehydes and acetone exhibited general trends of higher concentrations indoors compared to outdoor levels. Indoor concentrations of many VOCs were found to be 2–10 times higher during weekdays as compared to the weekend, exhibiting a strong correlation with human activities. A comparison with previous studies on the health risks due to selected VOCs indicates that long-term exposure to the peak values reported in this study has potential to develop adverse health effects to the occupants whereby reducing the efficiency in the workplace.

Introduction

In recent years, increased attention has been paid by the scientific community to understand and improve indoor workplace atmospheres. Indoor air quality is considered to be governed by high levels of outdoor pollutant concentrations, pollutant sources and sinks and movement of air between the building interior and outdoors. There has been substantial scientific enquiry in determining personal exposures to pollutants as people in developed countries spend more than 90% and people in developing countries more than 70% of their time indoors [1]. Although indoor pollution is not per se more dangerous than outdoor pollution, concentrations of indoor contaminants are often higher than those encountered outside, most of

DOI: 10.1177/1420326X08090822
Accessible online at http://ibe.sagepub.com
Figures 1–4 appear in colour online.

Dr S.J. Solomon,
Institute of Environmental Physics, University of Bremen, Otto-Hahn Allee-1,
D-28334, Bremen, Germany
Tel.: 0049 421 2183526, Fax: 0049 421 218455.
E-Mail juliet@iup.physik.uni-bremen.de

Atmos. Chem. Phys., 8, 3529–3562, 2008
www.atmos-chem-phys.net/8/3529/2008/

Atmospheric Chemistry and Physics

Validation of HNO_3, $ClONO_2$, and N_2O_5 from the Atmospheric Chemistry Experiment Fourier Transform Spectrometer (ACE-FTS)

M. A. Wolff[1], T. Kerzenmacher[1], K. Strong[1], K. A. Walker[1,2], M. Toohey[1], E. Dupuy[2], P. F. Bernath[2,3], C. D. Boone[2], S. Brohede[4], V. Catoire[5], T. von Clarmann[6], M. Coffey[7], W. H. Daffer[8], M. De Mazière[9], P. Duchatelet[10], N. Glatthor[6], D. W. T. Griffith[11], J. Hannigan[7], F. Hase[6], M. Höpfner[6], N. Huret[5], N. Jones[11], K. Jucks[12], A. Kagawa[13,14], Y. Kasai[14], I. Kramer[6], H. Küllmann[15], J. Kuttippurath[15,*], E. Mahieu[10], G. Manney[16,17], C. T. McElroy[18], C. McLinden[18], Y. Mébarki[5], S. Mikuteit[6], D. Murtagh[4], C. Piccolo[19], P. Raspollini[20], M. Ridolfi[21], R. Ruhnke[6], M. Santee[16], C. Senten[9], D. Smale[22], C. Tétard[23], J. Urban[4], and S. Wood[22]

[1]Department of Physics, University of Toronto, Toronto, Ontario, Canada
[2]Department of Chemistry, University of Waterloo, Waterloo, Ontario, Canada
[3]Department of Chemistry, University of York, York, UK
[4]Department of Radio and Space Science, Chalmers University of Technology, Gothenburg, Sweden
[5]Laboratoire de Physique et Chimie de L'Environment CNRS – Université d'Orléans, Orléans, France
[6]Forschungzentrum Karlsruhe and Univ. of Karlsruhe, Institute for Meteorology and Climate Research, Karlsruhe, Germany
[7]National Center for Atmospheric Research (NCAR), Boulder, CO, USA
[8]Columbus Technologies Inc., Pasadena, CA, USA
[9]Belgian Institute for Space Aeronomy, Brussels, Belgium
[10]Institute of Astrophysics and Geophysics, University of Liège, Liège, Belgium
[11]School of Chemistry, University of Wollongong, Wollongong, Australia
[12]Harvard-Smithsonian Center for Astrophysics, Cambridge, MA, USA
[13]Fujitsu FIP Corporation, Tokyo, Japan
[14]Environmental Sensing and Network Group, National Institute of Information and Communications Technology (NICT), Tokyo, Japan
[15]Institute of Environmental Physics, University of Bremen, Bremen, Germany
[16]Jet Propulsion Laboratory, California Institute of Technology, Pasadena, CA, USA
[17]New Mexico Institute of Mining and Technology, Socorro, NM, USA
[18]Environment Canada, Toronto, Ontario, Canada
[19]Atmospheric, Oceanic and Planetary Physics, University of Oxford, Oxford, UK
[20]Institute of Applied Physics "Nello Carrara", National Research Center (CNR), Firenze, Italy
[21]Dipartimento di Chimica Fisica e Inorganica, Università di Bologna, Bologna, Italy
[22]National Institute of Water and Atmospheric Research Ltd., Central Otago, New Zealand
[23]Laboratoire d'Optique Atmosphérique, Université des Sciences et Technologies de Lille, Villeneuve d'Ascq, France
[*]now at: LMD/CNRS Ecole polytechnique, Palaiseau Cedex, France

Received: 4 December 2007 – Published in Atmos. Chem. Phys. Discuss.: 11 December 2007
Revised: 5 June 2008 – Accepted: 5 June 2008 – Published: 7 July 2008

Correspondence to: M. A. Wolff
(mwolff@atmosp.physics.utoronto.ca)

Published by Copernicus Publications on behalf of the European Geosciences Union.

Atmos. Chem. Phys., 7, 4905–4934, 2007
www.atmos-chem-phys.net/7/4905/2007/

Atmospheric Chemistry and Physics

Validation of MIPAS HNO_3 operational data

D. Y. Wang[1,2], M. Höpfner[1], C. E. Blom[1], W. E. Ward[2], H. Fischer[1], T. Blumenstock[1], F. Hase[1], C. Keim[1], G. Y. Liu[1], S. Mikuteit[1], H. Oelhaf[1], G. Wetzel[1], U. Cortesi[3], F. Mencaraglia[3], G. Bianchini[3], G. Redaelli[4], M. Pirre[5], V. Catoire[5], N. Huret[5], C. Vigouroux[6], M. De Mazière[6], E. Mahieu[7], P. Demoulin[7], S. Wood[8], D. Smale[8], N. Jones[9], H. Nakajima[10], T. Sugita[10], J. Urban[11], D. Murtagh[11], C. D. Boone[12], P. F. Bernath[12,13], K. A. Walker[12,14], J. Kuttippurath[15,16], A. Kleinböhl[15,18], G. Toon[18], and C. Piccolo[19]

[1]Institut für Meteorologie und Klimaforschung (IMK),Forschungszentrum Karlsruhe und Universität Karlsruhe, Karlsruhe, Germany
[2]Physics Department, University of New Brunswick, Fredericton, New Brunswick, Canada
[3]Istituto di Fisica Applicata "N. Carrara" (IFAC) del Consiglio Nazionale delle Ricerche (CNR), Firenze, Italy
[4]Dipartimento di Fisica,CETEMPS, Universita' di L'Aquila, L'Aquila, Italy
[5]Laboratoire de Physique et Chimie de l'Environnement, Université d'Orléans (LPCE-CNRS), Orléans, France
[6]Belgian Institute for Space Aeronomy (BIRA-IASB), Brussels, Belgium
[7]Institut d'Astrophysique et de Géophysique, University of Liège (ULg), Liège, Belgium
[8]National Institute for Water and Atmospheric Research (NIWA), Lauder, Otago, New Zealand
[9]University of Wollongong, Wollongong, Australia
[10]National Institute for Environmental Studies, Tsukuba, Japan
[11]Department of Radio and Space Science, Chalmers University of Technology, Göteborg, Sweden
[12]Department of Chemistry, University of Waterloo, Waterloo, Ontario, Canada
[13]Department of Chemistry, University of York, Heslington, York, UK
[14]Department of Physics, University of Toronto, Toronto, Canada
[15]Institute of Environmental Physics, University of Bremen, Bremen, Germany
[16]CNRS/LMD Ecole Polytechnique, Palaiseau Cedex, France
[18]Jet Propulsion Laboratory, California Institute of Technology, Pasadena, CA, USA
[19]Department of Physics, Oxford University, Oxford, UK

Received: 29 March 2007 – Published in Atmos. Chem. Phys. Discuss.: 17 April 2007
Revised: 15 August 2007 – Accepted: 15 August 2007 – Published: 21 September 2007

Abstract. Nitric acid (HNO_3) is one of the key products that are operationally retrieved by the European Space Agency (ESA) from the emission spectra measured by the Michelson Interferometer for Passive Atmospheric Sounding (MIPAS) onboard ENVISAT. The product version 4.61/4.62 for the observation period between July 2002 and March 2004 is validated by comparisons with a number of independent observations from ground-based stations, aircraft/balloon campaigns, and satellites. Individual HNO_3 profiles of the ESA MIPAS level-2 product show good agreement with those of MIPAS-B and MIPAS-STR (the balloon and aircraft version of MIPAS, respectively), and the balloon-borne infrared spectrometers MkIV and SPIRALE, mostly matching the reference data within the combined instrument error bars. In most cases differences between the correlative measurement pairs are less than 1 ppbv (5–10%) throughout the entire altitude range up to about 38 km (∼6 hPa), and below 0.5 ppbv (15–20% or more) above 30 km (∼17 hPa). However, differences up to 4 ppbv compared to MkIV have been found at high latitudes in December 2002 in the presence of polar stratospheric clouds. The degree of consistency is further largely affected by the temporal and spatial coincidence, and differences of 2 ppbv may be observed between 22 and 26 km (∼50 and 30 hPa) at high latitudes near the vortex boundary, due to large horizontal inhomogeneity of HNO_3. Similar features are also observed in the mean differences of the MIPAS ESA HNO_3 VMRs with respect to the ground-based FTIR measurements at five stations, aircraft-based SAFIRE-A and ASUR, and the balloon campaign IBEX. The mean relative differences between the MIPAS and FTIR HNO_3 partial columns are within ±2%, comparable to the MIPAS

Correspondence to: D. Y. Wang
(dwang@unb.ca)

Published by Copernicus Publications on behalf of the European Geosciences Union.

Cover image credit: Philippe Cocquerez, CNES, Paris.
A balloon launch during the CONCORDIASI campaign in Antarctica in 2010